Flutes, megaflutes and erosional bedforms: a reappraisal of their dynamics

Heather Macdonald

Submitted in accordance with the requirements for the degree of Doctor of Philosophy

The University of Leeds

School of Earth and Environment

August 2010

The candidate confirms that the work submitted is her own, except where work which has formed part of jointly-authored publications has been included. The contribution of the candidate and the other authors to this work has been explicitly indicated overleaf. The candidate confirms that appropriate credit has been given within the thesis where reference has been made to the work of others.

This copy has been supplied on the understanding that it is copyright material and that no quotation from the thesis may be published without proper acknowledgement.

Declaration of authorship

Chapter 4 reproduces a manuscript that has been accepted by the Journal of the Geological Society London:

Macdonald, H.A., Peakall, J., Wignall, P. and Best, J. *In prep*. Sedimentation in deep-sea lobe elements: implications for the origin of thickening-upwards sequences.

Fieldwork was completed by Heather Macdonald. All presented data was collected by Heather Macdonald other than the data contained within Figure 4.5, which was collected by Jeff Peakall and Paul Wignall. All data was processed, interpreted and presented by Heather Macdonald. Ideas were shaped, and the model was developed during discussion with co-authors.

Chapter 6 reproduces a manuscript that is in review with Geosphere:

Macdonald, H.A. Wynn, R.B., Huvenne, V.A.I., Weaver, P.P.E., McPhail, S.D., Masson, D.G. and Peakall, J. *In review*. High-resolution imaging of deep-water erosional scours along the northeast Atlantic margin: Bridging the gap between modern and ancient turbidite systems.

Data were collected during the research cruise of JC027. Steven McPhail was responsible for data collection by Autosub6000, and Veerle Huvenne processed these data. Esther Sumner provided initial graphic logs of sediment cores. Phil Weaver performed coccolith dating on samples selected by Heather Macdonald. Heather Macdonald was responsible for all data presentation and interpretations.

Acknowledgements

First and foremost, I would like to thank my supervisors Jeff Peakall, Paul Wignall, Jim Best and Russell Wynn, for their support and guidance throughout this project and for making the research and fieldwork a really enjoyable experience.

Funding for this research has come from the Natural Environment Research Council (studentship NER/S/A/2006/14147) and via a CASE award from the NSRD Geology and Geophysics group at the National Oceanography Centre, Southampton.

I would like to thank Gareth Keevil for his endless support and inspiration during the course of the experimental aspect of this project. Thank you also to Esther Sumner, Rachael Dale and Karen Wignall for wonderful assistance in the field. I also extend thanks to John Thurmond for collecting, processing and providing LiDAR field data; Quentin Fisher for providing SEM and XRD analyses of field samples; Richard Connors for MATLAB advice, and Kirk Handley for assistance with experimental work. Also thank you to my examiners Nigel Mountney and Kevin Pickering, who greatly improved the clarity of the thesis.

I am especially grateful to Russ for including me on *RRS James Cook* cruise JC27, and for allowing me access to the spectacular data that were obtained. Special thanks also to the Captain, Officers and crew of JC027 for their assistance during data collection, and to Pete Stevenson, Maaten Furlong, Veerle Huvenne, Esther Sumner, Phil Weaver and Doug Masson.

I'd particularly like to thank Mary Benton, Jeff Trofimovs and Rich Brown for their inspiration and ongoing support during this during this project. Thank you.

I am most grateful to my family for their endless support. Thank you Mum, and thank you Matt.

This thesis is dedicated in loving memory of my father John, my grandfather Poppy, and our wonderful Jane.

Abstract

Erosional bedforms in deep-sea environments record the passage of highly erosive turbidity currents that are often voluminous and fully bypassing. This investigation focuses upon a subset of erosional bedforms that are elliptical in shape, and utilises a multidisciplinary approach to reappraise the occurrence and dynamics of the bedforms across all scales. The investigation provides highly detailed analyses for three scales of form: centimetre-scale flutes, metre-scale megaflutes, and large metre-to-kilometre scale scours. The results confirm that deep-water scours form a continuous spectrum from centimetre- to kilometre-scale. Furthermore, the investigation effectively 'bridges the scale gap' between traditional scales of analysis of outcrop and modern system

Laboratory modelling of the erosion of mud beds provides the first experimental generation of flutes upon a smooth mud-bed in open channel flows. High-resolution bathymetric data taken in time-series during experiments demonstrate that bedforms are stable, migrate downstream with time, and form in association with features not previously generated under experimental conditions, including pock-marks, gullies and potholes. The study also revisits the outcrops of the Carboniferous Ross Sandstone (SW Ireland) to address the stratigraphic occurrence, morphology and lithology of megaflutes and associated thickening-upward packages. This has identified that packages form via prograding lobe-elements, deposited by mud-rich sands, and record a vertical trend from distal- to proximal-deposits accompanied by an increasing frequency of megaflutes and broad erosional surfaces. Existing process-models for these packages are re-examined, and a six-stage model for lobe-element evolution is proposed that documents successive phases of deposition, sediment bypass, erosion and lobe abandonment.

High-resolution AUV data and well-constrained core control present the bathymetry (2x2 m pixel size), sedimentology and chronology of four large-scale modern deep-water canyon/channel systems along the northeast Atlantic continental margin. Scours range from 40-3170 m wide and 8-48 m deep and occur in zones of rapid flow expansion, such as channel mouths or overbank areas.

Table of contents

Declaration of authorship ii

Acknowledgements iii

Abstract iv

1. Thesis Rationale 1

1.1. Introduction 1

1.2. Scours that are between ‘linear’ and ‘transverse’ 2

1.3. Thesis objectives 5

1.4. Thesis structure 6

2. Scouring: scales, processes & morphologies 8

2.1. Introduction 8

2.2. Scours: scales of analysis 8

2.3. Experimental studies of centimetre-scale flutes 9

2.3.1. Terminology 11

2.3.2. Experiments of erosion by turbulent plaster of Paris flows 12

2.3.3. Experiments of erosion by turbulent plain water flows 14

2.3.4. Experiments of erosion by water with suspended sand 19

2.3.5. Mass transfer analogy 23

2.3.6. Flute morphology and terminology 24

2.3.7. A model for the development of flutes 24

2.4. Experimental studies: discussion and conclusions 26

2.5. Scours observed in modern deep-sea environments 28

2.5.1. Modern deep-sea scours: regions of formation 28

2.5.2. Modern deep-sea scours: morphological types 30

2.5.3. Modern deep sea scours: trigger mechanisms 30

2.5.4. Data collection in modern deep-sea environments 32

2.5.5. Discussion and conclusions 33

2.6. Scours observed in ancient deep-sea environments 34

2.7. Case Study: The Carboniferous Ross Sandstone, western Ireland 34

2.7.1. Model 1: Distal channel-lobe transition setting 36
2.7.2. Model 2: Basin floor deposition & erosion 38
2.7.3. Model 3: Sinuous channel and spillover system 38
2.7.4. Carboniferous Ross Sandstone case study summary 39
2.8. Discussion 40
3. Experimental simulations of erosional bedforms in muds 43
3.1. Introduction 43
3.2. Experimental equipment and procedure 45
3.2.1. Flume Tank 45
3.2.2. Creating artificial beds 45
3.2.3. Flow measurements 49
3.2.4. Bed measurements 51
3.2.5. Experimental method 52
3.3. Experimental results 54
3.3.1. Experimental beds of weakly cohesive china clay 54
3.3.2. Experimental beds made of potter's clay 55
3.4. Summary of experimentally produced bedforms 71
3.5. Description of experimentally produced erosional bedforms 72
3.5.1. Wavy topography 72
3.5.2. Pock-marks 72
3.5.3. Narrow, long flutes 74
3.5.4. Broad, shallow flutes 74
3.5.5. Gullies 74
3.5.6. Potholes 75
3.6. Discussion 75
3.7. Conclusions 78
4. Architecture and flow processes in deep-sea lobe-elements: the Carboniferous Ross Sandstone, western Ireland 79
4.1. Architecture of deep-sea lobe elements 79
4.2. Outcrop studies 81

4.3. The Carboniferous Ross Sandstone 82

4.3.1. Ross Sandstone thickening-upward packages 82

4.3.2. Methodology, dataset and study area 83

4.4. Results 85

4.4.1. Measured sections 85

4.4.2. Sedimentary model: erosive bypass within prograding lobe-elements 89

4.5. The occurrence of megaflutes, distributary channels and proximal lobe bypass surfaces 92

4.6. Discussion 93

4.6.1. Comparison with existing models 93

4.6.2. Progradation relative to aggradation in lobes 96

4.6.3. A mechanism for thickening-up distributions 98

4.7. Conclusions 101

5. The morphology, occurrence and genesis of megaflutes: the Carboniferous Ross Formation, western Ireland 102

5.1. Introduction 102

5.1.1. The Ross Formation 102

5.2. Field techniques and methodology 104

5.3. Results 1: sandstone properties 105

5.4. Results 2: scour types 109

5.4.1. Megaflutes 109

5.4.2. Stepped or flat-bottomed scours 118

5.4.3. Broad bypass surfaces 119

5.5. Summary: a spectrum of erosive features 120

5.6. Discussion 121

5.6.1. Cohesive properties of the Ross Sandstone 121

5.6.2. The relationship between megaflutes and ripples 122

5.6.3. Bed thickness as a control on the development of bedforms 123

5.6.4. Megaflute and scour genesis 125

5.7. Conclusions 126

6. High-resolution imaging of deep-water erosional scours along the northeast Atlantic margin 127

6.1. Introduction 127

6.2. High-resolution AUV imaging of deep-water scours 127

6.3. Study area 128

6.4. Methods and data 129

6.4.1. Geophysical data 129

6.4.2. Sedimentological data 129

6.4.3. Dating control 129

6.5. Results 130

6.5.1. Agadir Canyon mouth 130

6.5.2. Horseshoe Valley 134

6.5.3. Setúbal Canyon mouth 138

6.5.4. Whittard Channel margin 140

6.6. Interpretation and discussion 143

6.6.1. Isolated erosional scours 144

6.6.2. Amalgamated erosional scours 146

6.6.3. Sedimentary deposits within and adjacent to scours 147

6.6.4. Insights into scour genesis 149

6.6.5. Morphologic features associated with scours 150

6.7. Conclusions 150

7. Thesis synthesis 152

7.1. Introduction 152

7.2. Principal scientific advances 152

7.2.1. First experimental generation of flutes in open channel flows on initially smooth mud beds 152

7.2.2. Genetic model of megaflutes in sedimentary systems 153

7.2.3. First explanation of how megaflutes form within sand beds 154

7.2.4. First definition for megaflutes 154

7.2.5. First high-resolution imaging of deep-water scours along the northeast Atlantic margin 155

7.3. Do flutes, megaflutes and large-scale scours relate to one another in terms of morphology and genesis? 156

7.3.1. The morphology of spoon-shaped flute forms 157

7.3.1. The morphology of horseshoe-shaped flute forms 158

7.3.2. The genesis of spoon-shaped and horseshoe-shaped flute forms 161

7.3.3. The morphology and genesis of gully forms 161

7.4. Do erosional bedforms naturally form in three distinct size groups, or is this an artifact of how they are documented? 163

7.4.1. Future work 164

References 166

Appendix A 181

Appendix B 192

Appendix C 196

Appendix D 224

List of figures

Figure 2.1. Photograph of experimentally generated flute casts of Rucklin (1938), described as *conical flute casts*. Flute casts shown by red arrows, white arrow shows blocky degassing structure. Current direction from left to right. 11

Figure 2.2. Photographs of scour marks on soft mud surfaces settled from suspension, eroded by turbulent flows of plaster of Paris (Dzulynki and Walton 1963). Flow direction as indicated by arrows. 13

Figure 2.3. Schematic to show the apparatus used in fluid stressing experiments of Allen (1971). Flume measures 3.66 m long, 30.5 cm deep, 30 cm wide. A. Mud bed is settled from suspension within walled-off section over 3 days. B. Bed elevation is measured across the bed to ensure 6-8cm thickness. C. During run, the water surface level is set at a desired level. D. Following the experiment the bed elevation is measured at 5cm intervals, and an impression of the bed surface is taken using a plaster of Paris mixture. 14

Figure 2.4. Schematics showing the primary modes of small-scale fluid-stressing erosion in mud-beds in relation to local eddying patterns; of Allen (1969). A. Morphology of longitudinal ridges and V-shaped marks formed during high velocity flows (50 – 140 cm/s). B. Morphology of polygonal depressions formed as long-term trend during high-velocity flows; C. Grooves formed during low velocity flows (20 – 50 cm/s); mud flakes became held captive within the grooves during long runs. 16

Figure 2.5. Photographs from the same weakly cohesive fluid-stressing experimental bed, used by Allen (1969) to illustrate three morphologically intergrading flute types: (i) heel-shaped flutes that are symmetrical, and longer than they are wide; (ii) symmetrical flutes that are wider than long; and (iii) asymmetrical flutes that are longer than wide, and skewed to the mean flow direction. Widths of photographs are 15.5 cm (left) and 30.0 cm (right); flow direction is from bottom to top. Note, the three morphological types are hard to identify. The most convincing flute forms are illustrated with the red arrow. 17

Figure 2.6. Field example of mud ripples preserved on the sole of a sandstone bed (Allen, 1984, p. 260). Ripple wavelength is ~0.04 cm, palaeoflow direction is from bottom to top. Note their similarity of form to the features in Figure 2.5. From Kronso Beds (Oligocene), Wernejowka, Polish Carpathians. 18

Figure 2.7. Modified figure showing the apparatus used in corrasion experiments by Allen (1971) eroding a strong clay bed. Shop-bought modelling clay was hand moulded into the bed material holder, which is set into a Perspex pipe. Abrasive flows of water and sand were fed into the pipe from elevated tanks at controlled velocities, and the sand concentration monitored. 19

Figure 2.8. The growth of an experimentally produced flute via corrasion of a cohesive mud bed, by Allen (1971); his experimental run 41. The initial defect was a flat-bottomed, shallow and circular. Time-series times are approximate: a. t = 0; b. 19.8 minutes; c. 42.8 minutes; d. 74.1 minutes. 1 cm scale is indicated in a. Flow direction is from bottom to top.....21

Figure 2.9. Photographs of an experimentally produced flute via corrasion of a cohesive mud bed initiating from a deep, narrow defect aligned oblique to flow. After Allen (1971), his experimental run 42. Times are approximate: a. t = 0; b. 11.1

minutes; c. 27.8 minutes; d. 52.6 minutes; e. 74.3 minutes. 2 cm scale is shown in a; flow direction is from bottom to top. 22

Figure 2.10. Schematics showing the morphology of flute marks according to Allen (1971). Left hand side of each type shows longitudinal bed cross-section (along dividing plane) whereas the right hand-side illustrates planform morphology.....23

Figure 2.11. A schematic of a flute mark with terminology for morphological features, after Allen (1971). Bottom left figure shows longitudinal profile (along dividing plane), and bottom right figure shows transverse profile. 24

Figure 2.12. Schematic showing a downstream cross-sectional profile of an idealised flute and the patterns of motion associated with development, after Allen (1969). ..25

Figure 2.13. The development of flutes according to A. the passive bed theory, and; B. the defect theory (Allen, 1971).....26

Figure 2.14. Schematic figure showing the four principal formative locations of elliptical scours (and associated features) in modern systems, with referenced published examples. Thick black arrows indicate dominant flow direction. A. Channel-levee backslopes, B. Linear trends of cyclic stepped scours adjacent to channel bends, C. Channel-lobe transition zones (CLTZ), D. Basal slope plunge pools. Not to scale. 29

Figure 2.15. Summary figure showing the principal morphological types of elliptical scours in deep-sea environments, and published references. Features a - d are modified after Wynn et al. (2002b). Erosional lineations are included here because they are prominent features of channel-lobe transition zones and feature in Figure 2.14c. 31

Figure 2.16. Megaflute of the Carboniferous Ross Formation, western Ireland; with chalk lines etched on to show topography. Megaflute mesures ~6 m at its widest point; black and white metre ruler to right of photograph for scale. Palaeoflow is from top-right to bottom-left. Surrounding bedding surface is ornamented with lingoid ripples.....35

Figure 2.17. Contrasting models for the development of Ross Formation megaflutes: (A) Development in channel-lobe transition zones within an aggradational, sand-rich fan with small, coalescing mid-outer fan lobes with multiple shallow channels

(Chapin et al. 1994) (B) Megaflute development in channel-wing region along erosion surfaces that trace laterally into channel axis – specific location within basin is not stated (Elliott 2000a,b) (C) Development of megaflutes in the upper parts of spillover lobes at the bends of sinuous channels (Lien et al. 2003). 37

Figure 2.18. Photograph of the Albian Black Flysch deposits, Bakio Point, northern Spain. Foreground shows part of a megaflute surface (red line) and infilling sandstone (labelled), which is overlain by another erosional surface (red arrow); palaeoflow is from left to right. Sediments in photograph are all coarse grained sandstones. Three erosional surfaces in the background are also indicated (yellow arrows). Karen Wignall in photograph for scale. 40

Figure 3.1. Longitudinal profiles measured on experimental erosional marks generated at defects due to corrasion on strongly cohesive mud beds. Of Allen (1971, p. 279). A) originated from a shallow, circular defect – see Figure 2.8 for photograph. B) originated from a deep, narrow defect arranged oblique to flow – see Figure 2.9 for photograph. 44

Figure 3.2. Schematic showing the experimental flume tank used for generating flutes. The open-channel portion of the flume is glass-walled 29.5 cm wide and 8 m long..... 46

Figure 3.3. Experimental procedure for settling kaolin beds from suspension. (A) Perspex tray (designed to fit into artificial floor of Figure 3.2) is sealed into open top box. (B) Kaolin-water mixture of desired concentration is added to the open box, and begins to settle kaolin towards the base. (C) After 48 hours the kaolin bed is fully settled and the supernatant water has collected above. (D) The supernatant water is drained from the open top box, the tray is un-sealed and the kaolin bed may be placed into the flume. 47

Figure 3.4. Use of odometer in creating kaolin beds. The kaolin – water mixture is added to the box, then subjected to a normal load that expels water and forces consolidation. 48

Figure 3.5. Particle size distribution for the sand suspended within experimental flows for corrasion. Red line shows average of three distribution measurements; all of which were in perfect agreement. 51

Figure 3.6. A plan view schematic of arrangement for bathymetric profiling of experimental beds. (A) The probe holder with 12 mounted probes performs each scan at 2 mm intervals in the X-direction. The approximate positions of readings are shown for a single scan with spacing's of 15 mm in the Y-direction. Subsequent scans are initiatied at different Y=locations, and the scans are combined to provide a resolution of 2 mm x 2 mm. (B) Detailed illustration shown for a single scan, shown as the red box in A. 52

Figure 3.7. Plan view photographs of the experimental bed of Experiment 1 showing bedform development with time (in minutes). White arrows to left of each photograph shows the 30 cm flume width. Yellow arrow (T90) shows a void formed by plastic failure of the bed. White box (T300) indicates position of time-series photographs shown in Figure 3.8 Flow is from left to right. Note photo-series starts at T10. 58

Figure 3.8. Time series of photographs for Experiment 1 showing the development of two flutes, over 300 minutes. Location of photographs with respect to the whole bed is shown in Figure 3.7, T300, white box. Photograph widths are 14 cm. Flow from left to right. White dashed line shows a fixed position, marking the development of a flute that has an internal positive relief that is eroded to a depression between T90 and T120. White arrow (T45-T300) shows the position of a developing narrow, sinuous flute. 59

Figure 3.9. Plan view photographs of the experimental bed of Experiment 2 (17), showing bedform development with time (in minutes). White arrows to left of each photograph shows the 30 cm flume width. Flow is from left to right.....60

Figure 3.10. Planform view of the experimental bed for Experiment 2 after 120 minutes (T120). Two types of flutes are observed: i) narrow (4 mm – 10 mm), deep (4 mm – 8 mm) sinuous crested flutes that have a simple U-shaped across-stream profile; shown by yellow arrows, and (ii) broad (30 mm – 50 mm) more shallow (2 mm – 9 mm) flutes that are twisted 61

Figure 3.11. Downstream cross sectional profiles of experimental flutes; Experiment 2 (17). Flow direction is left to right; profile times shown in colours to the right. See Figure 3.10 for location. (A) Downstream cross-sectional profiles. (B) Downstream

profiles with position of broad flutes (BF) indicated and the downstream migration of their leading points (LP) and deepest points (DP) labelled.....62

Figure 3.12. Across stream, time-series, cross-sectional profiles of experimental flutes. Experiment 2 (17). Flow direction is away from the reader. Profile times shown in colours to the right. See Figure 3.10 for location. 63

Figure 3.13. Plan view photographs of the experimental bed of Experiment 3 (22), showing bedform development with time (in minutes). White arrows to left of each photograph shows the 30 cm flume width. Flow is from left to right.....64

Figure 3.14. A. Downstream time-series cross sectional profiles of experimental flutes; Experiment 3 (22). Flow direction is from left to right. Profile times shown in colours to the right. B. Plan view photograph of experimental bed; Experiment 3 (22). White dashed line shows the position of the profiles in A. Yellow arrows show the position of flute marks in the early stages of formation. Flow direction is left to right. 65

Figure 3.15. Plan view photographs of the experimental bed of Experiment 4 (24) showing bedform development with time (in minutes). White arrows to left of each photograph shows the 30 cm flume width. Flow is from left to right. Note photo-series starts at T10. 68

Figure 3.16. A. Downstream time-series cross sectional profiles of shallow wavy topography on experimental bed; Experiment 4. Flow direction is from left to right; profile times shown in colours to the right. (A) Downstream cross sectional profiles. (B) Downstream profiles indicating the crests *C* and troughs *T* of waves, and track their downstream migration with time. Note erosion is experienced across the whole bed. C. Plan view photograph of experimental bed at T45; white dashed line shows the position of the profiles in A and B. 68

Figure 3.17. Plastically failed erosional mark on experimental bed after 60 minutes. Experiment 4 (seen in Figure 3.15, T60, lower right from centre of photograph). Flow is from left to right, photograph shows 12 cm width. Note the sharp downstream rim to the top of the photograph. 69

Figure 3.18. Experimental bed after 240 minutes of erosion (T240), Experiment 4. Flow is towards the reader, and the glass walls of the flume are clearly visible to the

side of the photograph. The experimental bed is 29.5 cm wide. Yellow arrows indicate deep, hollow pock-marks. Blue arrows indicate the position of two pronounced gullies aligned downstream; one in the centre of the experimental bed and one in close proximity to the flume wall (on right).....69

Figure 3.19. Plan view photograph of experimental bedforms. Experiment 4. Flow direction was from left to right. Blue dashed lines highlight flat-bottomed erosional gully with gently sinuous margins. Yellow arrows indicate position of deep (6 – 12 mm) closed potholes. 70

Figure 3.20. Summary bedform diagram for results of experimental work on erosion of mud beds. 72

Figure 3.21. Schematics to illustrate the erosional bedforms produced during experimental runs presented in this chapter. Approximate dimensions are shown; bedforms are shown in planview and cross-section across flow. For planview figures, flow direction is left to right. Schematics shown are not to scale.....73

Figure 4.1. Schematic diagram of Deptuck et al. (2008), showing the hierarchy of compensation stacking observed in composite mid-fan lobes. 81

Figure 4.2. A typical, complete thickening-upward package of the Ross Formation at Ross Bay, recording an upward trend of (i) thick mudstone interval, (ii) interbedded sand and mud deposits, (iii) thick, amalgamated sandstone. 83

Figure 4.3. Location map showing the study area and overall location of the Carboniferous Shannon Basin, western Ireland (after Pyles, 2007). Inset maps show the location of studied areas, A. Ross Bay, B. Ross Point, and C. Kilbaha Bay. Low water mean (L.W.M.) and high water mean (H.W.M) are marked respectively. 84

Figure 4.4 Cross profiles of measured sections from three studied locations. Profiles show sandstone and mudstone deposits, major erosional surfaces, stepped scours and megaflutes. A. Ross Bay (52°35'3.12"N, 9°52'36.52"W), B. Ross Point (52°35'24.75"N 9°52'42.67"W), C. Kilbaha Bay (approx. 52°34'17.46"N 9°50'50.10"W). Time periods (t1-t6) are marked on the left hand side of each figure and link to the periods identified in Figure 4.6. 87

Figure 4.5. Sedimentary log showing the sedimentology of three thickening-upward packages from the upper Ross Sandstone, Ross Bay. Palaeocurrents measured from

ripples show a consistent NE flow direction. Where the palaeocurrent is the average of multiple readings the total number of readings is provided in brackets. Lateral variation within the central coarsening-up packages is depicted in Figure 3A.....88

Figure 4.6. A six-stage sedimentary model for erosive bypass within prograding terminal lobe-elements in the Ross Formation. The schematic lobe-elements are prograding relative to the fixed-position red dashed line. Cross-sections depict interbedded sandstone (yellow) and mudstone (grey), and illustrate the deposits associated with each stage at the fixed-position red dashed line. 91

Figure 4.7. Diagram showing vertical changes in sedimentation of sand (white) and mud (black), whereby packages are defined by lobe-element surfaces. A. Diagram showing the origin of compensation cycles (CC), and how thickness trends vary across the width of the cycles; upper part after Mutti and Sonnino (1981). Under this concept of compensation cycles, each cycle is capped by horizontal muds that accumulate during periods of shutdown. Note that across the diagram, thinning- and thickening-upward trends are observed together with regions of no thickness change. Only (iv) shows exclusively thickening-upward trends. B. Diagram showing the thickening-upward (TU) trends generated by prograding lobe-elements, as presented here. Thickening-upward trends are observed across the lobe-element, and are only interrupted by localised erosion generated by lobe-element bypass surfaces, as in (iii). Average total lobe with is ~1900 m (Pyles, 2007).....100

Figure 5.1. Planform exposures of megaflutes of the Carboniferous Ross Formation; A. 'Classic' spoon-shaped parabolic megaflute that exhibits extreme symmetry, palaeoflow is from top-right of photograph; measures 6.98 m wide and 0.5 m deep (corrected for dip, metre ruler highlighted in white for scale), white arrow highlights rippled infilling sediments; location: south side of Ross Bay. B. Parabolic shaped megaflute with median ridge showing positive relief within the limits of the megaflute; measures 2.02 m wide, 2.55 m long, 0.17 m maximum depth (corrected for dip), palaeoflow is from bottom-right to top–left. Location: Ross Slab. C. Water-filled megaflute that displays a median ridge, dimensions 3.05 m wide, 6.55 m long, 0.65 m maximum depth, metre-ruler highlighted in white for scale, palaeoflow is from back left towards the reader. Location: Ross Point. 103

Figure 5.2. Location of sandstone samples taken from thickening-upwards package at Ross Bay (see Figure 4.3). Strarigraphic context of the package is provided in Chapter 4. 17 sample sites shown by black circles; samples from sites labelled 1 to 8 were also analysed using a combination of backscattered electron microscopy (BSEM), cathode luminescence (CL) and x-ray diffraction (XRD). 105

Figure 5.3. BSEM image showing the typical microstructure of the sandstones analysed from the Ross Sandstone; dark black grains are quartz and albite, pale grey grains are chlorite, bright white grains are apatite. Note that the sample has very low porosity..... 106

Figure 5.4. BSEM images illustrating kaolin from the Ross Sandstone and Brent Formation. A) Image of Ross Sandstone sample (sample 1, Figure 5.2) showing illite (central in photograph) pseudomorphed after kaolin, that has experienced shallow burial. B) Image showing detrital kaolin from a Brent Formation reservoir in the North Sea; the reservoir has only been buried to around 2200 m and a maximum temperature of 75ºC (image courtesy of Quentin Fisher). Note how the kaolin structure is comparable between both images..... 108

Figure 5.5. Backscatter scanning electron microscope (BSEM) and cathode luminescence (CL) images showing the same area of a Ross Sandstone sample (Sample 1, Figure 5.2, Table 5-1). Note the lack of syntaxial quartz overgrowth... 109

Figure 5.6. Bathymetric image showing the interior morphology of horseshoe megaflute. Contour colours represent depth as shown in left of image; data have been rotated to correct for the dip of the bed. White line outlines megaflute rim, dashed line shows position of median ridge, inferred palaeoflow is indicated. Megaflute is only partly exposed in the far lower right of the image, and the exposure to the top left of the image is heavily weathered. A photograph of this megaflute is shown in Figure 5.1C..... 110

Figure 5.7. Cross sectional exposures of megaflutes of the Ross Formation; red arrows indicate position of megaflute surface. Yellow arrows indicate position of infilling deposits onlapping onto the megaflute surface. Metre rulers highlighted in red for scale. Locations: Kilbaha Bay (top), Ross Bay, south side (bottom)..... 111

Figure 5.8. Summary of scour types observed in the Ross Formation, showing typical dimensions and cross sectional profiles. Planforms are also shown for megaflutes. 111

Figure 5.9. Partly exposed elongate megaflute of the Ross Formation, seen from two different angles and shown as a scaled planform line drawing from surveying data. Exposure shows a significant portion of the upstream megaflute and rim. Red arrow shows the most upstream part of the megaflute in each case. Location: Bridge of Ross. 112

Figure 5.10. A plot of megaflute depth verses width for 9 fully exposed surveyed megaflutes from the Ross Sandstone. Dimensions listed corrected for the dip of the bed. Regression line is also shown. 113

Figure 5.11. Mud chip conglomerate veneer within a megaflute, mud chips highlighted by red arrows. Lens cap (5cm diameter) in top-right for scale. Location: Ross Point (megaflute shown in Figure 5.1c). 114

Figure 5.12. Images of a megafluted single bedding surface of the Ross Sandstone. (A) Photograph montage showing overall exposure and individual megaflutes. Top left photograph shows the single bedding surface exposed at ~080/60°N, Jeff Peakall in upper left of top photograph for scale. Individual megaflutes are numbered and shown in detail in inset photographs; note that the megaflutes all have an overall parabolic shape with a central medial ridge. (B) LiDAR image of whole bedding surface, courtesy of StatoilHydro. Note the megaflute depressions to the centre of the bedding surface, and dune-scale bedforms in the left of the image. Location: Ross Slab (52°36'10.94"N, 9°48'39.12"W), shown in Figure 4.3 115

Figure 5.13. Photograph and detailed bathymetric image showing two partly amalgamated horseshoe-shaped megaflutes. Data have been rotated to correct for the dip of the bed; contour colours indicate megaflute depth and morphology as indicated by the inset colour bar (top right). The megaflutes are not of equal dimensions, but share similar morphologies with a parabolic shaped rim, steep lee-slope and an interior hummock. The bathymetric image has been corrected for the dip of the bed. 116

Figure 5.14. Sandstone surface with 6.98 m wide megaflute, surrounded by linguoid ripples. Dashed white line shows megaflute rim; enlargement of photograph shows

the sharp truncation of the ripples at the megaflute rim. Red arrow indicates a rippled sandstone bed that drapes the megaflute interior. The megaflute surface itself is smooth. White arrow indicates palaeoflow direction. Black bucket shows scale.... 117

Figure 5.15. Photographs and representative schematics of stepped scours from the Ross Formation. Red shaded areas illustrate the eroded stepped surface. White arrows indicate palaeoflow. Black dashed lines mark the position of broad bypass surfaces (see Chapter 4). Top location: Ross Bay. Bottom location: Ross Point. ... 118

Figure 5.16. Flat-bottomed scour from the Ross Formation. White arrows highlight a sandstone bed at the point it is truncated at the margin of a stepped scour. The white dashed line indicates the location of the flat-bottomed scour where the sandstone bed is no longer present. Scour measures ~15 m across, and is exposed in cross-section only. Yellow hammer circled for scale. Location: Ross Bay..... 119

Figure 5.17. Schematic cross sectional profiles illustrating how sandstone bed thickness controls development of erosional bedforms during constant-rate erosional events. Not to scale. 124

Figure 6.1. Location map of the four study areas along the northeast Atlantic continental margin. White rectangles show areas covered by figures as labelled. .. 128

Figure 6.2. Erosional scours in Agadir Canyon mouth, offshore northwest Morocco. (A) Regional EM12 multibeam bathymetry showing the morphology of lower Agadir Canyon. Black arrows show interpreted flow pathways. Inset figure shows TOBI 30 kHz sidescan sonar profile of the scoured region (located by the red rectangle on EM12 data). Light tones are high backscatter. White rectangle shows location of Autosub6000 imagery. (B) High-resolution Autosub6000 image and cross sectional profiles of isolated and amalgamated spoon-shaped scours. Locations of piston cores shown in Figure 6.3 are provided..... 131

Figure 6.3. Core data from Agadir Canyon mouth scours. For locations see Figure 6.2. Data include core photos, graphic logs and interpretations, and coccolith ratios from hemipelagic sediments that provide dating control (see key for species). OIS = Oxygen Isotope Stage. Core JC27-09 recovered sediments from within a large amalgamated scour, JC27-12 was taken from within an isolated scour, and JC27-11 sampled sediments adjacent to the scoured..... 133

Figure 6.4. Erosional scours in Horseshoe Valley, offshore southwest Portugal. (A) Composite image of SWIM multibeam bathymetry data showing the regional morphology of Horseshoe Valley (Zitellini et al., 2009). Note the large scours in the central valley. Black arrows show interpreted flow pathways. Red box indicates the location of Autosub6000 data. (B) High-resolution Autosub6000 image and cross-sectional profiles across a giant oval-shaped scour in Horseshoe Valley. Additional depth information (pastel colors) is derived from AUV depth profiler data. Inset images show depositional chevrons and erosional lineations adjacent to the scour. Additional depth information (pastel colors) is derived from AUV depth profiler data. Locations of cores shown in Figure 6.5 are indicated. 136

Figure 6.5. Core data from Horseshoe Valley scour. For locations see Figure 6.4. Data include core photos, graphic logs and interpretations, and coccolith ratios from hemipelagic sediments that provide dating control (see key for species). OIS = Oxygen Isotope Stage. Core JC27-24 recovered sediments from smooth seafloor upslope of the scour headwall, while core JC27-25*3 was taken from within the scour. Note the thick mud deposits within the scour, compared to the zone of dominant bypass outside the scour. 138

Figure 6.6. Erosional scours in Setúbal Canyon mouth, offshore west Portugal. (A) Regional EM120 multibeam bathymetry showing the morphology of lower Setúbal Canyon. Black arrows show interpreted flow pathways. Inset figure shows TOBI 30 kHz sidescan sonar profile of the scoured region (located by the red rectangle on EM120 data and corresponding to the Autosub6000 image). Light tones are high backscatter. (B) High-resolution Autosub6000 image of crescent-shaped scours. Location of piston core shown in Figure 6.7 is shown. (C) Cross-sectional profiles across a series of crescentic scours. Profile locations shown in (B). 139

Figure 6.7. Core data from Setúbal Canyon mouth scour. For location see Fig. 6. Data include core photo and graphic log with interpretation. Core contains a thick mass transport deposit overlain by hemipelagic drape. 140

Figure 6.8. Erosional scours on Whittard Channel margin, northern Biscay margin. (A) Regional multibeam bathymetry showing the morphology of Whittard Canyon and Channel. Note the presence of large-scale sediment waves in overbank areas beyond channel bends. Red rectangle shows location of Autosub6000 image. (B)

High-resolution Autosub6000 image of scours adjacent to Whittard Channel, in an area of fine-grained sediment waves. Location of piston core shown in Figure 6.9 is shown. Note morphological contrast between smooth channel floor and scoured channel margins and sediment wave troughs. (C) Cross-sectional profiles across isolated and amalgamated scours. Profile locations shown in (B). 141

Figure 6.9. Core data from Whittard Channel margin scours. For locations see Figure 6.8. Data include core photos and graphic logs and interpretations. Core JC27-62 recovered sediments from a sediment wave crest just north of the imaged area, while core JC27-63 was taken from within a scour. Note the thick mud deposit within the scour, which is not present in the sequence recovered from outside the scour..... 143

Figure 6.10. Summary figure showing morphology and dimensions of the four isolated and amalgamated scour types documented in this study. Examples of comparable scours from both modern and ancient systems are also listed..... 146

Figure 7.1. Summary figure showing the principal morphological features and streamlines associated with spoon-shaped and horseshoe-shaped flute forms. Position of cross-sectional profiles in planview schematics is shown by red dashed line. Streamline figures modified after Allen (1971, 1984, p. 283). 158

Figure 7.2. A summary figure showing the morphology of bedforms belonging to the class of “spoon-shaped flute forms” observed in laboratory, ancient and modern systems. Position of cross-sectional profiles in planview schematics is shown by red dashed line. Illustrative 159

Figure 7.3. A summary figure showing the morphology of bedforms belonging to the class of “horseshoe-shaped flute forms” observed in laboratory, ancient and modern systems. Position of cross-sectional profiles in planview schematics is shown by red dashed line. Illustrative photographs (laboratory and ancient system) and bathymetric images (modern system) are presented; solid white lines indicate the location of bedform rims, and flow/palaeoflow directions are indicated by white arrows. 160

Figure 7.4. A summary figure showing the morphology of bedforms belonging to the class of “gully forms” observed in laboratory, ancient and modern systems. Illustrative photographs (laboratory and ancient system) and bathymetric images (modern system) are presented; solid white lines indicate the location of fully rims, and flow/palaeoflow directions are indicated by white arrows..... 163

List of tables

Table 2-1. The experimental conditions and associated references of previous studies used to model the formation of flutes and other erosional bedforms under laboratory conditions. 11

Table 2-2. Experimental conditions for fluid stressing experiments of Allen (1969). Run durations are not provided, but Allen (1969) comments on the duration of runs being brief. 15

Table 2-3. Experimental conditions for fluid stressing experiments of Allen (1971). 16

Table 2-4. Composition of mixtures used in fluid stressing experiments of Allen (1971) 18

Table 2-5. Experimental conditions of Allen (1971) investigating corrasion of strong clay beds. 20

Table 3-1. XRD analysis of potter's clay used as experimental beds. 49

Table 3-2. Shear vane analysis of potter's clay used as experimental beds in erosion experiments 49

Table 3-3. Open channel flow velocities for the experimental slurry pump at given flow depths. The relevant pump frequencies are also shown. 50

Table 3-4. Experimental parameters for experiments investigating corrasion of firm mud beds. 55

Table 3-5. Table showing the experimental time intervals used for experiments 1 to 4, and the nature of data collected during each paused interval; either bathymetric scans obtained via Seatek probes (*scanned*), or photographed from above *(photo'd)* 56

Table 5-1. Quantitative XRD results from analysed sandstone samples from the Ross Sandstone. The total clay estimate assumes that all the illite and chlorite formed from kaolinite: 105

Table 5-2. Dimensions of surveyed megaflutes from the Carboniferous Ross Formation. Data capture method TS is Leica Total Station (TCR805). See Figure 4.3 for locations.** denotes a partial measurement where the megaflute

is not fully exposed – the full downstream length of the megaflute is therefore greater than this measured value..... 112

Table 7-1. A summary table listing the morphological forms belonging to the three classes of erosional bedforms documented in this thesis..... 157

Table 7-2. Summary table showing the dimensions of documented examples of the class of “flute forms” presented in this thesis, for the three investigation environments of laboratory (experimental; Chapter 3), outcrop (Ross Sandstone, western Ireland; Chapters 4 and 5) and modern seafloor (Chapter 6). 164

1. Thesis Rationale

1.1. Introduction

Scours in deep-sea environments occur with a variety of morphologies that are often considered as either linear features, aligned parallel to flow; or transverse features, oriented transverse to flow (Allen, 1971; Stow et al., 2009). Linear features include grooves, ridges, lineations, obstacle/comet scours, ribbon marks and furrows (Tucholke, 1982; Tuckolke et al., 1985; Flood et al., 1983; Kuijpers et al., 2002; McCave et al., 2002; Stow et al., 2002a; Masson et al., 2004; Stow et al., 2009), and are significantly longer than they are wide, ranging greatly in length from tens of metres to many kilometres. Transverse features include gravel/sand bars and sediment waves (e.g. Piper et al., 1985; Roveri, 2002; Wynn et al., 2002c), and signify the significant reworking of sediments and flow bypass rather than perhaps true scouring. Transverse features may be extremely wide, with widths and wavelengths of several hundreds of metres, and wave heights of several metres. A third, unclassified group of scours exists that are not considered to be linear or transverse; they have comparatively equal downstream and across stream dimensions, with a overall spoon-shaped geometry and are elliptical or U-shaped in planform. Examples of these scours are *flutes* and *megaflutes* (e.g. Rucklin, 1938; Dzulynski and Walton, 1963; Dzulynski, 1965; Dzulynski and Simpson, 1966b; Allen 1969a, 1971; Chapin et al., 1994; Elliott 2000a,b; Lien et al., 2003), and are discussed in more detail in the following section.

It is widely assumed that deep-sea scours develop due to erosional processes that operate at the base of density currents (Normark et al., 1970, Winn and Dott, 1979; Mutti and Normark, 1987; 1991; Shor et al., 1990; Kenyon et al., 1995; Masson et al., 1995; Vicente Bravo and Robles, 1995; Elliott, 2000a,b; Morris and Normark, 2000; Lien et al., 2003; Fildani and Normark, 2004; Fildani et al., 2006; Jobe et al., 2009; Normark et al., 2009). However the nature of such scour-forming density currents ranges widely, from cold shelf-collapses driven by sea-water density contrasts (e.g. dense shelf water cascading, Canals et al., 2006), unidirectional bottom- and tidal-currents (Flood, 1983), and turbidity currents driven by river or

shallow-shelf processes (e.g. Wynn et al., 2002a; Bonnel et al., 2005). Scours caused by turbidity currents are the best documented, with scours developed down-fan at a variety of locations, including: channel/canyon termini (Mutti and Normark, 1987; 1991; Kenyon et al., 1995; Palanques et al., 1995; Torres et al., 1997; Morris et al., 1998; Wynn et al., 2002a, Bonnel et al., 2005); on channel levee backslopes or between/along active channels (Normark et al., 1979; 2009; Shor et al., 1990; Masson et al., 1995; Kidd et al., 1998; Klaucke et al., 2004), or in linear trends adjacent to channel bends (Fildani and Normark, 2004; Fildani et al., 2006). Early discussions regarding the formative processes of scours suggested that scours were most commonly cut and infilled by the same flow (e.g. Mutti and Normark, 1987); a concept recently revisited by (Kane et al., 2009b) but immediately proven inaccurate (Kane, 2010). Recent studies suggest scour formation and development is far more complex than this, whereby scours may form due to multiple events over long periods of time (Masson et al., 1995; Vicente Bravo and Robles, 1995, Wynn et al., 2002; Fildani and Normark, 2004; Fildani et al., 2006) or be cut by single large-scale events (Shor et al., 1990; Canals et al., 2006, Normark et al., 2009).

The numerous examples of scours in the literature highlight that they form a key component of many deep-water channels and fans, however it is clear that scour types vary considerably in size and geometry, location of formation and processes of initiation and development. This thesis investigates deep-sea scours that are roughly equal in across- and downstream dimensions, which are not considered to be linear or transverse. The thesis aims to reappraise the dynamics by investigating the sedimentary context, formational mechanism and role of scours in turbidite systems by utilising three approaches, specifically: (i) creating centimetre-scale scours under known experimental conditions; (ii) studying the morphology and stratigraphy of metre-scale examples in outcrop, and (iii) imaging and sampling modern seafloor scours that range from many hundreds to thousands of metres in width and length.

1.2. Scours that are between ‘linear’ and ‘transverse’

Scours that occur between the end-members of *linear* and *transverse* are herein considered in three broad categories: 1. small, centimetre-scale flutes; 2. metre-scale megaflutes, and; 3. large-scale scours that reach many hundreds to thousands of metres in width and length. Flutes are best observed in outcrop (e.g. Dzulynski, 1963, 2001), and their relatively small size has allowed them to be mechanically

studied and experimentally produced in laboratory environments (e.g. Rucklin, 1938; Dzulynski and Walton, 1963; Dzulynski, 1965; Dzulynski and Simpson, 1966b; Allen 1969a, 1971). Megaflutes are also observed in outcrop; with arguably the best planform examples exposed in the Carboniferous Ross Sandstone of western Ireland (Chapin et al., 1994; Elliott 2000a,b; Lien et al., 2003), the Albian Black Flysch of northern Spain (Vicente Bravo and Robles, 1995), and the Cerro Toro Formation of southern Chile (Winn and Dott, 1979; Jobe et al., 2009). The terms 'flute' and 'megaflute' have also been applied to scours in some modern seafloor environments (e.g. Shor et al., 1990), but this is relatively uncommon. Megaflutes in outcrop provide excellent insight into the nature of scoured substrates and infilling sediments (e.g. the multi-episodic scour-and-fill geometries visible in sandstones of the Albian Black Flysch; Vicente Bravo and Robles, 1995), however, limited exposure in outcrop can make precise palaeoenvironmental interpretation of scours challenging (e.g. the conflicting interpretations of megaflutes in the Carboniferous Ross Sandstone; Chapin et al., 1994; Elliott 2000a,b; Lien et al., 2003). Large-scale scours are exclusively documented in modern seafloor environments via deep-towed sidescan sonar and multibeam bathymetric images (see Appendix A). Importantly, many channels and large-scale scours have a considerable overlap in size range (Morris and Normark, 2000), and it is widely assumed that large-scale scours observed in outcrop are often misidentified as channels (e.g. Mutti and Normark, 1987; Morris and Normark, 2000). In addition, it has recently been shown that megaflute-scale scours can go undetected in side-scan sonar and multibeam studies of modern systems (Normark et al., 2009). Such incorrect or incomplete observations are of considerable importance for several reasons: 1. they create mis-interpretations for the processes operating within gravity-current systems; 2. the potential for large, voluminous, highly erosive or catastrophic flows remains undetected and may present geo-hazards to submarine installations or via the generation of tsunamis; 3. they may give rise to an erroneous view of the lateral connectivity of the deposits (Normark et al., 2009). Furthermore, although the variance in scales of erosional bedforms has long been acknowledged (Mutti and Normark, 1987; Normark and Piper, 1991; Morris and Normark, 2000), a single study has never been dedicated to erosonal bedforms across all scales. It therefore remains unclear:

1. if or how flutes, megaflutes and large-scale scours relate to one another in terms of morphology and generational process;
2. whether there are three distinct size groups, or whether this is an artifact of how they are documented.

This thesis focuses on addressing these issues. The work incorporates modern and ancient systems analysis, together with physical modelling of flute-development under experimental conditions. The first part of this thesis builds on the original experimental work on flutes of the 1930s – 1970s (Rucklin, 1938; Dzulynski and Sanders, 1962; Dzulynski and Walton, 1963; Dzulynski and Simpson, 1966; Allen, 1969a,b, 1971). Flute development is investigated in time-series, whereby scouring experiments at different erosional velocities are paused at 15 or 30 minutes and high-resolution bed morphology data are collected. The results of these experiments have implications for the development and morphology of flutes and other centimetre-scale erosional bedforms, and are discussed with reference to the development of centimetre-scale erosional bedforms at the base of turbidity currents. The second part of this thesis investigates megaflutes of the Carboniferous Ross Sandstone, western Ireland; firstly documenting the occurrence of megaflutes in the context of sedimentary models for the Ross Sandstone, and secondly reassessing the frequency, size, morphology and sedimentology of megaflutes and other erosional features. This investigation of the Ross Sandstone culminates in a new model for the development of megaflutes at this scale, and documents bed-scale lobe-element dynamics in the Ross Sandstone for the first time. The third part of this thesis comprises a pioneering high-resolution study of large-scale scours within four deep-water turbidite systems of the north-east Atlantic margin. The scours were sampled and imaged in high-resolution, at a scale usually only obtained in outcrop-studies, using a fully Autonomous Underwater Vehicle (AUV, or unmanned-submarine); this use of an AUV is the first of its kind in a deep-water environment. The results are discussed with reference to the erosional processes, morphology and evolution of large-scale deep-sea scours, and help to bridge the size gap between most metre-scale erosional scours documented in outcrop (i.e. megaflutes), and those imaged on the modern seafloor. Finally, the observations and conclusions gained from each area of research in the thesis are synthesised, and the range of erosional bedforms across the variety of environments are discussed.

It should be noted that the terms *flute* and *megaflute* have been applied to some subglacially developed scours (e.g. Boulton, 1987; Rose, 1987; Clark, 1994; Beaman and Harris, 2003; Todd et al., 2007), whereby the scours are generated by lateral pressures and stresses operating at the glacier-substrate interface (Gravenor and Meneley, 1958; Dreimanis, 1999). Despite the mutual terminology, the formative processes of subglacially eroded bedforms are very different to the submarine-formed bedforms that are generated by turbidity currents in the deep-sea. For this reason, subglacially eroded erosional bedforms are omitted from this study.

1.3. Thesis objectives

This thesis utilises a multidisciplinary approach to understand the formation, dynamics, sedimentology and morphology of the subset of scours described above. To achieve this, the following techniques were applied: 1. a series of laboratory experiments; 2. a detailed bed-scale field investigation of the Carboniferous Ross Sandstone (southwest Ireland); 3. a seabed investigation of scours along the northeast Atlantic continental margin seafloor. There are three key aspects to this thesis:

1. Investigating flutes under experimental conditions. Specifically:

a. whether it is possible to make flutes experimentally via fluid stressing or corrasion;
b. how flutes and other erosional bedforms develop with time,

2. A bed-scale investigation of the occurrence, morphology and sedimentological context of megaflutes in the Carboniferous Ross Sandstone, southwest Ireland, to establish:

a. the straigraphic occurrence of megaflutes in the Ross Sandstone;
b. if/how the new data vary from existing data in the literature, and how any differences may effect the way megaflutes are interpreted;
c. the significance of the megaflutes in relation to the wider stratigraphic framework of the Ross Sandstone, including their relation to packages of thickening-upward strata;
d. the morphology and sedimentology of megaflutes in the Ross Sandstone;
e. if the development of megaflutes is controlled by substrate type;

3. High resolution imaging, and precisely located sampling of scours and their surrounding sediments at four locations along the northeast Atlantic continental margin, with the pioneering use of AUV mounted multibeam. Data collected were used to ascertain:

a. the life cycle of scouring: their origin, ongoing processes, and cause for cessation;
b. the range in scales and precise morphology of scours on the modern sea floor;
c. whether the morphological types of scours may be classified;
d. the nature of the infilling and surrounding sediments of modern sea floor scours, and if/how they relate to one another;
e. the flow processes that operate within scours and in their surrounding areas
f. if scours are associated with a particular sedimentological environment;
g. whether regions of scour are linked to positions of hydraulic jumps;
h. the effectiveness of AUV mounted multibeam technology to image scours on the modern seafloor.

1.4. Thesis structure

Chapter 2 - "Scouring: processes, scales and morphologies" discusses the literature associated with the key aspects of the thesis, focusing upon erosion within deep-sea systems as observed in both modern and ancient environments, and the experimental simulation of erosional systems.

Chapter 3 – "Experimental simulations of erosional bedforms in muds" presents the experimental setup and results of experimentally generated erosional bedforms, and discusses the variety of generated bedforms.

Chapter 4 – "Architecture and flow processes in deep-sea lobe elements: the Carboniferous Ross Sandstone, western Ireland" provides the results of an outcrop based field investigation into the context of megaflutes and other erosional features with regard to the stratigraphic framework of the Ross Sandstone. This chapter discusses existing models for the development of megaflutes in the Ross Sandstone, and based upon new data, proposes a new sedimentary model for erosive bypass

within lobe-elements. The chapter also discusses this model as a mechanism for repeated thickening-upward distributions.

Chapter 5 – "The morphology, occurrence and genesis of megaflutes: the Carboniferous Ross Sandstone, western Ireland" presents further data in the field area of Chapter 4. These data are aimed specifically at investigating the morphology, occurrence and sedimentology of megaflutes. Survey and LiDAR data are presented that show the precise morphology and dimensions of a number of megaflutes. Additionally, XRD and SEM analysis of megaflute-hosting sandstones are presented and their implications for flow emplacement dynamics are discussed.

Chapter 6 – "High-resolution imaging of deep-water erosional scours along the northeast Atlantic margin" presents high-resolution images and sedimentological data from four deep-water erosional systems located along the northeast Atlantic margin.

Chapter 7 – "Thesis synthesis" summarises and integrates the laboratory, field and modern seafloor data presented in Chapters 3 – 6, and discusses how these findings may be used to further our generic understanding of flutes, megaflutes and large-scale scours. Finally, the relationship between these bedforms and the implications for the range of bedforms documented is discussed.

2. Scouring: scales, processes & morphologies

2.1. Introduction

Investigations of scours from deep-sea environments range include studies of scours in outcrop, in subsurface datasets, and in modern deep-sea environments. Results suggest that scours develop due to erosional processes that operate at the base of density currents (e.g. Rucklin 1938, Dzulynski and Sanders, 1962; Dzulynski, 1965; Allen, 1969; 1971; Normark et al., 1970; Pett and Walker, 1971a,b; Normark et al., 1979; Winn and Dott, 1979; Mutti and Normark, 1987; 1991; Shor et al., 1990; Kenyon et al., 1995; Masson et al., 1995; Pickering et al., 1995; Vicente Bravo and Robes, 1995; Kidd et al., 1998; Elliott, 2000a,b; Morris and Normark, 2000; Wynn et al., 2002a; Fildani and Normark, 2004; Klaucke et al., 2004; Canals et al., 2006; Fildani et al., 2006; Jobe et al., 2009; Normark et al., 2009). This chapter focuses upon these investigations to provide the reader with a background understanding of previous scour-related investigations.

2.2. Scours: scales of analysis

Small centimentre-scale scours and flutes were first recognized by Fuchs (1895), and were experimentally reproduced and subsequently documented in outcrop in the Lower Muschelkalk (Saarland, SW Germany) by Rucklin (1938). Later workers investigated their formation extensively using laboratory setups with mixed success but largely agreed that the bedforms were dependent upon the properties of the flows that formed them (e.g. Dzulynski and Walton, 1963; Dzulynski, 1965; Dzulynski and Simpson 1966b; Allen, 1968a,b, 1969, 1971, 1984). Flutes were included as a part of an ideal turbidite sequence, at the base of Bouma horizon *Ta,* which linked their development to the occurrence of dispersed high-density suspensions of turbidity currents (Bouma, 1962; Middleton, 1966a,b,c).

Research on significantly larger deep-sea scours began in the 1970s, when giant flute-shaped depressions over 500 m wide and 15 m deep were recognized during pioneering studies on Navy Fan offshore California (e.g. Normark, 1970; Normark et al., 1979). Subsequent investigations of modern and subsurface deep-sea systems have yielded an extensive catalogue of metre to kilometre scale scours in a

variety of morphologies, including (but not exclusive to): spoon shaped scours (Laurentian Fan, Shor et al., 1990; Agadir canyon mouth, Wynn et al., 2002b); chevron shaped scours (e.g. Lisbon canyon mouth, Wynn et al., 2002b; Lastras et al.. 2009); and, furrows grooves and ridges (e.g. Gulf of Cadiz, Stow et al., 2002a; Gulf of Lions margin, Canals et al., 2006). Around the time of Normark's (1970, 1979) pioneering modern seafloor observations, much smaller scours up to 1.5 m deep were documented in Upper Cretaceous submarine fan deposits of the Cerro Toro Formation (Magallanes Basin), southern Chile (Winn and Dott, 1979). Similarly sized metre-scale scours were later documented in outcrops of the Albian Black Flysch (northern Spain, Vicente Bravo and Robles, 1995) and the Carboniferous Ross Formation (western Ireland, Chapin et al., 1994; Elliott, 2000a,b; Lien et al., 2003).

These examples illustrate the major differences in the scale of feature that can be recognized in experimental, ancient and modern settings, and highlights the restrictive nature of the investigative methods currently utilised in each environment.

2.3. Experimental studies of centimetre-scale flutes

Experimental simulations of erosional bedforms began in the early 1910s, when the formation of 'conical flute casts' was said to be highly debated (Rucklin, 1938). At the time, the formative processes of flutes and flute casts were unclear; authors speculated about their way-up and whether they were formed: (i) via outflow from overlying beds (e.g. Fuchs, 1985); (ii) as remnant structures deposited during the passage of an otherwise non-depositional flow (in the case of the *flute casts* being of positive relief, rather than voids) Haentzschel (1935)); or (iii) if they were formed via the infilling of erosional hollows (Guerich, 1933; Freudenberg, 1933; Kraus, 1935).

Rucklin (1938) drew on observations from the Lower Muschelkalk (Saarland, SW Germany) and concluded that conical flute casts were generated by the infilling of erosional hollows. This was principally based upon three key observations, regarding (i) flute cast morphology (simple, corkscrew or flat), (ii) the regular distribution of flute casts (parallel-, pinnate-, and fan-shaped), and (iii) the consistent occurrence of flutes upon the base of un-faulted and un-rotated beds. Rucklin (1938) experimented with flows of water acting to erode cohesive clay and silty-clay beds, and hypothesized that the development of flutes and their resulting morphologies

were determined by current eddying, despite the lack of understanding with regard to the character of the erosive currents. Early experiments with a very fine-grained cohesive mud substrate (78% with average grain size <10 μ) failed to yield bedforms; Rucklin attributed this to the bed absorbing too much water and becoming unstable. However, subsequent experiments with a substrate of 5.8% clay grains (4 – 10 μ) and 94.2% coarse grains (of quartz grains 20 – 80 μ and mica 50 – 200 μ) yielded bedforms. Images of Rucklin's experimentally produced bedforms show topography (Figure 2.1), but individual flutes are hard to identify and it is unclear whether true flutes were generated. Allen (1971) suggested Rucklin's (1938) experimental bedforms were simply relief features on the bed, not true flutes; but recognized from these experiments that fluid stressing alone (i.e. without suspended sediments) is sufficient to sculpt and erode a substrate (Allen, 1969).

Subsequent experiments by Allen (1968a,b, 1969, 1971) and Dzulynski and co-workers (Dzulynski and Walton, 1963; Dzulynski, 1965; Dzulynski and Simpson 1966) were conducted using a combination of different turbulent flows and substrates, including flows of plaster of Paris, plain water and sandy water, over substrates formed by plaster of Paris, china clay settled from suspension, and hand-moulded modelling clay: see Table 2-1 for experimental conditions and references. Other experiments aimed at investigating cave scallops and the erosion of limestone bedrock via dissolution or mass transfer were conducted using plain water flows over plaster of Paris beds (Allen, 1971). Allen (1971) conducted 18 experiments in this way, however the results are omitted here because they do not directly model flute-forming processes, but mass-transfer or dissolution processes.

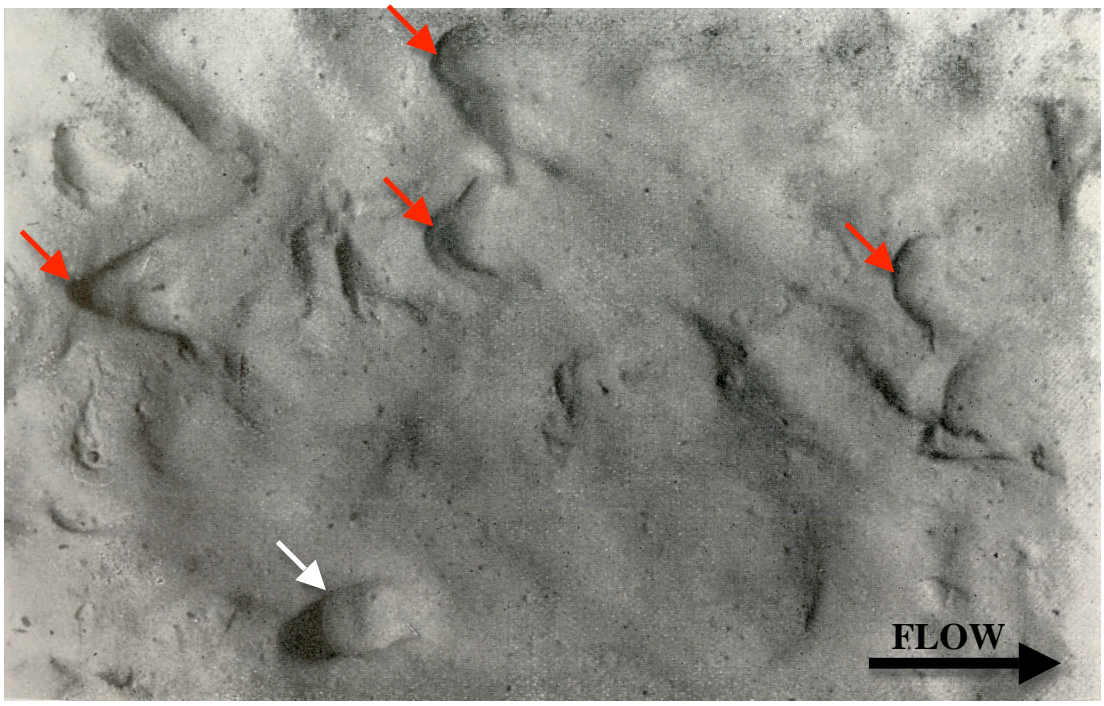

Figure 2.1. Photograph of experimentally generated flute casts of Rucklin (1938), described as *conical flute casts*. Flute casts shown by red arrows, white arrow shows blocky degassing structure. Current direction from left to right.

	Plain Water Flows	**Plaster of Paris Slurry Flows**	**Water flows carrying suspended sand particles**
Plaster of Paris substrate	Allen (1971, 1973, 1975)	No experiments	No experiments
Settled substrates of china clay	Rucklin (1938)	Dzulynski and Walton (1963) Dzulynski (1965) Dzulynski and Simpson (1966b)	No experiments
Hand shaped substrates of modelling clay	No experiments	No experiments	Allen (1971)

Table 2-1. The experimental conditions and associated references of previous studies used to model the formation of flutes and other erosional bedforms under laboratory conditions.

2.3.1. Terminology

Dzulynski and Sanders (1962) distinguished the difference between *scour marks*, which develop via the impingement of (usually sediment-laden) eddies on mud beds, and *tool marks* that are created when objects being carried within a turbulent flow strike the muddy substrate. Dzulynski and Sanders (1962) also clarified the usage of

the terms mark and cast, whereby *marks* are the original features that developed upon the beds, and *casts* are impressions of marks and develop on the base of the overlying bed.

2.3.2. Experiments of erosion by turbulent plaster of Paris flows

Experiments using turbulent flows of plaster of Paris were conducted over mud beds settled from suspension over short (unspecified) and longer (1-3 hours) periods, that aimed to create weak and firm substrates respectively (Dzulynski and Walton, 1963; Dzulynski, 1965). The experiments were conducted in small experimental tanks, but the exact dimensions or figures showing the apparatus are not provided. Experiments conducted over weak substrates formed flutes around the area of discharge, and longitudinal ridges and furrows further downstream. This led to the characterization of zones of bedforms within experimental turbidity currents (Dzulynski and Walton, 1963). The zones are potentially controlled by the distance of the deposits from the discharge, and were arranged from distal to proximal as follows: 1. zone of flute marks; 2. zone of longitudinal furrows (not always present); 3. zone of longitudinal and dendritic ridges; 4. zone of smooth surfaces (not always present). Experiments conducted using mud beds where settling occurred over longer periods (1-3 hours) were subject to three different types of turbulent plaster of Paris flow: (i) slow, dense currents (1:1 water to mixture of plaster of Paris) that formed pronounced, deep, irregular load structures, but no flutes (Figure 2.2a); (ii) rapid, less concentrated currents of ~10 cm/s that formed long, flat flutes and longitudinal ridges and furrows (no images presented); (iii) very dilute currents (3:1) that developed long, flat, slightly flaring flute marks (no images presented). Similar experiments were conducted using fish bones and hardened plaster of Paris fragments within the flow, to act as tools (Dzulynski and Walton, 1963). For these experiments the mud beds were allowed to settle for longer than one day, and the currents were very dilute (3:1 by vol.). Results showed the proximal zone (upstream) to be dominated by flutes, and tool marks developed further downstream, outside the zone of greatest turbulence (Figure 2.2b). Dzulynski (1965) suggested the development of these flutes was controlled by turbulence associated with the passage of tools close to the bottom of the flow. However the features identified as flutes by Dzulynski and his co-workers (Dzulynski and Walton, 1963; Dzulynski, 1965; Dzulynski and Simpson (1966) are often difficult to identify as true flutes, owing to weakly defined rims,

shallow profiles, and the close proximity to other erosional features. Dzulynski (1996) later critiqued these early experiments, commenting that without tools in the flow, the experiments failed to yield flute marks. Allen (1971) also questioned the validity of the flutes created by Dzulynski and his co-workers, on the basis that flute development could not be observed and could therefore have been deformational in origin. Photographic evidence of the flutes created by Dzulynski and his coworkers (Dzulynski and Walton, 1963; Dzulynski, 1965; Dzulynski and Simpson, 1966) is unconvincing, and implies the experimental flows produced tool marks and loading bedforms, rather than flutes (see Figure 2.2). Owing to these factors, together with Dzulynski's (1996) own dismissal of the flute-like nature of these bedforms, the bedforms created by Dzulynski and his coworkers are herein considered to have not been true flutes.

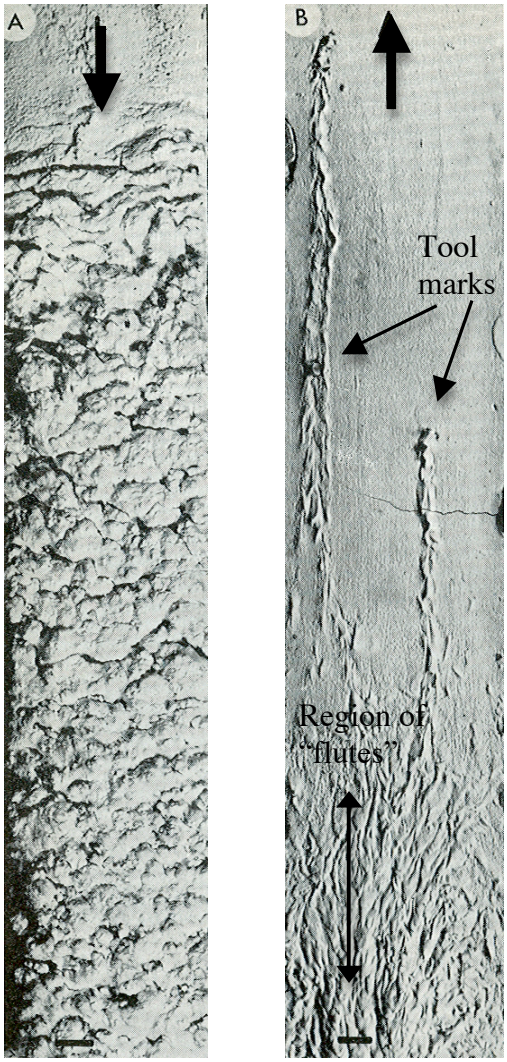

Figure 2.2. Photographs of scour marks on soft mud surfaces settled from suspension, eroded by turbulent flows of plaster of Paris (Dzulynki and Walton 1963). Flow direction as indicated by arrows.

A. Bedforms created by a high-density current. The surface is dominated by deformation marks and no flutes are present.

B. Bedforms created by rapid, very dilute (3:1 by vol.) currents of plaster of Paris, loaded with tools (fish vertebrae and hardened plaster of Paris pieces). Dzulynki and Walton (1963) claim the photograph shows "flutes" in the upstream region (lower photograph) that pass downstream into tools marks (upper photograph); however the validity of these flutes is called into question.

2.3.3. Experiments of erosion by turbulent plain water flows

Rucklin (1938) first experimented with eroding mud beds with flows of plain water (see Page 9), and created erosional topographic features within silty mud beds. Allen (1969, 1971) continued with these experiments, investigating the process of fluid stressing with a number of variables, including: substrate strength, flow velocity, flow depth and flow duration, using relatively weak mud beds that settled from suspension over 3 days. The experiments were conducted in a non-recirculating flume, into which the experimental beds were settled and subsequently eroded (Figure 2.3).

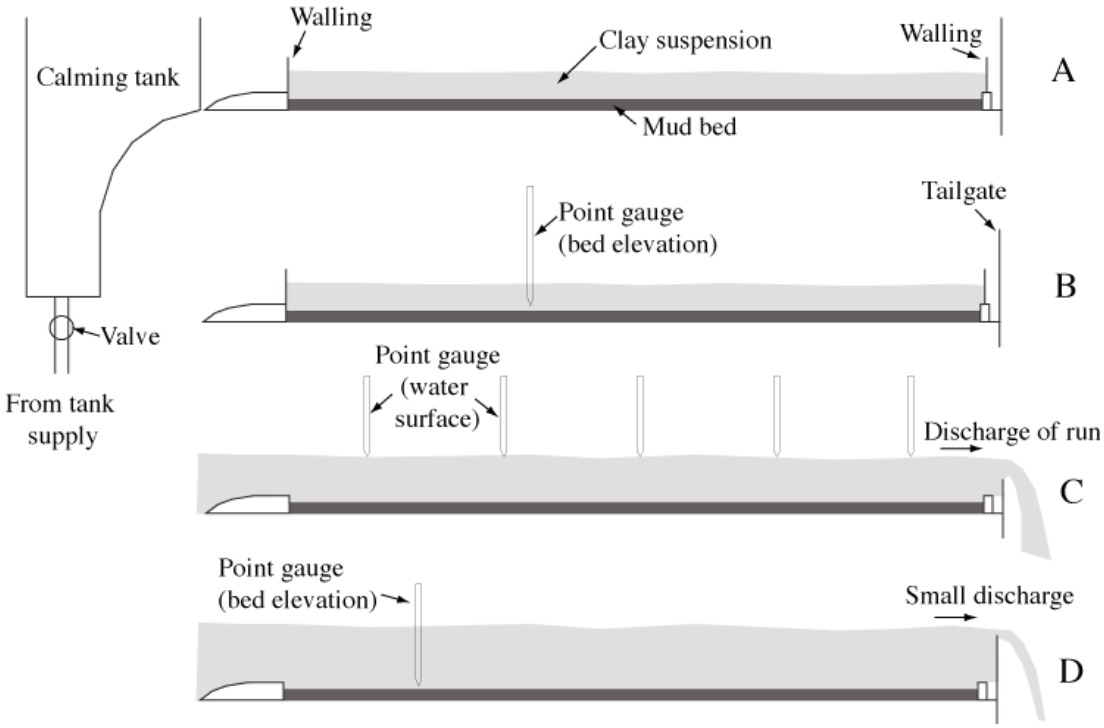

Figure 2.3. Schematic to show the apparatus used in fluid stressing experiments of Allen (1971). Flume measures 3.66 m long, 30.5 cm deep, 30 cm wide. A. Mud bed is settled from suspension within walled-off section over 3 days. B. Bed elevation is measured across the bed to ensure 6-8cm thickness. C. During run, the water surface level is set at a desired level. D. Following the experiment the bed elevation is measured at 5cm intervals, and an impression of the bed surface is taken using a plaster of Paris mixture.

Allen (1969, 1971) conducted and published two sets of experiments on *weakly cohesive* beds using this apparatus; the experimental conditions of this work are summarized in Table 2-2 and Table 2-3. Allen (1969) experimented on a consistent bed type, and presented three sets of results. These are summarized: 1. At high flow velocities (50 – 140 cm/s), 2. Long-term trend during high velocity flows, 3. At low flow velocities (20 – 50 cm/s), and 4. Long-term trend during low velocity flows.

Run	Mean low velocity cm/sec	Mean flow depth /cm	Re	Bed water concent /wt. %	Erosion rate cm/sec	Principal erosional structure
1	20.6	6.1	11000	53 – 59%	0.0000085	rectilinear grooves
2	29.8	5.8	14000	53 – 59%	0.000026	rectilinear grooves
3	32.4	5.4	17000	53 – 59%	0.000018	rectilinear grooves
4	37.8	4.1	12000	53 – 59%	0.000019	meandering grooves
5	46.7	5.3	20000	53 – 59%	0.0002	meandering grooves
6	59.8	7.2	39000	53 – 59%	0.0084	flute marks
7	84.4	3.3	42000	53 – 59%	0.011	flute marks
8	138	3.1	37000	53 – 59%	0.025	Transverse erosional markings

Table 2-2. Experimental conditions for fluid stressing experiments of Allen (1969). Run durations are not provided, but Allen (1969) comments on the duration of runs being brief.

(1) At high flow velocities (50 – 140 cm/s) a topmost 'soupy' layer was quickly washed away, before strong eddies plastically deformed the clay into ridges arranged roughly parallel to flow (1 – 3 cm long) (Figure 2.4a). (2) The long-term trend during these high velocity runs was for erosion to occur more rapidly in some places compared to others, resulting in features of substantial relief (termed *polygonal depressions*) developing in zones of accelerated areas of erosion (Figure 2.4b). (3) At low flow velocities (20 – 50 cm/s), fluid stressing eroded the mud bed flake-by-flake, principally in the topmost layer, to develop grooves and ridges (Figure 2.4c). (4) Later, during these same experiments, loose clay fragments collected in the lower parts of the ridges and became entrained in trapped vortices that further eroded the base of the grooves and ridges (Figure 2.4c).

Run	Mean flow velocity cm/sec	Mean flow depth cm	Re	Bed water content /wt. %	Duration of run /s	Mean bed erosion velocity cm/sec
43	58.6	3.45	29600	70.6	33.2	0.042
44	71.8	4	40900	70.1	36.6	0.048
45	79.3	4.6	50300	70.1	40.9	0.054
46	65.2	6.6	51300	70.8	49.2	0.034
47	53.4	8.05	53200	70.8	56.2	0.019
48	49.8	8.65	46900	71.4	116	0.001
49	47.3	9.1	49700	70.8	210	0.006
50	43.9	9.8	47100	70.4	172	0.003
51	39.1	11	50000	70.6	200	0.0021
52	33.6	12.8	42100	70.5	183	0.00006
53	57.4	1.95	17900	64.8	44.4	0.041
54	34.7	2.65	13400	65	28.9	0.019
55	54.7	2.75	22900	65	36.3	0.036
56	53.6	3.42	26200	64.7	46.7	0.023
57	73.7	3.88	40200	64.6	40.9	0.038
58	49.3	4.1	28600	64.7	74.2	0.012
59	69.1	5.28	48700	64.2	22.6	0.073
60	55.2	7.79	52600	64.7	39.8	0.033
61	40.8	10.5	48200	64.3	252	0.0023
62	31.6	13.6	36700	63.8	2920	0.000058

Table 2-3. Experimental conditions for fluid stressing experiments of Allen (1971).

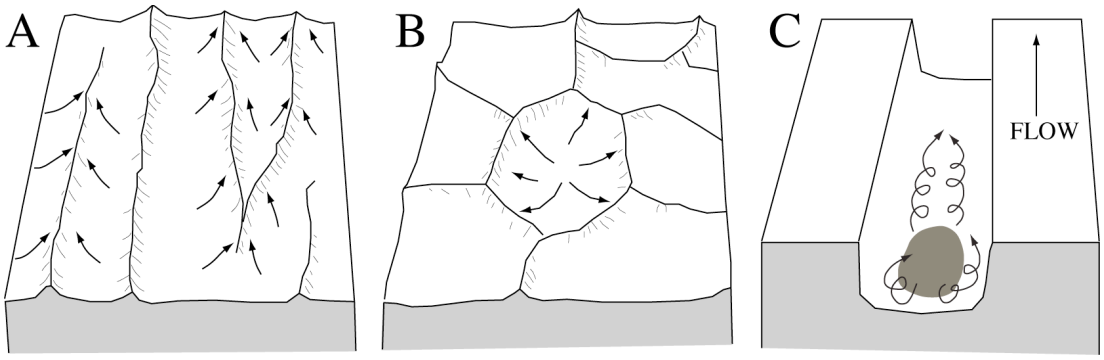

Figure 2.4. Schematics showing the primary modes of small-scale fluid-stressing erosion in mud-beds in relation to local eddying patterns; of Allen (1969). A. Morphology of longitudinal ridges and V-shaped marks formed during high velocity flows (50 – 140 cm/s). B. Morphology of polygonal depressions formed as long-term trend during high-velocity flows; C. Grooves formed during low velocity flows (20 – 50 cm/s); mud flakes became held captive within the grooves during long runs.

Bedforms generated during high-velocity runs were divided into three morphologically intergrading types (Allen, 1969): (i) heel-shaped flutes that are symmetrical, and longer than they are wide; (ii) symmetrical flutes that are wider than long; (iii) asymmetrical flutes that are longer than wide, and skewed to the mean flow direction. Allen (1969) refers the reader to Figure 2.5 to illustrate these three types; however the features are unconvincing and only two 'flute-like' features can be easily identified (see red arrow). Instead the photographs illustrate the presence of numerous mud ripples that are comparable in morphology to Allen's (1984) own image of mud ripples (Figure 2.6). This suggests that during fluid stressing experiments, Allen (1969) generated mud ripples in addition to flute marks. Furthermore, these photographs are taken from the same experimental bed during the same experimental run, suggesting the different features are coeval.

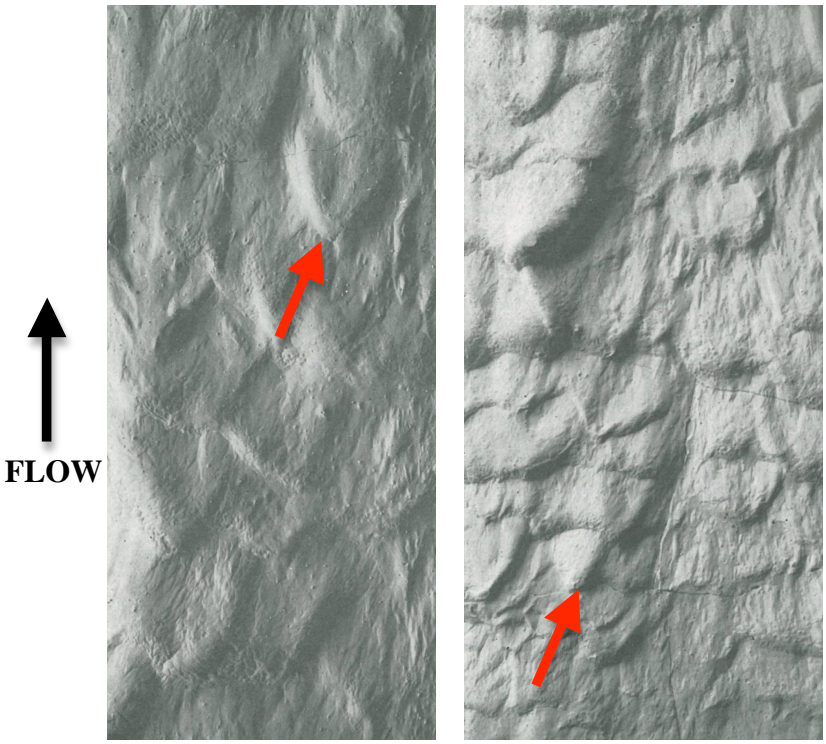

Figure 2.5. Photographs from the same weakly cohesive fluid-stressing experimental bed, used by Allen (1969) to illustrate three morphologically intergrading flute types: (i) heel-shaped flutes that are symmetrical, and longer than they are wide; (ii) symmetrical flutes that are wider than long; and (iii) asymmetrical flutes that are longer than wide, and skewed to the mean flow direction. Widths of photographs are 15.5 cm (left) and 30.0 cm (right); flow direction is from bottom to top. Note, the three morphological types are hard to identify. The most convincing flute forms are illustrated with the red arrow.

Figure 2.6. Field example of mud ripples preserved on the sole of a sandstone bed (Allen, 1984, p. 260). Ripple wavelength is ~0.04 cm, palaeoflow direction is from bottom to top. Note their similarity of form to the features in Figure 2.5. From Kronso Beds (Oligocene), Wernejowka, Polish Carpathians.

Later fluid stressing experiments by Allen (1971) produced wave-like erosional features in at least 17 different experiments, using two different bed mixtures to create two different substrate strengths (Table 2-4). Beds produced by mixture 1 were stronger than those made by mixture 2, but had the higher water content. Allen (1971) identified the features as regularly spaced, conjugate, transverse ridges and hollows that are commonly many times wider than they are long. Allen (1971) noticed their similarity to long-crested sand ripples, and observed that separated flows in the lee of the features were slow moving roller vortices. Importantly, these fluid-stressing experiments did not yield flutes.

	Mixture 1	**Mixture 2**
China Clay (median fall diameter 4μ)	19.5%	20%
Water	80%	80%
Bentonite	0.5%	none

Table 2-4. Composition of mixtures used in fluid stressing experiments of Allen (1971)

2.3.4. Experiments of erosion by water with suspended sand

To investigate the erosion of firmer beds, Allen (1971) conducted experiments that eroded firm clay beds with flows charged with sand particles. These experiments modelled the physical process of *corrasion* whereby suspended particles erode a surface via sand-blasting. The mud beds used in these experiments were made of artist's modelling clay in shop-bought condition (a kaolin-based plastic clay that could be shaped by hand) and the abrasive particles added to the turbulent flow were dry quartz sand discharged to obtain a concentration of 0.3 - 0.4 g/l. The apparatus used is shown in Figure 2.7 and indicates the experimental bed is held within a closed pipe; this suggests the experiments were conducted in closed-channel flow conditions, although this is not mentioned in the experimental setup description (Allen, 1971).

These experiments form what is arguably the best example of the experimental generation of flutes in the literature. Allen (1971) conducted 13 corrasion experiments (Table 2-5), and placed a defect on the experimental bed (pressed into the clay surface) prior to each run, which aided the development and positioning of flutes.

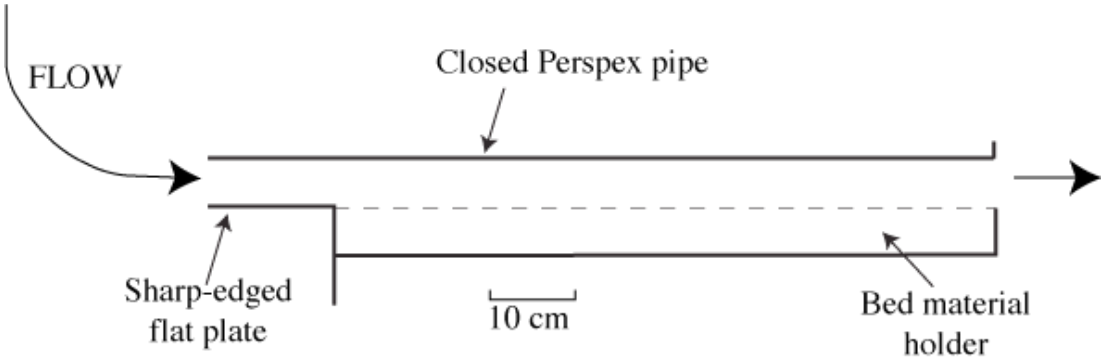

Figure 2.7. Modified figure showing the apparatus used in corrasion experiments by Allen (1971) eroding a strong clay bed. Shop-bought modelling clay was hand moulded into the bed material holder, which is set into a Perspex pipe. Abrasive flows of water and sand were fed into the pipe from elevated tanks at controlled velocities, and the sand concentration monitored.

Run No.	Mean Flow Velocity cm/sec	Conc^{n} of sand g/l	Duration of run /s	Duration /mins	Character of initial defect	Defect length /cm	Defect amplitude /cm
30	97	0.33	2100	35.0	circular pit	0.86	0.26
31	148	0.3	2790	46.5	circular pit	0.96	0.3
32	148	0.34	1640	27.3	circular pit	1.18	0.28
33	148	0.34	1640	27.3	circular pit	1.18	0.38
34	148	0.34	1640	27.3	circular pit	1.18	0.44
35	148	0.3	3050	50.8	circular pit	1.22	0.54
36	148	0.44	2380	39.7	circular pit	2.51	0.46
37	148	0.44	2380	39.7	circular pit	2.7	0.72
38	148	0.4	2360	39.3	groove (102° to flow)	1.6	0.44
39	148	0.4	2360	39.3	groove (150° to flow)	2.7	0.48
40	148	0.4	2360	39.3	groove (150° to flow)	2.82	0.38
41	148	0.32	4450	74.2	circular pit	1.54	0.24
42	148	0.4	4460	74.3	groove (150° to flow)	3.98	0.36

Table 2-5. Experimental conditions of Allen (1971) investigating corrasion of strong clay beds.

Two of these flute-generating experiments are described in detail and presented as photographs (Figure 2.8, Figure 2.9) (Allen, 1971); one originated with a shallow, circular, flat based initial defect, and the other with a deep, narrow initial defect aligned oblique to flow (Runs 41 and 42 respectively, Table 2-5). Both defects grew rapidly following the initiation of the run, the circular defect developed into a parabolic flute with a rounded, symmetric form (Figure 2.8), and the oblique defect became an asymmetric flute with an elongate and deepened form (Figure 2.9). Allen (1971) documented that the parabolic flute developed via one captive vortex that later developed into a complex of vortices that led to the development of furrows in the lateral region of the flute; in contrast the asymmetric flute generated a single, powerful vortex. Further results showed: (i) circular defects generally developed scours with lateral furrows and ridges, but rarely developed median ridges (median

ridges never developed in larger or younger scours); (ii) defects arranged oblique to flow resulted in flaring asymmetric scours; (iii) elongate defects arranged parallel to flow became spindle-shaped with lateral and distal secondary furrows. Allen (1971, 1984) illustrates these, and other flute assemblages and morphologies according to their planform appearance (Figure 2.10).

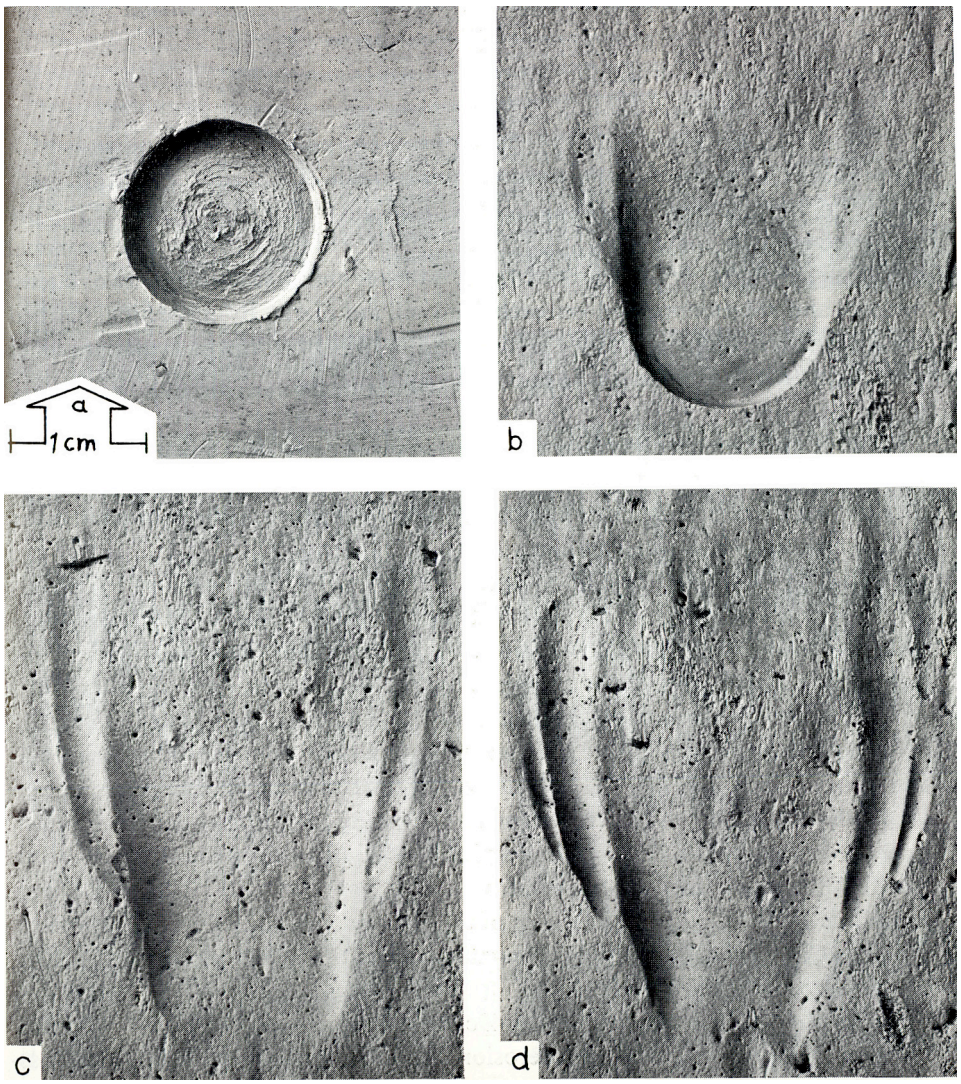

Figure 2.8. The growth of an experimentally produced flute via corrasion of a cohesive mud bed, by Allen (1971); his experimental run 41. The initial defect was a flat-bottomed, shallow and circular. Time-series times are approximate: a. t = 0; b. 19.8 minutes; c. 42.8 minutes; d. 74.1 minutes. 1 cm scale is indicated in a. Flow direction is from bottom to top.

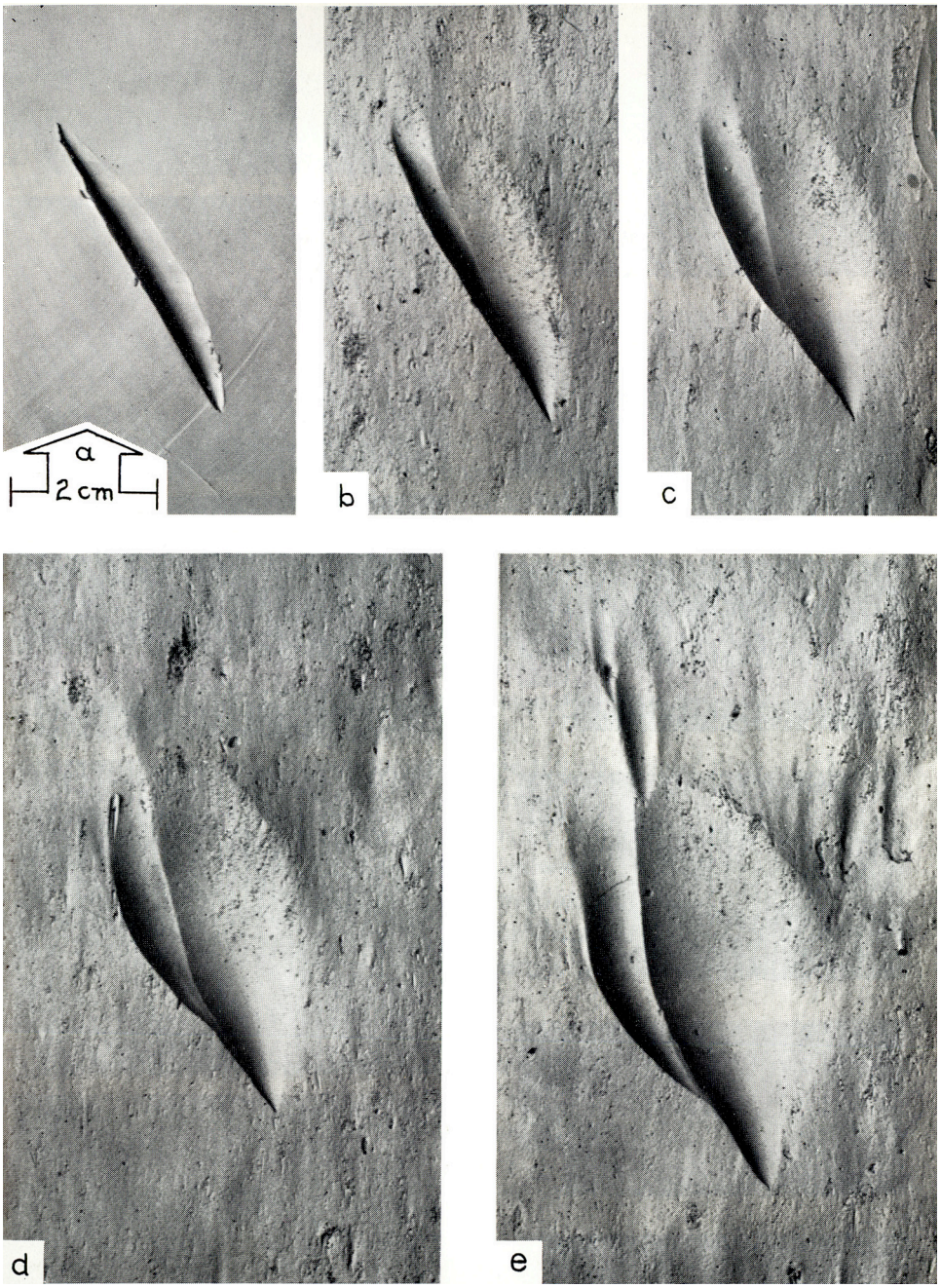

Figure 2.9. Photographs of an experimentally produced flute via corrasion of a cohesive mud bed initiating from a deep, narrow defect aligned oblique to flow. After Allen (1971), his experimental run 42. Times are approximate: a. t = 0; b. 11.1 minutes; c. 27.8 minutes; d. 52.6 minutes; e. 74.3 minutes. 2 cm scale is shown in a; flow direction is from bottom to top.

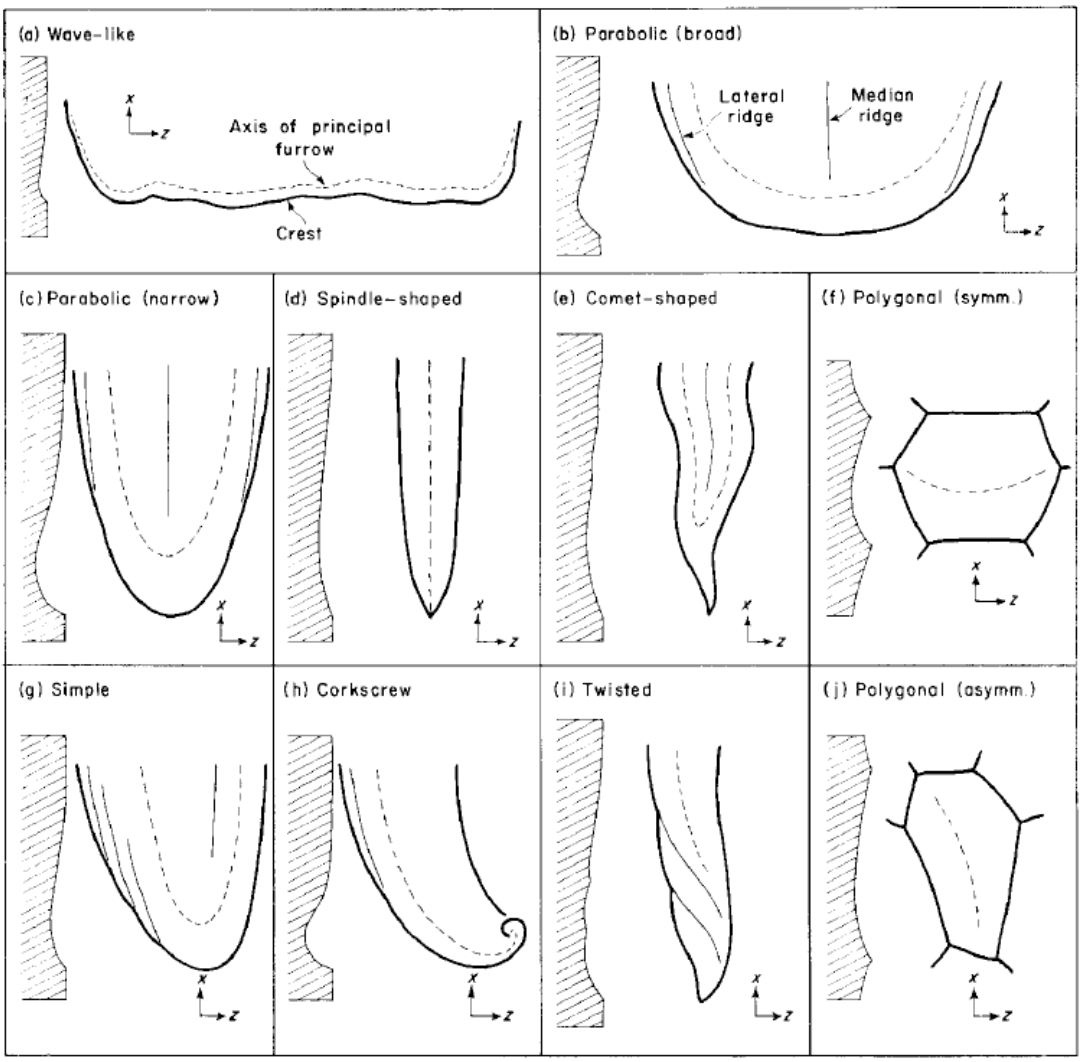

Figure 2.10. Schematics showing the morphology of flute marks according to Allen (1971). Left hand side of each type shows longitudinal bed cross-section (along dividing plane) whereas the right hand-side illustrates planform morphology.

2.3.5. Mass transfer analogy

Allen (1971, 1973, 1975) investigated the mass transfer of plaster of Paris beds with a view to the experiments becoming analogous to the fluid stressing and/or corrasion of cohesive mud beds. These experiments were conducted with hardened mixtures of water and plaster of Paris (hydrated calcium sulphate) that are easily shaped and only dissolve in turbulent streams of water (Allen, 1984, p. 272). Experiments were initiated with a defect of known shape and size made on the bed, and results indicated that flute development was dependent upon the spacing, pattern and orientation of these defects. Closely located defects would develop and expand as isolated features until their rims coalesced, at which point the feature would develop

as a partly-conjugate mark; ongoing development resulted in a single, large, bilaterally symmetrical flute via the gradual loss of features of the initial defects.

2.3.6. Flute morphology and terminology

The principal terms applied to flute morphology by Allen (1971, 1984) are shown in Figure 2.11.

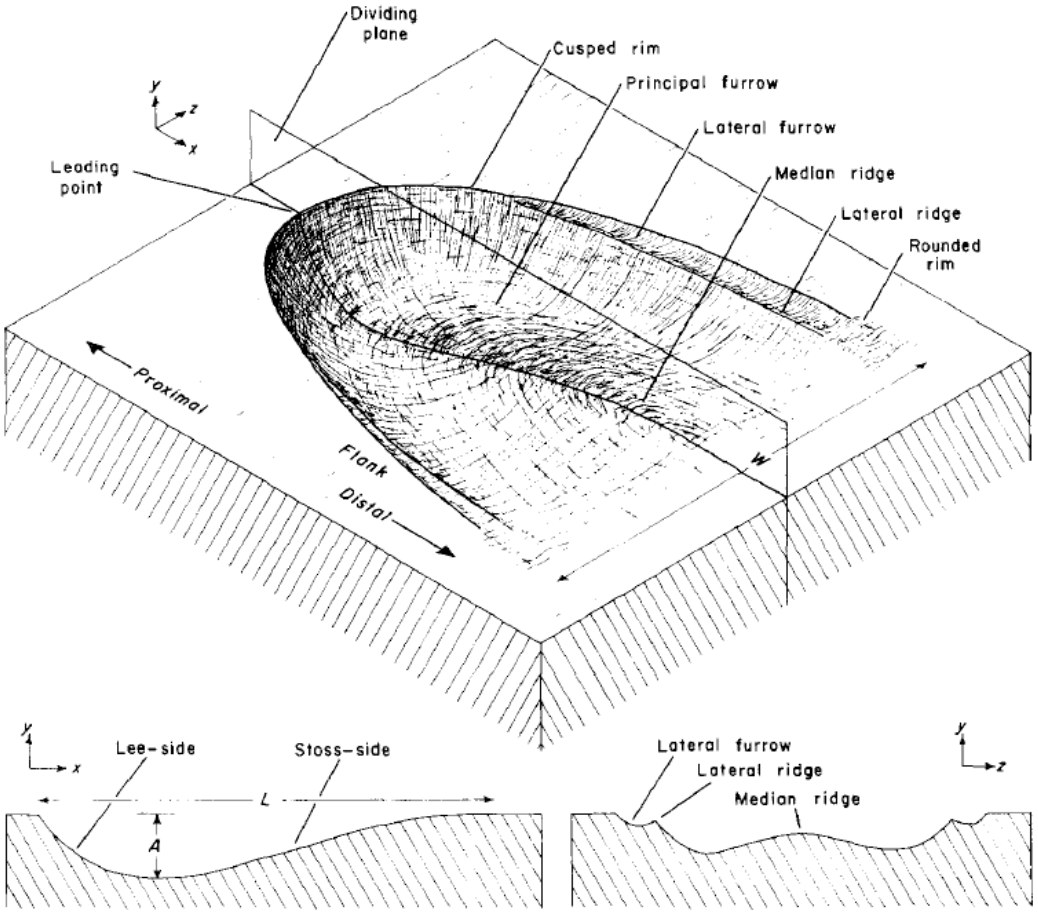

Figure 2.11. A schematic of a flute mark with terminology for morphological features, after Allen (1971). Bottom left figure shows longitudinal profile (along dividing plane), and bottom right figure shows transverse profile.

2.3.7. A model for the development of flutes

Allen (1984, p. 268) concluded that the size and growth of a flute mark cannot be predicted, but confirmed the development of flutes is linked to the physical process of flow separation and reattachment (Allen, 1968a,b, 1969, 1971). Flow separation occurs in regions of abrupt flow expansion, such as over irregularities on the surface of a bed or where there is a negative step along the path of a flow. At these points,

there is a sufficient transition in the fluid for the flow to become detached from the physical boundary, and develop a free-shear layer before reattaching to the boundary further downstream (Figure 2.12). This free-shear layer divides the external stream from a recirculating separation bubble that is captive and attached to the step for as long as the flow persists (Allen, 1968a,b, 1969). During fluid-stressing this results in increased rates of mass-transfer and mud-bed erosion, and during corrasion this results in greater rates of mud-bed erosion (Allen, 1984). Allen (1968a,b, 1971) used a two-dimensional theoretical model to predict that the point of most rapid erosion occurs at the point of reattachment (Figure 2.12). Allen (1971) then used physical modelling to observe that the point of most rapid erosion occurred just downstream of the deepest point within a flute, which, together with the 2-D theoretical model, was used to locate the site of flow reattachment (Figure 2.12). Allen (1968) further develops the theoretical investigation by creating models for a flow over an infinite three-dimensional step that is skewed in various planes; results suggest that over skewed steps the free shear layer does not attach along a specific boundary but fades away into the main external stream. It is unclear how this dwindling of the free shear layer may affect the growth of flutes over a skewed step.

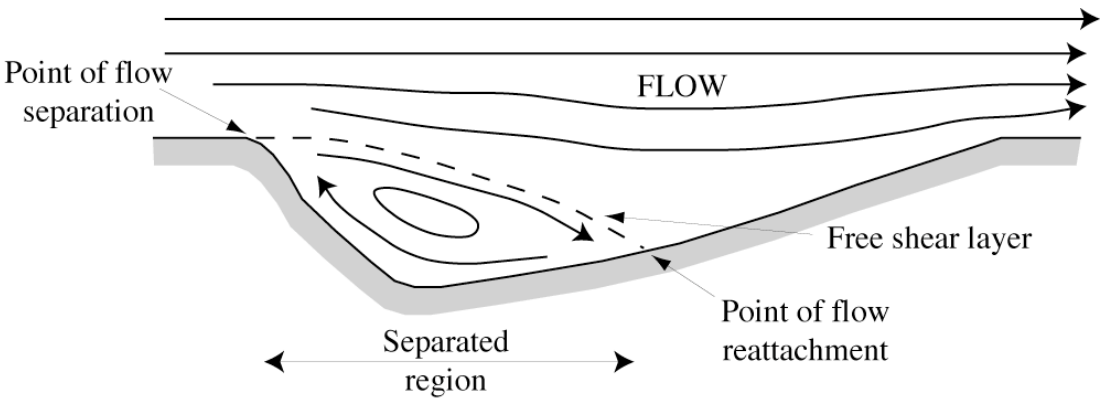

Figure 2.12. Schematic showing a downstream cross-sectional profile of an idealised flute and the patterns of motion associated with development, after Allen (1969).

This model of flute development and positioning theoretically relates the size, shape and structure of flutes to the nature of defects present on the bed prior to erosion (principally the number and character of defects), and the nature of the erosive flow. This is the so-called *defect theory* of Allen (1971). Its rival, the *passive bed theory*,

assumes that flutes are the imprint of flow structures held within the boundary layer of the erosive flow, and therefore the nature of the bed and the details of the erosion process are irrelevant (Allen, 1971; Richardson and Carling, 2005). These theories are summarised in Figure 2.13; bedforms made via the passive bed theory rely purely on flow properties, whereas bedforms made via the defect model only form in the presence of defects.

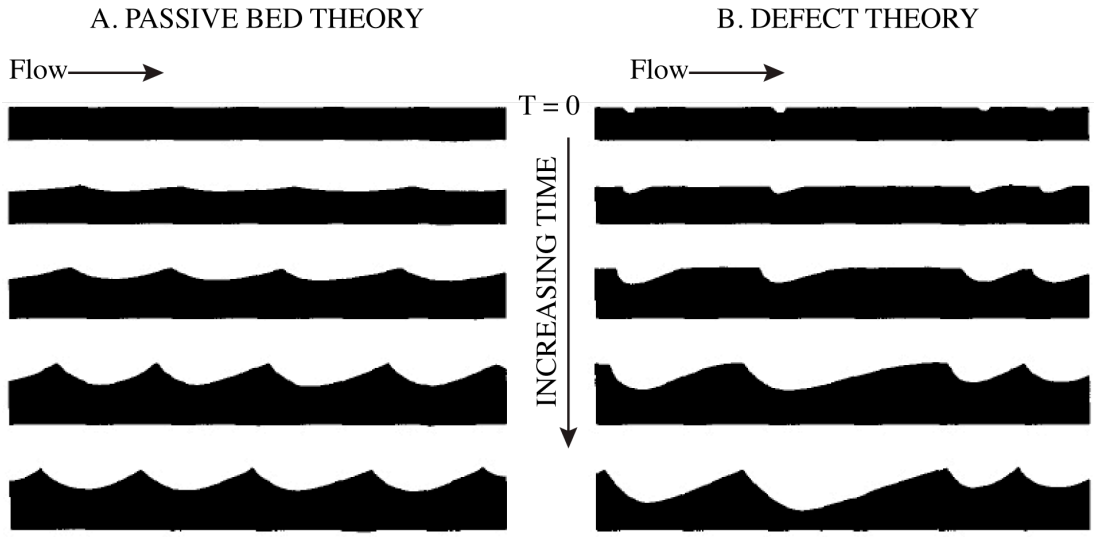

Figure 2.13. The development of flutes according to A. the passive bed theory, and; B. the defect theory (Allen, 1971).

2.4. Experimental studies: discussion and conclusions

Previously conducted experimental work that investigated flute formation reveals that while some clay-based substrates developed erosional bedforms during the experiments, the bedforms were lost when the erosive current was stopped (e.g. Rucklin, 1938). These experiments reveal a number of challenges and limitations that may be experienced when trying to create flutes experimentally. These are principally 1. Finding a method to create flutes, together with the materials that allow their development and preservation, and 2. Monitoring and measuring flute development, and quantifying this process. It is worth noting that previously conducted work comprises a small number of experiments, with only around 30 experiments dedicated to fluid stressing of mud beds (Rucklin, 1938; Allen, 1969, 1971) and 12 to corrasion of clays (1971). Many experiments with materials other

than mud and clay substrates failed to yield flutes, but rather modelled the development of deformation structures (e.g. Dzulynski and Walton, 1963; Dzulynski, 1965; Dzulynski and Simpson, 1966b).

This previous experimental work shows that flutes can be developed by the fluid stressing of weakly cohesive mud beds in closed channel conditions (see Figure 2.7), during very 'brief' flows (e.g. Allen, 1969). Although the length of these experiments are only defined as 'brief', comparison with experiments of Allen (1971) suggests they are only of the order of tens of seconds, and were developed in a narrow range of flow velocities and depths. Furthermore, the experimental flutes generated by fluid stressing show similarities with very transverse features such as mud ripples (e.g. Allen, 1969); this suggests either the mud ripples or flute marks were only temporarily stable while spatial changes between the bedforms took place. Additionally, some experimental flutes were discovered only to form if hardened fragments were suspended in the flow (e.g. Dzulynski and Walton, 1963; see also Dzulynski, 1996). The current catalogue of experimental flute development substantially lacks quantitative data, with very little control over substrate strength and limited time-series data with non-defined time intervals. Key questions remain as to whether the experimentally generated flutes are stable over longer time scales, across a wider range of flow velocities, and if flute development is synonymous with mud ripples.

2.5. Scours observed in modern deep-sea environments

Subsequent to the early findings of the 1970s, increasingly detailed deep-towed sidescan sonar and multibeam bathymetry images of the modern seafloor revealed that large-scale erosional scours are in fact a common feature of many deep-water turbidite systems (for a comprehensive listing of examples, see Appendix A). As described in Chapter 1, scour forms range from longitudinal to transverse (see page 1 and references therein) and this thesis aims to investigate the elliptical or spoon-shaped scours that form the middle ground to the linear/transverse end-members. Previously published studies of scours in deep-sea environments provide a broad understanding of their formative locations and general morphological shapes; a summary of these findings is presented herein.

2.5.1. Modern deep-sea scours: regions of formation

In modern deep-sea scour literature, four different areas occur as typical regions of scour formation (Figure 2.14), and include: 1. on channel-levee backslopes, where scours are up to 20 m deep and 400 m long (e.g. Navy Fan, Normark et al., 1979; Laurentian Fan, Shor et al., 1990; Stromboli Canyon, Kidd et al., 1998; Monterey Fan, Masson et al., 1995; Klaucke et al., 2004; and Redondo Fan, Normark et al., 2009); 2. parabolic features arranged in linear, stepped trends that may extend for several kilometres adjacent to tight channel bends (e.g. Monterey Canyon, Fildani and Normark, 2004; Fildani et al., 2006; and Eel Canyon, Lamb et al., 2008); 3. at the transition zone between canyons or channels and depositional fans and basins, either as fields of isolated scours (250-1000 m wide, 500-1000 m long and 14-20 m deep) or as broad zones of amalgamated scour up to 3 km wide (e.g. Valencia Channel mouth, Palanques et al., 1995; Morris et al., 1998; Rhône Neofan, Kenyon et al., 1995; Torres et al., 1997; Wynn et al., 2002b; Bonnel et al., 2005; Umnak Channel mouth, Kenyon and Millington, 1995; and Setubal and Agadir Canyon mouths, Wynn et al., 2002b); 4. in areas where slope canyons encounter a marked slope break at the base-of-slope where submarine plunge pools form up to 1.1 km wide and 75 m deep (e.g. along the US continental slope, Lee et al., 2002).

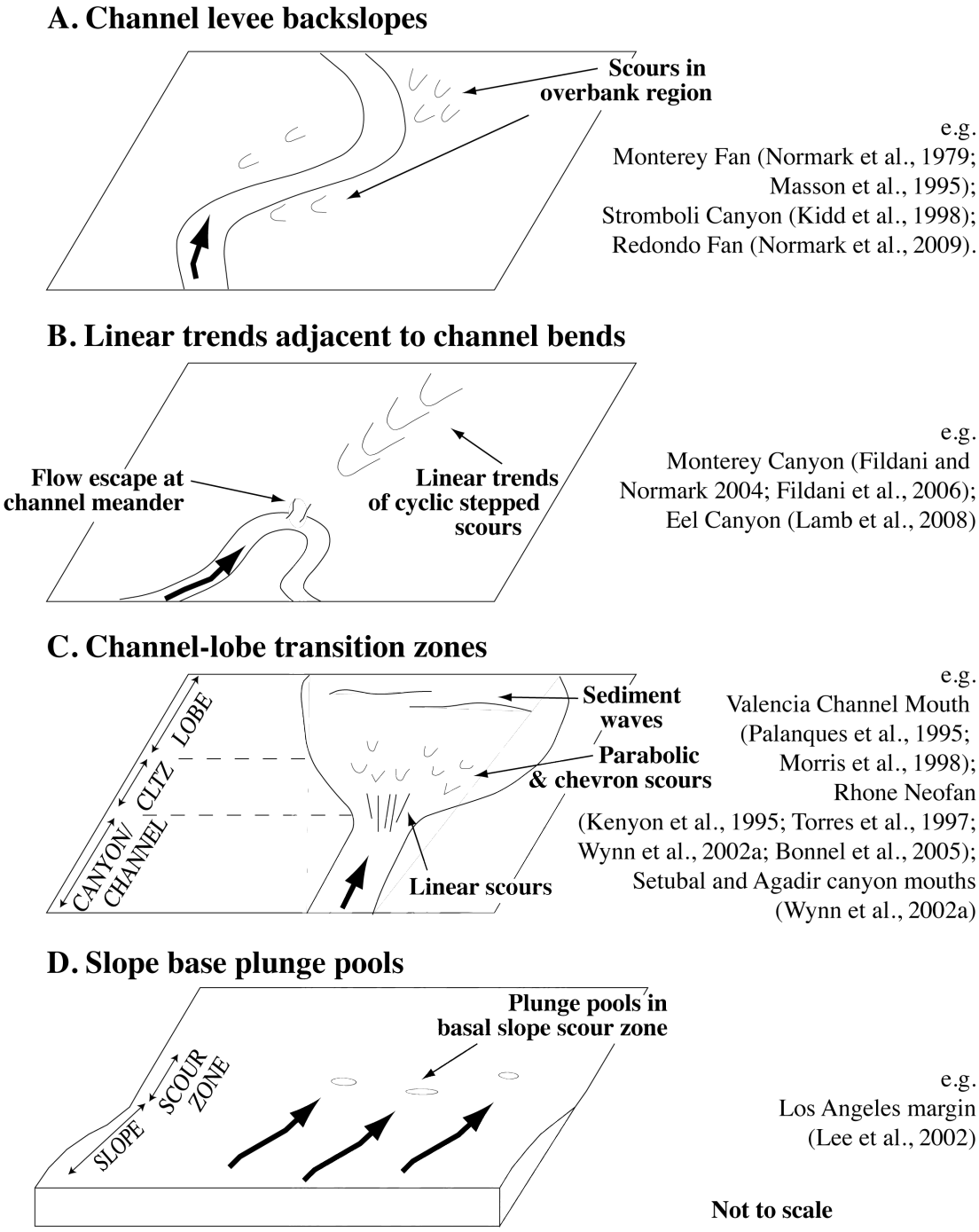

Figure 2.14. Schematic figure showing the four principal formative locations of elliptical scours (and associated features) in modern systems, with referenced published examples. Thick black arrows indicate dominant flow direction. A. Channel-levee backslopes, B. Linear trends of cyclic stepped scours adjacent to channel bends, C. Channel-lobe transition zones (CLTZ), D. Basal slope plunge pools. Not to scale.

2.5.2. Modern deep-sea scours: morphological types

The dimensions, planform and cross-sectional morphology of elliptically shaped deep-sea scours are summarized in Figure 2.15; erosional lineations are included in the summary because they are key features observed in channel-lobe transition zones (see Figure 2.14c). Wynn et al. (2002b) identified the following types of scours in modern and ancient channel-lobe transition zones (Figure 2.15a-d): (i) spoon-shaped scours; (ii) amalgamated scours; (iii) isolated chevron-shaped scours; (iv) erosional lineations. Further to these four types are plunge pools formed at the base of steep slopes (Figure 2.15f), such as on the Los Angeles margin (Lee et al., 2002), and the linear trains of parabolic or rounded scours arranged in step-like sequences that extend down-fan from the bends of sinuous channels (Figure 2.15e); examples include Monterey East channel (Fildani and Normark, 2004; Fildani et al., 2006) and Redondo Fan (Normark et al., 2009).

2.5.3. Modern deep sea scours: trigger mechanisms

Most large-scale scours are associated with regions of flow expansion where increased flow turbulence is implied (Mutti and Normark, 1987; Normark and Piper, 1991), such as at the locations illustrated in Figure 2.14. Experimental and theoretical work suggests that turbidity currents may undergo an hydraulic jump at these locations, transforming from supercritical to subcritical flows and leading to locally increased turbulence and scouring of underlying sediments (Komar, 1971; Normark et al., 1979; Mutti and Normark, 1987; Lee et al., 2002). Hydraulic jumps are also shown to occur in linear sequences where the flow repeatedly alternates between supercritical and sub-critical states (also seen in fluvial systems, e.g. Wohl, 2000): a process that has been physically demonstrated (Koyama and Ikeda, 1998; Brooks, 2001) and theoretically modelled (Parker and Izumi, 2000). Each hydraulic jump (i.e. each transition from supercritical to sub-critical flow) leads to the development of a *cyclic step* that may be net-depositional (which form sediment waves) or net-erosional that develop scours (e.g. Monterey East channel, Fildani and Normark, 2006; Fildani et al., 2006; see also Figure 2.14b and Figure 2.15e).

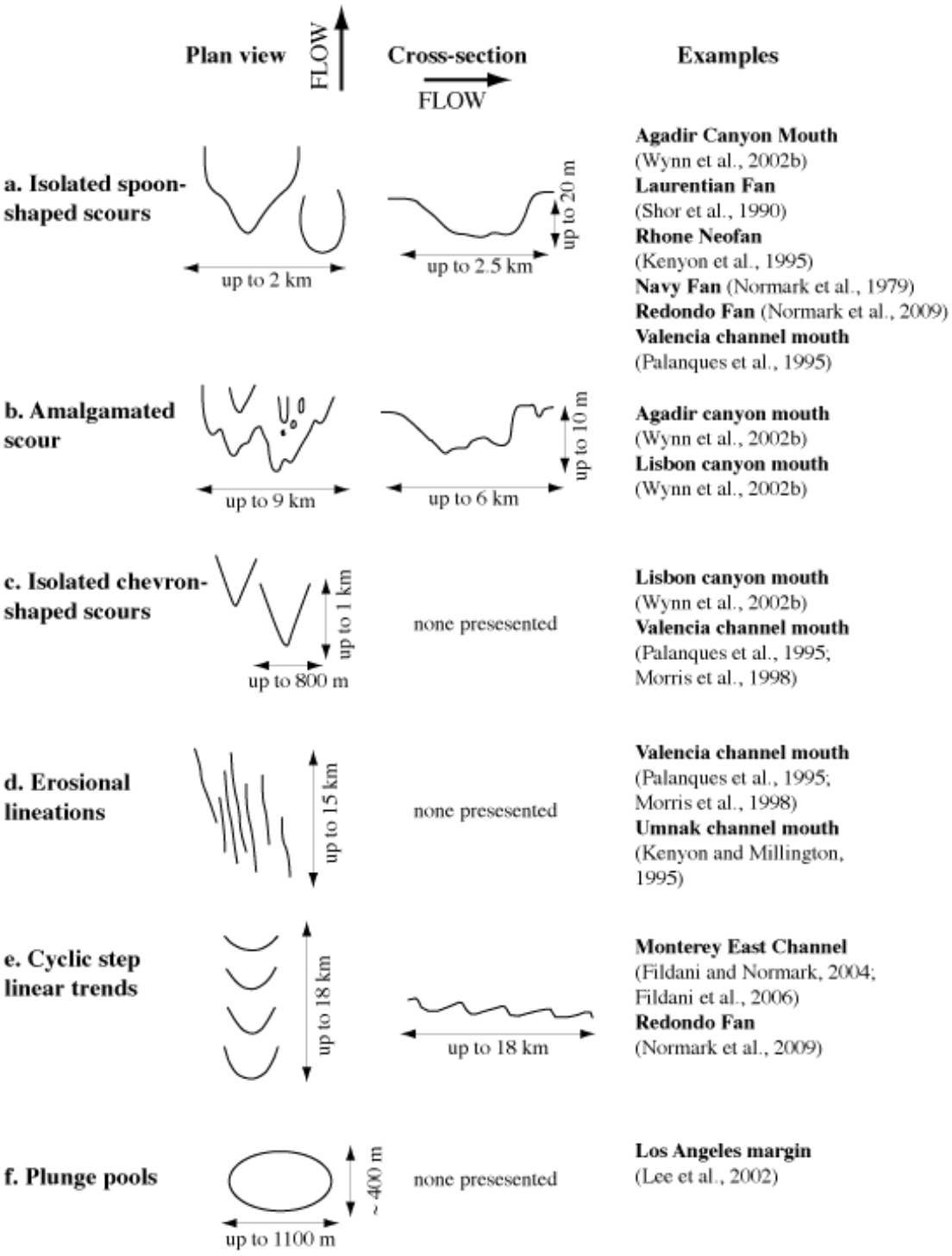

Figure 2.15. Summary figure showing the principal morphological types of elliptical scours in deep-sea environments, and published references. Features a - d are modified after Wynn et al. (2002b). Erosional lineations are included here because they are prominent features of channel-lobe transition zones and feature in Figure 2.14c.

Existing work demonstrates that incisional cyclic steps are intrinsically linked to the presence of hydraulic jumps and therefore require an initially supercritical flow to form (Fildani et al., 2006). Although hydraulic jumps are proposed as a scouring mechanism for some erosional systems (Mutti and Normark, 1987; Kenyon et al., 1995; Lee et al., 2002), it has been suggested that the erosional processes are probably more complex than this, and are dependent upon variables such as current magnitude and composition (Wynn et al., 2002b). Aside from the development of cyclic steps, scouring mechanisms that are unrelated to hydraulic jumps have also been suggested, such as the impact of high momentum flows or vortices caused by local disturbances in the flow (Normark and Piper, 1991; Chapin et al., 1994; Lee et al., 2001). Additionally, underlying structural controls are thought to determine scour locations and further influence their formation (e.g. Horseshoe Valley, Duarte et al., 2009).

A key factor to be considered in the mechanism for scouring is the common distribution of scours in some systems, such as where many tens of scours are located within close proximity of each other (e.g. Valencia channel mouth, Palanques et al., 1995; Morris et al., 1998; Agadir canyon mouth, Wynn et al., 2002b). With the exception of linear sequences of cyclic steps, it is unclear whether multiple hydraulic jumps develop across wide regions of flow expansion; this does not appear to be discussed in published literature.

2.5.4. Data collection in modern deep-sea environments

Numerous scours are catalogued from modern environments, but at a limited resolution. Significant portions of the data were collected via deep-towed ocean bottom instruments (e.g. TOBI), hull mounted multibeam bathymetry systems, and sub-bottom profilers, yet in deep-sea environments (>3000 m) the resolution of these systems is reduced to tens of metres (Normark et al., 2009). As a result, the dimensions of documented scours are often given within ranges (e.g. the Agadir canyon mouth: ~500 m long and 250-500 m wide, Wynn et al., 2002b), and the true morphology of the imaged scours cannot be obtained. Furthermore, without a precise understanding of scour morphology, difficulties arise when trying to place core sites at specific locations either within or adjacent to scours, and the sedimentology of the scours, the manner in which they expand, infill, and bypass, remains unclear. One

notable exception to this however, is Redondo Fan, offshore California, where Normark et al. (2009) utilised an Autonomous Underwater Vehicle (AUV) to obtain unprecedented images of sea-floor scours at water depths up to 700 m. They obtained high-resolution multibeam bathymetry and sub-bottom profiles by flying the AUV at a height of ~70 m above seafloor, and obtained multibeam bathymetry data of 1.5 m lateral resolution and 0.3 m vertical accuracy, which is approaching outcrop-scale resolution (Normark et al., 2009). This pioneering study was a first step towards producing high-resolution data for modern deep-sea scours, but further data are now required to assess the dimensions and morphology of scours in true deep-sea systems (*true* meaning >1000 m depth), and how these are influenced by local factors, e.g. structural controls, substrate type, flow conditions/frequency, and nature and volume of infilling sediments.

2.5.5. Discussion and conclusions

Aside from this new style of high-resolution AUV mapping, the strength of modern deep-sea mapping lies in providing excellent constraint on the overall formative location of scours, together with approximate control on their geomorphology and dimensions. Through modern deep-sea mapping, it has become clear that large-scale scours are common features of submarine fans; however the processes of scour formation remain unclear, and key questions remain regarding the sediments that host, cut and infill scours.

2.6. Scours observed in ancient deep-sea environments

Erosional scours documented in outcrop commonly have metre-scale geometries, such as megaflutes in the Carboniferous Ross Sandstone of western Ireland (Figure 2.16) (Chapin et al., 1994; Elliott 2000a,b; Lien et al., 2003), the Albian Black Flysch of northern Spain (Vicente Bravo and Robles, 1995), the Lower Eocene Charo Canyon mouth of the Spanish Pyrenees (Millington and Clark, 1995) and the Eocene-Oligocene Annot Sandstone in the French Alps (Hilton, 1995; Morris and Normark, 2000). It is likely that larger scours are preserved in the rock record, but are misidentified as channels (Mutti and Normark, 1987). Outcrop-based studies have helped document the nature of scoured substrates and infilling sediments, e.g. the multi-episodic scour-and-fill geometries visible in sandstones of the Albian Black Flysch (Vicente Bravo and Robles, 1995). However, precise palaeoenvironmental interpretations of scours in outcrop can be challenging, as exemplified by observations of the well-studied Carboniferous Ross Sandstone. In this system, scours have been interpreted as occurring in a channel-lobe transition zone (Chapin et al., 1994), on channel flanks via single high-magnitude channel-initiating flows (Elliott, 2000a,b), and in spillover lobes at the bends of sinuous channels (Lien et al., 2003). The megaflutes of the Ross Sandstone form the fieldwork component of this thesis.

2.7. Case Study: The Carboniferous Ross Sandstone, western Ireland

The Carboniferous Ross Sandstone is a 500 m thick turbiditic sandstone formation that outcrops in western Ireland. It developed in the Shannon Basin, a structurally-confined basin that formed in response to subsidence over the Iapetus suture (Collinson et al., 1991; Martinsen et al., 2000, 2003; Wignall and Best, 2000, 2002; Martinsen and Collinson, 2002; Pyles, 2007, 2008). The basin-fill comprises an initially deepening, then shallowing-upward succession, punctuated by laterally-continuous condensed sections (termed “marine bands”) that provide a biostratigraphic framework (Hodson, 1954a,b; Hodson and Lewarne, 1961; Rider, 1974; Collinson et al., 1991; Hampson et al., 1997; Wignall and Best, 2000, 2002; Martinsen and Collinson, 2002; Pyles, 2008). The basin consists of a Visean

Figure 2.16. Megaflute of the Carboniferous Ross Formation, western Ireland; with chalk lines etched on to show topography. Megaflute mesures ~6 m at its widest point; black and white metre ruler to right of photograph for scale. Palaeoflow is from top-right to bottom-left. Surrounding bedding surface is ornamented with lingoid ripples.

---

limestone overlain by a clastic Namurian (upper Mississippian-lower Pennsylvanian) fill, including deep-water shales (Clare Shale Formation ~100% shale), turbiditic sandy submarine-fan deposits (Ross Formation ~ 60% sandstone), unstable muddy delta-slope deposits (Gull Island Formation ~ 23% sandstone) and fluvio-deltaic shelf margin deposits (Central Clare Group cyclothems ~ 25% sandstone) (Rider, 1974; Collinson et al., 1991; Wignall and Best, 2000, 2002; Martinsen and Collinson, 2002; Pyles, 2008).

The submarine fan deposits of the Ross Formation have been intensively studied in recent years, in part owing to their excellent and continuous exposure along the coast of County Clare, but also because their sedimentary architecture is analogous to many deep-sea petroleum reservoirs in the Gulf of Mexico (e.g. Chapin et al., 1994; Sullivan et al., 2000; Pyles, 2008). The Ross Formation comprises interbedded sandstones, siltstones and mudstones that have been interpreted as mudstone sheets, turbidites, channels and associated slumps (Rider, 1974; Collinson et al., 1991; Martinsen et al., 2000; Wignall and Best, 2000; Strachan, 2002; Lien et

al., 2003; Pyles, 2007, 2008). The Ross Formation documents an overall progradational history recorded by the progressive north-eastward expansion of the area of turbidite sandstone deposition (Wignall and Best, 2000). In outcrops in SW County Clare, the progradational trend is shown by the vertical change in the proportions of internal architectural elements, where mudstone sheets dominate the lowermost deposits, the middle Ross Formation is dominated by lobes, and both channels and slumps become more common in the upper Ross Formation (Pyles, 2008). Many of the mid- to upper-Ross deposits comprise interbedded sandstones and mudstones organised into broad thickening-upward packages, each typically 1-7 m thick, subdivided into three parts (Elliott, 2000a,b; Lien et al., 2003; Pyles 2007): i) an initial finely parallel-laminated mudstone unit; ii) a series of interbedded silty mudstone and sandstone deposits, and iii) an overlying structureless amalgamated sandstone bed. The degree of amalgamation within the upper sandstone varies across the beds, allowing some bedding surfaces and intervening mudstone deposits to be preserved. The distribution of megaflutes and the depositional environment of these cyclical packages has been widely debated; several depositional models regarding their development have been proposed, and their key attributes are discussed here.

2.7.1. Model 1: Distal channel-lobe transition setting

Some of the earliest work on the Ross Sandstone created a model for deposition invoking deep-sea lobes, and placed megaflutes at channel to lobe transition zones and at overbank positions (Figure 2.17a), which are related to areas of slope change and therefore possibly hydraulic jumps (Chapin et al., 1994). This work found megaflutes to be ubiquitous within the Ross Sandstone, but interestingly reported an absence of coarsening- or thickening-upward packages; lobes were instead identified by the dominance of sheet sandstones, composed of fine-grained turbidites with Bouma horizons T_{ac} and T_{ace} present. This model was later adapted by Pyles (2007, 2008) who documented large-scale architectural elements and found the dominant architectural element to be lobes (56% average by area; Pyles, 2007). Chapin et al. (1994) alternatively suggest that megaflute development might be invoked by local flow disturbances caused by irregular depositional topography (such as compensation bedding), and are not related to hydraulic jumps.

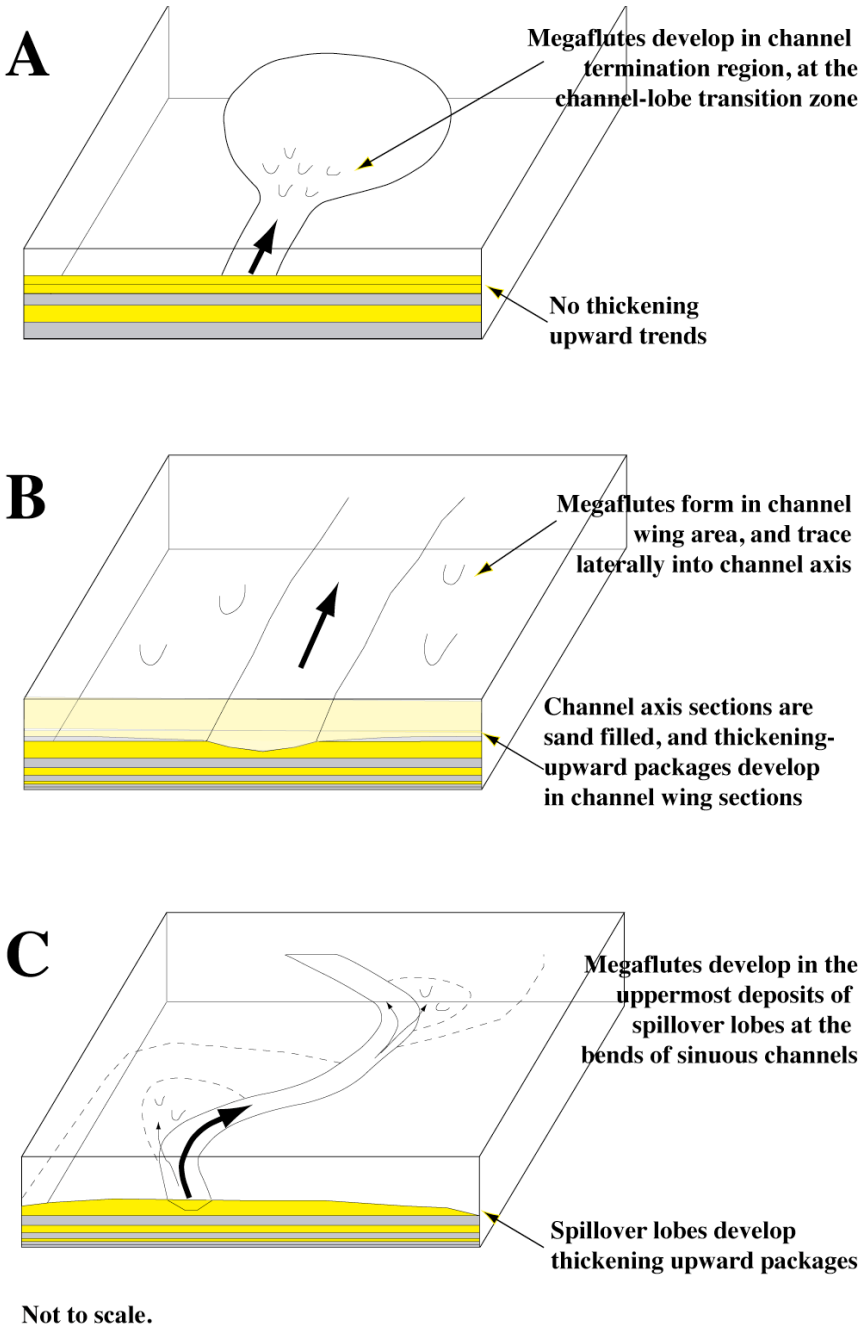

Figure 2.17. Contrasting models for the development of Ross Formation megaflutes: (A) Development in channel-lobe transition zones within an aggradational, sand-rich fan with small, coalescing mid-outer fan lobes with multiple shallow channels (Chapin et al. 1994) (B) Megaflute development in channel-wing region along erosion surfaces that trace laterally into channel axis – specific location within basin is not stated (Elliott 2000a,b) (C) Development of megaflutes in the upper parts of spillover lobes at the bends of sinuous channels (Lien et al. 2003).

2.7.2. Model 2: Basin floor deposition & erosion

A subsequent model (Elliott, 2000a,b) suggests that sandstone dominated channels are prevalent in the upper part of the Ross Sandstone, and typically consist of two components: 1. a locally developed channel axis defined by a master basal erosion surface; 2. laterally extensive channel wings that flank the channel axis and overlie megaflute erosion surfaces (Elliott, 2000a,b). The model notes channel axes are overlain by massive, highly amalgamated turbidites, whilst channel wings comprise turbidites with varying degrees of amalgamation, and a pronounced thickening-upward trend above the basal megaflute erosion surfaces (Elliott, 2000a,b) (Figure 2.17b). This stratigraphy is considered to have developed in two phases: 1. an erosional phase that was the product of a single, high-magnitude/low frequency turbidity current event that produced erosion throughout the study area, 2. a depositional phase involving numerous lower magnitude/higher frequency turbidity current events. Under this model, the erosional phase is recorded by channel axes that trace laterally into widespread erosional surfaces ornamented with numerous megaflutes. The depositional phase is recorded by thick sand bodies that fill the channel axes, and fine-grained deposits in overbank regions. The final phase of deposition is a blanket of sandy turbidites, resulting in vertical sandstone-only successions within the channel axes, and thickening-upward trends that overlie megaflute ersoional surfaces at the channel-wings (Figure 2.17b).

2.7.3. Model 3: Sinuous channel and spillover system

A later model associates megaflute development with spillover lobes at the bends of sinuous channels (Lien et al., 2003; Figure 2.17c). These findings were based upon a number of palaeocurrents and sedimentary logs recorded from the eastern outcrops of the Ross Sandstone, and document the thickening-upward packages described in Section 2.6. The model proposes that overspill from low-sinuosity channels resulted in thickening-upward successions in the overbank settings (Lien et al., 2003). Megaflute formation in the upper amalgamated beds is attributed to turbulence associated with later spillover and amalgamation.

2.7.4. Carboniferous Ross Sandstone case study summary

Data collected on the Ross Sandstone are inconsistent, with recent debates regarding the presence of thickening-upward packages, megaflutes, channels, lobate elements and turbidite sheets (Elliott, 2000a,b; Lien et al., 2003; Higgs, 2004; Pyles, 2007, 2008). One of the most significant differences in the data is regarding the stratigraphic location of megaflutes, specifically whether megaflutes are restricted to the tops of thickening-upward packages (e.g. Elliott, 2000a,b), the uppermost deposits of packages (e.g. Lien et al., 2003) or whether they are unrelated to packages (e.g. Chapin et al., 1994). Clearly such observations affect palaeoenvironmental reconstructions, which range widely from: i) aggrading lobes within a structurally-confined, rapidly subsiding basin (Pyles, 2007, 2008), where scouring developed in regions of channel-to-lobe transition (Chapin et al., 1994), through ii) scouring on channel flanks via single, catastrophic, channel-initiating flows that subsequently infilled via low-magnitude, high-frequency turbidity currents (Elliott, 2000a,b), to iii) deposition and scouring within spillover lobes at the bends of sinuous submarine channels (Lien et al., 2003).

Curiously, the Ross Sandstone megaflutes are erosive into sandstone and are common in sheet sandstone deposits (Chapin et al., 1994; Elliott, 2000a,b; Lien et al., 2003). An alternate example of megaflutes in outcrop is the Albian Black Flysch (northern Spain), where scours 5 – 50 m wide may be observed in cross-section and planview (Figure 2.18); however these deposits are in significantly more coarse-grained sandstones which grade up from conglomeratic deposits with clasts up to ~5 cm across. These are the only two published examples of deep-sea megaflutes exposed in planform, and comprise a very small dataset. Key questions remain regarding the occurrence and formative dynamics of megaflutes in the Ross Sandstone, especially in light of the many conflicting datasets in the literature (e.g. Chapin et al., 1994; Elliott, 2000a,b; Lien et al., 2003). Furthermore, it remains unclear whether there is a typical morphology to the Ross Sandstone megaflutes, or whether there is a wide range in morphologies.

Figure 2.18. Photograph of the Albian Black Flysch deposits, Bakio Point, northern Spain. Foreground shows part of a megaflute surface (red line) and infilling sandstone (labelled), which is overlain by another erosional surface (red arrow); palaeoflow is from left to right. Sediments in photograph are all coarse grained sandstones. Three erosional surfaces in the background are also indicated (yellow arrows). Karen Wignall in photograph for scale.

2.8. Discussion

It has been previously hypothesized that there is a continuous size spectrum between small-scale flute marks and larger scours (tens of metres) observed on the sea floor (e.g. Normark et al., 1979). However difficulties arise when trying to test this because the scales of observation between small-scale flutes and scours on the seafloor differ by several orders of magniude. Furthermore, there are major differences in the sedimentology of the flutes, megaflutes and scours presented in this chapter. Nominally, flutes erode into cohesive muds and are infilled and cast by sands; megaflutes erode into coarse sands and may be infilled by a variety of sediments, and very little is known about the sedimentology of large-scale (kilometre-sized) modern seafloor scours owing to the difficulties encountered in precisely sampling their sediments.

However, one attempt has been made to link these smallest and largest features, by testing whether Allen's (1971) defect theory can be up-scaled to large-scale modern scours. Shor et al. (1990) applied the defect theory to the generation of a giant flute-shaped scour on Laurentian Fan (100 m deep and 1000 m long), which is believed to have been generated by the 1929 Grand Banks turbidity current. Shor et al. (1990) performed calculations using both empirical parameters (from Allen, 1971) and measurements taken from the giant scour. However, both calculations produced durations of scour generation that were considered too short to realistically generate the observed scour; it was therefore assumed that the scour became unusually deep because the surrounding sediments were protected by a conglomerate veneer, however once this veneer has been broken erosion became focused and the scour rapidly deepened. It therefore remains unclear whether flow processes operating on both small- and large-scale scours are comparable, and whether experimental studies of erosion can be up-scaled to natural examples on the modern seafloor.

In contrast to Allen's (1971) defect theory is the widely hypothesized hydraulic jump theory (see also page 30) which links scouring to increased turbulence associated with a hydraulic jump (Komar, 1971; Mutti and Normark, 1987, 1991; Normark and Piper, 1991; Garcia et al., 1993; Kenyon et al., 1995; Millington and Clark, 1995; Palanques et al., 1995; Wynn et al., 2002b; Ito, 2008). The hydraulic jump theory is most commonly applied in positions of rapid flow expansion such as at slope breaks (e.g. Lee et al., 2002) and channel/canyon-lobe transition zones (Kenyon et al., 1995; Wynn et al., 2002a; Bonnel et al., 2005); however, it remains unclear whether the hydraulic jump theory translates to other environments of scouring such as in proximal lobe positions (Chapin et al., 1994). Increasingly, some authors are suggesting that scouring may arise from increased turbulence associated with local disturbances in the flow (such as compensation bedding) or the impact of high momentum flows (Normark and Piper, 1991; Chapin et al., 1994; Lee et al., 2001).

Key questions remain, therefore, regarding flutes, megaflutes and scours and the relationship between them, if indeed they are related. Firstly, the experimental production of flutes must be revisited in order to establish whether these flutes:

(i) are stable over long time scales; (ii) develop at different flow velocities/depths to those previously produced; (iii) are synonymous with mud ripples. Secondly, megaflutes preserved in outcrop must be re-examined in order to investigate the contrasting models for their development and establish a much-needed definition for the *megaflute* term. Thirdly, deep-sea scours in modern systems must be revisited in an attempt to establish an understanding of their typical dimensions, formative locations, dynamics and sedimentology. Finally, and crucially, these newly obtained results may be used to directly compare the morphology, sedimentology and occurrence of deep-sea scours across all scales, to establish whether there is a continuum of erosional bedforms from centimetre- to kilometre-scale, and whether these processes translate across the wide range of scales and different sedimentologies.

3. Experimental simulations of erosional bedforms in muds

3.1. Introduction

Previous experimental investigations into the development of flutes comprise a few experiments across a variety of experimental conditions (e.g. Rucklin 1938, Dzulynski and Sanders, 1962; Dzulynski and Walton, 1963; Dzulynski, 1965; Dzulynski and Simpson 1966b; Allen, 1968a,b, 1969, 1971) see Chapter 2 for detailed discussion. Only a small number of these experiments yielded flutes. Many experiments developed deformational and loading structures and other shallow erosional features. Crucially, at the time of this experimental work (1930s – 1970s), the technology had not been developed whereby the bathymetry of the experimental bedforms could be obtained electronically; therefore any quantitative measurements were taken by hand. Furthermore, there was no way to measure flow velocities, and therefore shear stress, of experimental flows (Allen, 1969). Key experimental observations were made following experiments and were largely qualitative, made visually, and illustrated with photographs (e.g. Rucklin 1938, Dzulynski and Sanders, 1962; Dzulynski, 1965; Allen, 1969, 1971). Allen (1971) provides one exception to this, whereby six experiments (four eroding plaster of Paris beds via mass transfer, and two eroding clay beds by corrasion) were paused at intervals during the flow so that measurements of the flute could be taken. Allen (1971) provided a dimensionless age ($V_B t/X$) for each interval, and did not provide real time ages. For this:

V_B = time averaged areal mean velocity on the bed upstream from the flute

t = duration of the erosion process

X = initial streamwise length of defect

Assuming V_B remains constant during the course of each experiment, it is possible to back calculate the dimensionless age to obtain a real time age. Although this is not an accurate time, it is a reasonable guide to the experimental times that Allen (1971) used. These calculated real-time ages are shown in Figure 3.1 and indicate that bed profiles were not taken at regular intervals; it is unclear why Allen (1971) used these specific time intervals. At each interval, Allen (1971) measured the flute depth (amplitude) using a point gauge reading to ±0.002 cm, and took plasticine moulds of

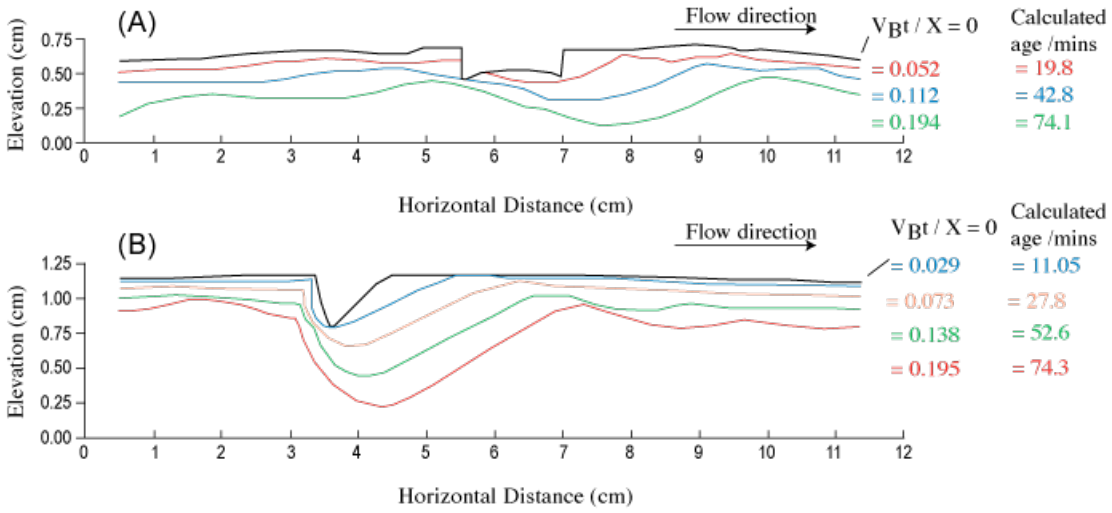

Figure 3.1. Longitudinal profiles measured on experimental erosional marks generated at defects due to corrasion on strongly cohesive mud beds. Of Allen (1971, p. 279). A) originated from a shallow, circular defect – see Figure 2.8 for photograph. B) originated from a deep, narrow defect arranged oblique to flow – see Figure 2.9 for photograph.

---

the marks from which flute length and width were measured. Results suggest the upstream rim of the flute (the leading point) migrates upstream, and the lowest point of the profile migrates downstream with time (Figure 3.1). Results also show the highest erosion velocity is observed slightly downstream of the deepest point along the profile, at the point of reattachment (see Figure 2.13; in agreement with theoretical predictions, Chapter 2). However it appears that no other studies have attempted to make such time-series observations, and our current understanding of real-time flute development in mud beds consequently relies upon the findings of Allen's (1971) two experiments.

This study utilises physical modelling to investigate the experimental conditions required to create flutes in mud and clay beds. The experiments assess:

(i) the development of flutes in weakly cohesive mud beds via fluid stressing;

(ii) the development of flutes in stong clay beds via corrasion;

(iii) how these flutes develop with time.

3.2. Experimental equipment and procedure

3.2.1. Flume Tank

The experiments presented here were conducted in the Sorby Environmental Fluid Dynamics Laboratory of the University of Leeds. The flume tank used is a recirculating slurry flume, with an open-channel that measures 8 m long, 29.5 cm wide, and 35 cm deep (Figure 3.2). The flume recirculates flow via a large pipe that runs beneath the flume, and re-introduces the flow to the channel within a large header tank. This header tank is fitted with a number of steel pipes 20 cm long and 3.8 cm diameter aligned parallel to flow that act to calm the flow and suppress turbulence within the open channel. The flume is also fitted with flow baffles at the upstream and downstream ends of the flume, which further suppress turbulence within the flow (Figure 3.2). The downstream-end baffle also prevents air being sucked into the pump and recirculating pipes, which can cause extreme pump vibrations and flume damage. The flume was fitted with an artificial floor raised 8 cm from the open channel floor, with an open space measuring 40 cm long (located 2.5 m down the flume) into which mud and clay beds could be inserted. The axial slope of the flume may be adjusted, and for these experiments was set to 1/500, to minimize standing waves. The pump that generated flow was a slurry pump capable of achieving flow velocities of 1.5 m/s for plain water flows.

3.2.2. Creating artificial beds

Two types of bed were created for use in these experiments. Type 1: weakly cohesive mud beds of kaolin (china clay), and; Type 2: stronger clay beds of potter's clay purchased from a pottery vendor. Two methods were used to create the weakly cohesive mud beds: (i) via settling from suspension and (ii) in a shear-box intended to extract excess fluid.

A five-step process was followed for bed formation by the settling from suspension: 1. a removable Perspex tray designed to fit within the artificial floor (Figure 3.3) was sealed within an open top box; 2. mixtures of between 30 and 40 wt. % kaolin mixed by hand with tap water added to the box and left to settle for 48 hours – the total depth of the settled bed was generally 15% of the original

mixture depth; 3. the supernatant water was drained from the top of the box, leaving only the

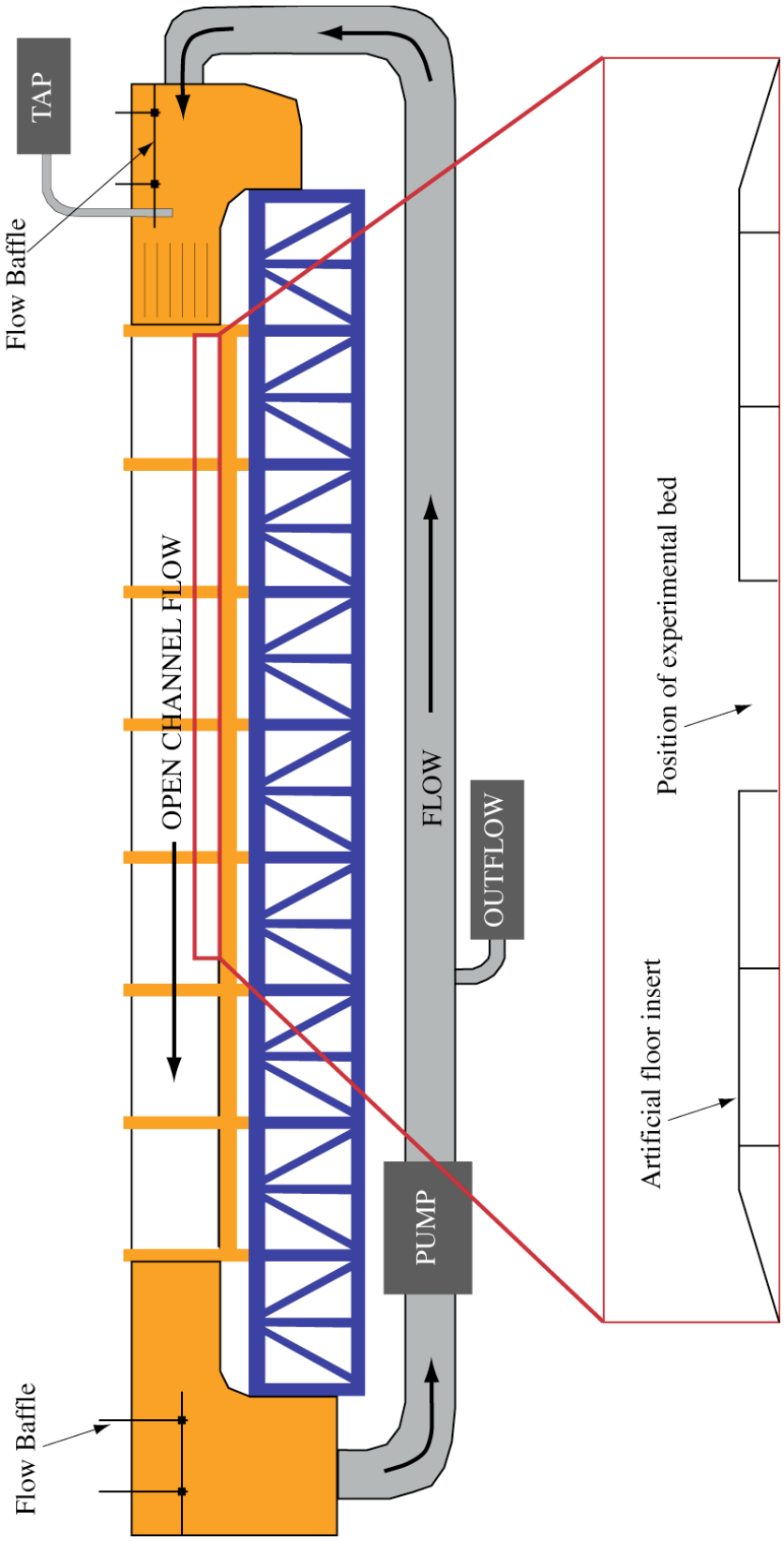

Figure 3.2. Schematic showing the experimental flume tank used for generating flutes. The open-channel portion of the flume is glass-walled 29.5 cm wide and 8 m long.

settled bed within the inner Perspex tray (Figure 3.3c); 4. the sealant around the tray was removed and the open box also removed; 5. the settled bed within the Perspex tray was placed into the opening within the artificial floor in the flume. An alternate method of preparing the bed within an odometer was intended to expel the water from the mixture while under compression (Figure 3.4). A Wykcham Farrance 50 mm odometer was used, in the Engineering Geology Laboratory at University of Leeds. Kaolin-water mixtures of between 31 and 75 % kaolin were poured into the odometer, and were bound above and below by soaked porous ceramic plates. The mixture was then subjected to a load of 111 kPa (the minimum load possible), which forced the consolidation of the kaolin and allowed water to escape via the porous plates. This sample could then be transferred to the flume tank.

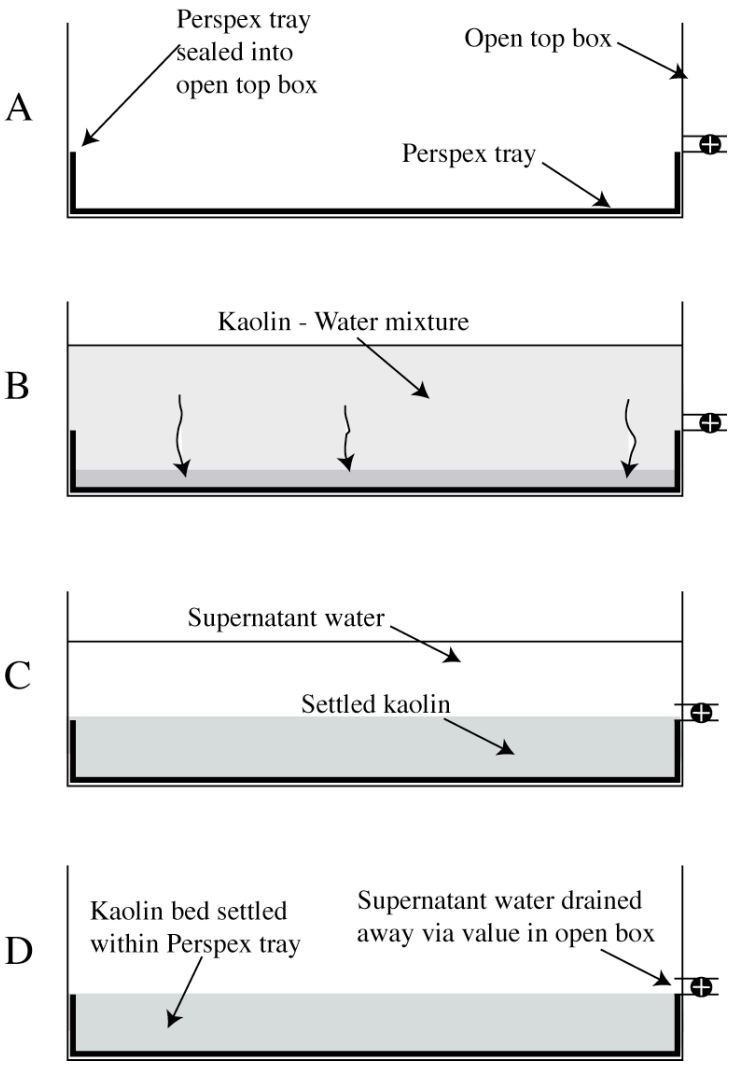

Figure 3.3. Experimental procedure for settling kaolin beds from suspension. (A) Perspex tray (designed to fit into artificial floor of Figure 3.2) is sealed into open top box. (B) Kaolin-water mixture of desired concentration is added to the open box, and begins to settle kaolin towards the base. (C) After 48 hours the kaolin bed is fully settled and the supernatant water has collected above. (D) The supernatant water is drained from the open top box, the tray is un-sealed and the kaolin bed may be placed into the flume.

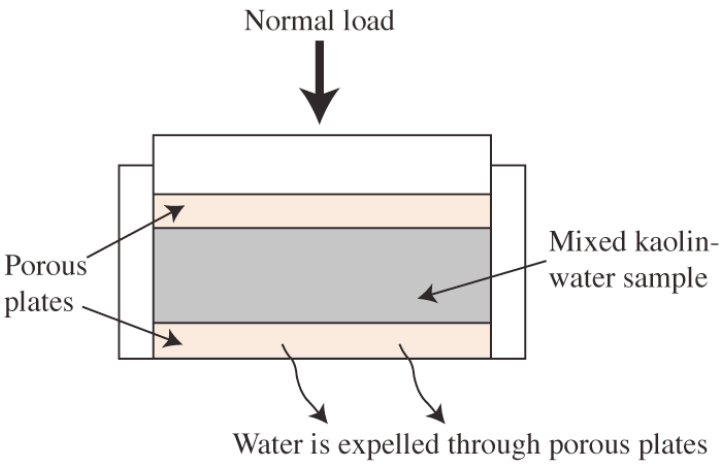

Figure 3.4. Use of odometer in creating kaolin beds. The kaolin – water mixture is added to the box, then subjected to a normal load that expels water and forces consolidation.

To create the stronger Type 2 clay beds, potter's clay was purchased though a potter's clay vendor (Valentine's Clays, www.valentineclays.co.uk). XRD analysis of the clay is shown in Table 3-1. The clay was firm enough so that it would stay in rigid blocks, but was sufficiently soft so it could be shaped by hand. Three of the experimental beds were tested for their shear strength; bed samples were taken following the end of each experimental run and sealed in a watertight container for 2 to 3 days before being measured. Shear strengths were measured using a mechanised laboratory shear vane (VJ Technology – VJT5300) that measured bulk strengths from the centre of the sample. Three repeat measurements were taken for each sample (the container was moved between measurements in order to place each one away from previously disturbed material) the resulting average value of 1.10 kPa (Table 3-2). The blocks were made to 'soft cake' specifications and delivered in individually wrapped 20 kg packets; each one was more than enough to fill the insert in the artificial floor of the flume. The bed was then hand-shaped into the insert, aiming to exclude air bubbles and irregularities as much as possible, and made level with the artificial floor of the flume using the sharp edge of a metal ruler. Following placement of the bed, the flume was filled to the desired level with tap water using a fully opened regular tap at mains water pressure; the tap is not fitted with a flow-meter and the rate of filling is unknown.

Mineral	Quartz	Albite	Microcline	Mica	Illite-smectite	Kaolinite	Chlorite	Hematite	Total
Percent content	33.7	1.0	1.0	1.5	30.8	18.0	7.7	5.7	99.4

Table 3-1. XRD analysis of potter's clay used as experimental beds.

	Test 1 /kPa	Test 2 /kPa	Test 3 /kPa	Ave /kPa
Sample 1	0.87	1.07	1.11	1.02
Sample 2	0.56	2.12	0.61	1.10
Sample 3	0.38	1.90	1.29	1.19
			Overall Ave /kPa	1.10

Table 3-2. Shear vane analysis of potter's clay used as experimental beds in erosion experiments.

3.2.3. Flow measurements

Flow velocities within the flume were calculated for different flow depths by use of a Sontek 10 MHz ADV (Acoustic Doppler Velocimeter) probe with 5 cm focal length. The ADV probe uses Doppler technology to measure 3-dimensional velocities at a fixed distance from the end of the probe, and calculates a downstream average velocity. The ADV was inserted into the flow from above so it measured the velocity of the flow at 0.4 of the flow depth, which is the height at which the velocity gradient of a turbulent open channel flow becomes independent of the basal boundary (von Karman, 1930). The calibrated results are shown in Table 3-3.

Flow Depth /cm	Flow Velocity cm/s	Pump Frequency /Hz
12.5	77.6	20
13	81.9	22
14	78.5	20
14	83.8	22
14	89.5	24
15	94.5	26
15	95.9	28
16	98.4	30
16	97.2	32
17	101.6	32
17	103.6	34
17	104.1	36

Table 3-3. Open channel flow velocities for the experimental slurry pump at given flow depths. The relevant pump frequencies are also shown.

For corrasion experiments, sand was gradually added to the flow manually so that it stayed fully suspended in the flow and never travelled as bedload within the channel. The sand was added to the flow downstream of the bed insert of the artificial floor so the sand had almost one full recirculation through the flume before it came in contact with the experimental bed. Initially, 5 kg of sand was added. In order to measure the concentration of sand in the flow, samples of the flow were taken using sample pots 6 cm long and 3 cm diameter. Samples were taken from just downstream of the experimental bed so that their presence in the flow did not affect the flow around the experimental bed. Sampling was performed at approximately one third of the flow depth by being placed into and then immediately removed from the flow; the sampling process lasted <1 second. These samples were then weighed and dried, then weighed again to calculate the concentration of sand in the sample containers. Each time the flume was drained during a pause in an experiment (such as to take photographs), some sediment was lost via the drain and an additional 3.5 kg of sand was added each time to compensate. This quantity of sand added to "top-up" the sand level was selected on a trial and error basis, however the average concentration was ~0.3 g/l, which is approximately the same concentration used during Allen's (1971) corrasion experiments (concentration of 0.30 – 0.44 g/l). The grain-size

distribution of the sand was determined using a Malvern Mastersizer 2000 laser grain-sizer; the nominal grainsize distribution is 190.9 μm (D10), 299.6 μm (D50) and 462.1 μm (D90) (Figure 3.5).

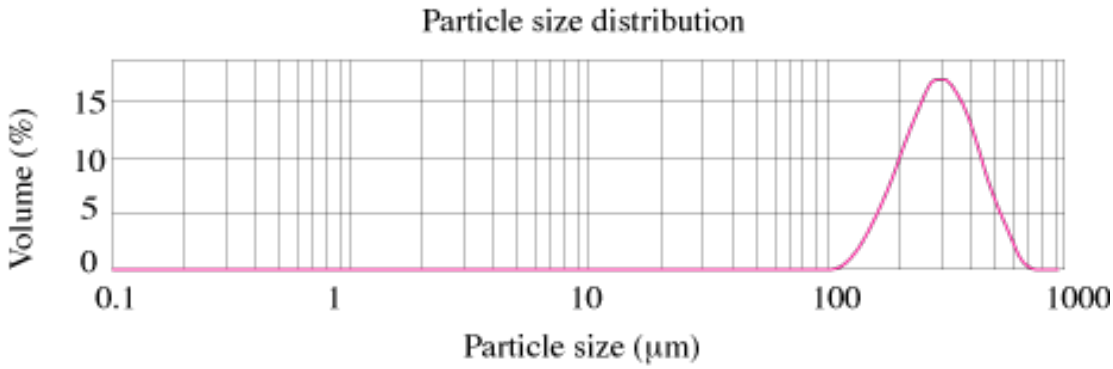

Figure 3.5. Particle size distribution for the sand suspended within experimental flows for corrasion. Red line shows average of three distribution measurements; all of which were in perfect agreement.

3.2.4. Bed measurements

The morphology of the experimental beds was measured via bathymetric profiling. twelve ultrasonic 5 MHz SeaTek probes were used to take depth measurements at 2 mm increments across the entire bed; the probes were arranged in a line 15 mm apart from one another, and mounted onto an XY traverse capable of moving the probes upstream (X) and across-stream (Y) with millimetre precision. Each single scan measured at a 2 mm (X) by 15 mm (Y) resolution (Figure 3.6a). In order to obtain a 2 mm resolution in both the X and Y directions, multiple scans were taken, each at different Y values to the previous. For each profile, 8 scans were taken that were subsequently stitched together to produce a 2 mm by 2 mm grid (Figure 3.6b). However one interval within this grid has a 1 mm by 2 mm resolution; because the 15 mm probe spacing would not allow 2 mm grid spacing throughout (see Figure 3.6b). These bathymetric data were processed using MATLAB coding (see Appendix B for data processing and interpolating codes) to provide accurate bathymetric and cross-sectional profiles along any plane.

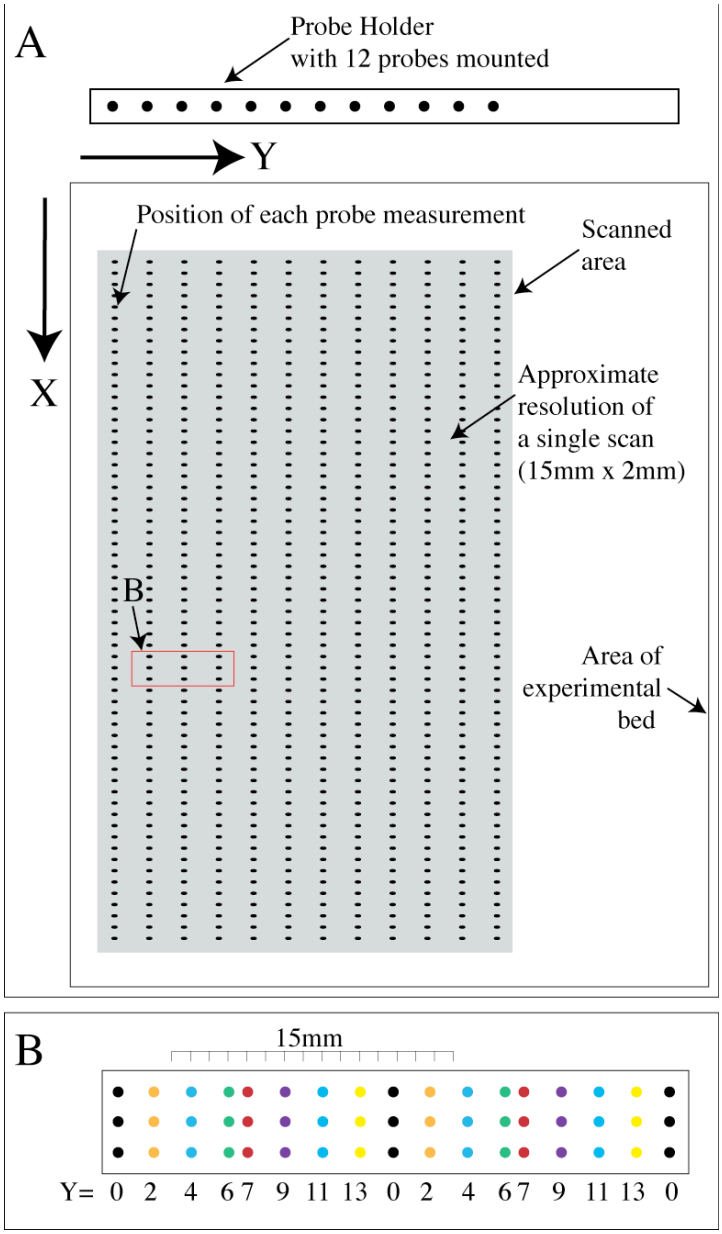

Figure 3.6. A plan view schematic of arrangement for bathymetric profiling of experimental beds. (A) The probe holder with 12 mounted probes performs each scan at 2 mm intervals in the X-direction. The approximate positions of readings are shown for a single scan with spacing's of 15 mm in the Y-direction. Subsequent scans are initiatied at different Y=locations, and the scans are combined to provide a resolution of 2 mm x 2 mm. (B) Detailed illustration shown for a single scan, shown as the red box in A.

3.2.5. Experimental method

During the course of each experiment the flows were temporarily stopped so that time-series bathymetric data and photographs could be collected. A 12 step experimental method was followed to ensure that consistency was maintained between experiments:

1. The experimental bed is placed into the insert in the artificial floor;
2. Bed surface was made flush with the surrounding artificial floor;
3. Flume tank was filled and the first scan (T0) initiated;

4. Flow was started within the flume and the experimental run begun;
5. For corrasion runs sand was added to the flow then sampled for concentration;
6. After the desired duration, the run was completed and the pump turned off;
7. The flume was drained and visual observations and photographs were taken (in the case of corrasion experiments some sand collected within the bedforms, often making them easier to see in photographs);
8. Flume was refilled;
9. Using a pipette, grains were gently flushed and loosened from within the bedforms (especially important in corrasion runs) so the surface that remained was a true representation of the eroded surface;
10. Bed morphology was scanned using the ultrasonic SeaTek probes;
11. For ongoing runs, the experiment returned to step 4.

3.3. Experimental results

3.3.1. Experimental beds of weakly cohesive china clay

The formation of Type 1 experimental beds via expelling water from a dilute china clay mixture within an odometer proved unsuccessful. The 111 kPa minimum load applied to expel water from the bed was too severe and caused the china clay mixture to be expelled though cracks in the odometer. The highest concentration mixture used (75% china clay) did not behave in this way, but produced an extremely hard clay bed that cracked the upper ceramic plate and was considered too hard to experiment with.

The formation of experimental beds by settled kaolin from suspension worked effectively, however they did not yield erosional bedforms and did not contribute morphological data to this investigation. After 48 hours of settling, a weakly consolidated bed had settled within the tray insert; the shear strength of the fresh beds was too small to be measured but they were estimated to be ~100 Pa (estimated via investigative shear vane tests by David Harbottle in the Faculty of Engineering, University of Leeds), which is comparable to those Allen (1971) formed via the same method. The tray inserts were awkward to insert into the flume (but could be inserted without compromising the bed). When the flow was initiated, the topmost layer of sediment became incorporated into the flow, making the flow opaque and preventing visual observations. When the flow was stopped and drained, the draw of the draining fluid across the surface of the bed sculpted low-profile (<2 mm height) wavy bedforms across the bed, obliterating any pre-existing bedforms that developed under the experimental flow. It was clear at the time of draining that these bedforms were actively developing under the draining flow, rather than being generated by the experimental flow as intended. Furthermore, the bathymetry of the beds could not be measured because the topmost layer of sediment was ‘transparent’ to the ultrasonic probes. The resulting scans were not a true representation of the morphology of the beds. As such, no data are presented for the morphology of kaolin experimental beds formed from suspension.

3.3.2. Experimental beds made of potter's clay

Experimental beds formed from potter's clay proved successful. A number of experiments were conducted in order to establish stable erosional experimental conditions, whereby the substrate was firm enough to develop and preserve bedforms, but not so firm that erosional bedforms did not develop. XRD analysis of the experimental beds demonstrate its likeness to naturally formed seafloor deposits, owing to its high quartz content and significant but lesser content of illite/smectite, kaolinite and chlorite. However regional studies suggest natural seafloor compositions vary in chlorite and kaolinite with latitude (Biscaye, 1965; Naidu et al., 1971). Experiments conducted with potter's clay were initially run without abrasive particles in the flow, thereby investigating the fluid stressing of firm beds. Experiments were conducted at a flow velocity of 96 cm/s and flow depth of 15 cm, using both an initially smooth bed and one with defects. The experiments were initially paused at 15-minute intervals but it quickly became apparent that no changes in bed morphology were developing. Subsequently, the experiments were paused at 2-hour intervals, and conducted for up to 24-hour durations. However all of these fluid stressing experiments failed to yield any bedforms.

The second set of experiments investigated the corrasion of firm mud beds made of potter's clay. All these experiments proved successful. A number of test experiments were conducted before a satisfactory experimental method was established, and the data from these early test experiments are not presented. Four representative experiments are presented herein; see Table 3-4 for experimental parameters. Each experiment was paused at 15 minute intervals so bathymetric scans and photographs could be taken, but in some cases towards the end of experiments only photographs were taken (see Table 3-5 for scanning and photographing details).

Experiment number	Flow velocity /cm.s^{-1}	Flow depth /cm	Total flow duration /mins
1	95	14	300
2	85	14	120
3	95	14	120
4	90	14	240

Table 3-4. Experimental parameters for experiments investigating corrasion of firm mud beds.

Time	Experiment 1		Experiment 2		Experiment 3		Experiment 4	
	Scanned	Photo'd	Scanned	Photo'd	Scanned	Photo'd	Scanned	Photo'd
0	✓	✓	✓	✓	✓	✓	✓	✓
10	✓	✓	✓	✓	✓	✓	✓	✓
30	✓	✓	✓	✓	✓	✓	✓	✓
45	✓	✓	✓	✓	✓	✓	✓	✓
60	✓	✓	✓	✓	✓	✓		✓
75	✓	✓	✓	✓	✓	✓		✓
90	✓	✓	✓	✓	✓			✓
120	✓	✓	✓	✓				✓
180	✓	✓						✓
240	✓	✓						✓
300		✓						

Table 3-5. Table showing the experimental time intervals used for experiments 1 to 4, and the nature of data collected during each paused interval; either bathymetric scans obtained via Seatek probes (*scanned*), or photographed from above *(photo'd)*.

Experiment 1 was performed with a flow velocity of 95 cm/s and a flow depth of 14cm, for a total of 300 minutes. The time series photographs illustrate the development of bedforms (Figure 3.7). During the first 60 minutes, the initially smooth bed surface developed low profile (<1 – 2 mm) wavy topography with some small pock-marks 5 – 10 mm across. These small marks expanded between 60 and 90 minutes, developing limbs that flared widely downstream becoming deeper; many of these flutes developed in the locality of pock-marks. The experimental bed had a clearly 'fluted' appearance from T90 onwards; comprising numerous narrow (5 – 15 mm), sinuous crested flutes and several heel-shaped flutes. One section of the bed failed plastically, leaving a 3 cm wide circular void in the centre of the bed (see void, T90, Figure 3.7, indicated by yellow arrow). With further erosion time, this void developed into a widely flaring, shallow flute, and by T300 the mark had developed lateral furrows upon each limb (see T300, Figure 3.7). The development of two other flutes during the same experiment is presented in Figure 3.8; one is a widely flaring flute (white dashed line); the other is a narrower sinuous flute (white arrow). The widely flaring flute develops from a pock-mark (Figure 3.8, T10), and appears to be expanding via the downstream propagation of the erosional hollow (see above dashed line, T10 - T90, Figure 3.7). However this hollow developed into a

30cm
T10

T30

T45

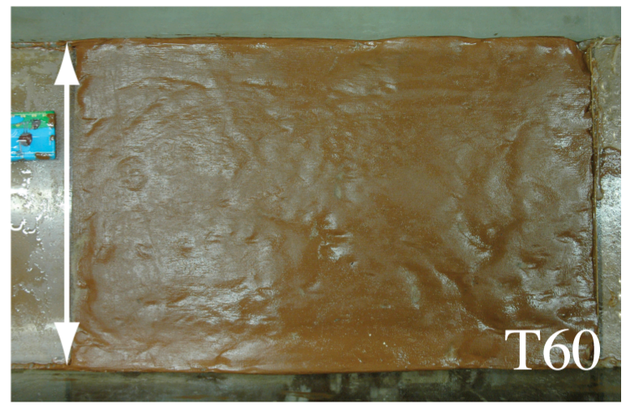
T60

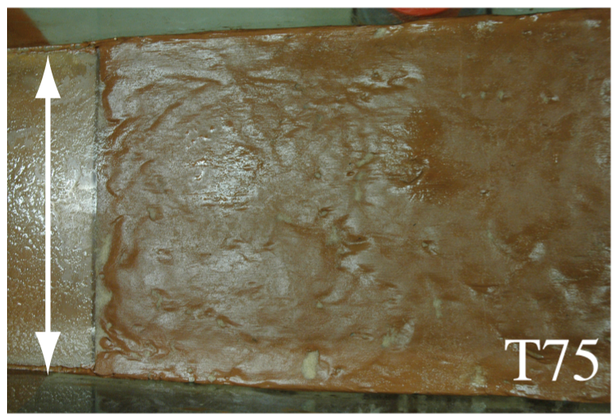
T75

T90

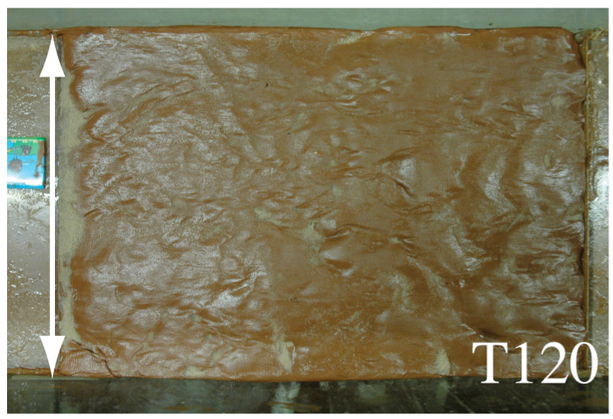
T120

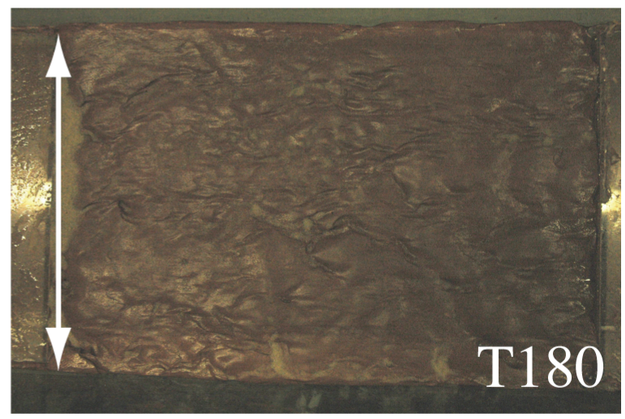
T180

T240

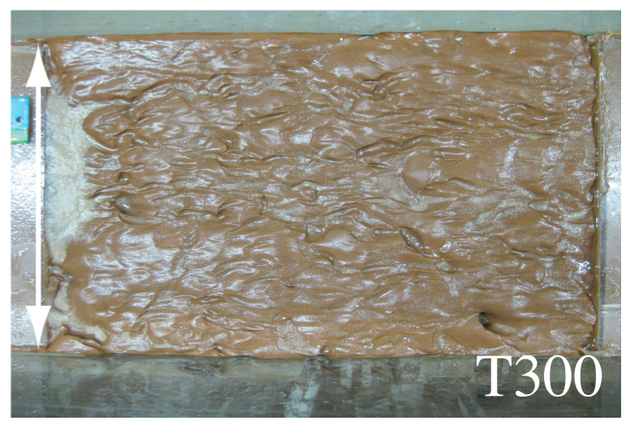
T300

Figure 3.7. Plan view photographs of the experimental bed of Experiment 1 showing bedform development with time (in minutes). White arrows to left of each photograph shows the 30 cm flume width. Yellow arrow (T90) shows a void formed by plastic failure of the bed. White box (T300) indicates position of time-series photographs shown in Figure 3.8 Flow is from left to right. Note photo-series starts at T10.

downstream extending limb and the flute grew with a median ridge during T90 to T180, which was then eroded into a single furrow ~4 cm wide (T180 – T300, Figure 3.7). In contrast, an immediately adjacent pock-mark developed into a narrow flute (see white arrow, T10 – T180, Figure 3.8) before becoming slightly twisted (T240 – T300, Figure 3.8). At T300, an isolated flute with downstream pointing limbs developed that was much deeper than all the other features (14 mm deep) (Figure 3.7, T300, see far bottom right of photograph).

Experiment 2 (17) was run with a low flow velocity at 85 cm/s and initially developed low profile waves (T0 – T30, Figure 3.9) similar to those in experiment 1. However, unlike in experiment 1, the bed developed low profile gullies (2 – 3 mm deep) that extended downstream along the length of the experimental bed ~ 6 cm in from the walls of the flume; the most noticeable of these is seen in the upper part of the photographs T15 – T45 (Figure 3.9, white arrows). These low profile gullies did not develop into prominent gullies on the bed, however after 120 minutes of experimental time one developed into a 30 cm-long sinuous crested flute, immediately adjacent to the flume wall (Figure 3.9, Figure 3.10, red arrow). Pock-marks developed across the bed during T30 – T45, and developed into flutes from T60 onwards; two types of flute are recognisable on the bed: (1) a narrow (4 mm – 10 mm) and deep (4 mm – 8 mm) sinuous crested flute that has a simple U-shaped across-stream profile (Figure 3.11, yellow arrows), and; (2) a broad (30 mm – 50 mm) more shallow (2 mm – 9 mm) flute that is twisted downstream and has one or more lateral furrows, creating a cuspate across-stream profile (Figure 3.11, red circles). Two time-series cross sectional profiles are presented - one downstream (Figure 3.11) and one across stream (Figure 3.12) - both of which pass through the same broad, shallow flute, as well as other features (see also Figure 3.10). The profiles show the whole experimental bed has been eroded so that the bed at each

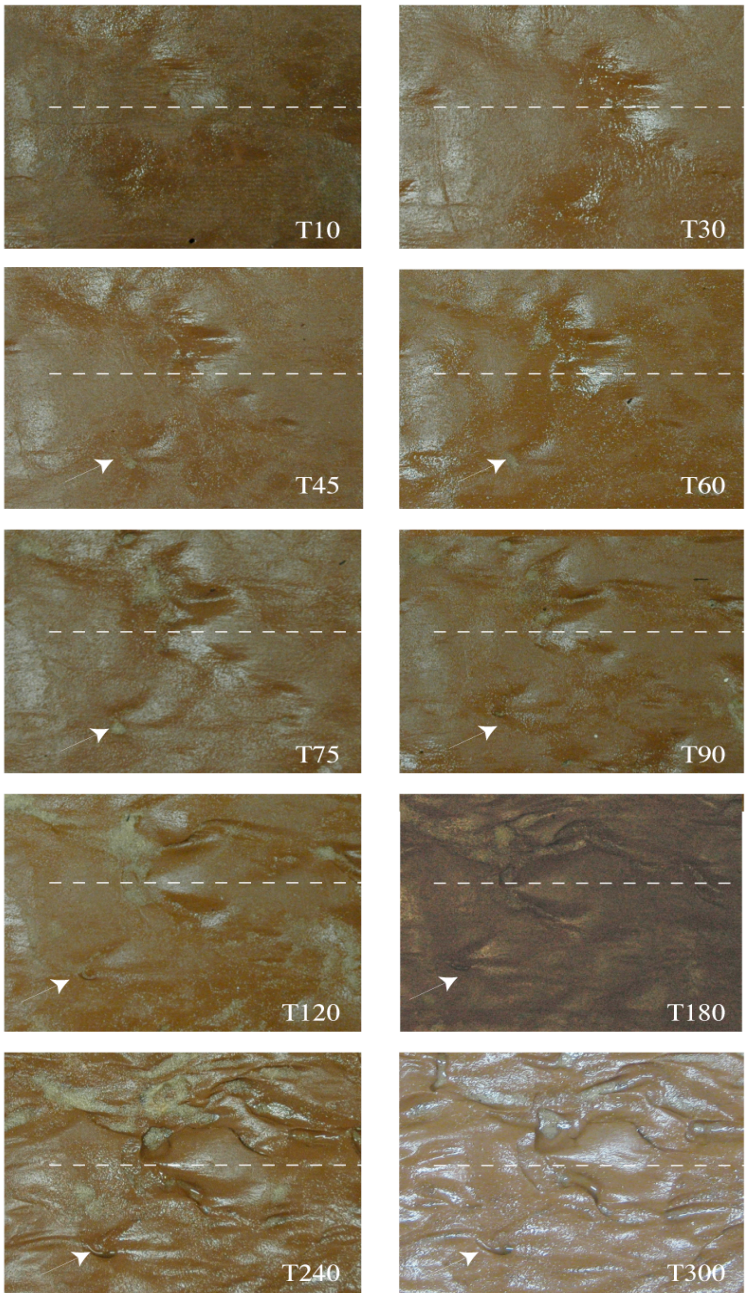

Figure 3.8. Time series of photographs for Experiment 1 showing the development of two flutes, over 300 minutes. Location of photographs with respect to the whole bed is shown in Figure 3.7, T300, white box. Photograph widths are 14 cm. Flow from left to right. White dashed line shows a fixed position, marking the development of a flute that has an internal positive relief that is eroded to a depression between T90 and T120. White arrow (T45-T300) shows the position of a developing narrow, sinuous flute.

time interval is progressively deeper than the previous; this also indicates that no deposition occurred along these profiles. The downstream profile (Figure 3.11) shows all topographic features have migrated downstream with time, including the flutes leading point and deepest point. Two features of interest, the broad flutes BF1 and BF2 (see Figure 3.11), have both expanded with time and become progressively deeper and longer with continued erosion. The across stream profiles show progressive erosion across the whole bed, with the narrow, deep flute becoming narrower with time, and the broad shallow flute becoming deeper, and developing from a W-shaped cross sectional profile into a U-shaped one (Figure 3.12).

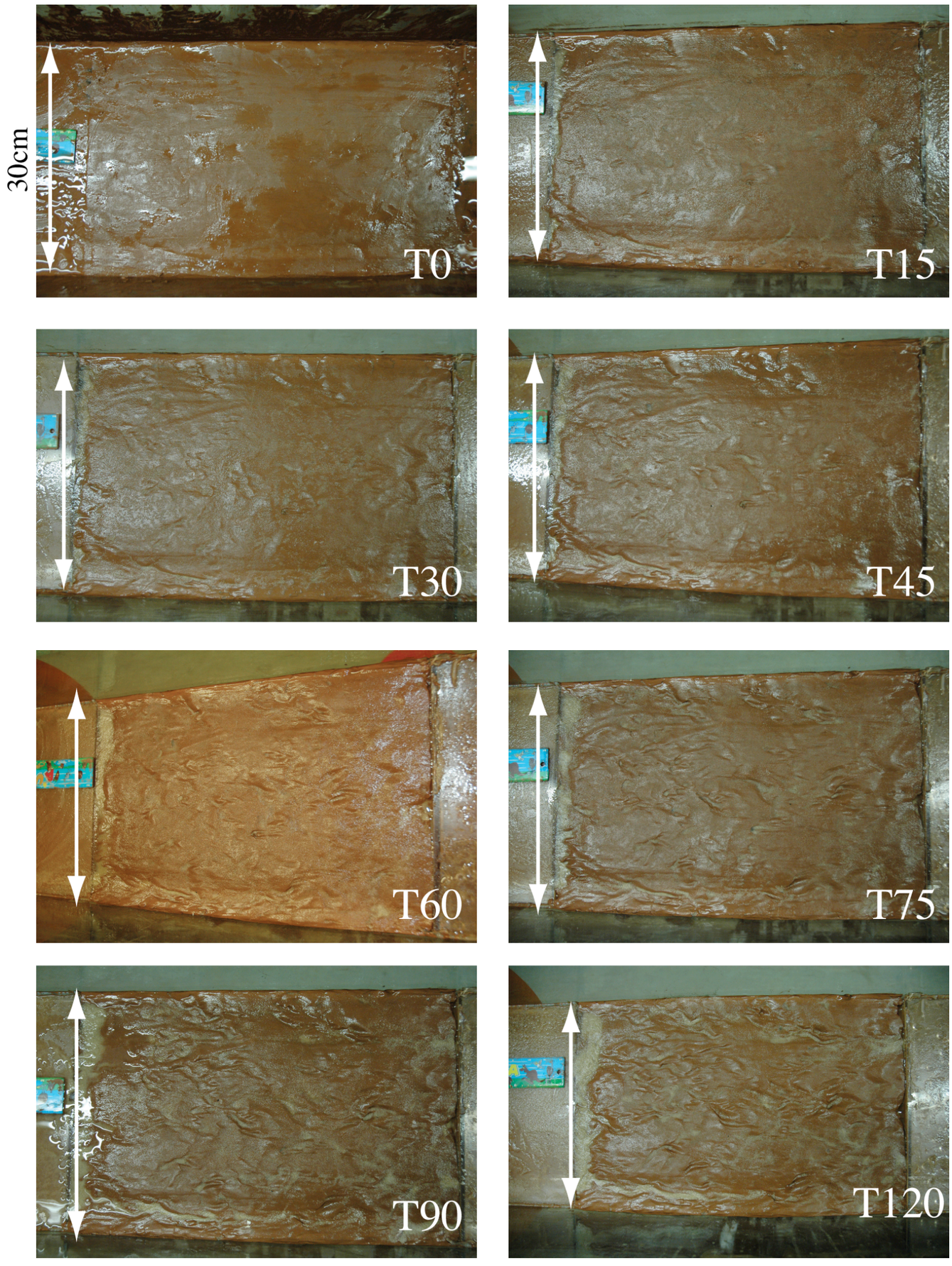

Figure 3.9. Plan view photographs of the experimental bed of Experiment 2 (17), showing bedform development with time (in minutes). White arrows to left of each photograph shows the 30 cm flume width. Flow is from left to right

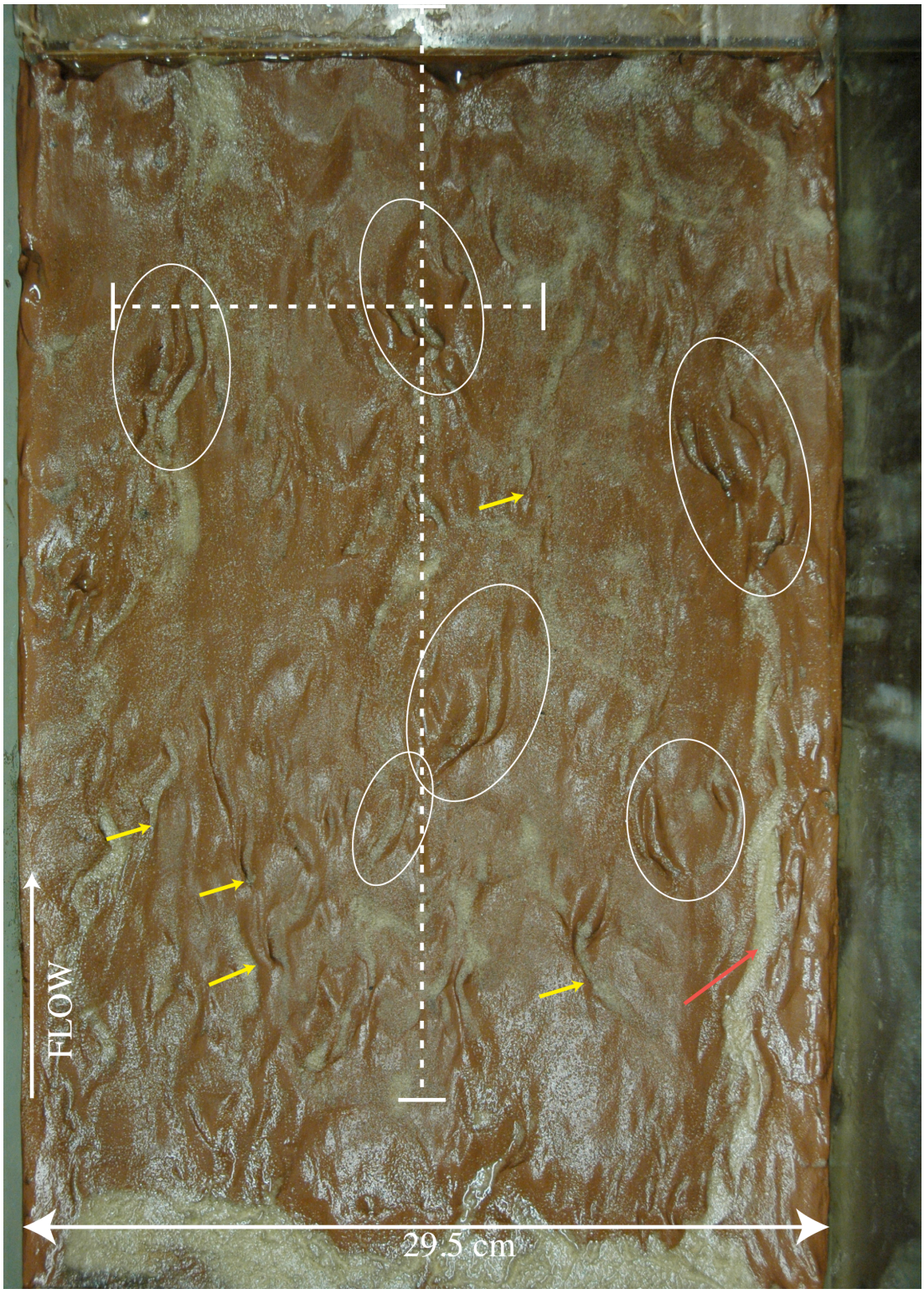

Figure 3.10. Planform view of the experimental bed for Experiment 2 after 120 minutes (T120). Two types of flutes are observed: i) narrow (4 mm – 10 mm), deep (4 mm – 8 mm) sinuous crested flutes that have a simple U-shaped across-stream profile; shown by yellow arrows, and (ii) broad (30 mm – 50 mm) more shallow (2 mm – 9 mm) flutes that are twisted

downstream and have one or more linear ridges, shown by white circles. The red arrow shows a 26 cm long narrow sinuous flute that originated from a gully. Dashed white lines show the positions of the cross sectional profiles of Figure 3.11 (downstream) and Figure 3.12 (across stream). The experimental bed is 29.5 cm wide.

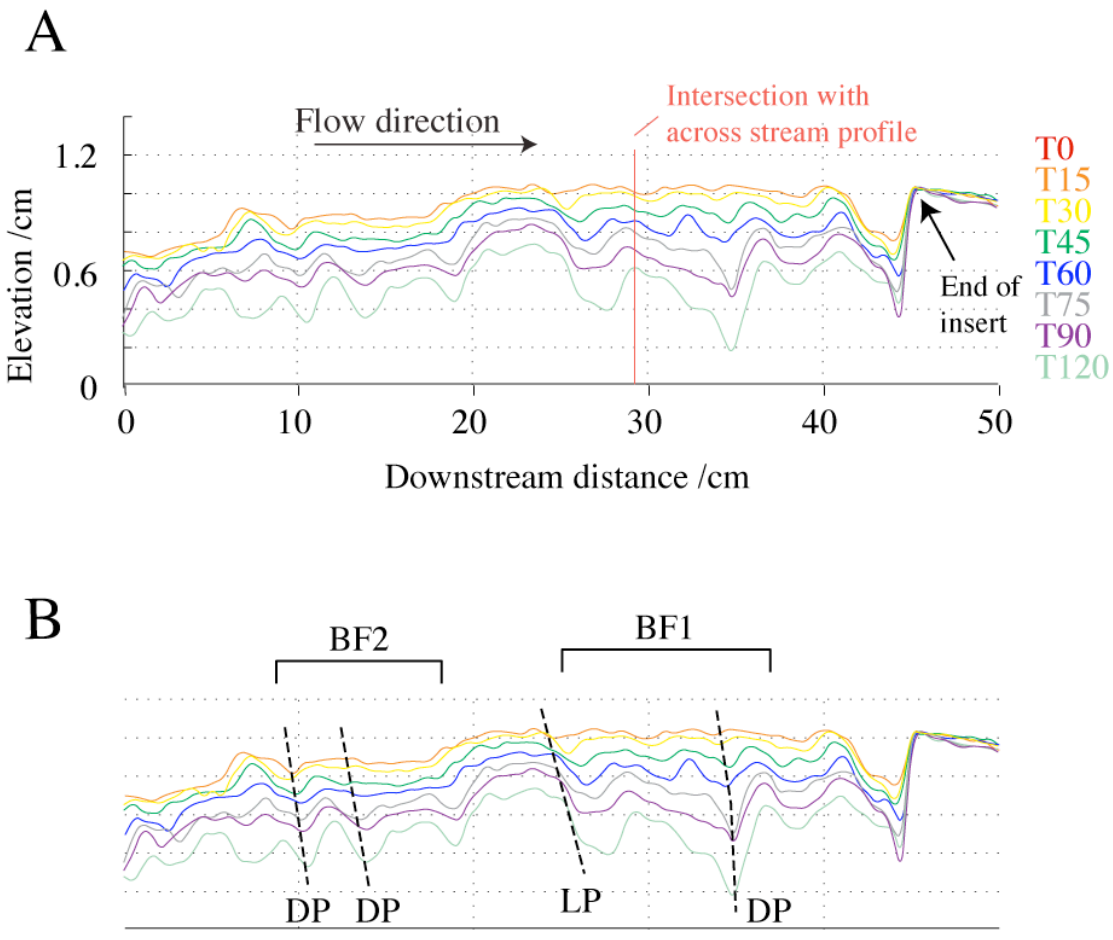

Figure 3.11. Downstream cross sectional profiles of experimental flutes; Experiment 2 (17). Flow direction is left to right; profile times shown in colours to the right. See Figure 3.10 for location. (A) Downstream cross-sectional profiles. (B) Downstream profiles with position of broad flutes (BF) indicated and the downstream migration of their leading points (LP) and deepest points (DP) labelled.

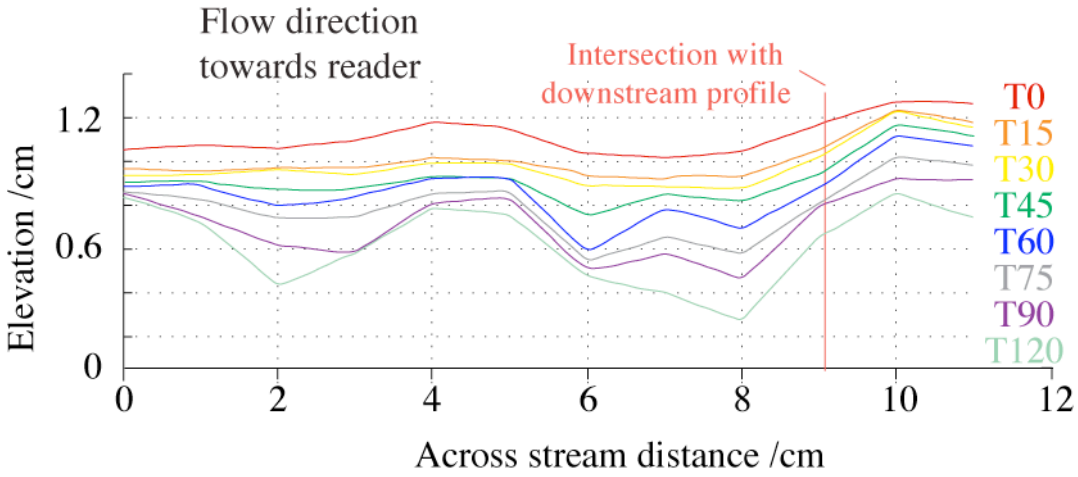

Figure 3.12. Across stream, time-series, cross-sectional profiles of experimental flutes. Experiment 2 (17). Flow direction is away from the reader. Profile times shown in colours to the right. See Figure 3.10 for location.

Experiment 3 was a repeat of experiment 1, with the same experimental conditions and parameters of 95 cm/s flow velocity and 14 cm flow depth. However, the experiment was stopped at 90 minutes after the probes were accidentally knocked out of alignment, thus making any following scans incompatible with the earlier ones. As in experiment 1, the bed initially developed low profile wavy topography with some small pock-marks 1 – 10 mm across; the downstream cross-sectional profile shows the downstream migration of these low-profile waves (Figure 3.14). By T75 some of these pock-marks developed into flutes 20 – 30 mm long and up to 15 mm wide, however the bed did not have an overwhelming fluted appearance such as at T300 of Experiment 1 (Figure 3.7). The profile also shows the bed morphology presented at any given time interval is very similar to the scan before it, indicating a very even rate of erosion across the bed. It is also worth noting that the experimental bed had ~ 4 mm of relief at T0, and the morphology of the eroded beds bears a resemblance to this initial T0 bed (Figure 3.14b).

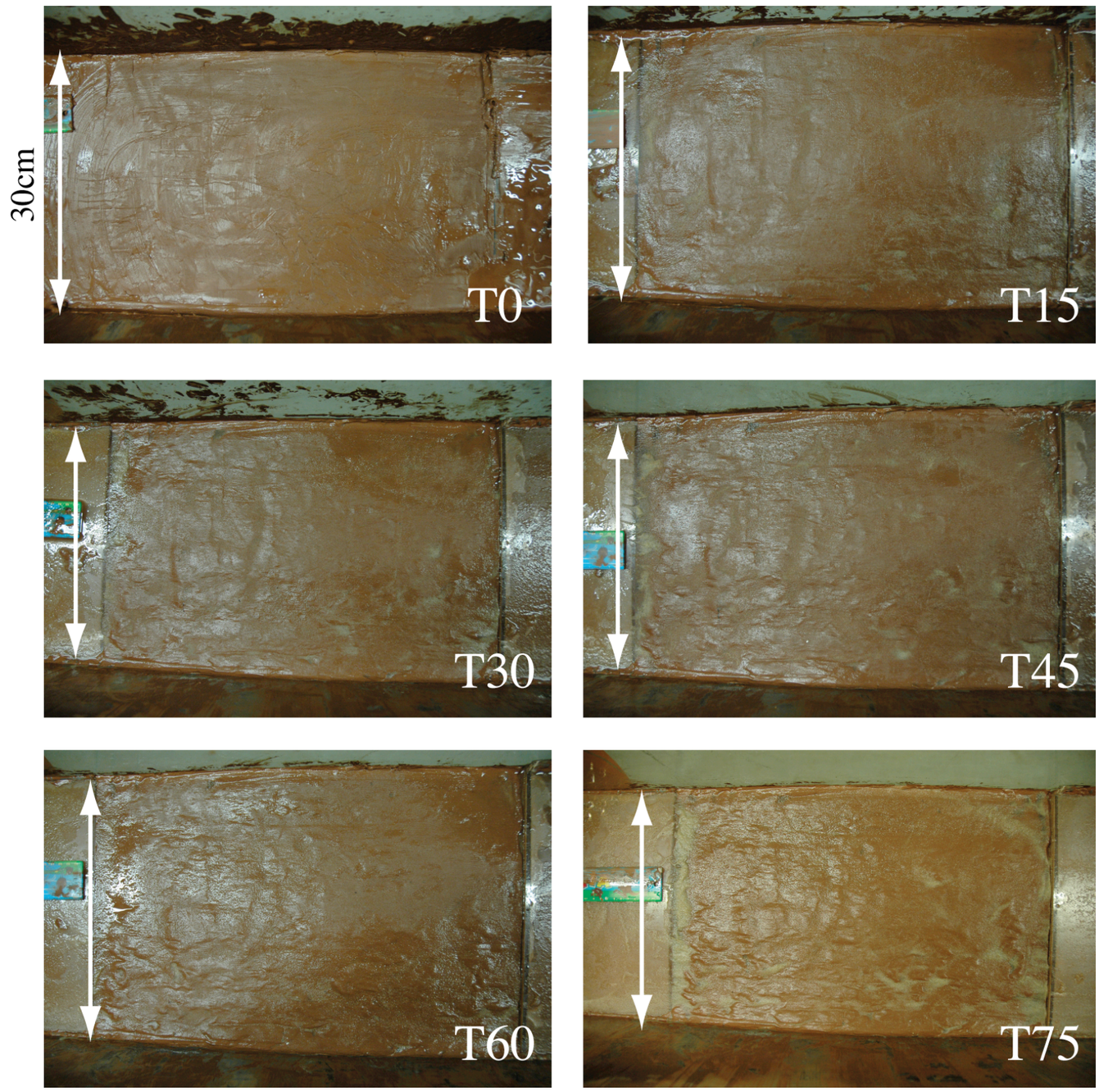

Figure 3.13. Plan view photographs of the experimental bed of Experiment 3 (22), showing bedform development with time (in minutes). White arrows to left of each photograph shows the 30 cm flume width. Flow is from left to right

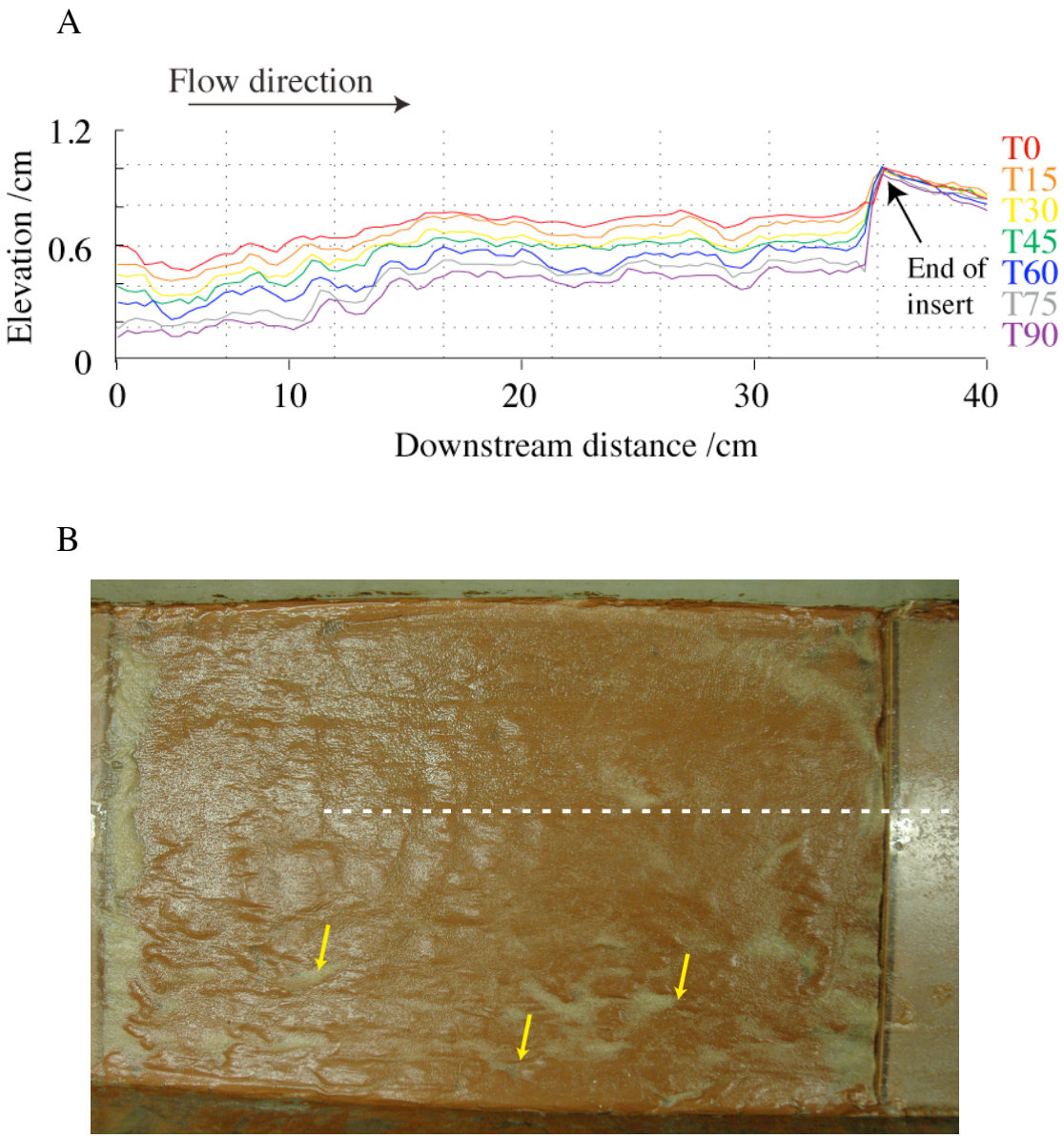

Figure 3.14. A. Downstream time-series cross sectional profiles of experimental flutes; Experiment 3 (22). Flow direction is from left to right. Profile times shown in colours to the right. B. Plan view photograph of experimental bed; Experiment 3 (22). White dashed line shows the position of the profiles in A. Yellow arrows show the position of flute marks in the early stages of formation. Flow direction is left to right.

Experiment 4 was performed at a flow velocity of 90 cm/s with a flow depth of 14 cm, for a total of 240 minutes. The experimental bed developed in a similar manner to previous experiments, with low-profile wavy topography developing up to T45 (Figure 3.15). These sediment waves are visible on the time-series cross-sectional profiles (Figure 3.16); though curiously, the profiles show the sediment waves were present at T0. The sediment waves were not observed on the bedding surface at the time of the experiment, and are not visible on the T0 photograph (Figure 3.15). The waves must therefore have developed between smoothing/photographing the bed, and taking the bathymetric data. The downstream time-series cross sectional profiles indicate the bed experienced net erosion and the sediment waves migrated downstream with time (Figure 3.16). Pock-marks were clearly visible on the experimental bed by T45, and one had failed plastically by T60, developing into an irregularly shaped hollow 5 cm long and wide, with a sharp outer rim (Figure 3.17). Despite being the most prominent feature on the bed at T60, this hollow did not develop into a major flute, and was no longer recognizable on the bed by T120. By T120, the experimental bed was fully fluted, featuring mostly narrow (5 – 10 mm), deep (2 - 6 mm) flutes of between 2 and 7 cm length, but notably lacking the broad, flat flutes that were observed in Experiment 2 at T120. Between T120 and T240 the bed morphology changed character and started to develop a series of straight, flat-bottomed gullies between 3 and 5 cm wide (Figure 3.15 and Figure 3.18); the best developed of these ran along the flume wall (~ 6 cm away from the wall) and down the centre of the bed. The gullies are aligned downstream, parallel to flow (Figure 3.19) and are flanked by a series of deep (6 – 12 mm) sub-circular or sub-lunate closed features, referred to herein as potholes (Figure 3.18 and Figure 3.19). These potholes are located in two groups ~ 5 cm distance from the gullies, and occur among flutes. Two of the potholes have overhanging rims (see Figure 3.19, lower left two features). The intermediate region between the gullies and potholes is not fluted or gullied, but is smoothed with low-profile (1 – 3 mm) undulating topography (Figure 3.18).

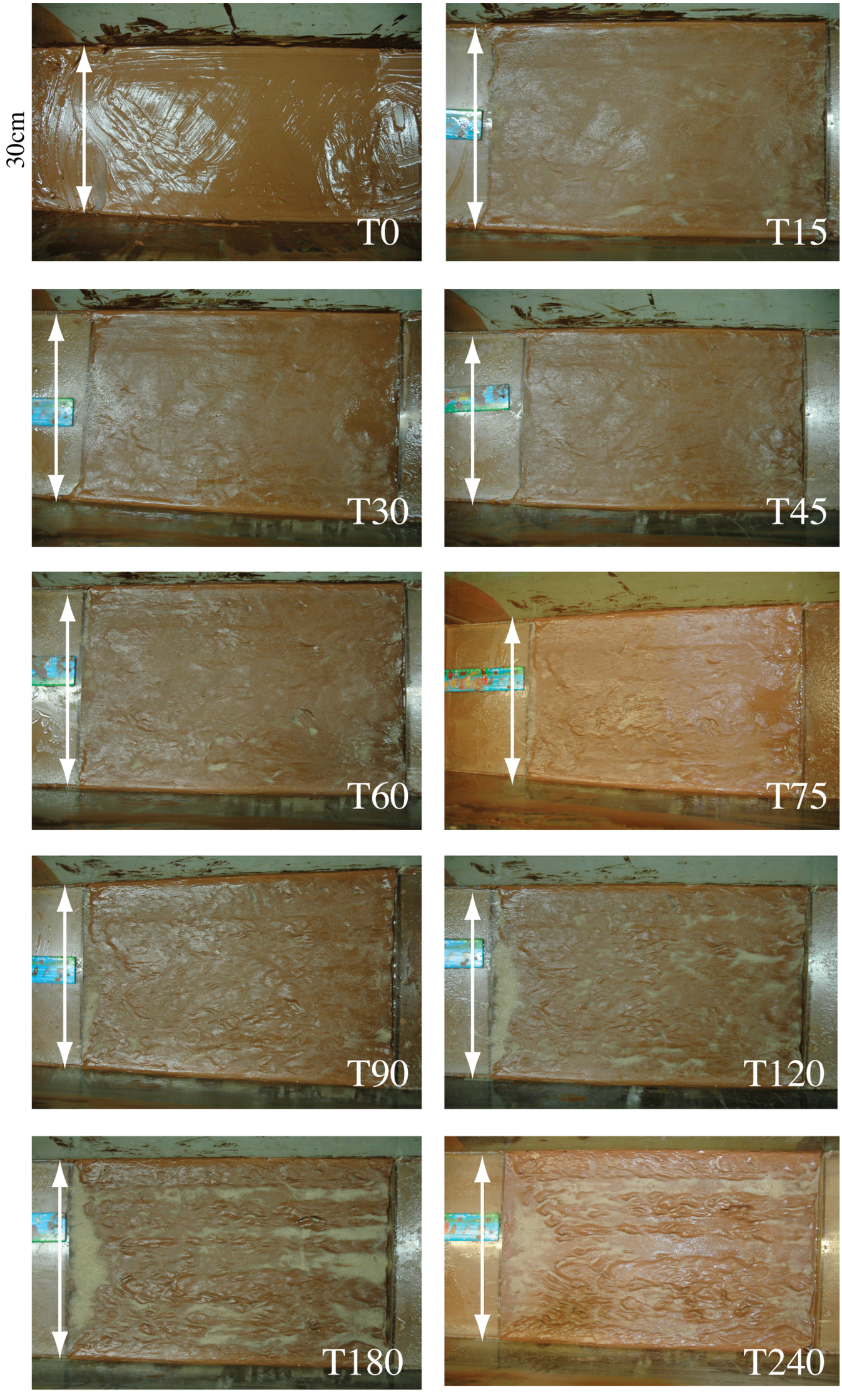
30cm
T0
T15
T30
T45
T60
T75
T90
T120
T180
T240

Figure 3.15. Plan view photographs of the experimental bed of Experiment 4 (24) showing bedform development with time (in minutes). White arrows to left of each photograph shows the 30 cm flume width. Flow is from left to right. Note photo-series starts at T10.

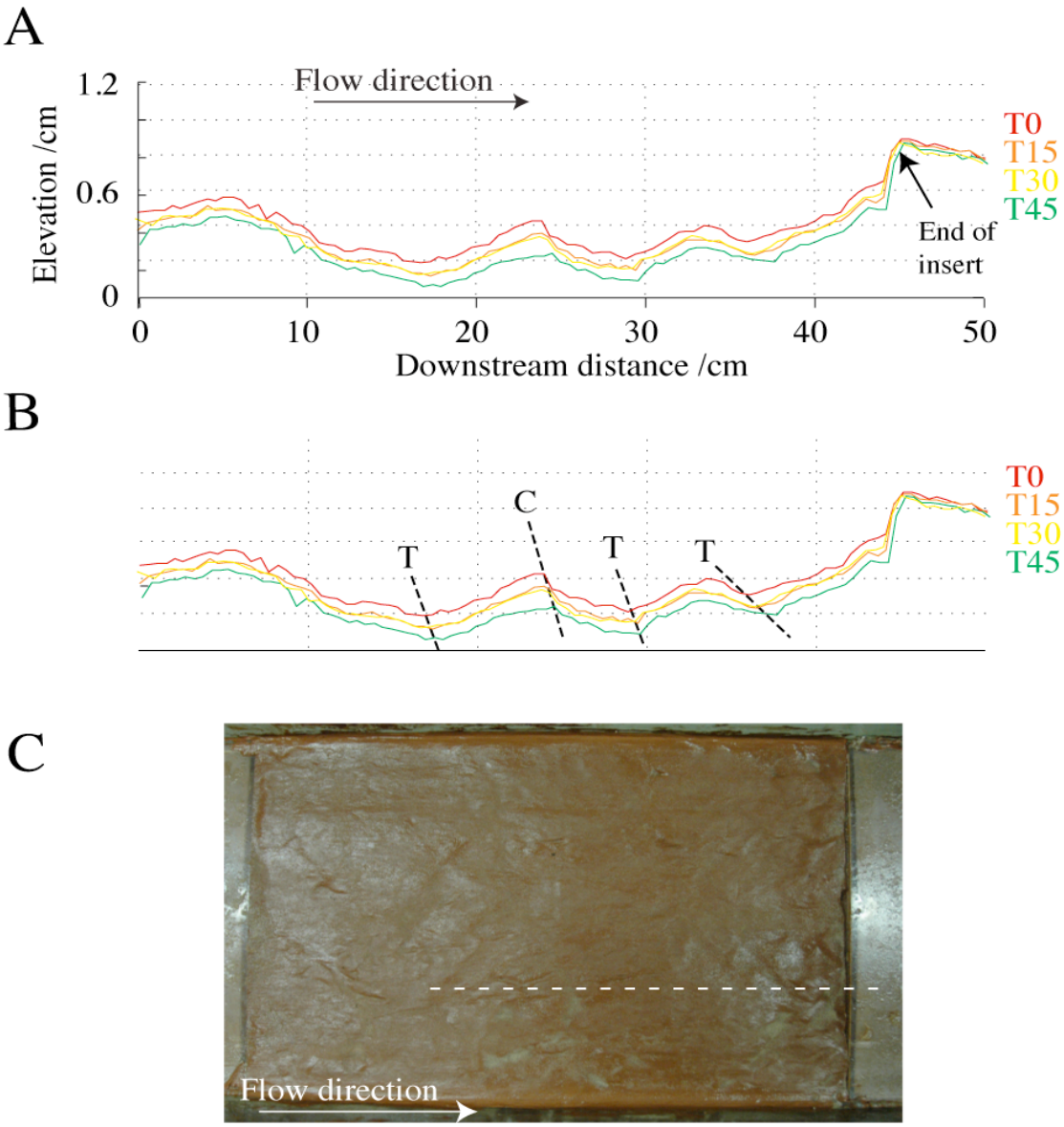

Figure 3.16. A. Downstream time-series cross sectional profiles of shallow wavy topography on experimental bed; Experiment 4. Flow direction is from left to right; profile times shown in colours to the right. (A) Downstream cross sectional profiles. (B) Downstream profiles indicating the crests *C* and troughs *T* of waves, and track their downstream migration with time. Note erosion is experienced across the whole bed. C. Plan view photograph of experimental bed at T45; white dashed line shows the position of the profiles in A and B.

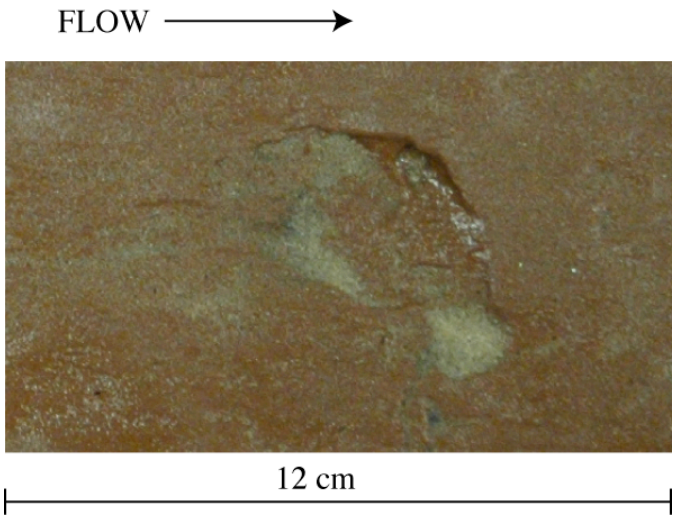

Figure 3.17. Plastically failed erosional mark on experimental bed after 60 minutes. Experiment 4 (seen in Figure 3.15, T60, lower right from centre of photograph). Flow is from left to right, photograph shows 12 cm width. Note the sharp downstream rim to the top of the photograph.

Figure 3.18. Experimental bed after 240 minutes of erosion (T240), Experiment 4. Flow is towards the reader, and the glass walls of the flume are clearly visible to the side of the photograph. The experimental bed is 29.5 cm wide. Yellow arrows indicate deep, hollow pock-marks. Blue arrows indicate the position of two pronounced gullies aligned downstream; one in the centre of the experimental bed and one in close proximity to the flume wall (on right).

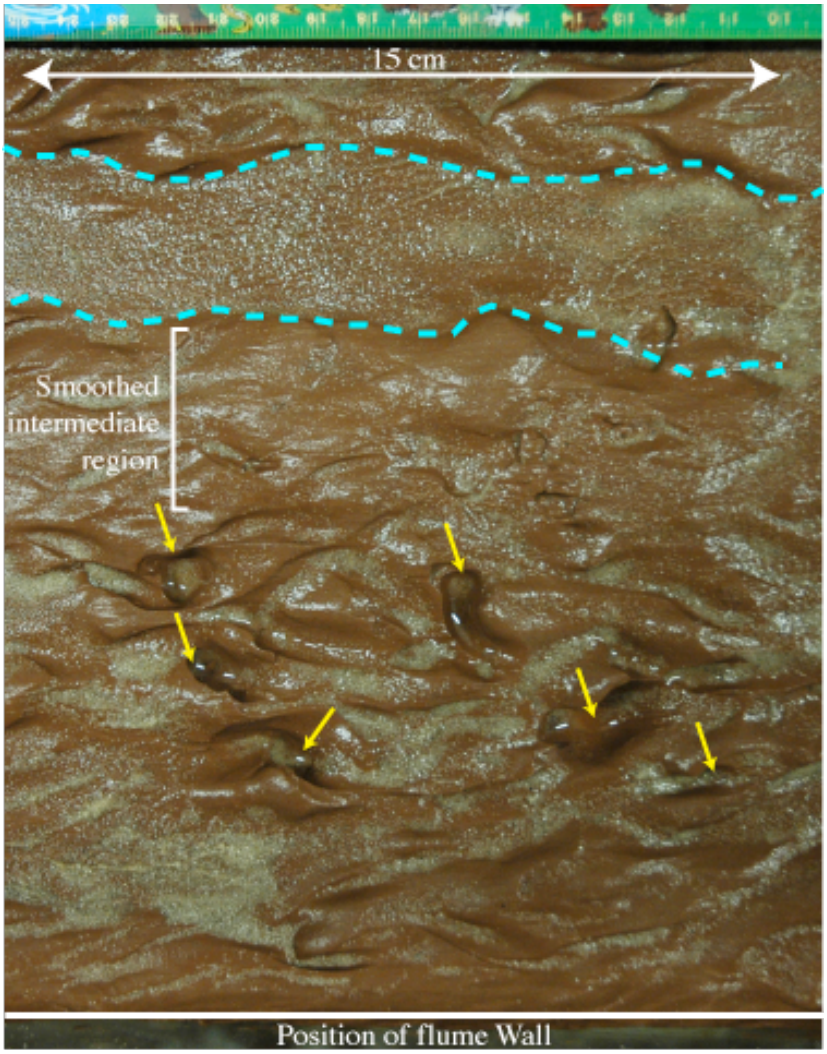

Figure 3.19. Plan view photograph of experimental bedforms. Experiment 4. Flow direction was from left to right. Blue dashed lines highlight flat-bottomed erosional gully with gently sinuous margins. Yellow arrows indicate position of deep (6 – 12 mm) closed potholes.

3.4. Summary of experimentally produced bedforms

In each of the experiments documented here, the experimental bed developed in an initially similar way with the generation of low profile (0.5 – 2 mm deep) wavy topography during at least the first 30 minutes. However, in experiment 4, the waves appear to have developed following the photographing of the bed, but prior to the scanning of the bed (Figure 3.15a, Figure 3.16). Subsequent bedform development included the generation of shallow (1 – 3 mm deep), sub-circular (5 – 10 mm across) hollows, termed pock-marks which were present on all beds by T45. The low velocity experiment (Experiment 2; 85 cm/s) developed shallow (2 – 3 cm deep) gullies in close proximity to the flume walls during the first 75 minutes of experimental flow. By T120, other features on the bed had obscured one of these gullies, and the second gully had developed into a long (30 cm), sinuous crested flute with U-shaped cross-section. This experiment developed two recognisable types of flute: 1. narrow (4 mm – 10 mm) and deep (4 mm – 8 mm) sinuous crested flutes that have a simple U-shaped across-stream profile; 2. broad (30 mm – 50 mm) more shallow (2 mm – 9 mm) flutes that are twisted downstream and have one or more linear ridges, creating a cuspate across-stream profile. The medium velocity experiment (Experiment 4 (24; 90 cm/s) yielded the narrow variety of flute, but did not develop the broad shallow type. However during the final stages of the medium velocity experiment two features developed that were unique across all the experiments: 1. a series of straight, flat-bottomed gullies between 2.5 and 4 cm wide (Figure 3.15, T240), that ran down the sides (~ 6 cm from the flume wall) and the centre of the experimental bed, and; 2. a series of deep (6 – 12 mm) sub-circular or sub-lunate closed features, referred to as potholes (Figure 3.18, Figure 3.19). Both features developed upon a fully fluted surface; the gullies developed first at ~ T120 onward, followed by the potholes at ~T180 onward. A single pothole also developed after T180 in experiment 1. Notably in experiment 4, the region between the gullies and potholes became progressively more smoothed with continued erosion. Direct comparisons between photographs of the two high-velocity experimental beds show the bedforms to be developing equally in each experiment. A summary figure is presented in Figure 3.20.

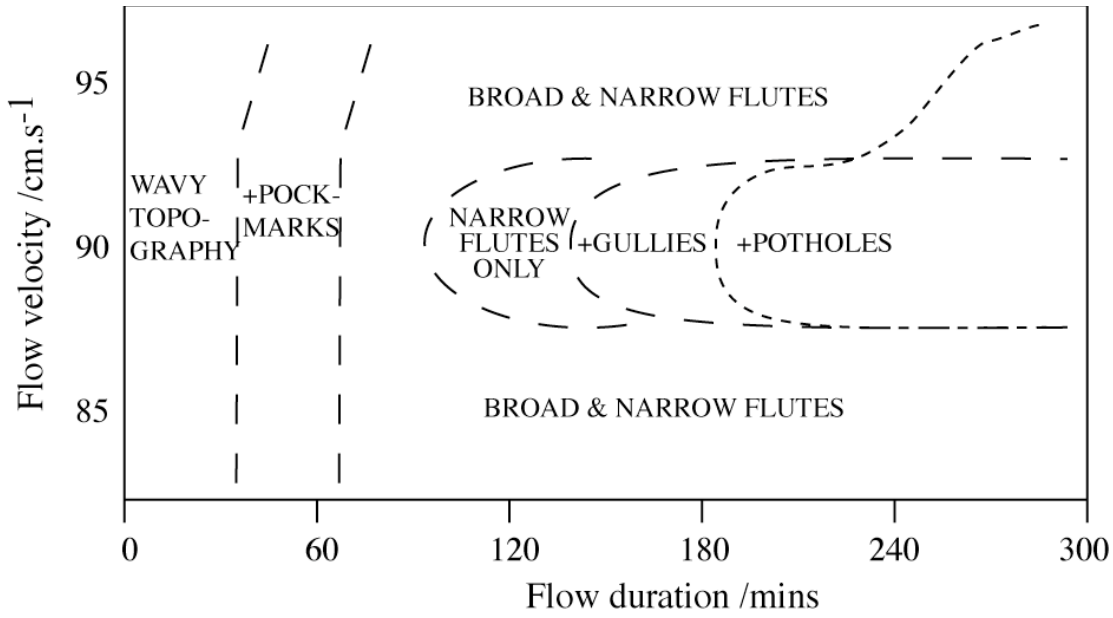

Figure 3.20. Summary bedform diagram for results of experimental work on erosion of mud beds.

3.5. Description of experimentally produced erosional bedforms

3.5.1. Wavy topography

Wavy transverse topographic features (<1 – 6 mm height and 20 – 50 mm wavelength) developed across the width of the experimental bed (Figure 3.21a). The waves were the first features to develop upon the initially smooth experimental bed, but were later lost due to the formation of other morphological features. Downstream cross-sectional profiles through the waves indicated that they were associated with net erosion across the bed, and their troughs and crests migrated downstream (e.g. Figure 3.14 and Figure 3.16).

3.5.2. Pock-marks

Pock-marks developed on the experimental beds after the formation of transverse waves (Figure 3.21b). The marks developed as shallow (1 – 3 mm deep), sub-circular (5 – 10 mm across) hollows that were present on all beds by T45. They developed throughout the wavy bed, apparently unrelated to wave crests or troughs.

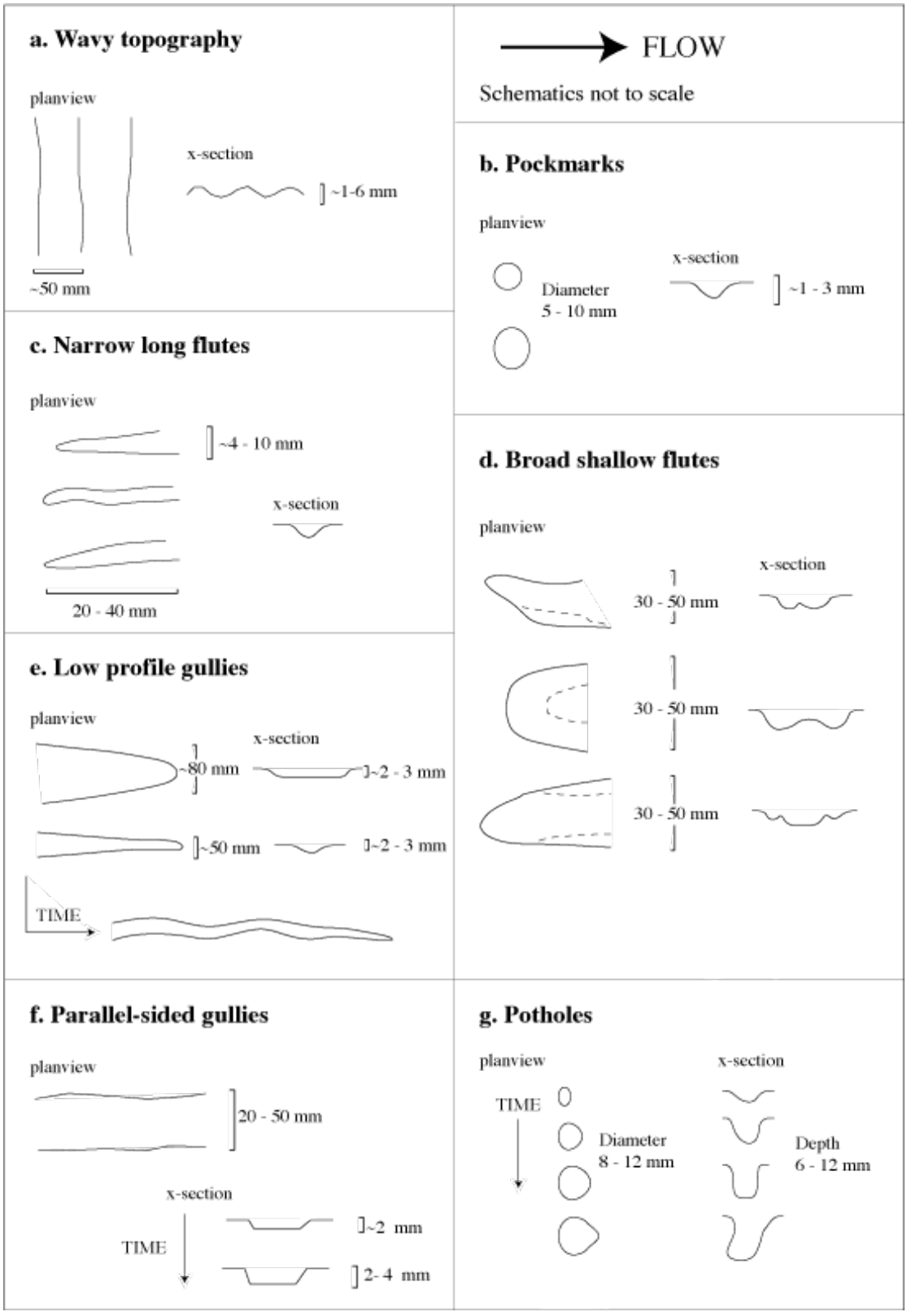

Figure 3.21. Schematics to illustrate the erosional bedforms produced during experimental runs presented in this chapter. Approximate dimensions are shown; bedforms are shown in planview and cross-section across flow. For planview figures, flow direction is left to right. Schematics shown are not to scale.

3.5.3. Narrow, long flutes

Narrow, long flutes (Figure 3.21c) formed after the development of pock-marks in every experiment. They were between 4 – 10 mm wide, 20 – 40 mm long and 4 – 8 mm deep, with sinuous crests and a simple U-shaped across-stream profile. They bear resemblance to the comet-, corkscrew- and twisted-flutes of Allen (1971), being many times longer than they are wide, and having between 1 and 4 curves down the length of the mark. In contrast to Allen's (1971) comet- and twisted-flutes, the narrow long flutes created here never develop a median ridge, and commonly comprise just one furrow, rather than a number of lateral furrows and ridges. Their formative location is closely associated with the location of previously formed pock-marks.

3.5.4. Broad, shallow flutes

Broad shallow flutes created here formed dominantly in the medium velocity experiment as broad (30 mm – 50 mm width) more shallow (2 mm – 9 mm) flutes that are approximately as wide as they are long (Figure 3.21d). The flutes are generally twisted downstream and have one or more lateral ridges, creating cuspate across-stream profiles. These flutes are comparable to the 'broad parabolic' and 'simple' flutes of Allen (1971), but almost always deviate away from a simple parabola.

3.5.5. Gullies

Gullies formed on the experimental bed during two different experiments, each at different stages. The first type developed parallel to flow along the sides of the experimental bed, during the first 15 minutes of experimental erosion. This type of gully became narrower along its length (Figure 3.21e; from 8 cm to a point) and remained low profile, not exceeding 3 mm depth at any stage during the experiment. The second variety of gullies developed during the latter stages of erosional runs; they were flat-bottomed with gently sinuous edges (aligned parallel to flow) and were low in profile, initially being ~2 mm deep (Figure 3.21f). With time, these gullies did not expand in width, but became gradually deeper, to ~4 mm depth.

3.5.6. Potholes

Potholes developed following T180, as shallow (4 – 12 mm deep), sub-circular (5 – 10 mm across) marks that have an approximate U-shape both across-stream and downstream (Figure 3.21g); more mature marks (experimental duration >T180) developed a skewed downstream cross sectional profile so that the upstream-facing rim becomes gently inclined downstream, whereas the downstream edge remains steep-to-vertical and in some cases even becomes overhanging (Figure 3.21g). Potholes appear to have not previously been documented in fluid stressing or corrasion experiments.

3.6. Discussion

The experimental work presented here produced flutes successfully but only for certain experimental conditions. Attempts to experiment with weakly cohesive mud beds failed because the bed was too soupy and did not preserve bedforms. Previously conducted work investigating flutes in weakly cohesive muds reported similar results, whereby the fine-grained substrate became unstable after absorbing too much water (Rucklin, 1938). Even experiments conducted with silty substrates (Rucklin, 1983; 5.8% clay, 94.2% fine quartz/mica) and more cohesive substrates (Allen, 1971; 0.5 wt.% bentonite, 20 wt.% china clay, 80 wt.% water) failed to yield flutes, instead forming features that more closely resemble the *wave-like* variety of transverse marks (Figure 2.6). There appears to be only one claim of experimental flutes formed in weakly cohesive mud beds via fluid stressing (Allen, 1969; formed at intermediate velocities 59 – 85 cm/s); however the validity of these flutes is called into question owing to their close association with wavy topography. Additionally, they only formed during two experiments, each at different velocities, and were not repeated. When considered together with the production of wavy topography in all other experiments, it remains possible that the *flutes* formed by Allen (1969) were not true flutes, but rather transient features associated with the development of wavy topography. This suggests that *all* existing experimental work investigating the fluid stressing of weakly cohesive mud beds have produced wave-like topography only, and no flutes. Allen (1984, p. 290) however suggests waves and flutes are genetically related, but Allen does not revisit this idea.

Preceding this study, only one investigation into the formation of flutes via corrasion in cohesive mud beds had been conducted (Allen, 1971). All of Allen's (1971) experiments were initiated with a bed defect, and experiment durations were mostly limited to 4 minutes and 12 seconds (one test run lasted 48 minutes) owing to the development of ripples (possibly Finnie's Ripples; Finnie and Kabil, 1965). Newly conducted experiments presented in this chapter lasted up to 300 minutes and did not generate the same type of ripples as created during Allen's experiments. Both investigations (Allen, 1971 and those presented here) confirmed the processes of the defect theory, however all the experiments presented here were initiated with an initially smooth bed. This suggests that the interactions between a turbulent flow and an initially smoothed cohesive bed are sufficient to generate defects. Furthermore, the results presented here indicate that naturally formed defects evolve with time to produce wavy-topography, pock-marks, narrow-flutes, broad-flutes, gullies and potholes - an observation not yielded during Allen's (1971) experimental work. These results suggest these bedforms develop as a continuum of features that continue to evolve with time. It is likely that Allen's (1971) experiments were not conducted over sufficient periods of time to document this. These bedform types are briefly discussed below.

In at least one test here, waves were present prior to the initiation of the experiment. The only explanation for this is that they formed during the infilling of the experimental flume, as the current of water flowed over the bed. It is likely that the development of these waves was driven by standing waves on the surface of the open channel flow, as is also documented by Richardson and Carling (2005, p. 90) in the case of open bedrock channels. The transverse erosional waves produced in these experiments developed during the earliest stages of each experiment and did compromise bed development at any stage; therefore it is unlikely they are of the same origin as those observed during the experiments of Allen (1971).

Pock-marks may have originated in two ways: (i) via the impinging of highly localised turbulent cells in an apparently chance arrangement across the experimental bed, perhaps influenced by the presence of pre-existing wavy topography; or (ii) by the exposure of weaknesses in the experimental bed and resulting plucking of material. The pock-marks are similar in morphology to the *Type A*- or *incipient*-

potholes seen in bedrock channels (Nemec et al., 1982; Lorenc et al., 1994; Richardson and Carling, 2005, p. 20), where they form part of a continuum between well-developed potholes, shallow shaped depressions (morphologically similar to flutes) and subangular hollows (Richardson and Carling, 2005, p. 20). Once these pock-marks are present on the experimental bed, they act as defects upon which other features nucleate.

It is unclear what determined the development of either narrow or broad flutes, and it is further unclear whether there may be a continuum of flute sizes and morphologies between them, which would make narrow and broad flutes end-members of the same feature. They have previously been documented as different features within the overall class of erosional marks (Allen, 1971). However it is well documented that their formation is dependent upon the pre-existence of a pock-mark; supporting the defect theory of Allen (1971).

Gullies formed here bear resemblance to the parallel-sided furrows in open bedrock channels of Richardson and Carling (2005, p. 30). Potholes are also documented in open bedrock channels, with a range of plan-view forms including circular, ovoid, spiral and undercut (Richardson and Carling, 2005, p.18), all of which were documented in these experiments. Studies show the most important mechanism of formation for potholes in bedrock channels is abrasion by suspended load (Alexander, 1931; Maxson and Campbell, 1925; Allen, 1982, p. 261; Whipple et al., 2000; Richardson and Carling, 2005, p. 18). Intriguingly, potholes are not commonly associated with deep-sea density currents, and Allen (1982, p. 261, 288) only discusses potholes with reference to bedrock channels and glacially formed features.

Important questions remain regarding the development of the described bedforms; a key finding of this investigation is the indication that the bedforms may form in a time-dependent continuum. With regards to natural systems, such a finding would emphasise the importance of the duration of density currents, whereby short-lived currents might not lead to the development of the full spectrum of bedforms. Furthermore, the final two bedforms of the continuum observed in these experiments (gullies and potholes) are common features in open bedrock channels, suggesting that they require rock or extremely firm substrates in order to form. It is possible that

they *exclusively* form in substrates of a certain strength (or cohesion), and may only reach this level of substrate strength following a significant period of erosion that acts to first remove the topmost layer of softer sediments.

3.7. Conclusions

Here, for the first time, flutes have been generated in open channel conditions via corrasion over a flat surface. The experimental investigations produced a wide range of erosional bedforms, including large numbers of flutes, all of which originated from an initially smooth surface. Furthermore, these features did not develop in association with transverse features such as mud waves, and are clearly not transient features of the bed as previous work indicates. The erosional bedforms occurred within a time-dependent continuum of: wavy-topography, pock-marks, narrow-flutes, broad-flutes, gullies and potholes. The two types of flute may form end-members of a generic flute form. Parallel-sided gullies and potholes were the final features to form and had never previously formed in muds under experimental conditions. As such, they are thought to form within firmer substrates, such as when firmer muds are exposed following a sustained period of erosion. In fluid-stressing flows of weakly cohesive mud beds, flutes either (i) do not form, or (ii) form only as transient features in association with low profile waves.

4. Architecture and flow processes in deep-sea lobe-elements: the Carboniferous Ross Sandstone, western Ireland

The Carboniferous Ross Sandstone, western Ireland, presents exceptionally well-preserved and exposed deepwater deposits, and has been used as a deepwater outcrop analogue in many studies (e.g. Chapin et al., 1994; Sullivan et al., 2000; Pyles, 2008; Pyles and Jennette, 2009). Models for the development of the Ross Sandstone are discussed in Chapter 2; however the dominant architectural element within the Ross Sandstone is interpreted to be lobes, based in part on regional palaeocurrent directions forming a radial fan-like pattern (Pyles, 2007; 2008).

4.1. Architecture of deep-sea lobe elements

Submarine lobes form a key component of submarine fans, and although they have been extensively studied (e.g., Walker and Mutti, 1973; Mutti, 1974; Ricci-Lucchi, 1975; Hiscott, 1980; Mutti and Normark, 1987; Twichell et al., 1992; Nelson et al., 1992; Piper et al., 1999; Piper and Normark, 2001; Ribeiro Machado et al., 2004; Gervais et al., 2006; Deptuck et al., 2008; Bourget et al., 2009; Prélat et al., 2009), their formative processes remain relatively poorly understood. Recent advances in understanding the sedimentary architecture of submarine fans have been made based upon analysis of large-scale geometries interpreted from seismic, bathymetric or acoustic datasets (e.g., Gervais et al., 2006; Deptuck et al., 2008; Jegou, 2008; Bourget et al., 2009). These studies have led to the recognition of hierarchies of internal sedimentary architecture (e.g. Twichell et al., 1992; Piper et al., 1999; Deptuck et al., 2008; Prélat et al., 2009), and culminated in two very similar four-level hierarchies, based on subsurface data (Deptuck et al., 2008) and outcrop data (Prélat et al., 2009). The hierarcy of Deptuck et al. (2008) was based upon small, confined lobes of the Corsican trough, and comprises bed/bed-sets, lobe-elements, composite-lobes and lobe complexes Figure 4.1. However, understanding the detailed process mechanics within and between these individual levels has been limited by the poor resolution of these techniques and the absence of detailed facies and bed-level descriptions.

Outcrop studies often provide bed-level detail, although they typically lack both the scale and three-dimensional control on architecture observed in seismic data

and modern studies, although Prélat et al. (2009) present a recent notable exception to this rule. Early work concentrated on analysis of vertical sequences and placed much emphasis on the presence of asymmetrical sequences, particularly thickening-upwards packages (Walker and Mutti, 1973; Mutti, 1974; Ricci-Lucchi, 1975; Ghibaudo, 1980; Ricci-Lucchi and Valmori, 1980). These sequences were interpreted either as the result of progradation (e.g., Mutti, 1974; Ricci-Lucchi, 1975, 1984) or the subtle lateral shifts that form compensation cycles (Mutti and Sonnino, 1981, and later by Pickering, 1981; Mutti, 1984; Pickering et al., 1989). Mutti and Sonnino's (1981) work was questioned by Hiscott (1981) who argued that the sequences recognised by Mutti (1974), Ricci-Lucchi (1975) and Ghibaudo (1980) could simply be the result of the chance distribution of beds. Subsequent statistical analysis of a broader range of deep-marine sequences (Chen and Hiscott, 1999) also concluded that in the studied sections the lobe deposits showed no consistent thickness trends. The absence of asymmetric vertical stacking patterns was attributed both to the myriad factors controlling turbidite thickness and distribution, and to the importance of aggradation relative to progradation in turbidite lobes (Hiscott, 1981; Chen and Hiscott, 1999). In the lobes of deep-sea fans, sediment aggradation is not controlled principally by sea-level, as in fluvio-deltaic lobes, and therefore accommodation space is always available and progradation is deemed less important (Hiscott, 1981; Chen and Hiscott, 1999). However, despite these arguments, thickening-upwards packages in lobes have continued to be recognised (e.g., Mutti and Normark, 1991; Mutti, 1992; Anderton, 1995; Carr and Gardner, 2000; Hodgson et al., 2006; Pyles 2007), including in the Carboniferous Ross Formation, western Ireland (Elliott, 2000a,b; Lien et al., 2003) but their origin and frequency of occurrence remains enigmatic.

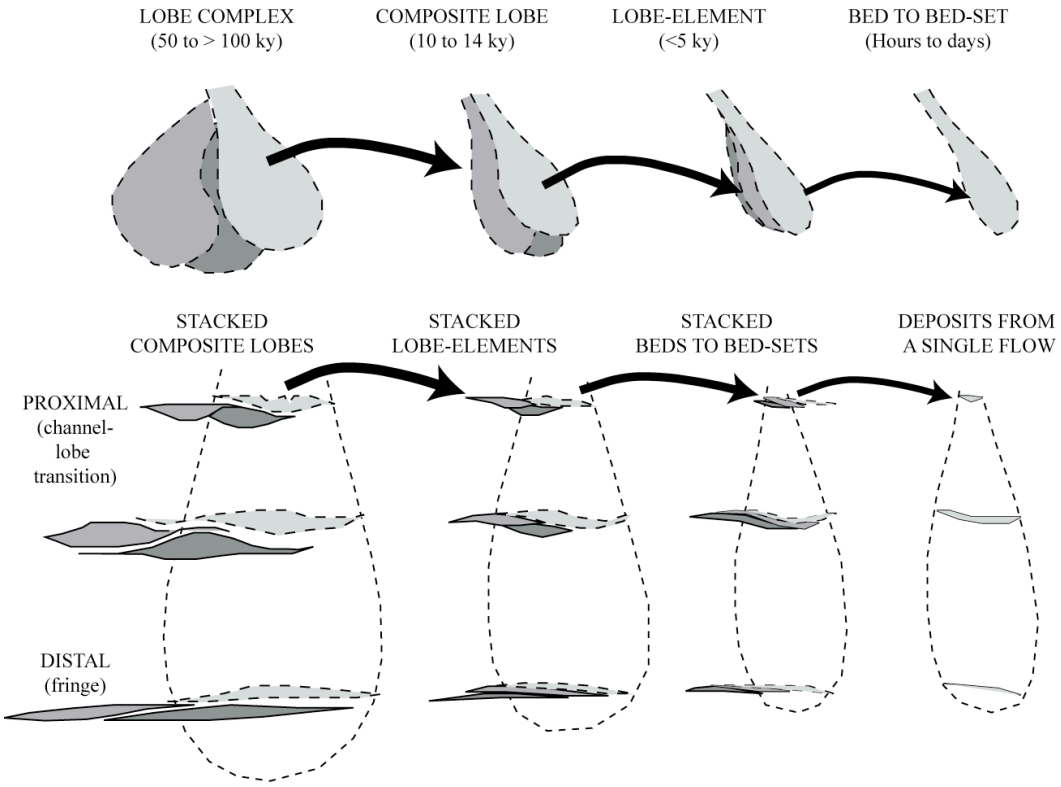

Figure 4.1. Schematic diagram of Deptuck et al. (2008), showing the hierarchy of compensation stacking observed in composite mid-fan lobes.

4.2. Outcrop studies

Outcrop studies have examined lobes in two and three-dimensional exposures (e.g., Chapin et al., 1994; Carr and Gardner, 2000; Johnson et al., 2001; Remacha and Fernandez, 2003; Hodgson et al., 2006; Pyles, 2007, 2008; Prélat et al., 2009), and have concentrated principally on the nature, dimensions and hierarchy of the architectural elements, and the overall evolution of these lobe systems. However, these studies have not specifically addressed the detailed process mechanics of small-scale (*c*. several metres) packages, or the origins of cyclicity. This chapter examines lobe-element dynamics (*sensu* Deptuck et al., 2008) and thickening-up sequences, through the analysis of parts of the Carboniferous Ross Formation, Western Ireland. It is widely recognised that these outcrops exhibit thickening-upwards packages (Elliott, 2000a,b; Lien et al., 2003; Pyles 2007). Past research has interpreted these sequences as deep-sea lobes or spillover lobes adjacent to channels (Chapin et al., 1994; Sullivan et al., 2000; Lien et al., 2003; Pyles, 2007, 2008), or as channels and channel wings on the basin-floor (Elliott, 2000a,b), see Figure 2.23.

4.3. The Carboniferous Ross Sandstone

The Ross Formation has a maximum thickness of 500 m and comprises interbedded sandstones, siltstones and mudstones that have been interpreted as mudstone sheets, turbidites, channels and associated slumps (Rider, 1974; Collinson et al., 1991; Martinsen et al., 2000; Wignall and Best, 2000; Strachan, 2002; Lien et al., 2003; Pyles, 2007, 2008); see Section 2.6 for detailed summary. The Ross Formation documents an overall progradational history and is observed in two ways: (i) by the progressive north-eastward expansion of the area of turbidite sandstone deposition (Wignall and Best, 2000), and (ii) by the vertical change in the proportions of internal architectural elements, such as where mudstone sheets dominate the lowermost deposits, the middle Ross Formation is dominated by lobes, and both channels and slumps become more common in the upper Ross Formation (Strachan, 2002; Pyles, 2008). However, the dominant architectural element in the Ross Sandstone has been shown to be that of lobes (56% average by area; Pyles, 2007).

4.3.1. Ross Sandstone thickening-upward packages

Much of the Ross Sandstone is characterised by interbedded sandstones and mudstones that are organised into thickening-upward packages (Elliott, 2000a,b; Lien et al., 2003; Pyles 2007). Packages are typically 1 - 7 m thick, and where complete, can be subdivided into three parts (Figure 4.2): (i) an initial finely parallel-laminated mudstone unit; (ii) a series of interbedded silty mudstone and sandstone deposits, (iii) an overlying structureless amalgamated sandstone unit. The degree of amalgamation within the upper sandstone varies across the beds, allowing some bedding surfaces and intervening mudstone deposits to be preserved. As will be shown here, megaflutes are important features that occur at varying heights through these packages; they provide evidence for localized erosion within an otherwise largely depositional environment. The distribution of megaflutes, together with the depositional environment of these cyclical packages, has been widely debated, with palaeoenvironmental reconstructions ranging from: (i) aggrading lobes within a structurally-confined, rapidly subsiding, basin (Pyles, 2007, 2008), where scouring developed in regions of channel-to-lobe transition (Chapin et al., 1994), through (ii) scouring on channel flanks via single, catastrophic, channel-initiating flows that subsequently infilled via low-magnitude, high-frequency turbidity currents (Elliott, 2000a,b), to (iii) deposition and scouring within spillover lobes at the bends of

sinuous submarine channels (Lien et al., 2003). These previous studies have dominantly used single vertical sedimentary logs, or larger-scale correlation panels of 'key' identified surfaces. However many of these logs are conflicting, outlining the need for a collection of more detailed logs and correlation panels.

Figure 4.2. A typical, complete thickening-upward package of the Ross Formation at Ross Bay, recording an upward trend of (i) thick mudstone interval, (ii) interbedded sand and mud deposits, (iii) thick, amalgamated sandstone.

4.3.2. Methodology, dataset and study area

The present-day geomorphology of the study area consists of both cliff exposures and extensive foreshore platforms. The cliffs allow laterally continuous lobe deposits to be traced across distances of up to 2000 m revealing that average lobe dimensions are 1900 m wide and 2 m thick (Pyles, 2007). In order to evaluate depositional processes, this work has studied accessible coastal exposures at Ross Bay, Ross Point and Kilbaha Bay (Figure 4.3). The former two locations have not previously been

recorded in bed-set detail, whereas the sections at Kilbaha Bay (Figure 4.3b) have been previously studied by Elliott (2000a; his Channel 4). The present dataset comprises 53 sedimentary logs that were used to construct three correlation panels. The study has constructed a series of detailed bed-by-bed scale correlation panels from multiple closely spaced logs, in combination with laterally tracing continuous individual surfaces, in order to examine the lateral and vertical variations of all beds within these sections. The presence of an array of different erosional features is used in combination with the spatial distribution of beds, to re-examine previous palaeoenvironmental interpretations, and propose a new model for the development of thickening-upward lobe-elements within the Ross Sandstone. This model recognizes major phases of sediment deposition, bypass, erosion and lobe abandonment, and is used to discuss the origin of some thickening-up sequences in deep-sea lobes.

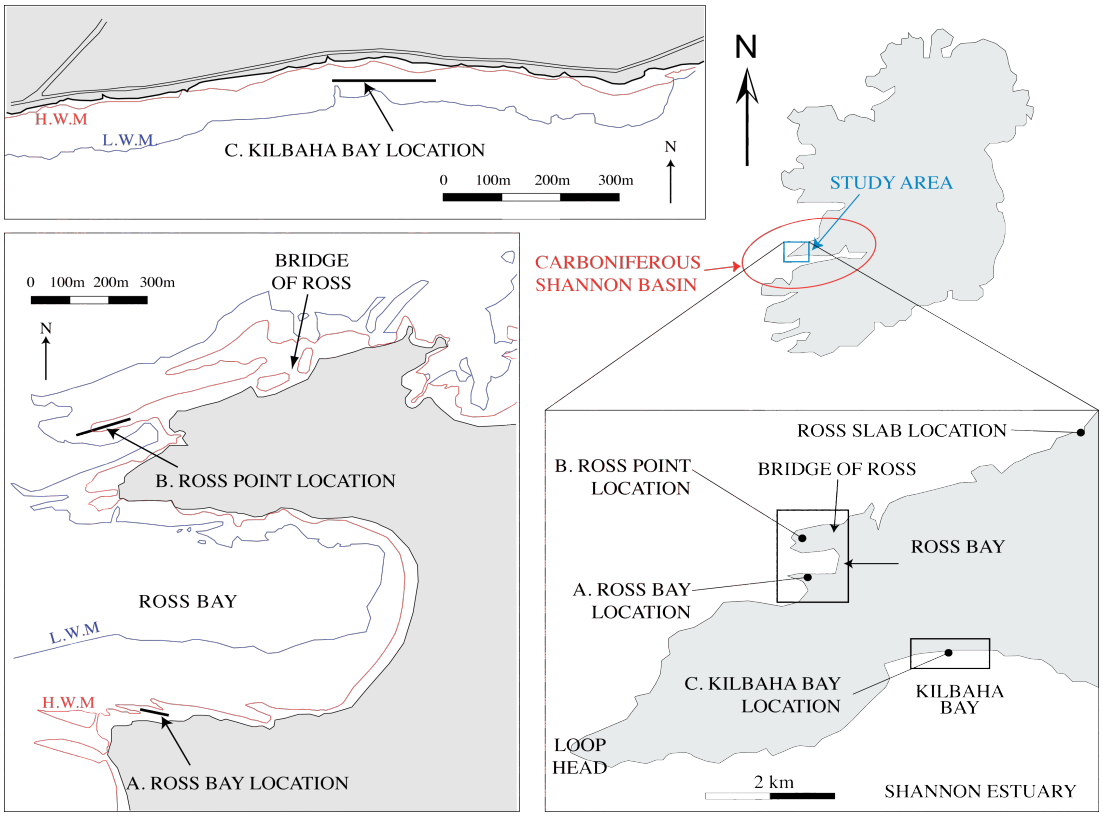

Figure 4.3. Location map showing the study area and overall location of the Carboniferous Shannon Basin, western Ireland (after Pyles, 2007). Inset maps show the location of studied areas, A. Ross Bay, B. Ross Point, and C. Kilbaha Bay. Low water mean (L.W.M.) and high water mean (H.W.M) are marked respectively.

4.4. Results

4.4.1. Measured sections

The three stratigraphic intervals detailed herein occur within the middle (Kilbaha Bay) and upper Ross Sandstone Formation (Ross Bay and Ross Point). The intervals comprise cyclical thickening-upwards packages (Figure 4.2). The sandstones are fine-grained and are almost exclusively structureless (Bouma horizon Ta), although some rarely possess planar laminae 4 – 10 mm thick (Bouma horizon Tb) and have irregular or fluted bases and/or ripple cross-laminated or wavy surfaces (Bouma horizon Tc). In some cases, mud chips are contained within sandstone beds, particularly with thicker (>0.30 m) and/or amalgamated sandstones where clasts are 0.02 – 0.15 m long. Mudstone beds are nearly always planar laminated with some very thin (<1 mm) fine-sand stringers. Within the thickening-upward packages, two scales of erosional surfaces and structures exist: (i) broad scour surfaces with steps that may fully, or almost-fully, cut out thick (>0.50 m) sandstone beds (Figure 4.4A,B), and (ii) megaflutes that show a much wider range of styles and sizes than previously recorded (e.g. Chapin et al., 1994; Elliott 2000a,b; Lien et al., 2003), including cross-sectional profiles with a U-shape (Figure 4.4A,B) or internal hummocks (Figure 4.4B) and planform shapes that range from widely-flaring (Figure 4.4A) to arcuate (Figure 4.4B). These various types of erosive feature are often preserved on the same bedding surface, where the scalloped rims of megaflutes occur along broad erosional surfaces.

Ross Bay (Figure 4.4A)

The interval documented from Ross Bay (Figure 4.3 and Figure 4.4A) is situated 7.2 m above the previously described “classic megaflute” surface (Leeder, 1999; Elliott, 2000b; Lien et al., 2003). It occurs within a succession of >10 thickening-up packages that begin with mudstone intervals that vary considerably in thickness (Figure 4.5). Contrary to previous reports that considered the packages to exhibit solely a coarsening-up motif (e.g. Elliott, 2000a; Lien et al., 2003; Pyles, 2008), the basal strata show a fining-upward with thin interbedded ripple sandstone and siltstone passing upwards into dark shale’s although the predominant trend is one of

coarsening-upwards (Figure 4.5). This is manifested as a progressive increase in sandstone bed thickness and an associated decline in the thickness of shale/siltstone interbeds. The thickest beds are ~1 m thick although this is attributable to amalgamation of 2-3 or more beds (Figure 4.5).

The package chosen for study exhibits a sequence of distinct erosional events, with the lowest erosion surface (labelled 'a', Figure 4.4A) truncating a thin-sand that is only 0.25 m from the base of the package. Overlying this thin sand is a 0.50 m thick tabular sand that has two megaflutes eroded into its upper surface (labelled 'b', Figure 4.4A), each measuring ~3 m wide and possessing ~0.25 m of erosive relief. Despite being immediately adjacent to one another, these megaflutes have different sediment infills, with one being firstly infilled with 0.1 m of sand whereas the other is initially infilled with 0.1 m of mud. Overlying both of these initial infills is a series of interbedded muds and sands that show amalgamation up-section. These muds and sands are themselves partially eroded by a broad scour surface (labelled 'c', Figure 4.4A) that extends across the width of the exposure and has a vertical relief of ~1.5 m. This scour surface is the main erosive feature within the package, and hosts at least 3 megaflutes and one stepped-scour (inset figures, Figure 4.4A). This major erosional surface is infilled by interbedded sand-rich deposits, some of which display further megaflutes (labelled 'd', Figure 4.4A), which are then overlain by amalgamated sandstone beds. This whole thickening-up package is overlain by a significant thickness of mudstone at the base of an overlying thickening-upward package.

Ross Point (Figure 4.4B)

The Ross Point section is located in an intertidal position, immediately below the Ross Slump (Figure 4.3 and Figure 4.4B). A thickening-upward package lies on a laterally continuous amalgamated sandstone that has an undulating, erosive upper contact (labelled 'a', Figure 4.4B). The earliest interbedded muds and sands of the overlying thickening-upward package have ponded within the erosive topography of this upper surface. The first major erosional surface (1.3 m from the base of package

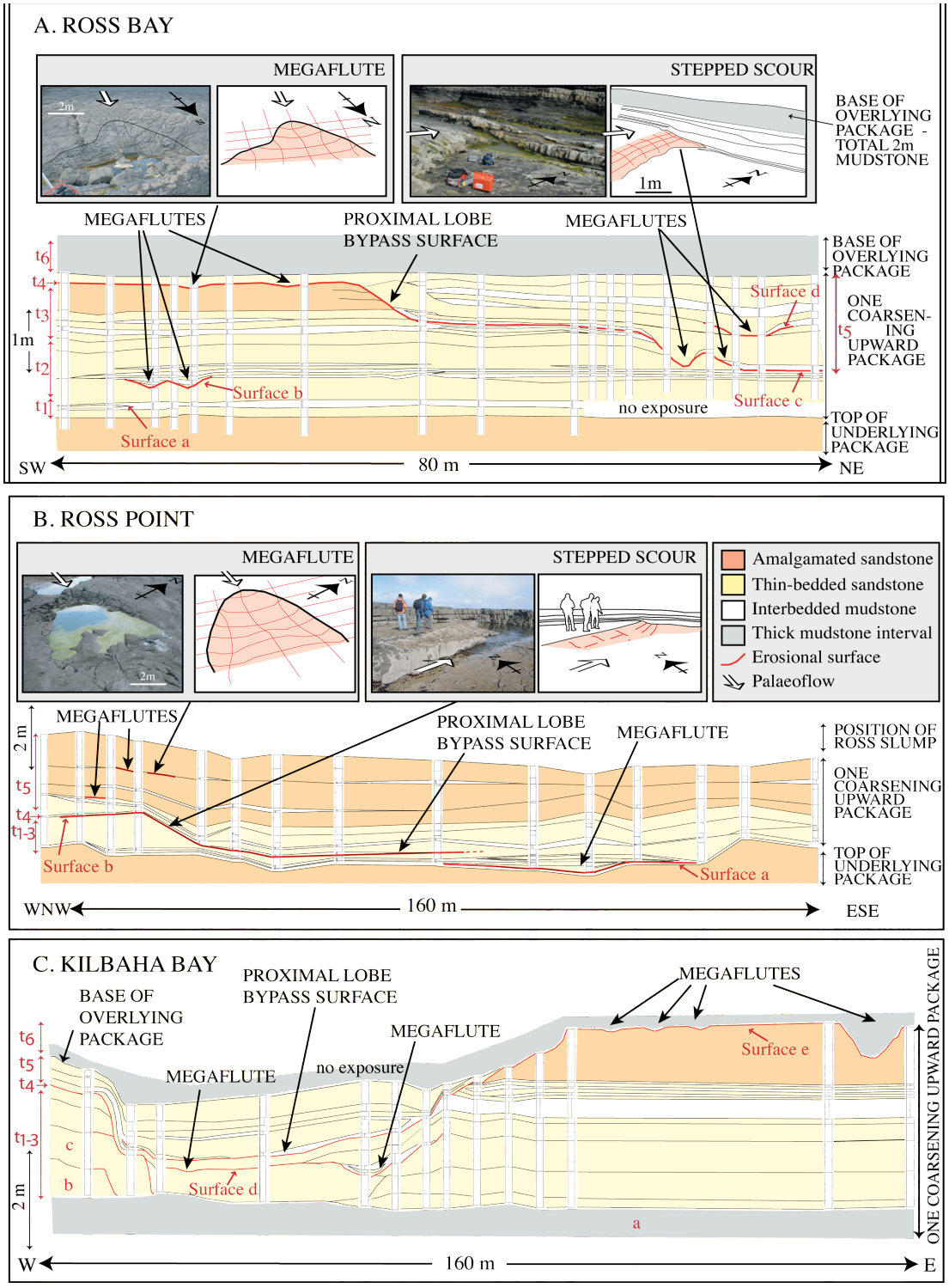

Figure 4.4 Cross profiles of measured sections from three studied locations. Profiles show sandstone and mudstone deposits, major erosional surfaces, stepped scours and megaflutes. A. Ross Bay (52°35'3.12"N, 9°52'36.52"W), B. Ross Point (52°35'24.75"N 9°52'42.67"W), C. Kilbaha Bay (approx. 52°34'17.46"N 9°50'50.10"W). Time periods (t1-t6) are marked on the left hand side of each figure and link to the periods identified in Figure 4.6.

in the northwest; labelled ‘b’ Figure 4.4B) is laterally persistent and hosts a stepped scour that almost enitrely removes a 1.1 m thick tabular sand. To the south-east, the erosional surface becomes difficult to discern within an erosive amalgamated sandstone (Figure 4.4b). This major erosional surface is progressively infilled by interbedded sands and muds, which are then succeeded by amalgamated sands. Megaflutes occur in these upper sandstones; one fully exposed example (inset figure, Figure 4.4B) measures 3 m wide, 7 m long and 0.55 m in vertical relief, and is initially draped with a mud-chip conglomerate with clasts up to 0.25 m long. These megaflutes are otherwise passively filled with sandstone and thin discontinuous muds (Figure 4.4B).

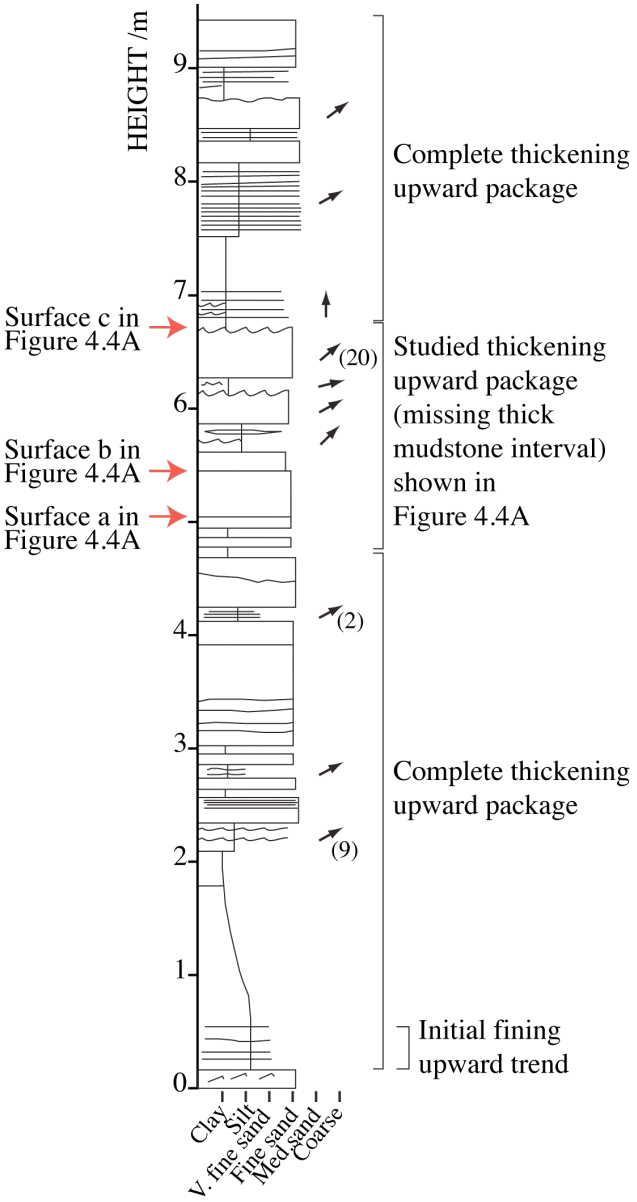

Figure 4.5. Sedimentary log showing the sedimentology of three thickening-upward packages from the upper Ross Sandstone, Ross Bay. Palaeocurrents measured from ripples show a consistent NE flow direction. Where the palaeocurrent is the average of multiple readings the total number of readings is provided in brackets. Lateral variation within the central coarsening-up packages is depicted in Figure 3A

Kilbaha Bay (Figure 4.4C)

The Kilbaha Bay section (Figure 4.3 and Figure 4.4C) is located at the easternmost headland of the bay approximately 5 m below the top of the exposure. The base of the package is marked by a laterally continuous mudstone (labelled 'a', Figure 4.4C), which is overlain by ~2 m of interbedded sandstone beds (with some mudstone intervals) that shows progressive amalgamation to the west. Two of the lowermost interbedded sandstones (labelled 'b' and 'c', Figure 4.4C) have erosional upper surfaces and are cut-out locally by stepped scours. These surfaces are passively filled with other thick interbedded sandstones, one of which has a widespread upper erosional surface that hosts megaflutes (>2 m wide; labelled 'd', Figure 4.4C). Overlying this is a series of interbedded sandstones and mudstones, which culminate in a thick, amalgamated sandstone. This succession is partially eroded by a widespread erosional scour surface, with a vertical relief of up to 2 m, which also hosts megaflutes (3 – 15 m wide) upon the amalgamated sandstone (labelled 'e', Figure 4.4C). This broad scour surface is then passively filled with interbedded sands and mud, and is overlain by a thick mudstone interval that marks the beginning of the next thickening-upward package.

4.4.2. Sedimentary model: erosive bypass within prograding lobe-elements

Based on these detailed sections, the thickening-up packages observed in the Ross Formation are attributed to deposition on prograding lobes within a distributary submarine fan. The deposits exhibit the classical features of deep-sea lobes (e.g., Mutti and Normark, 1987): 1) relatively tabular and laterally-extensive beds; 2) distinct packages bounded by parallel surfaces; 3) a dominance of thick sandstone beds alternating with mudstones and thinner-bedded sandstones; 4) amalgamation of sandstone beds; 5) scours and 6) thickening-up packages. By analogy with other studies in turbiditic environments (Twichell et al., 1992; Piper and Normark, 2001; Gervais et al., 2006; Deptuck et al., 2008; Bourget et al., 2009; Hanquiez et al., 2009), and in accord with Pyles and Jennette (2009), this work interprets each

thickening-up package to represent one lobe-element, which in turn stack to produce composite lobes. The basal part of the packages marks a period of rapid lobe-element shutdown, recorded by thin, fining-upward successions, and its presence is dependent upon the degree of avulsion (lateral distance and time scale) experienced by a subsequent lobe-element.

Based on these observations, a six-stage model for the development of each lobe-element and its erosive features can be proposed (Figure 4.6): (t1) Initially, in a dominantly depositional distal lobe-element setting, interbedded sands and muds accumulate from successive turbidity currents, and the bed shear stresses from these expanding and decelerating flows are insufficient to generate any erosional bedforms. (t2) As the lobe-element progrades and aggrades, increasing erosion is manifested by the generation of megaflutes. Thicker sands are deposited by higher velocity flows that deposit erosively amalgamated beds. (t3) With further progradation and aggradation of the lobe, the frequency of megaflutes becomes greater as the intensity of sediment bypass increases. (t4) The period of maximum bypass represents arrival of the distributary channel at a proximal position within the lobe-element; the erosive surface is here termed a proximal lobe bypass surface. At this stage, megaflutes may develop and join laterally or become incorporated into the margin of the bypass surface. (t5) Bypass intensity decreases as lobe-element abandonment is initiated; deposition rates increase resulting in a net accumulation of sediment and the passive filling of the proximal lobe bypass surface. The remaining erosive features become draped or compensationally-filled by larger flows. (t6) Complete avulsion, perhaps linked to the infill of these erosive features, leads to the prograding lobe-element being abandoned. Sediment accumulation at this locality is initially composed of thin sand/mud interbeds and then solely by mud that marks the beginning of a new thickening-up package, and the generation of a new lobe-element.

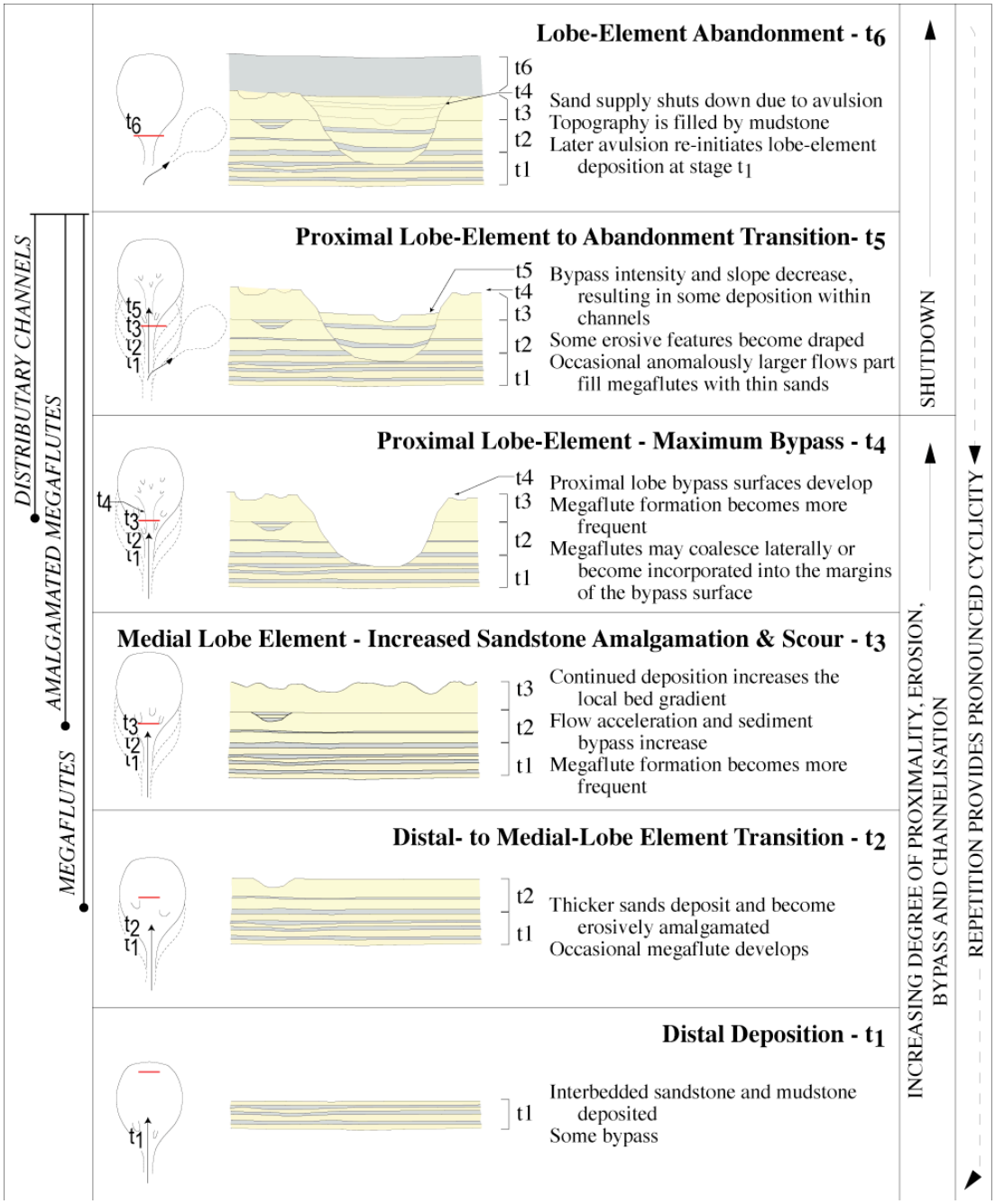

Figure 4.6. A six-stage sedimentary model for erosive bypass within prograding terminal lobe-elements in the Ross Formation. The schematic lobe-elements are prograding relative to the fixed-position red dashed line. Cross-sections depict interbedded sandstone (yellow) and mudstone (grey), and illustrate the deposits associated with each stage at the fixed-position red dashed line.

4.5. The occurrence of megaflutes, distributary channels and proximal lobe bypass surfaces

In the model proposed herein, the location of erosive features within the lobe-element deposits, including megaflutes and broader bypass surfaces, is determined by their proximality within the prograding and aggrading lobe. Furthermore, megaflutes form as a result of the increased flow velocities that may be expected at the channel to lobe-element transition region, and develop in a proximal lobe-element position. Such localities have also been proposed to be zones in which hydraulic jumps occur that favour the production of local scour (Normark et al., 1979; Chapin et al., 1994). Their occurrence within the upper portions of thickening-up packages therefore spans medial-fan deposits to late-stage proximal deposits (Fig. 3). In the lowermost parts of the packages, the megaflutes likely represent the erosive products of larger flows, and with continued progradation an increasing proportion of the flows generate more megaflutes. At this stage, the largest flows begin to develop broad erosive surfaces on which megaflutes can form, grow and coalesce. With continued progradation, a more proximal setting is reached and the phase of maximum sediment bypass occurs via the arrival of the lobe-element distributary channel, eventually culminating in formation of a proximal lobe bypass surface. This surface erodes through earlier proximal and medial fan deposits, and precedes the initiation of lobe abandonment. The observed increase in erosional intensity within these thickening-upwards packages points to a gradual and progressive increase in the local velocity of the turbidity currents at any given location.

Support for this model is provided by recent work on modern deep-sea environments, which shows repeated erosion and the formation of megaflutes in regions of flow expansion between confined and unconfined flow. Examples include the San Lucas Fan, and the Agadir, Lisbon and Setubal Canyons where scours are common in these modern channel-lobe transition zones, and in the Rhône Neofan and Monterey Fan, where flows are beginning to initiate new lobe / overbank deposits (Normark, 1970; Masson et al., 1995; Wynn et al., 2002; Bonnel et al., 2005; Fildani et al., 2006).

4.6. Discussion

4.6.1. Comparison with existing models

The model presented here builds on earlier interpretations of lobes for these sequences (Chapin et al., 1994, Pyles, 2007, 2008) but is in contrast to models invoking 'channels with channel-wings' (Elliott, 2000a,b) and channel spillover lobes (Lien et al., 2003).

Channels, channel wings and channel initiation

Elliott (2000a,b) suggested that the successions examined here were channels with broader, sheet-like, thickening-upward, and overall coarsening-upward, channel wing deposits. The basal surfaces of the channel wings in Elliott's model exhibit megaflutes along discrete surfaces and were interpreted as marking periods of widespread erosion and subsequent localised channelization by giant single flows. These discrete surfaces, termed *megaflute erosion surfaces* were envisaged to occur on the upper surface of thick, amalgamated sandstones, and pass laterally into channel axes. Several problems exist with this 'channel-wing' model: (1) it fails to record the occurrence of megaflutes both within the amalgamated sandstones and upon interbedded sands lower in the packages (as also recorded by Lien et al., 2003), and does not account for the fact that there is therefore a progressive increase in the degree of erosion that occurs within each package; (2) it fails to recognise that once the main megaflute erosion surface is formed, it may continue to be subjected to subsequent *filling-and-cutting* events, i.e. it does not have to form via a single catastrophic event explicit in the model; (3) the model provides no explanation for the repetition of numerous thin packages, which presumably must arise through frequent channel avulsion in this model. However, trunk channels (rather than the distributary channels as envisaged here) are typically long-lived conduits with low avulsion rates (e.g., Weimer, 1991; Pirmez and Flood, 1995; Savoye et al., 2009); (4) it implies the proportion of channels-fills in the Ross Sandstone would be very high. Indeed, Elliott (2000a) considered such channel fills the dominant element of the mid-and upper parts of the Ross Sandstone, much higher than in any other example (Clark and Pickering, 1996; Wynn et al., 2007); (5) it contrasts with previous work on the infill of submarine channels that have typically been shown to be fining-

upwards successions, sometimes associated with thinning-upwards packages, but not thickening- and coarsening-upwards sequences (e.g., Chen and Hiscott, 1999); (6) paradoxically, the 'channel-wing' model suggests that the packages predominantly consist of 'laterally extensive sheet-like' deposits (Elliott, 2000a p. 367), and thus presumably must be dominantly unconfined, yet are all considered as channel elements.

The model presented herein addresses all of these points and recognises distributary channels and broad erosion surfaces within dominantly unconfined lobe sequences. Critically, 'megaflute erosion surfaces' are shown to be just one of many erosional surfaces in each thickening-upward package, and they represent erosion by many of the most erosive flows (see also Pyles and Jennette, 2009). This suggests that channels, at least distributary channels such as these, are formed by multiple events rather than single catastrophic events. It further suggests that the previous consensus on the initiation of trunk channels via numerous erosive events (e.g., Clark and Pickering, 1996; Imran et al., 1998; see also Posamentier, 2003) remains valid.

Spillover lobes

A contrasting model associates megaflute development with spillover lobes at the bends of sinuous channels (Lien et al., 2003). This 'spillover' model proposes that mudstones at the base of the packages represent deposition furthest from the channel, and that the coarser-grained, thickening-up, sequences represent spillover lobes formed as the channels migrated laterally, with channel avulsion occurring at the top of each thickening-up unit. Overbank flow is assumed to occur only at the outside of channel bends, with homogeneous mudstones occurring immediately adjacent to other parts of the channel representing older overbank deposits or the deposits of distal flows that are overspilling at the outer channel bend (Lien et al., 2003; their figure 23). A number of key difficulties arise with this model: (1) overbank sediment from submarine channels does not comprise solely homogeneous muds in more distal locations, but rather displays thin interlaminated beds, graded beds and base-missing sequences (Stow and Bowen, 1980; Mutti and Normark, 1987; Kane et al., 2007, 2009); (2) there is substantial evidence to suggest that fine-grained overbank flow occurs at all points along a channel, particularly for the largest flows. Therefore, overbank areas immediately adjacent to channels are proximal deposits, not older

deposits or the distal deposits of overspill from outer channel bend apices (as implied by figure 23 of Lien et al., 2003) (e.g. Hesse and Dalton, 1995; Peakall et al., 2000a; Kane et al., 2007, 2008, 2010; Crane and Lowe, 2008); (3) the deposits in channel overbank areas typically fine-upwards (e.g., Hiscott et al., 1997; Piper and Deptuck, 1997; Beaubouef, 2004; Kane et al., 2007) and would also be expected to typically show decreasing erosional features with time as flow confinement increases. In fact, levees typically show only minimal erosional features (e.g., Kane et al. 2007); (4) true levee sequences do not show thickening-upwards cyclicity, but are instead marked by complex patterns with both thinning-up and thickening-upwards packages (e.g., Mutti and Normark, 1987; Kane et al., 2007); (5) similarly repeated thickening-upwards cycles are not observed in other spillover lobes (e.g., Dutton et al., 2003); (6) trunk channels, rather than the distributary channels envisaged herein, are typically long-lived conduits with low avulsion rates (e.g., Weimer, 1991; Pirmez and Flood, 1995; Savoye et al., 2009); (7) given the high proportion of lobes in this environment (56%; Pyles 2007) and high avulsion rates, channels should be more abundant and show higher degrees of inter-connectivity (e.g., Mackey and Bridge, 1995; Leeder et al., 1996; Larue and Hovadik, 2006); (8) The model of Lien et al. (2003) is, in part, predicated on the idea that the thin (~2 m thick) thickening-upwards packages seen in the Ross Formation are interpreted as lobe fringe deposits (when compared to typical 3-15 m thickening-upwards lobe deposits; Mutti and Normark, 1987), but this is not commensurate with observations of significant erosion.

Existing lobe models

The present thesis shows how erosional features develop on widespread erosional surface and that erosion is distributed in a systematic manner within the stratigraphic architecture of these sediments. The bed-scale analysis used herein reveals the erosive and depositional processes involved in building the fundamental element of the depositional system: the lobe element (sensu Prélat et al., 2009), and is in agreement with the history of depositional lobes that focuses on much larger, inaccessible, cliff-sections that are laterally-extensive and continuous (Pyles, 2004, 2007, 2008; Pyles and Jennette, 2009).

4.6.2. Progradation relative to aggradation in lobes

The relative importance of aggradation versus progradation in deep-sea lobes has been controversial (e.g., Mutti, 1974; Ricci-Lucchi, 1975, 1984; Hiscott, 1981; Chen and Hiscott, 1999). Although it is clear that aggradation is a rapid process in deep-sea lobes as accommodation space is always available, there is less clarity on the degree of progradation, if any, that may occur. Progradation was considered to be prevalent in deep-sea lobes from early field studies (e.g., Mutti, 1974; Ricci-Lucchi, 1975, 1984), yet the thickening-up cyclical packages used in support of this argument were challenged (see below), leading to a view that there was only limited progradation in deep-sea lobes (Chen and Hiscott, 1999). In particular, evidence for progradation from outcrop studies, other than from putative asymmetric cyclical packages, is lacking. The integrated model of lobe-element evolution postulated herein addresses this limitation, combining a number of key lines of evidence: i) progressive increases in the periodicity of erosion, ii) the associated increasing magnitude of this erosion over time, iii) increasing flow confinement over time, and iv) clearly-defined repetative thickening-upwards bed packages. Such evidence indicates that over time flow velocities at-a-point increased, in part driven by increasing confinement. The proposed model can be explained through purely autocyclic behaviour, where a lobe develops and the distributary channel progressively progrades over the lobe. As the lobe-element aggrades, and the lateral gradients consequently increase, then avulsion becomes progressively more likely (cf. Mackey and Bridge, 1995; Jones and Schumm, 1999; Peakall et al. 2000b; Parsons et al., 2002). Once avulsion takes place, there is a relatively rapid decrease in the energy of flows received at the original location, and a new lobe-element is initiated elsewhere. Repetition of this autocyclical sequence results in repeated thickening-upwards packages.

An alternative explanation is that the cyclical increases in erosion frequency, erosion magnitude, bed thickness and flow confinement are the result of progressive and repeated changes in externally-controlled flow magnitude. In this scenario, lobe progradation is not required, and lobe aggradation could be more dominant; yet, even here, a degree of progradation would be expected given that flow sizes would be increasing. There are, however, two main weaknesses of such an explanation. Firstly, it is unclear what external factor(s) might lead to such repeatable changes in external

conditions. The timescales of formation for lobe-elements are very rapid; whereas avulsion frequency of lobe-elements in the Ross Formation is unknown, modern systems have avulsion frequencies for lobe-elements of <5 kyr for smaller systems (Deptuck et al., 2008) such as the Ross, and even higher frequencies (0.6-1.5 kyr) in larger systems such as the Amazon and Zaire Fans (Dennielou et al., 2003; Jegou et al., 2008). These rates are orders of magnitude faster than Milankovitch sequences but may scale to the types of millennial-scale fluctuations identified in Pleistocene records such as Isotope Stage 3 (e.g. Cutler et al., 2003; Siddall et al., 2008) and linked to channel avulsion in the Amazon channel (Maslin et al., 2006). It is unknown whether such high frequency fluctuations were present in the Namurian (Haq and Schutter, 2008), but even if these are assumed, then it is questionable whether most millennial fluctuations are sufficiently high-frequency and repeatable, with the possible exception of Dansgaard-Oeschger events (e.g. Schulz, 2002; Siddall et al., 2008). Secondly, recent experimental work has shown that submarine channels act to regulate the size of flows that travel through them (Keevil et al., 2008; Straub et al., 2008; Amos et al., 2010), thus in large part eliminating the influence of any external forcing, even if present. The rationale behind these experiments is relatively simple; consider the case of a larger than average flow in a channel with any significant sinuosity such as those identified in the Ross (e.g., Elliott, 2000a; Sullivan et al., 2000; Lien et al., 2003). As this larger flow approaches the first bend, enhanced overspill occurs due to centrifugal forces; the process is repeated at each subsequent bend until the flow has been regulated to a similar size that is able to traverse the main channel with only limited progressive overbank loss of material.

In summary, the autocyclic model proposed herein honours the field-data and provides a set of coherent process explanations for the formation of these packages. The alternative explanation of repeated and progressive external forcing of flows appears improbable, as it lacks underlying forcing mechanisms. Furthermore, even if such external drivers were present, then autocyclic behaviour operating within the trunk channels would act to reduce the impact of these variations at the point of lobe-element deposition. The underlying processes have implications for the relative amounts of progradation to aggradation observed; the proposed lobe-element

dynamics model, in contrast to the ideas on external forcing, demonstrates an important component of progradation at the lobe-element scale.

4.6.3. A mechanism for thickening-up distributions

The presence and origin of thickening-up sequences in deep-sea lobes has also been much debated. A number of workers have suggested that thickening-up distributions do not generally occur in lobes and have demonstrated that some early interpretations were incorrect (Hiscott, 1981; Anderton, 1995; Chen and Hiscott, 1999). However, thickening-up packages continue to be recognised within lobe sequences, and have been attributed either to lobe progradation or to subtle lateral migration producing compensation cycles (e.g., Mutti, 1974; Mutti and Sonnino, 1981, Pickering et al., 1989; Lien et al., 2003; Pyles, 2007). Given that progradation in lobes has previously been considered to be limited (Chen and Hiscott, 1999), then the compensation-cycle model has been prevalent, relating sequences to lateral changes (Mutti and Sonnino, 1981; Mutti, 1984; Pickering et al., 1989). Given the widespread application of compensation cycles, it is perhaps instructive to revisit the basis of the compensation cycle model. A progressive shift in a single direction will make for a localised thickening-up sequence (e.g., Hiscott, 1981). However, to examine full compensational cycles, the original block model of Mutti and Sonnino (1981) is used herein (Figure 4.7), and shows that only some areas exhibit thickening-up sequences, whilst others predict thinning-up or more complex sequences. Consequently, a succession consisting only of thickening-up cycles is very unlikely to form from compensation cycles (e.g. Chen and Hiscott, 1999).

The model presented herein provides a mechanism for generating thickening-up sequences at all points laterally across a section (Figure 4.7B), with the exception being low-relief distributary channels that would typically show local fining-up, and possibly thinning-up sequences. However, such channels are volumetrically of limited importance. The thickening-up sequences occur as a consequence both of larger flows at-a-point over time, due to progradation and enhanced flow confinement, and critically to consequent increased bed erosion and amalgamation. The presence of erosion is key since it will act to partly offset any natural variability in initial flow volumes, because the thickening-upwards trend is not purely a bed-by-bed variation but instead is largely envisaged to be a function of the extent of progressive bed amalgamation. Importantly, the degree of progradation relative to

aggradation that is required to achieve such thickening-up sequences is greatly reduced when the dominant control is not the individual flow size and associated bed thickness, but instead a relatively subtle shift from preservation of mud interbeds to progressive erosion of these mud caps.

Support for such a progradational and aggradational model for submarine lobes is provided by both high-resolution seismic studies of modern lobes, and outcrop examples with excellent three-dimensional control. Some small-scale modern fans have been observed to undergo significant progradation whilst undergoing aggradation (e.g., Gervais et al., 2006; Hanquiez et al., 2009), and bed-correlations in the Permian Karoo Basin demonstrate the progradation of submarine lobes in this basin (Hodgson et al., 2006; Prélat et al., 2009). Although aggradation is dominant in these examples, progradation still occurs, with consequent implications for the preserved sedimentary characteristics as demonstrated in the present model.

The model presented herein thus demonstrates how thickening-up trends may form in prograding lobes with periodic erosive flows. However, it is not proposed that all lobes will display such trends, as originally postulated by early outcrop studies. Lobes that exhibit more limited erosion are less likely to display thickening-up sequences. Equally, lobes that display more limited progradation and commensurately greater relative aggradation (e.g., Deptuck et al., 2008) and / or lateral migration, will be less likely to exhibit thickening-up packages. The ultimate controls on the degree of progradation, aggradation, and lateral migration remain to be explored.

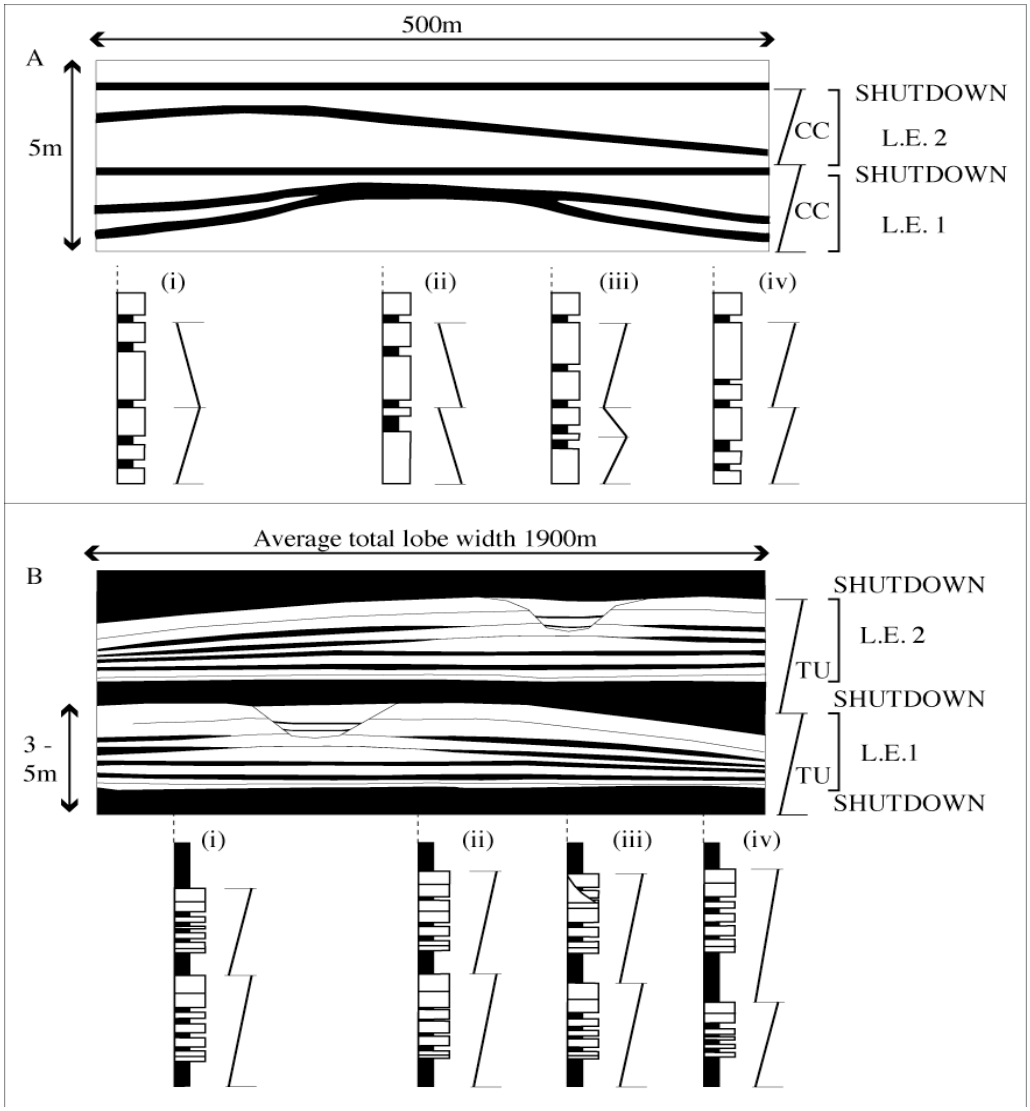

Figure 4.7. Diagram showing vertical changes in sedimentation of sand (white) and mud (black), whereby packages are defined by lobe-element surfaces. A. Diagram showing the origin of compensation cycles (CC), and how thickness trends vary across the width of the cycles; upper part after Mutti and Sonnino (1981). Under this concept of compensation cycles, each cycle is capped by horizontal muds that accumulate during periods of shutdown. Note that across the diagram, thinning- and thickening-upward trends are observed together with regions of no thickness change. Only (iv) shows exclusively thickening-upward trends. B. Diagram showing the thickening-upward (TU) trends generated by prograding lobe-elements, as presented here. Thickening-upward trends are observed across the lobe-element, and are only interrupted by localised erosion generated by lobe-element bypass surfaces, as in (iii). Average total lobe with is ~1900 m (Pyles, 2007).

4.7. Conclusions

Repeated thickening-upwards trends within the Ross Formation are shown to exhibit progressive increases in erosional periodicity, bed amalgamation, and scour, culminating in broad erosional surfaces and an abrupt return to mud-deposition. A model of lobe-element dynamics is proposed that integrates these observations. Lobe-element progradation in association with aggradation leads to a progressive increase, at any given point in the system, in the local magnitude of flows, resulting in increased erosion and sediment bypass, and ultimately the development of broad erosive surfaces associated with low-relief distributary channels. Avulsion and lobe-element switching, most likely as a result of increased lateral gradients, subsequently lead to rapid abandonment and a return to background sedimentation.

This model of lobe-dynamics has led to a reassessment of previous environmental interpretations, including spillover lobes, and channels with channel wings. These alternative models are shown to be inconsistent with the outcrop observations. Additionally, implications from the model include the rejection of previous arguments (based on these sections) that submarine channel initiation is the product of giant single flows. Instead the previous consensus on channel initiation via numerous erosive events is reasserted.

The model of lobe-element dynamics outlined herein provides a mechanism for thickening-upwards trends within lobes. Furthermore, this work suggests that the progressive thickening-upwards pattern occurs through a combination of locally larger flows, and increased bed amalgamation. This produces thickening-upwards sequences at all points, with the exception of volumetrically insignificant low-relief channel infills. In contrast, existing models based on the lateral movement of deposits in compensation cycles result in a variety of vertical sequences and are unlikely to result in cyclical thickening-upwards packages. The present dataset thus demonstrates that progradation can, in certain cases, form thickening-upwards sequences, and furthermore that as a result of bed amalgamation the degree of progradation to aggradation does not have to be high.

5. The morphology, occurrence and genesis of megaflutes: the Carboniferous Ross Formation, western Ireland

5.1. Introduction

The significance of megaflutes within turbidite systems has been intensely debated in recent years. In particular, their relationships to bypass surfaces and phases of channel initiation have been highlighted, such as in the Carboniferous Ross Formation, western Ireland (see Chapter 4). The Ross Formation reveals many examples of "classic" megaflutes, with their crescentic planform and broad U-shaped profile (Figure 5.1) (Morris and Normark, 2000; Elliott, 2000a,b), but also contains numerous examples of other metre to 100 metre-scale erosive bedforms that have hitherto escaped attention. This chapter aims to document the inter-related spectrum of these erosive bedforms, their formational processes and examine their location within the stratigraphic architecture of the system.

5.1.1. The Ross Formation

The sedimentology and architecture of the Ross Formation has been the subject of several, highly detailed studies in the past few years (Collinson et al., 1991; Higgs, 1991; Lien et al. 2003; Pyles, 2008), making it one of the best documented turbidite systems. However the location of megaflutes within the system remains controversial, with interpretations regarding their formative locations ranging from lobes (Chapin et al., 1994), to spillover lobes at the bends of sinuous channels (Lien et al., 2003), and deflation surfaces lateral to feeder channels (Elliott, 2000a,b). These interpretations are presented and discussed in detail in Chapter 2 (see Chapter 2.7; Figure 2.23); and a new alternate model for the environmental setting of megaflute development is presented in Chapter 4 (Figure 4.6). This chapter furthers this investigation, with special emphasis on the character of individual megaflutes and their associated features. These bedforms were analysed to establish: (i) the morphology of megaflutes and other erosional beforms, in order to develop a classification scheme; (ii) the lithology of scour substrates, specifically to evaluate

cohesive properties at time of deposition; (iii) an understanding of bedform genesis, and how the bedforms might be related.

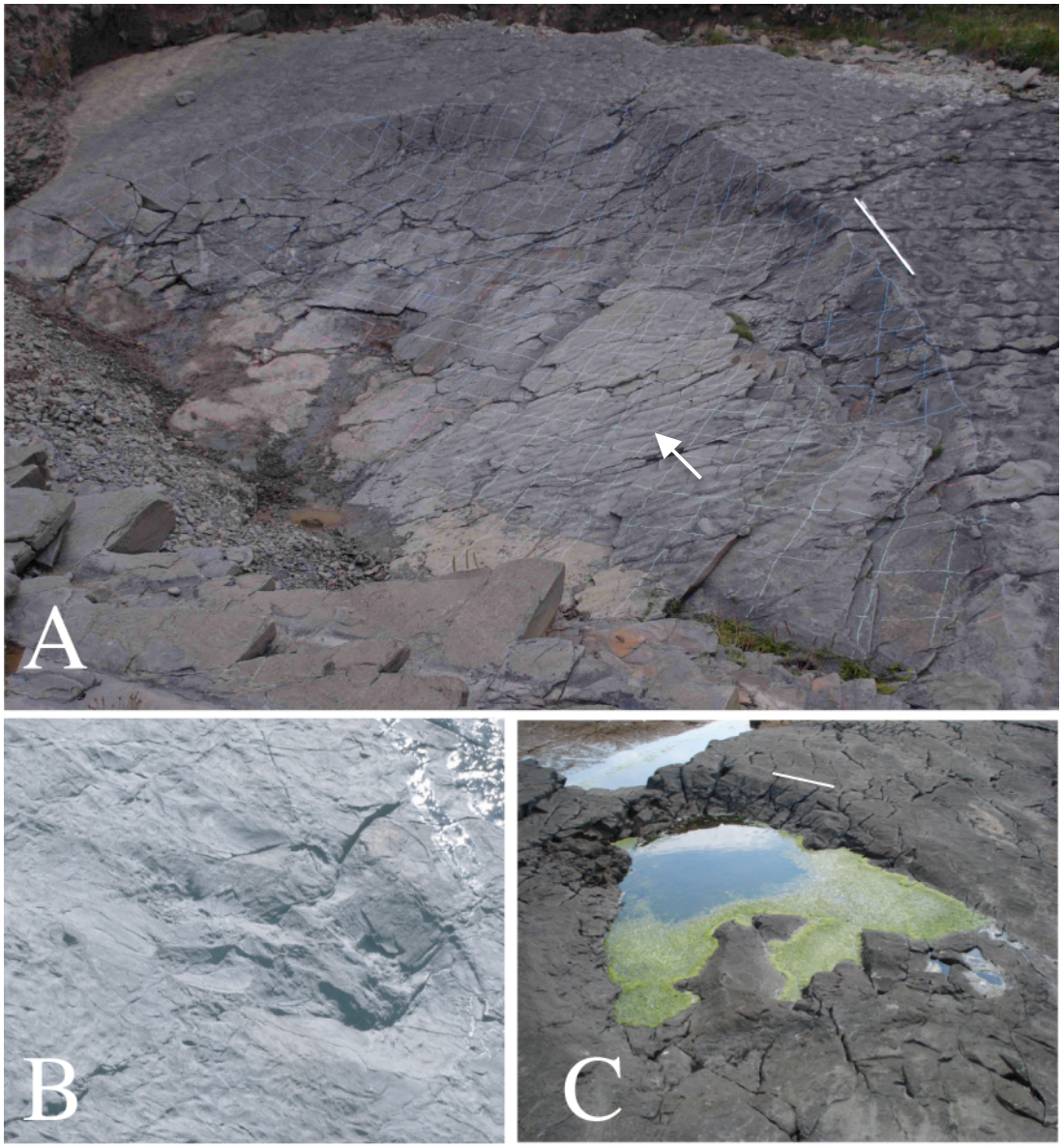

Figure 5.1. Planform exposures of megaflutes of the Carboniferous Ross Formation; A. 'Classic' spoon-shaped parabolic megaflute that exhibits extreme symmetry, palaeoflow is from top-right of photograph; measures 6.98 m wide and 0.5 m deep (corrected for dip, metre ruler highlighted in white for scale), white arrow highlights rippled infilling sediments; location: south side of Ross Bay. B. Parabolic shaped megaflute with median ridge showing positive relief within the limits of the megaflute; measures 2.02 m wide, 2.55 m long, 0.17 m maximum depth (corrected for dip), palaeoflow is from bottom-right to top–left. Location: Ross Slab. C. Water-filled megaflute that displays a median ridge, dimensions 3.05 m wide, 6.55 m long, 0.65 m maximum depth, metre-ruler highlighted in white for scale, palaeoflow is from back left towards the reader. Location: Ross Point.

5.2. Field techniques and methodology

Data presented here are all based upon samples and measurements collected from the outcrops of the Ross Formation. The data collected fall into two broad categories: 1. locating, documenting and sampling megaflutes, and 2. surveying megaflute morphology:

(1) Megaflutes were located by simply searching the outcrops, and their associated stratigraphy was recorded in stratigraphic logs. Sandstone beds were also sampled; 17 samples were taken from one thickening-upward package at Ross Bay (Figure 4.3) and sampled both thick (~40 cm) and thin (1 cm) megaflute-hosting and non megaflute-hosting sandstones; thicker beds were sampled at the base and top of the beds (Figure 5.2). In order to evaluate any lithological control on the genesis of megaflutes, the samples were made into polished thin-sections and analysed using a scanning electron microscope (SEM) in the Electron Optics Unit at the University of Leeds. Eight of the samples were examined using a combination of backscattered electron microscopy (BSEM) and cathode luminescence (CL) to determine the microstructure, diagenesis and mineralogy of the sandstones. Some samples were also selected for x-ray diffraction (XRD) analysis to investigate quantitative mineralogy; the key aim was to establish the original clay content of the sandstones. These samples were crushed into a fine power and analysed in the x-ray laboratory also at the University of Leeds.

(2) Megaflutes exposed in three-dimensions were surveyed in two ways. Most of the surveys were performed manually with a Leica Total Station (TCR805) that produced an array of XYZ data of 2 mm accuracy. For megaflutes with limited access, a LiDAR was used to survey the whole outcrop exposure. All the survey files were processed in the same way using MATLAB, so that the data could be presented as contour images to present 3D morphology and as line plots to illustrate cross sectional profiles across specific lines (see Appendix B for code files). All of the megaflutes were also photographed at high resolution; those with limited access were photographed at high resolution with a 600 mm zoom lens.

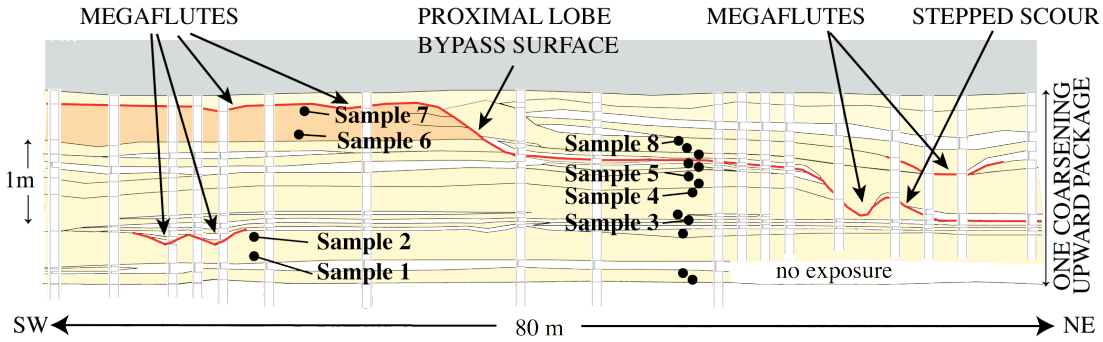

Figure 5.2. Location of sandstone samples taken from thickening-upwards package at Ross Bay (see Figure 4.3). Strarigraphic context of the package is provided in Chapter 4. 17 sample sites shown by black circles; samples from sites labelled 1 to 8 were also analysed using a combination of backscattered electron microscopy (BSEM), cathode luminescence (CL) and x-ray diffraction (XRD).

5.3. Results 1: sandstone properties

All of the analysed samples, including thick/thin sandstone deposits and those hosting/not-hosting megaflutes, showed identical compositional and textural properties. As a result, the images and results presented herein are considered representative of all the samples. BSEM and QXRD results (Table 5-1) reveal that the samples are composed of quartz, albite, chlorite and illite. BSEM reveals that the samples have a very low (<5%) porosity (Figure 5.3), and suggest the main processes that have reduced the porosity of the sample are: (i) mechanical compaction, and (ii) illite and chlorite precipitation.

Sample Number	Host bed to mega-flutes?	Quartz (wt. %)	Albite (wt. %)	Chlorite IIb (wt. %)	Illite 2M1 (wt. %)	Maximum estimated original clay (wt. %)
1	Yes	63.2	11.8	9.1	15.9	18.9
2	Yes	61.6	12.1	10.6	15.7	20.3
3	No	48.7	12.5	12.9	26.0	29.1
4	Yes	66.5	15.5	7.6	10.5	14.0
5	No	59.1	11.2	11.8	17.9	22.8
6	Yes	55.0	8.7	6.4	30.0	25.5
7	Yes	69.9	10.0	9.0	11.1	15.7
8	Yes	50.9	7.2	8.1	33.9	29.6

Table 5-1. Quantitative XRD results from analysed sandstone samples from the Ross Sandstone. The total clay estimate assumes that all the illite and chlorite formed from kaolinite:

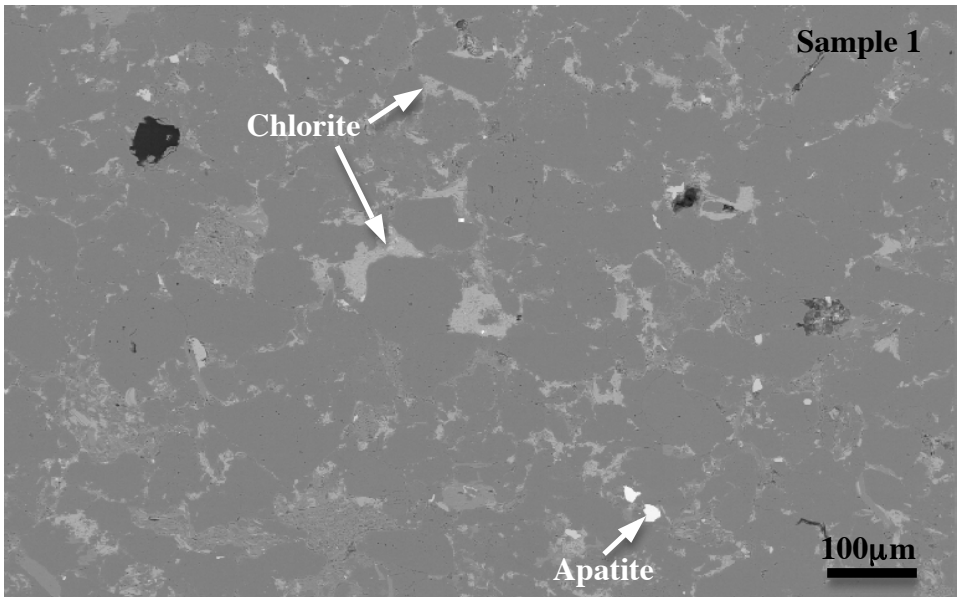

Figure 5.3. BSEM image showing the typical microstructure of the sandstones analysed from the Ross Sandstone; dark black grains are quartz and albite, pale grey grains are chlorite, bright white grains are apatite. Note that the sample has very low porosity.

The maximum estimates of original clay (Table 5-1) assume: (i) all illite within the rock formed as a result of the reaction between kaolin and K-feldspar, and (ii) all chlorite within the rock formed as a result of the reaction between kaolin and chlorite. Such assumptions require that:

Original Illite + 2Quartz + Water -> Kaolin + K-feldspar

And:

Dolomite + Kaolin -> **Current Chlorite** + CO_2

So that:

Current chlorite wt.% + Estimated original Illite wt.% -> Total estimated original clay

Further evidence for these reactions are presented:

1. The reaction of kaolin and K-feldspar to form illite is a very common reaction in sedimentary rocks (Chuhan et al., 2001) and is assumed here as the formative mechanism of illite in these rocks. Such an assumption is supported by the morphological similarities between the illite documented here and kaolinite

found in petroleum reservoirs that have not experienced high temperatures (e.g. Figure 5.4).

2. The coarse crystal structure of the illite and chlorite suggests that they formed at high temperatures (>150ºC) (e.g. Wilcoxon et al., 1990), and the chlorite crystal structures (IIb chlorites) suggest the samples experienced very late diagenetic/metamorphic conditions (Karpova, 1969). The high temperatures of formation for chlorite and mica suggest that they are either detrital deposits, or that the Ross Sandstone experienced late diagenesis or early metamorphic conditions. It is possible that the chlorite could have formed from an early authigenic or detrital clay. For example, the reaction between siderite and kaolin or the transformation of early authigenic bertherine during late diagenesis could all produce high temperature chlorite.
3. BSEM and CL analysis further reveals that the Ross Sandstone samples do not contain significant amounts of quartz overgrowth (Figure 5.5). It has previously been shown that the amount of authigenic quartz overgrowths tends to increase rapidly once sandstones are buried to a depth where the temperature exceeds ~80ºC (Walderhaug, 1996); therefore given the high temperatures that these rocks are known to have experienced during burial, they would be expected to show extensive quartz overgrowth. However, the main mechanism that restricts the progress of quartz overgrowths is the presence of clay minerals (e.g. Walderhaug, 1996). It is therefore argued that the lack of overgrowths within these samples is an indication that samples contained a large concentration of clay minerals prior to their burial beyond 80ºC.

An attempt has been made to quantify the amount of clay minerals that were potentially present within the rocks either upon deposition or soon after deposition (Table 5-1), and assumes all illite present formed via the reaction between kaolin and K-feldspar, and all chlorite present formed as a result of the reaction between kaolin and chlorite. Even if these values are over-estimated (for example some or all chlorite could be of detrital origin), the results indicate that the pre-alteration composition of the rocks, and therefore the original turbidite deposits, could have contained up to 18 - 30% clay.

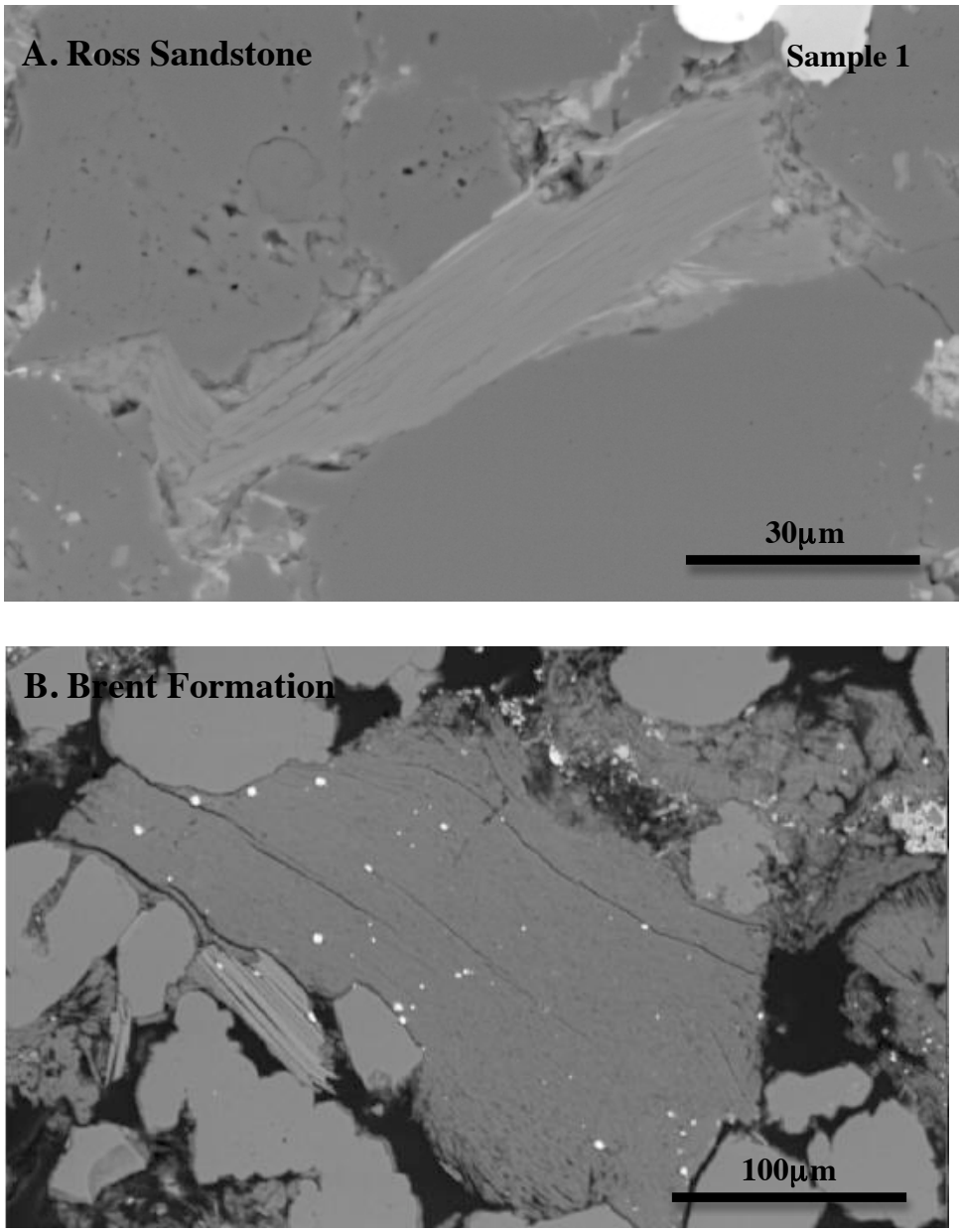

Figure 5.4. BSEM images illustrating kaolin from the Ross Sandstone and Brent Formation. A) Image of Ross Sandstone sample (sample 1, Figure 5.2) showing illite (central in photograph) pseudomorphed after kaolin, that has experienced shallow burial. B) Image showing detrital kaolin from a Brent Formation reservoir in the North Sea; the reservoir has only been buried to around 2200 m and a maximum temperature of 75ºC (image courtesy of Quentin Fisher). Note how the kaolin structure is comparable between both images.

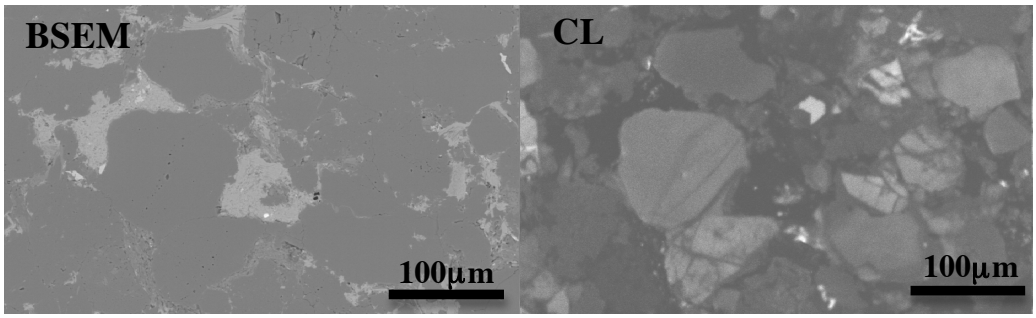

Figure 5.5. Backscatter scanning electron microscope (BSEM) and cathode luminescence (CL) images showing the same area of a Ross Sandstone sample (Sample 1, Figure 5.2, Table 5-1). Note the lack of syntaxial quartz overgrowth.

5.4. Results 2: scour types

Several scour types were documented, including megaflutes, flat-bottomed scours and stepped scours. These are each described herein.

5.4.1. Megaflutes

Megaflutes are developed exclusively in sandstone beds. Their rims are parabolic in planform and point upstream and widen and flare downstream. Using flute terminology of Allen (1971), megaflute interiors are either spoon-shaped with a steep lee-slope and more gently angled stoss slope (Figure 5.1a) or raised towards their centre with a median ridge (Figure 5.1b,c, Figure 5.6) producing a 'horseshoe' shaped form, and are herein referred to as "horseshoe megaflutes". The internal ridges are formed of remnant original substrate and are not depositional in origin. Spoon-shaped megaflutes are U-shaped in cross-section (Figure 5.7, Figure 5.8) whereas horseshoe megaflutes are W-shaped across the same profile (Figure 5.8). Thirteen megaflutes were surveyed, 7 of which were fully exposed and 6 were only exposed in their upstream region; their dimensions are presented in Table 5-2. Widths ranged from 0.44 – >8.00 m, depths ranged from 0.10 – 0.65 m, and lengths ranged from 0.80 – 6.55 m; however one exceptionally long megaflute exceeds 25 m length (Figure 5.9). A width verses depth plot of megaflute dimension data is presented in Figure 5.10 and the data points are colour-coded according to whether they have a spoon-shape or a central median ridge.

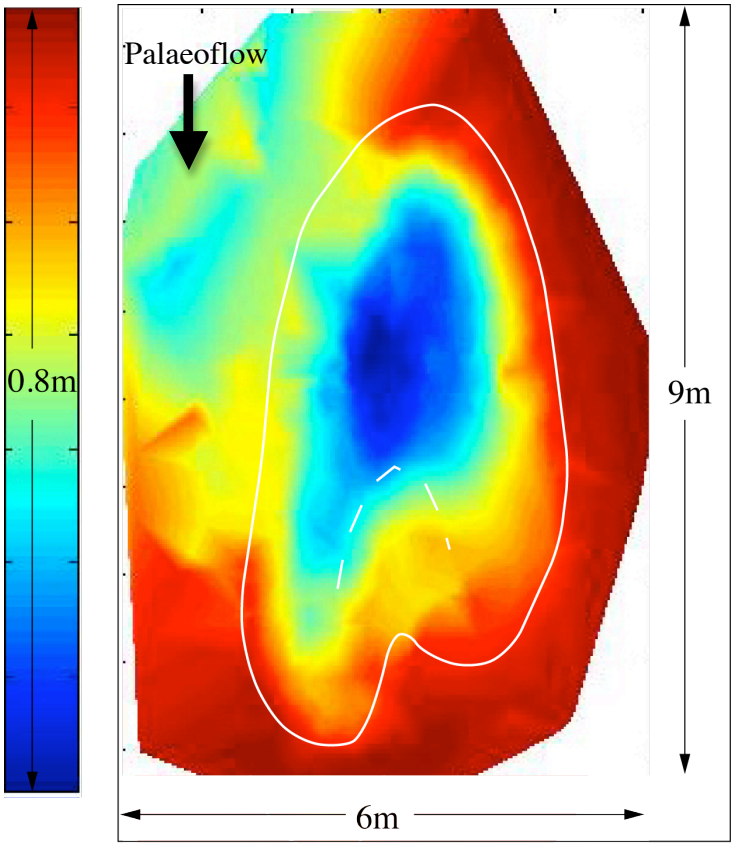

Figure 5.6. Bathymetric image showing the interior morphology of horseshoe megaflute. Contour colours represent depth as shown in left of image; data have been rotated to correct for the dip of the bed. White line outlines megaflute rim, dashed line shows position of median ridge, inferred palaeoflow is indicated. Megaflute is only partly exposed in the far lower right of the image, and the exposure to the top left of the image is heavily weathered. A photograph of this megaflute is shown in Figure 5.1C.

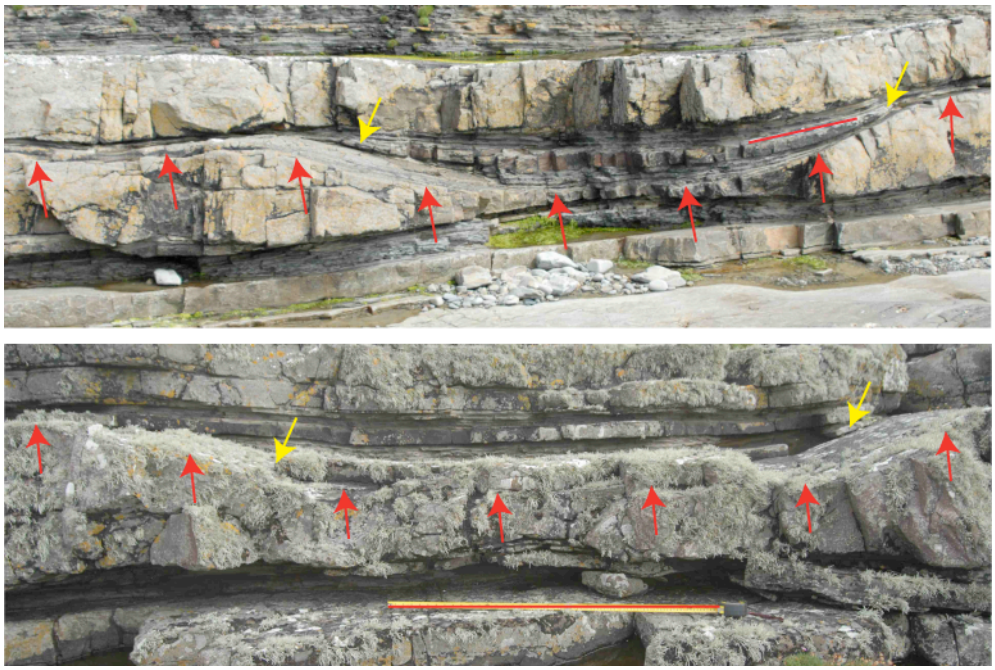

Figure 5.7. Cross sectional exposures of megaflutes of the Ross Formation; red arrows indicate position of megaflute surface. Yellow arrows indicate position of infilling deposits onlapping onto the megaflute surface. Metre rulers highlighted in red for scale. Locations: Kilbaha Bay (top), Ross Bay, south side (bottom).

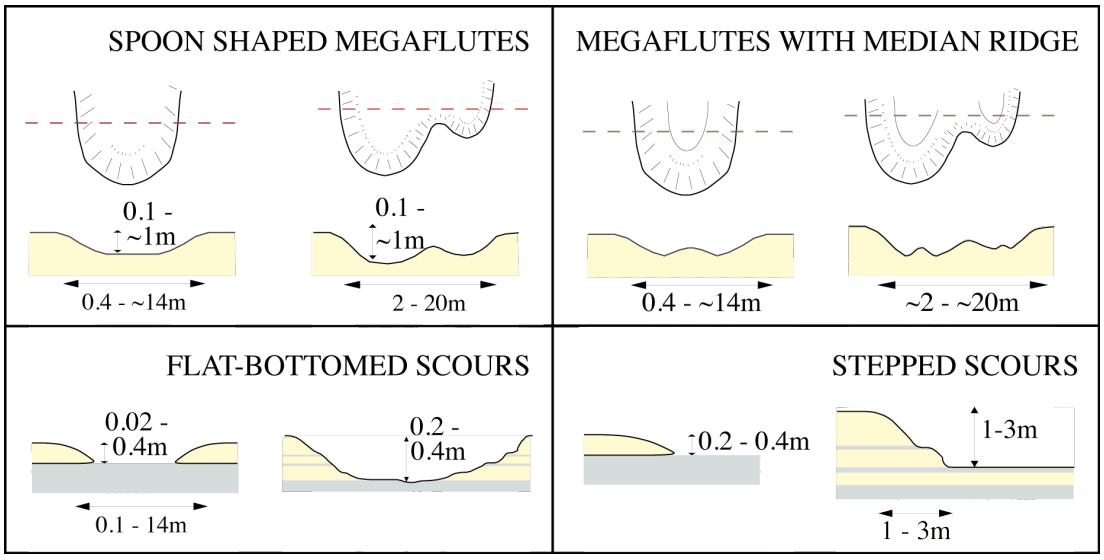

Figure 5.8. Summary of scour types observed in the Ross Formation, showing typical dimensions and cross sectional profiles. Planforms are also shown for megaflutes.

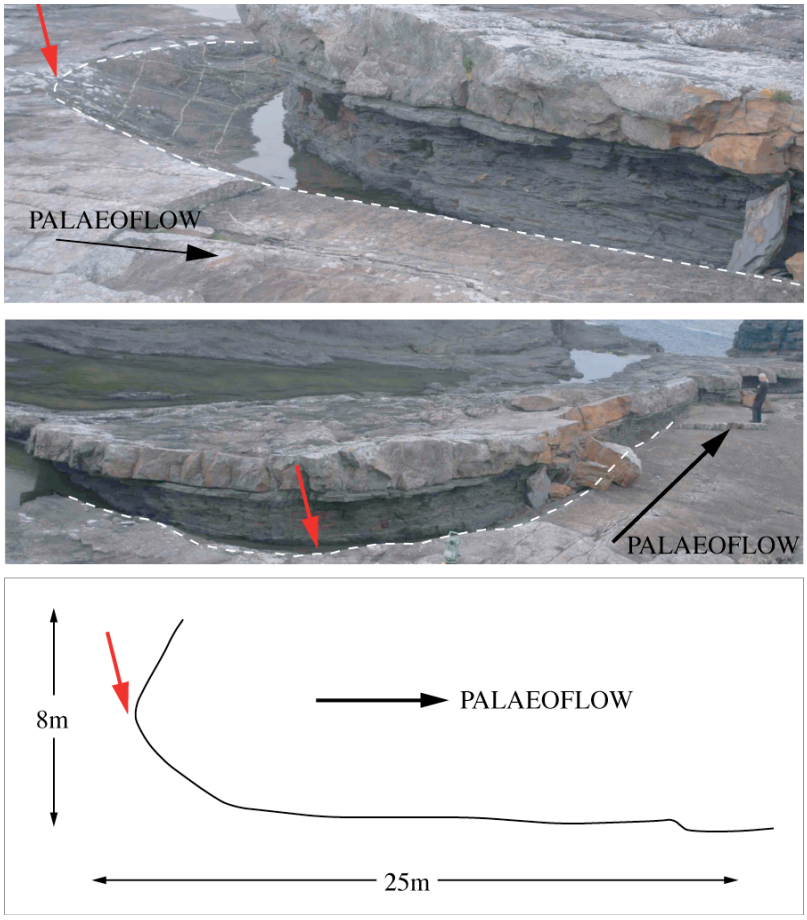

Figure 5.9. Partly exposed elongate megaflute of the Ross Formation, seen from two different angles and shown as a scaled planform line drawing from surveying data. Exposure shows a significant portion of the upstream megaflute and rim. Red arrow shows the most upstream part of the megaflute in each case. Location: Bridge of Ross.

Location	Data capture method	Width /m	Depth /m	Length / /m	Depth-Width Ratio
Ross Slab	LiDAR	2.24	0.20	2.26	0.089
Ross Slab	LiDAR	3.26	0.29	3.65	0.089
Ross Slab	LiDAR	1.70	0.15	1.60	0.088
Ross Slab	LiDAR	2.08	0.19	2.21	0.091
Ross Slab	LiDAR	1.23	0.15	1.08	0.122
Ross Slab	LiDAR	2.02	0.17	2.55	0.084
Ross Bay	TS	3.31	0.24	>3.55 **	0.073
Ross Point	TS	3.05	0.65	6.55	0.213
Ross Bay	TS	4.85	0.26	>2.50 **	0.054
Ross Bay	TS	2.94	0.16	>1.00 **	0.054
Ross Bay	TS	6.98	0.50	>4.41 **	0.072
Kilbaha Bay	TS	3.62	0.41	4.41	0.113
Kilbaha Bay	TS	0.44	0.10	0.80	0.227
Bridge of Ross	TS	>8 **		>25	n/a

Table 5-2. Dimensions of surveyed megaflutes from the Carboniferous Ross Formation. Data capture method TS is Leica Total Station (TCR805). See Figure 4.3 for locations.** denotes a partial measurement where the megaflute is not fully exposed – the full downstream length of the megaflute is therefore greater than this measured value.

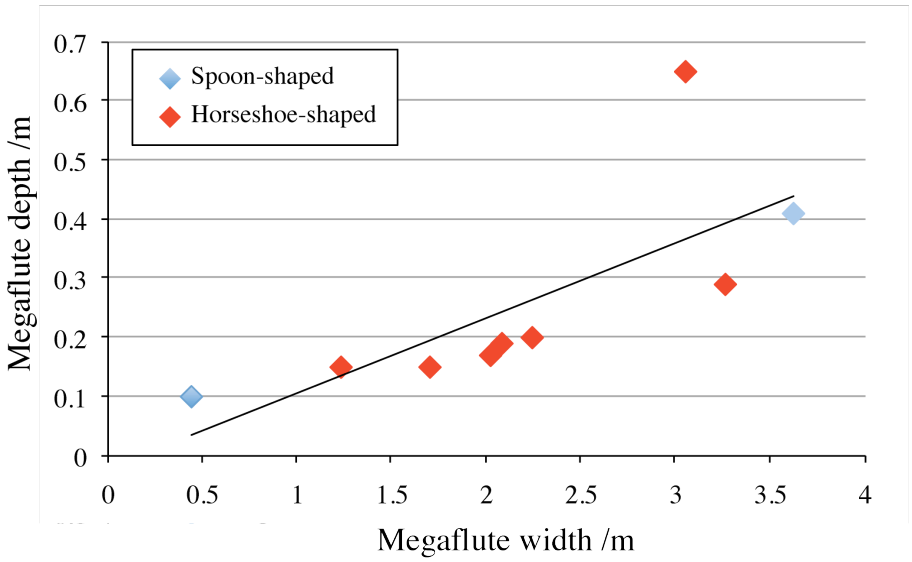

Figure 5.10. A plot of megaflute depth verses width for 9 fully exposed surveyed megaflutes from the Ross Sandstone. Dimensions listed corrected for the dip of the bed. Regression line is also shown.

The infilling sediments of megaflutes comprise either multiple or single beds of mudstone and/or sandstone, and often do not extend beyond the limits of the megaflute but onlap onto the interior (Figure 5.7). The first deposit within megaflutes may be a mud-chip conglomerate with mud-chip sizes of 1 cm – 20 cm (Figure 5.11).

Megaflutes may be located in groups along the same bedding surface (Figure 5.12, Figure 4.4a,c), and often their rims may coalesce laterally to produce amalgamated megaflutes that have irregular, cuspate rims and a series of concave-up depressions to their interior (Figure 5.13). Amalgamated megaflutes are commonly (but not always) larger than isolated megaflutes, and are usually wider (up to 20 m) than they are long.

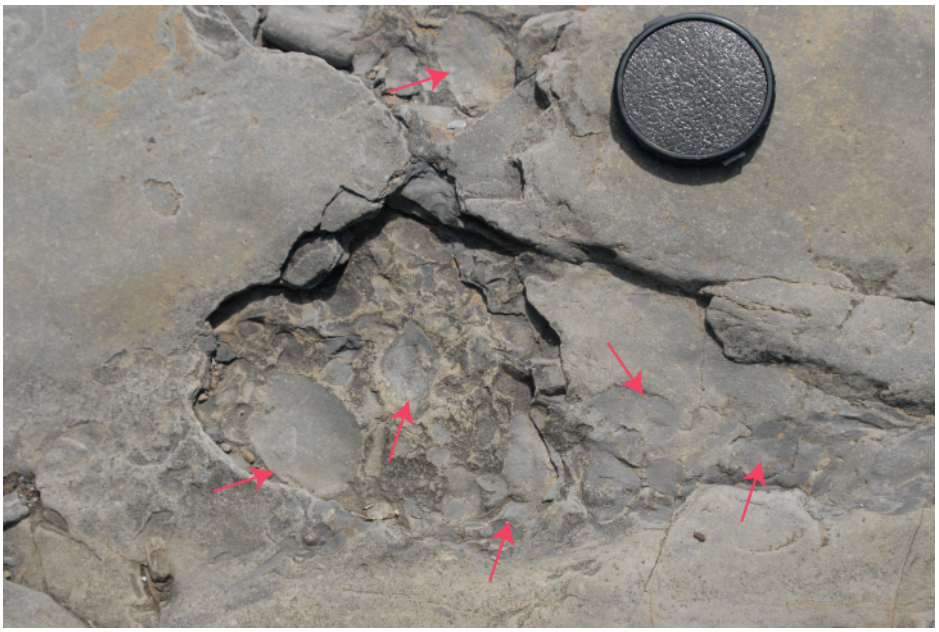

Figure 5.11. Mud chip conglomerate veneer within a megaflute, mud chips highlighted by red arrows. Lens cap (5cm diameter) in top-right for scale. Location: Ross Point (megaflute shown in Figure 5.1c).

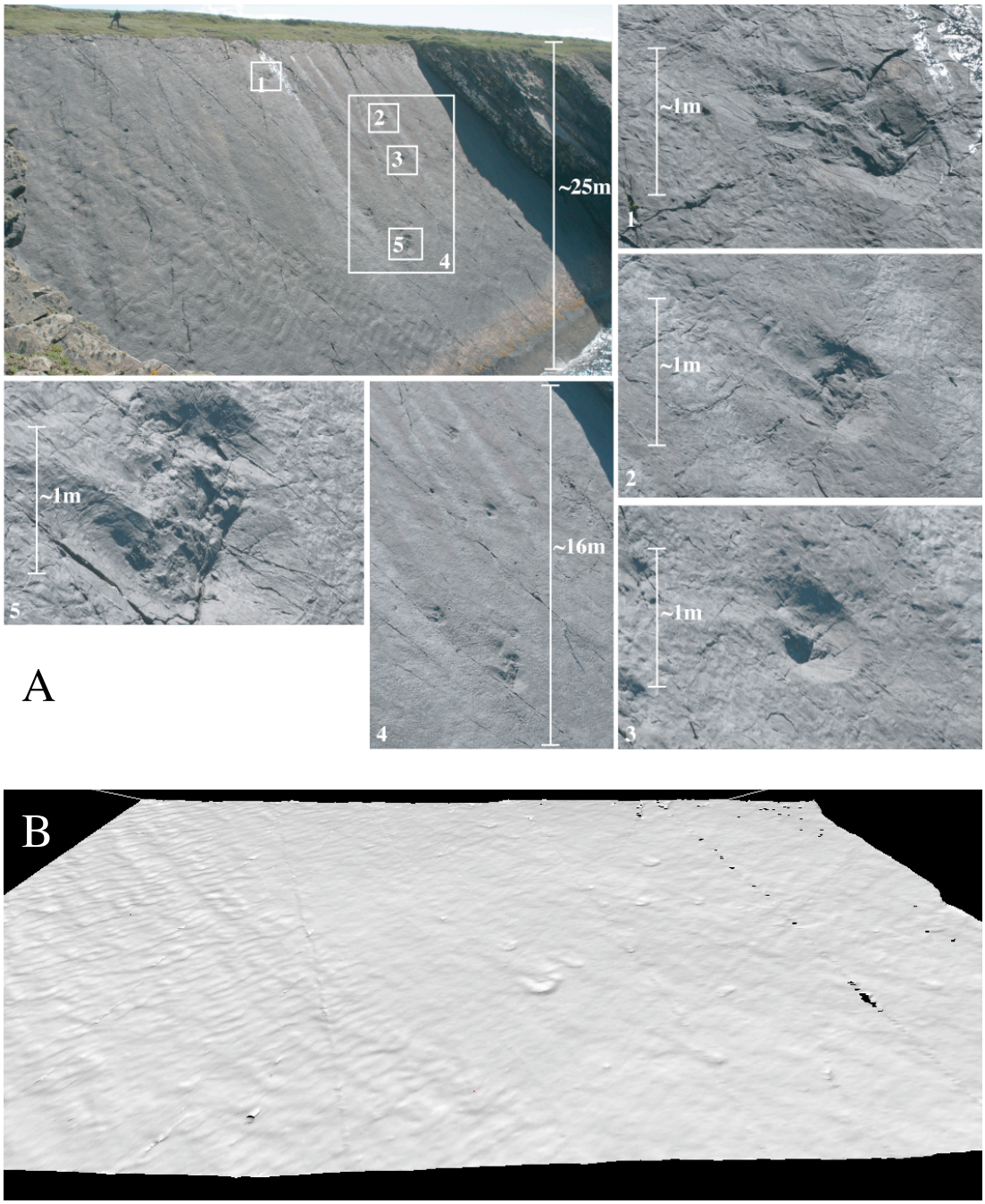

Figure 5.12. Images of a megafluted single bedding surface of the Ross Sandstone. (A) Photograph montage showing overall exposure and individual megaflutes. Top left photograph shows the single bedding surface exposed at ~080/60ºN, Jeff Peakall in upper left of top photograph for scale. Individual megaflutes are numbered and shown in detail in inset photographs; note that the megaflutes all have an overall parabolic shape with a central medial ridge. (B) LiDAR image of whole bedding surface, courtesy of StatoilHydro. Note the megaflute depressions to the centre of the bedding surface, and dune-scale bedforms in the left of the image. Location: Ross Slab (52º36'10.94"N, 9º48'39.12"W), shown in Figure 4.3

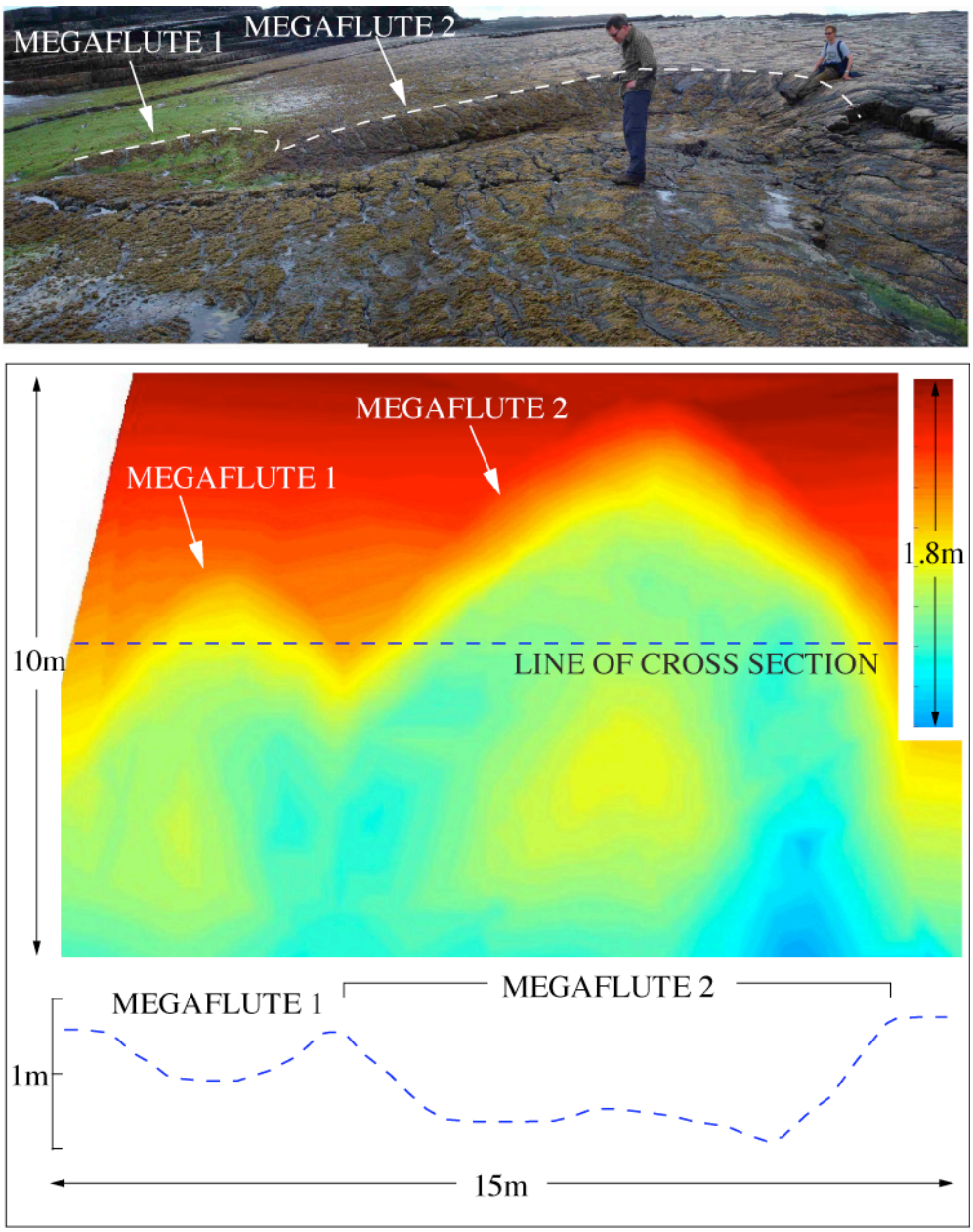

Figure 5.13. Photograph and detailed bathymetric image showing two partly amalgamated horseshoe-shaped megaflutes. Data have been rotated to correct for the dip of the bed; contour colours indicate megaflute depth and morphology as indicated by the inset colour bar (top right). The megaflutes are not of equal dimensions, but share similar morphologies with a parabolic shaped rim, steep lee-slope and an interior hummock. The bathymetric image has been corrected for the dip of the bed.

Most megaflutes are developed on rippled surfaces, with straight-, wavy-crested or linguoid ripples of ~1 cm height and 10 – 15 cm wavelength. In one locality, dune-scale bedforms (height ~10 cm, wavelength ~1 m) are seen on the same bedding surface as a number of megaflutes (Figure 5.12B). Megaflute interiors are generally smooth, although the infilling beds can be rippled (e.g. Figure 5.1a). Megaflute rims exhibit a sharp boundary between the smooth megaflute interior and the rippled surrounding surface, and the ripples do not show any interference or bending of crests with increased proximity to megaflutes (Figure 5.14). In one unique example, ripples that surround a conjugate pair of extremely shallow (<10 cm deep, ~2 m total width) megaflutes descend into the interior of the megaflutes; the ripples crests are deflected by the topography of the megaflute. This occurrence is located at Ross Point ~15 m southwest of the stratigraphic panel shown in Figure 4.4c (see also Figure 4.3); however it is poorly exposed (a rockpool in an intertidal position) and not photogenic.

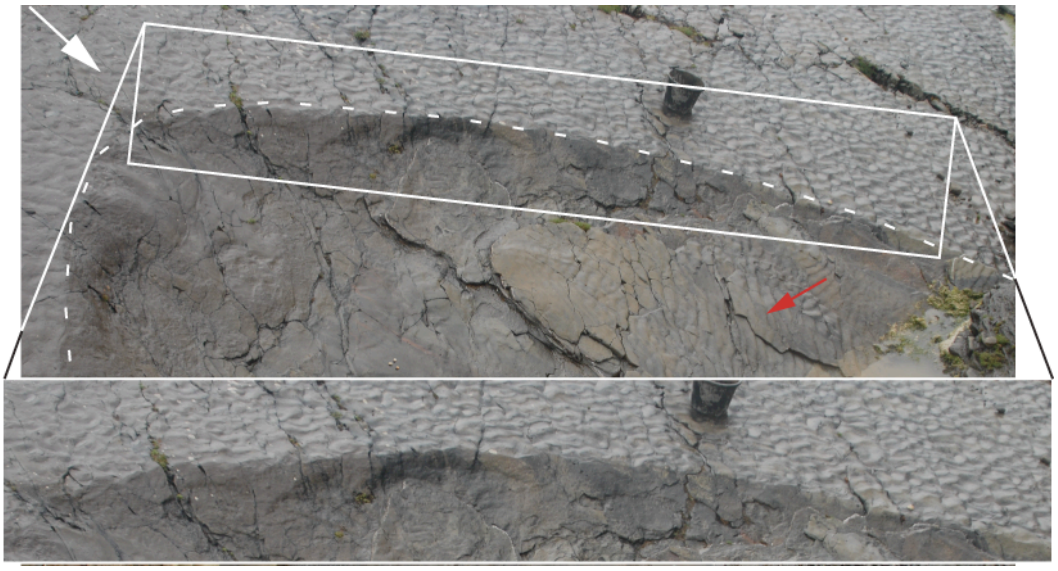

Figure 5.14. Sandstone surface with 6.98 m wide megaflute, surrounded by linguoid ripples. Dashed white line shows megaflute rim; enlargement of photograph shows the sharp truncation of the ripples at the megaflute rim. Red arrow indicates a rippled sandstone bed that drapes the megaflute interior. The megaflute surface itself is smooth. White arrow indicates palaeoflow direction. Black bucket shows scale.

5.4.2. Stepped or flat-bottomed scours

Stepped and flat-bottomed scours cut steeply into the surface of sandstone beds, and are only distinguished from each other according to their symmetry (Figure 5.8). Stepped scours cut entirely through a bed, providing a stepped appearance (Figure 5.15), whereas flat-bottomed scours have two steep erosional 'sides' and a flat-bottomed interior (Figure 5.16). Both stepped and flat-bottomed scours may erode through single or multiple beds. In planform, the step of the erosional surface is linear and arranged approximately parallel to paleoflow. Depths of these scours vary from 1-40 cm, and they commonly bottom-out on mudstone beds.

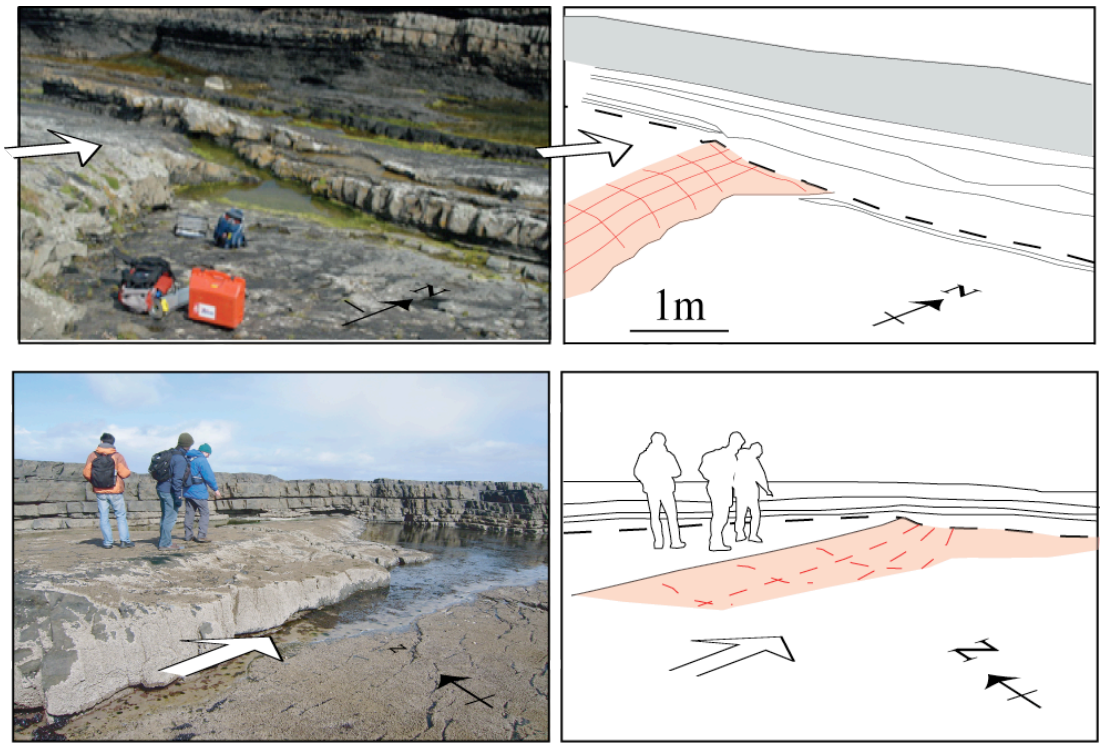

Figure 5.15. Photographs and representative schematics of stepped scours from the Ross Formation. Red shaded areas illustrate the eroded stepped surface. White arrows indicate palaeoflow. Black dashed lines mark the position of broad bypass surfaces (see Chapter 0). Top location: Ross Bay. Bottom location: Ross Point.

Figure 5.16. Flat-bottomed scour from the Ross Formation. White arrows highlight a sandstone bed at the point it is truncated at the margin of a stepped scour. The white dashed line indicates the location of the flat-bottomed scour where the sandstone bed is no longer present. Scour measures ~15 m across, and is exposed in cross-section only. Yellow hammer circled for scale. Location: Ross Bay.

5.4.3. Broad bypass surfaces

Broad bypass surfaces are the largest form of erosional feature documented in this study, with widths >160 m and depths >2 m (Figure 5.8). The surfaces cut through multiple beds of coarsening-up cycles, and commonly adopt a stepped nature at each new bedding surface that it cuts through. The broad surfaces often show smaller erosional features, including megaflutes, stepped-scours and flat-bottomed scours, as is indicated in Figure 5.15. The broad surfaces are infilled by a range of mudstone, sandstone and mud-chip conglomerate beds, which often host further erosional bedforms. Broad bypass surfaces are illustrated in Figure 4.4 are termed proximal lobe bypass surfaces.

5.5. Summary: a spectrum of erosive features

The erosional bedforms observed in this study occur across and range of scales and dimensions, so that they develop a spectrum of erosive features. Flat-bottomed scours have the broadest range in size, ranging from centimetres in width and height, and scale-up into the size range of megaflutes. Megaflutes reach widths of ~14m and depths of up to ~1m, and overlap marginally with stepped scours, which reach depths of 0.4 m (through single beds) to 3m (multiple beds). Broad erosional surfaces occur across many tens of metres in width and several metres in depth, and comprise flat-bottomed scours, megaflutes and stepped scours.

This spectrum of erosional bedforms indicates that there is a continuum of bedforms ranging from centimetres in width and depth, to >100 m wide and >3 m deep. However each type of bedform occurs within a different type of bed (or beds). Thus: (i) flat-bottomed scours erode mostly or fully through sandstone or sandstone/mudstone interbeds, and commonly 'bottom-out' on mudstone beds; (ii) megaflutes are preserved entirely within sandstone horizons formed either of single or amalgamated beds, but are never associated with erosion through mudstone deposits; (iii) stepped scours erode through any number of beds of either mudstone or sandstone. Broad bypass surfaces are the largest erosional feature and are inferred to be the final member of the erosive spectrum; they are here considered as proximal-lobe bypass surfaces, eroded by feeder-channel processes operating in the proximal region of prograding lobe-elements (Chapter 4.4.2). Although they are considered within the spectrum of erosional features, it is clear that their processes of formation are different to megaflutes, stepped- and flat-bottomed scours.

These bedforms are systematically developed in thickening upward packages within the Ross Formation (described in Chapter 4.3.1). They occur throughout the sandstone beds within the thickening-upward packages but are especially prevalent in the uppermost deposits, which may explain why previous studies erroneously document megaflutes exclusively or primarily within the upper surface of these thickening-upward packages (e.g. Elliott, 2000a,b; Lien et al., 2003). Chapter 4 describes the sedimentology of thickening-upward packages at three locations within the Ross Formation (Figures 5.3 and 5.4), and documents the distribution of erosional features within the packages. The packages are interpreted as the deposits

of prograding lobe-elements within a distributary submarine fan, and a six-stage model is provided to explain their formation (Figure 4.6).

5.6. Discussion

5.6.1. Cohesive properties of the Ross Sandstone

As described in Chapter 4.4.1, the Ross Sandstone sandstones consists of predominantly fine-grained, structureless sands. SEM and XRD analyses presented in this chapter provide strong evidence to suggest that these sandstones originally consisted of up to 18 – 30 % clay at the time of deposition. This high clay content has not previously been documented in published literature. Unfortunately, experimental investigations into the deposits and transport regimes of mud and sand mixtures (e.g. Baas et al., 2009; Sumner et al., 2009) are not directly comparable to the Ross Sandstone deposits analysed here, simply because they contain much higher mud levels than is inferred for the analysed samples. For example, the least mud-rich mixture investigated by Sumner et al. (2009) was 6 vol% mud (10 vol% silica sand, 84 vol% water), which excluding water, provides a mud content of 38%. However these experimental investigations did reveal that flows with lower mud contents deposited structured sands with a well-defined mud cap, whereas more mud-rich flows deposited structureless and ungraded deposits with a mud cap (Sumner et al., 2009). This, although not directly comparable to the deposits analysed here, does qualitatively suggest that the structureless and ungraded sandstone deposits of the Ross Sandstone are more mud rich than those that exhibit grading or Bouma divisions.

The structural and mineralogical analysis of the Ross Sandstone samples indicates that there is no variance in sandstone properties: (i) between megaflute-hosting and non megaflute-hosting sandstones, or (ii) with increasing height through thickening-upward packages. The six-stage model for the development of thickening-upward packages presented in Chapter 4 implies that each package is deposited by distal- through to proximal-deposition of prograding lobe-elements (Figure 4.6). This, together with the consistency in sandstone properties through the thickening-upward packages, suggests that the distal reaches of erosive flows (i.e. the basal package deposits) are of the sedimentary composition as the increasingly proximal more erosive flows (i.e. upper package deposits). The only stage of

complete bypass, and therefore the only stage that is not recorded within the sedimentary deposits of the package, is an erosive phase in the upper-part of the package (t_4 in Figure 4.6).

These new compositional data for the Ross Sandstone have therefore created numerous new questions regarding the original composition of the sandstones and their emplacement mechanisms. Yet in the absence of experimental analogues, it is not yet possible to infer a transport regime to the sandstones of the Ross Sandstone. Importantly, it appears necessary to question the reliability of calculating the composition of early diagenetic/low grade metamorphic sandstones.

5.6.2. The relationship between megaflutes and ripples

This investigation documents two forms of megaflute – ripple interaction: (i) an erosive megaflute-ripple boundary where the megaflute rim sharply intersects the ripples, and indicates the ripples were present prior to the formation of the megaflute, and, more rarely, (ii) a gradual boundary at which the ripples pass into the interior of the megaflute, indicating the ripples formed following the development of the megaflute, but before it was infilled. Both types of boundary have been previously reported, however, the only previous claim of the second type (Elliott, 2000b) is curiously supported with a photograph that shows a sharply erosive megaflute rim and smooth megaflute interior (Elliott, 2000b; his Figure 2). This same megaflute is presented here in Figure 5.1a. Additionally, Lien et al. (2003) refute Elliott's claim.

In the case of megaflutes forming after ripples, the high clay content documented by compositional analysis presented in this chapter may have provided additional cohesive strength to the ripples shortly after deposition. Additionally, Lien et al. (2003) suggest that the ripples remain intact and unaffected by the erosive megaflute-generating flow because they were shielded by a protective layer of mudstone. This seems a plausible explanation and would further explain how the ripples resist re-working to become deflected towards the megaflute. However the presence of a mudstone veneer would have implications for the development of megaflutes because it suggests the megaflute initially eroded through a veneer of mudstone, before developing in the sandstone bed. Nevertheless, it is also possible that the mudstone veneer was absent at the site of megaflute formation, and had

some influence on the positioning of the megaflute. This suggests that megaflutes may develop at sites of substrate weakness.

5.6.3. Bed thickness as a control on the development of bedforms

Observations made here suggest that bed thickness can control development of a specific bedform. This is illustrated in a schematic in Figure 5.17, which assumes the rate of erosion and the duration of erosive flow remains constant between examples. If an erosional bedform develops on a sandstone bed, it will continue to expand for as long as the flow remains erosive. If the host sandstone is of sufficient thickness, bedform development will not be interrupted and will develop into a smooth megaflute (Figure 5.17a). If the host sandstone is situated immediately above another sandstone bed, the bedform will propagate through both beds and may experience minor 'stepping' at the bedding interface (Figure 5.17b). However if the sandstone is relatively thin but overlies a thick mudstone bed (Figure 5.17c), or if erosion propogates through multiple thin mudstone and sandstone beds (Figure 5.17d), the bedform may develop as either a flat-bottomed scour (if the scour is recognizable on both sides) or a stepped-scour (if the scour is only seen to descend).

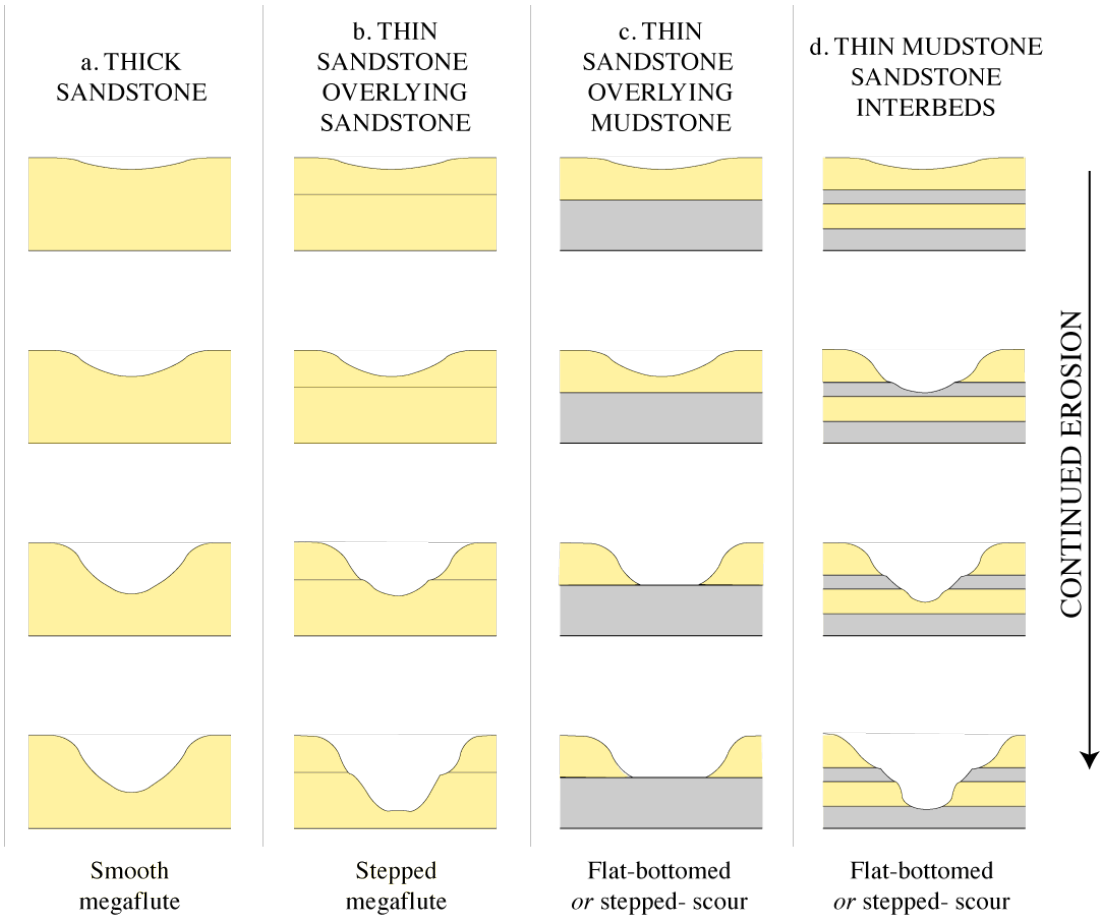

Figure 5.17. Schematic cross sectional profiles illustrating how sandstone bed thickness controls development of erosional bedforms during constant-rate erosional events. Not to scale.

This also has implications for the classification of flat-bottomed scours and stepped-scours as separate bedforms. Stepped scours observed in the Ross Sandstone are typically deeper than flat-bottomed scours, but this may be partly controlled by the thickness of its host bed(s). Furthermore, their greater depth (where the host bed allows) may also be associated with greater width (as is the case for megaflutes, see Figure 5.10); and the larger the bedform is, the less likely it is to be fully exposed in outcrop. Therefore the "one-sided" nature of stepped-scours may in fact be an artifact of how they are exposed. If the bedforms are related, it further suggests that the linear nature of stepped-scours may also translate to flat-bottomed scours. Although this is a tentative observation, other such linear features have previously

been documented in modern (Flood, 1983; Wynn et al., 2002b) and subsurface (Gervais et al., 2006) turbidite systems; termed lineations, furrws or gullies.

5.6.4. Megaflute and scour genesis

Previous authors attribute scour and megaflute development to hydraulic jumps associated with a change in flow regime, specifically at the transition of supercritical to subcritical flows (Komar, 1971; Mutti and Normark, 1987, 1991; Normark and Piper, 1991; Chapin et al., 1994; Kenyon et al., 1995; Palanques et al., 1995). Such transitions are thought to occur in positions of significant flow expansion, such as in channel/canyon mouths, in overbank positions at the bends of sinuous channels, and at the base of steep slopes (Figure 2.18). However in reality this is probably a highly complex situation, and dependent upon a number of local environmental controls including current volume and composition (Wynn et al., 2002a) and substrate properties.

The environment of formation favoured for the Ross Formation erosional bedforms is a channel-lobe transition setting seen at the terminus of prograding lobe-elements. In this setting, the region of expansion occurs at a feeder-channel to lobe-element transition; see Chapter 4.4.2 and Figure 4.4. It is unlikely whether this scale of transitional zone is sufficient to invoke hydraulic jumps, especially considering the degree of expansion is not as extreme as in larger-scale canyon/channel mouths (e.g. Wynn et al., 2002b; Kostic and Parker, 2006). Further to this are the considerations that: (1) the lobe-elements are in a terminal position and located too distally upon the fan to invoke hydraulic jumps; (2) megaflutes are very common implying numerous individual hydraulic jumps for their development. Importantly however, many published examples of scours in deep-sea environments that discuss development via hydraulic jumps do not discuss alternative mechanisms for formation (e.g. Wynn et al., 2002b; Normark et al., 2009). One exception to this is Chapin et al. (1994) who suggest megaflute-scouring vortices unrelated to hydraulic jumps "*may be induced by irregular depositional topography implied by compensation bedding that cause local disturbances in the flow*". In agreement with Chapin et al. (1994) it is suggested that megaflutes, flat-bottomed and stepped-scours of the Ross Sandstone are caused by erosive turbulent vortices that impinge on sand bedding surfaces in a medial- to proximal- lobe-element locality, and that these vortices are unrelated to hydraulic jumps. Furthermore, owing to their development

in a medial to proximal setting within prograding lobe-elements, it is highly likely that their development is influenced by the topography associated with earlier distal deposits over which the subsequent deposits prograde.

The manner in which the bedforms evolve further is dependent upon: (1) the nature of the deposits they are eroding into: (2) their proximity to other erosive features, and (3) the duration and power of the erosive flow. Bedform development, erosion and/or bypass is maintained for as long as the system remains non-depositional at that locality.

5.7. Conclusions

Conclusions to this chapter comprise 7 parts:

1. Sandstone beds of the Ross Sandstone are of consistent microstructure and mineralogy had an original depositional clay content of 18 – 30 %;
2. The Ross Sandstone likely experienced early diagenetic or low grade metamorphic conditions;
3. Megaflutes of the Ross Sandstone are parabolic in planform with rims that point upstream and flare out downstream; they may be spoon shaped or have a central median ridge;
4. These megaflutes range in size from 0.44 – >8.00 m wide, 0.10 – 0.65 m deep and 0.80 – 25 m long; amalgamated megaflutes also develop where megaflutes coalesce laterally;
5. Megaflutes almost exclusively cut into rippled surfaces, and exhibit smooth megaflute interiors;
6. Megaflutes form part of a spectrum of erosive features, comprising a spectrum of flat-bottomed scours, stepped-scours and megaflutes;
7. The development of the erosive bedforms is partly dependent on host-bed thickness;
8. The erosive features develop in a medial- to proximal-lobe element position.

6. High-resolution imaging of deep-water erosional scours along the northeast Atlantic margin

6.1. Introduction

Large-scale erosional scours are indicative of the passage of highly erosive turbidity currents that are often voluminous and fully bypassing. They are a key component of many deep-water channels and fans. However, although existing data capture methods (e.g. side-scan sonar) have provided a broad understanding of their formative locations (see Chapter 2), their processes of formation, morphologies and dimensions are still relatively poorly understood. This low level of understanding is primarily based upon the difficulties encountered when collecting bathymetric and/or sedimentological data from deep-sea environments. In order to address this, this study presents high-resolution images of deep-water scours from 4 different deep-water channel/canyon systems along the northeast Atlantic continental margin (Figure 6.1), and their sedimentology is analysed via sediment cores. The images were obtained via an Autonomous Underwater Vehicle (AUV) instrumented with a high-resolution multibeam bathymetry system. These images are the first such images obtained from a deep-water environment. Using this approach, each of the scours is evaluated by assessing the scour size, morphology and sedimentology.

Data presented in this chapter were collecting during a research expedition on RRS *James Cook* in August 2008 (JC27). The author was part of the scientific crew upon JC27 and worked in a team that handled, cut and archived sediment cores. Additional responsibilties of Macdonald included the logging, sampling and direct interpretation of cores, the interpretation of high-resolution AUV images, and the preparation of all illustrative figures.

6.2. High-resolution AUV imaging of deep-water scours

This study utilises data obtained by Autosub6000, which is a newly developed AUV capable of operating close to the seafloor at water depths of up to 6000 m (Huvenne et al., 2009). The AUV was instrumented with a high-resolution multibeam bathymetry system, in order to map the planform morphology of deep-water scours in unprecedented detail. These high-resolution images are combined with accurately

targeted piston cores, in order to provide information on erosion history and scour fill. The results provide new insights into scour genesis (particularly large-scale amalgamated scours) and highlight the variability in scour morphology and fill in different turbidite systems along a single stretch of continental margin.

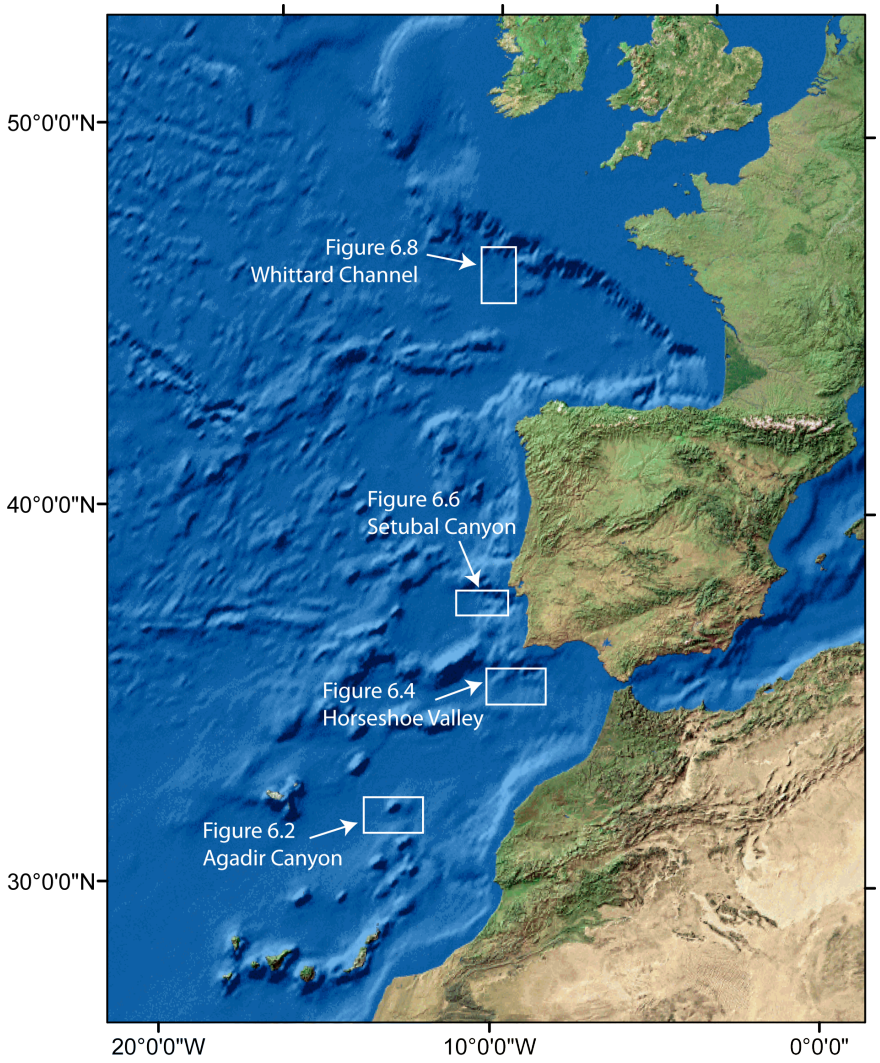

Figure 6.1. Location map of the four study areas along the northeast Atlantic continental margin. White rectangles show areas covered by figures as labelled.

6.3. Study area

This study investigates erosional scours in four deep-water canyon/channel systems along the northeast Atlantic continental margin (Figure 6.1). These are: 1) Agadir Canyon mouth, 2) Horseshoe Valley, 3) Setúbal Canyon mouth, and 4) Whittard Channel margin (see also Chapter 2). These locations were selected because they cover several tectono-climatic settings with a variety of shallow- to deep-water sediment transport regimes (Weaver et al., 2000). For example, Agadir Canyon is

dominated by infrequent (1 every ~10,000 yrs), large-volume flows (>10 km^3 of sediment), sourced from the Morocco Shelf (Wynn et al., 2002b), whereas Whittard Channel is dominated by frequent (up to 130 per 1000 yrs) smaller flows, mostly during glacial lowstands when fluvio-glacial outwash supplied sediments directly to the head of Whittard Canyon (Toucanne et al., 2008).

6.4. Methods and data

6.4.1. Geophysical data

The majority of geophysical data presented here were collected during a research expedition on RRS *James Cook* in August 2008 (JC27). Data collected using hull-mounted multibeam bathymetry (EM120) and sub-bottom profilers (SBP120 and 3.5kHz) provide information on the overall planform and cross-sectional geometry of the seafloor. However, the main dataset presented here is high-resolution AUV multibeam bathymetry, collected using an EM2000 system housed within the Autosub6000 AUV. Autosub6000 was able to cover an area of ~25 km^2 within a 24-hour mission, and the EM2000 system was able to image seafloor features with a pixel size of 2x2 m. Data were subsequently processed using the IFREMER software suite 'Caraibes'.

6.4.2. Sedimentological data

A series of shallow piston cores were collected from each of the four work areas, with a maximum penetration of 6.5 m. Core sites were chosen once high-resolution multibeam bathymetry images were downloaded and visualised, and were selected to hit targets >50 m across. RRS *James Cook* is equipped with a Dynamic Positioning (DP) system, while any potential offset created by drift of the corer was monitored using an Ultra Short Base Line (USBL) acoustic positioning system located on the coring wire at depths of up to 2.5 km. Visual core logging included sediment facies, colour and grain size. All logged deposits were ultimately identified as turbidite, debrite or hemipelagite.

6.4.3. Dating control

Microfossil-based dating of hemipelagic sediments in the studied cores was used to identify erosional hiatuses. Ratios of different coccolith species were identified and a combination of first and last appearance and overall abundance of dominant species

then used to develop a chrono-stratigraphy that is tied into the oxygen isotope stratigraphy at specific oxygen isotope stages (OIS) (Weaver and Kuijpers, 1983; Weaver, 1994; Wynn et al., 2002b). Bioturbation of hemipelagic sediments and other potential errors mean that ages are accurate to within ~10%.

6.5. Results

6.5.1. Agadir Canyon mouth

Agadir Canyon extends northwestwards over 450 km from the Morocco Shelf (100-200 m water depth) to the eastern Agadir Basin (~4500 m water depth) (Figure 6.1, Figure 6.2a) and acts as a conduit for large-volume siliciclastic flows (Wynn et al., 2002b; Frenz et al., 2009). Previous studies mapped a major zone of erosion in the canyon mouth area immediately downstream of an intra-canyon slope break (slope change of 0.2° to 0.04°; Wynn et al., 2002a). Existing low-resolution data reveal kilometre-scale isolated and amalgamated scours.

The new high-resolution imagery presented here (Figure 6.2) confirms the presence of both isolated and amalgamated scours, covering an area of ~15 km^2 in the canyon mouth. The deepest erosion is focused within isolated scours along the northern margin of the broad, flat canyon axis; these scours cut into the gently sloping margin of the canyon floor. Isolated scours are spoon-shaped and elongated downslope, with U-shaped cross-sectional profiles that shallow and taper downstream. Maximum scour depths and sidewall slope angles are consistently within the upstream 60% of the scours; the steepest slope angles (20°-50°) are largely confined to scour headwalls and sidewalls (see profiles A-A' and B-B', Figure 6.2b). Scour dimensions vary between 150-600 m long, 40-225 m wide and 8-20 m deep. Scours 1 and 2 (Figure 6.2b) are the largest identified isolated scours. Scour 2 exhibits a rim opening and low sidewall slopes (0.5°-6.5°) along its southwest margin, where it borders a region of amalgamated scour. This amalgamated scour displays a broadly flat-bottomed morphology, but includes several erosional remnants within the scour floor and in cuspate rims at scour margins (see cross section C-C', Figure 6.2b). The imaged area of amalgamated scour extends across >4 km^2 and can be subdivided into smaller zones of amalgamation that are bound by

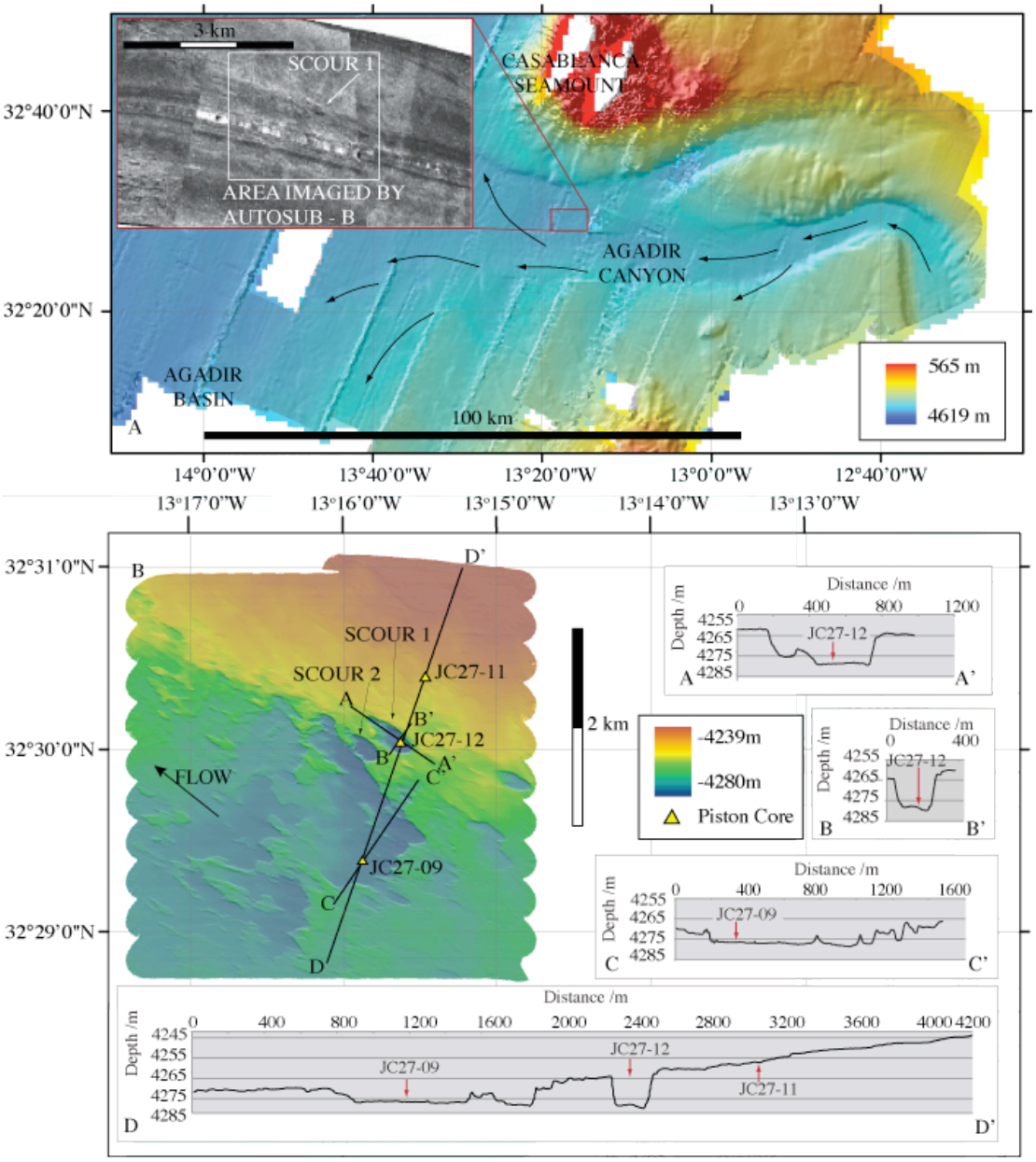

Figure 6.2. Erosional scours in Agadir Canyon mouth, offshore northwest Morocco. (A) Regional EM12 multibeam bathymetry showing the morphology of lower Agadir Canyon. Black arrows show interpreted flow pathways. Inset figure shows TOBI 30 kHz sidescan sonar profile of the scoured region (located by the red rectangle on EM12 data). Light tones are high backscatter. White rectangle shows location of Autosub6000 imagery. (B) High-resolution Autosub6000 image and cross sectional profiles of isolated and amalgamated spoon-shaped scours. Locations of piston cores shown in Figure 6.3 are provided.

high-standing topography. The headwall of the amalgamated scour comprises a series of cuspate scars, similar in apparent dimensions and morphology to the headwalls of adjacent isolated scours.

Three piston cores were obtained from within the imaged region along a SSW-NNE transect: JC27-09, JC27-12 and JC27-11 (Figure 6.2b and Figure 6.3). Core JC27-09 targeted the floor of the amalgamated scour, and recovered ~4.0 m of sediment including a total of 13 turbidites. The youngest turbidites comprise thin (<5 cm), normally-graded, very fine-grained and well-sorted basal sands, with thin planar and cross-laminations (*Tc* and *Td*; Bouma, 1962). Overlying mud caps are up to 65 cm thick, and intervening hemipelagites are present between each turbidite (dated at OIS 1-3; <60 ka). In contrast, older deposits (below 1.8 m core depth and dated at OIS 4-5; 60-130 ka) display 5-10 cm thick, normally graded, medium-grained, planar and cross-laminated basal sands (*Tc* and *Td*), with erosive bases and rip-up clasts; these sands are overlain by comparable thicknesses of turbidite mud. A thin clast-rich muddy debrite overlies an apparent erosional hiatus at 3.4 m that likely occurred around the OIS 5/6 boundary at ~130 ka (Figure 6.3). Immediately beneath this hiatus are the oldest hemipelagic sediments sampled in the core, which contain *P. lacunosa* and are therefore older than OIS 13 or ~450 ka (Weaver and Kuijpers, 1983; Weaver, 1994). The hiatus therefore corresponds to at least 320 kyrs of erosion and probably represents several metres of missing sediment.

Core JC27-12 targeted the floor of the deepest isolated scour, and recovered 1.0 m of sediment including five turbidites (Figure 6.3). These turbidites typically display thin (<5 cm), fine- to medium-grained, planar- and cross-laminated basal sands (*Tb* and *Tc*), with 5-15 cm thick overlying mud-caps. Coccolith dating of intervening hemipelagites reveals that the upper three turbidites were deposited during OIS 1-3 (<60 ka). These turbidites are immediately underlain by a hemipelagite dated at OIS 7 (190-245 ka), indicating an erosional hiatus of ~130 kyrs (Figure 6.3). A further hiatus of >200 kyrs occurs above the lowermost turbidite in the core, as hemipelagite overlying this deposit contains *P.lacunosa* and is therefore older than OIS 13 (>450 ka).

Core JC27-11 sampled ~3.0 m of sediment from an area of relatively smooth seafloor immediately northeast of the scoured area, and contains six texturally

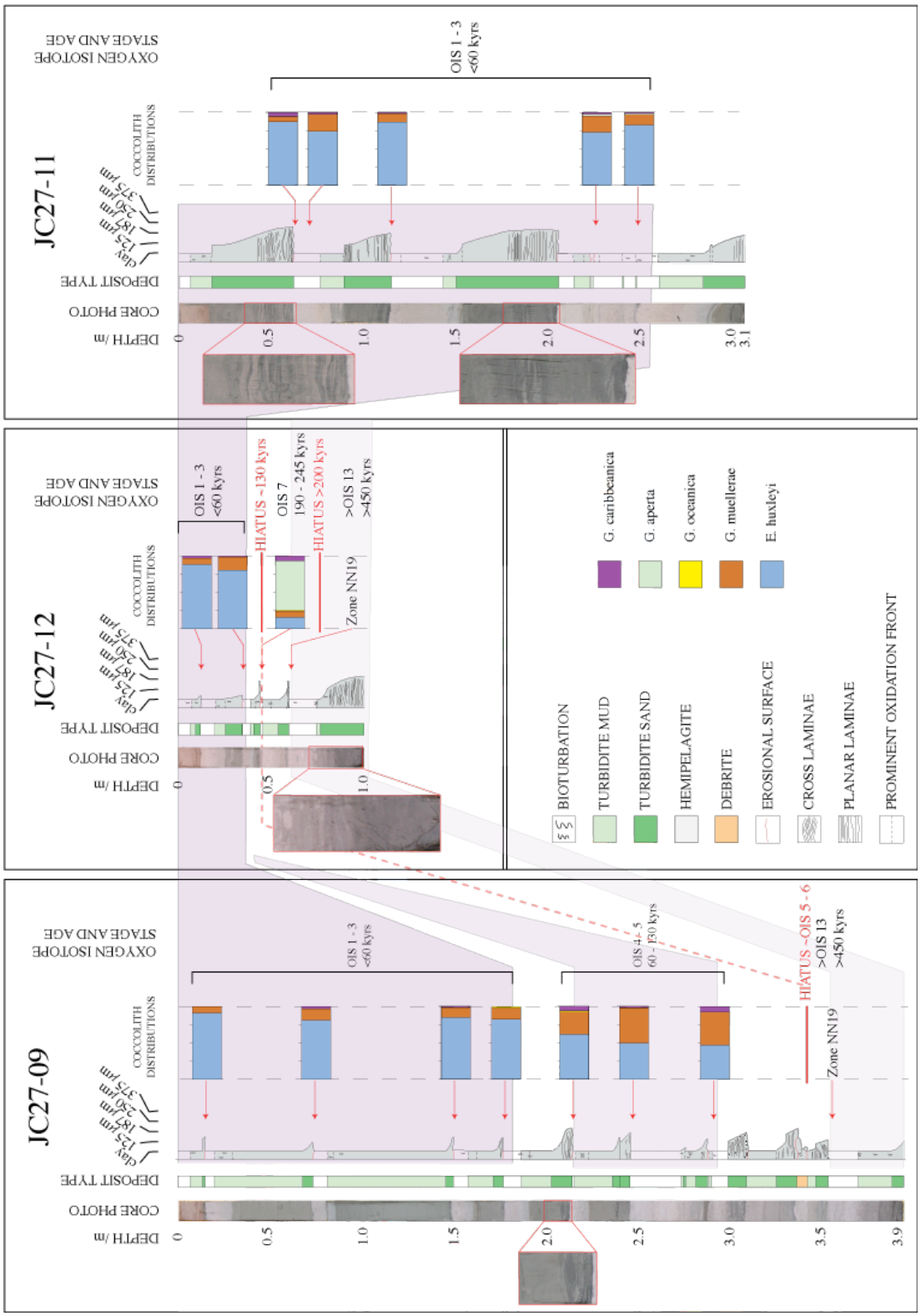

Figure 6.3. Core data from Agadir Canyon mouth scours. For locations see Figure 6.2. Data include core photos, graphic logs and interpretations, and coccolith ratios from hemipelagic sediments that provide dating control (see key for species). OIS = Oxygen Isotope Stage. Core JC27-09 recovered sediments from within a large amalgamated scour, JC27-12 was taken from within an isolated scour, and JC27-11 sampled sediments adjacent to the scoured

zone. Note the marked variability in abundance, thickness and grain size of turbidite deposits, across an area of just over 2 km.

---

cross laminations that are rarely disturbed by convolute bedding. Coccolith dating reveals an absence of significant hiatuses in JC27-11 (Figure 6.3), instead showing a relatively young and continuous sequence of sand-rich turbidites (all OIS 1-3; <60 ka).

Visual analysis of the three cores provides compelling evidence for a correlative relationship between the upper three turbidites, based upon turbidite mud colour, relative stratigraphic position, and thickness and colour of intervening hemipelagic intervals. Coccolith dating supports these correlations and indicates that the upper three turbidites were deposited in the last 60 ka (Figure 6.3). However, the turbidite deposits show remarkable variation between cores, in terms of bed thickness, grain size and sedimentary structures (Figure 6.3). Cores JC27-09 and JC27-12 also show evidence for significant hiatuses beneath these turbidites, indicating phases of active erosion prior to 60 ka and removal of several metres of sediment.

6.5.2. Horseshoe Valley

The Horseshoe Valley is located offshore southwest Iberia, and is a broad conduit for sediments transported southwestwards from the Lagos and Portimao Canyons to the Horseshoe Abyssal Plain (Figure 6.1, Figure 6.4a) (Terrinha et al., 2009). Hull-mounted multibeam bathymetry data reveal a series of giant scours on the floor of the central fairway, on an overall slope of ~0.5° (Terrinha et al., 2009; Duarte et al., 2010; Figure 6.4a). The largest scours are up to 5 km wide and 120 m deep, with long axes aligned parallel to slope. Seismic profiles indicate that scour locations are controlled by the underlying thrust fault morphology (Duarte et al., 2010).

Our new high-resolution AUV data focus on a single large-scale, erosional scour that is U-shaped in cross-section and measures ~3 km wide and 50 m deep (Crescentic Depression 1 of Duarte et al., 2010). The scour is oval in planform and, unlike the Agadir Canyon scours, is elongate along slope (i.e. perpendicular to downslope flow). The scour is at ~4600 m water depth and displays average

headwall slope angles of 30º, with maximum angles locally reaching 56º (Figure 6.4b). Profiles of the headwall slope vary across the scour, ranging from smooth and constant to stepwise with distinctive terraced morphology (Profiles A-A' and C-C'; Figure 6.4b). Two areas of morphologically distinct bedforms flank the scour: V-shaped chevrons to the west and lineations to the southeast and east (see inset figures in Figure 6.4b). The chevrons are V-shaped positive relief features that are up to 200 m across. Chevron limbs bound a hollow and flat-bottomed central region, and open out in a downstream direction. The lineations are negative relief features that may be fully isolated or amalgamated with other surrounding lineations; they are 40-80 m wide, 250-1000 m long and up to 3 m deep. All lineations >80 m in length appear to be amalgamated.

Two piston cores were recovered from the area imaged by high-resolution data (Figure 6.4b and Figure 6.5). Core JC27-24, recovered from outside the scour ~700 m upslope of the scour headwall, contains 4.7 m of dominantly hemipelagic sediments interbedded with about 20 thin turbidites. Turbidite deposits are 0.2-12 cm thick, and comprise thinly laminated fine sand bases overlain by structureless muds. In some cases the basal sand is absent. Coccolith ratios reveal that these deposits range in age from OIS 1-3 (<60 ka) to OIS 8-12 (450 ka), and do not appear to be separated by significant hiatuses (Figure 6.5). In contrast, core JC27-25*3, recovered from the scour floor, is dominated by seven thick turbidites with very different character to those seen outside the scour. The turbidites display texturally mature, normally-graded, fine- to medium-grained sand bases that are erosive, up to 25 cm thick and laminated or cross-laminated (*Tb* and *Tc*). Sand bases are overlain by up to 1.5 m of structureless ungraded turbidite mud, and bounding hemipelagites are thin or absent (Figure 6.5). Coccolith dating shows that the turbidite sequence cored inside the scour is relatively young, with ages restricted to OIS 1-5 (<75 ka). Net accumulation rates during the last 75 kyrs are therefore over three times higher inside the scour compared to the adjacent seafloor.

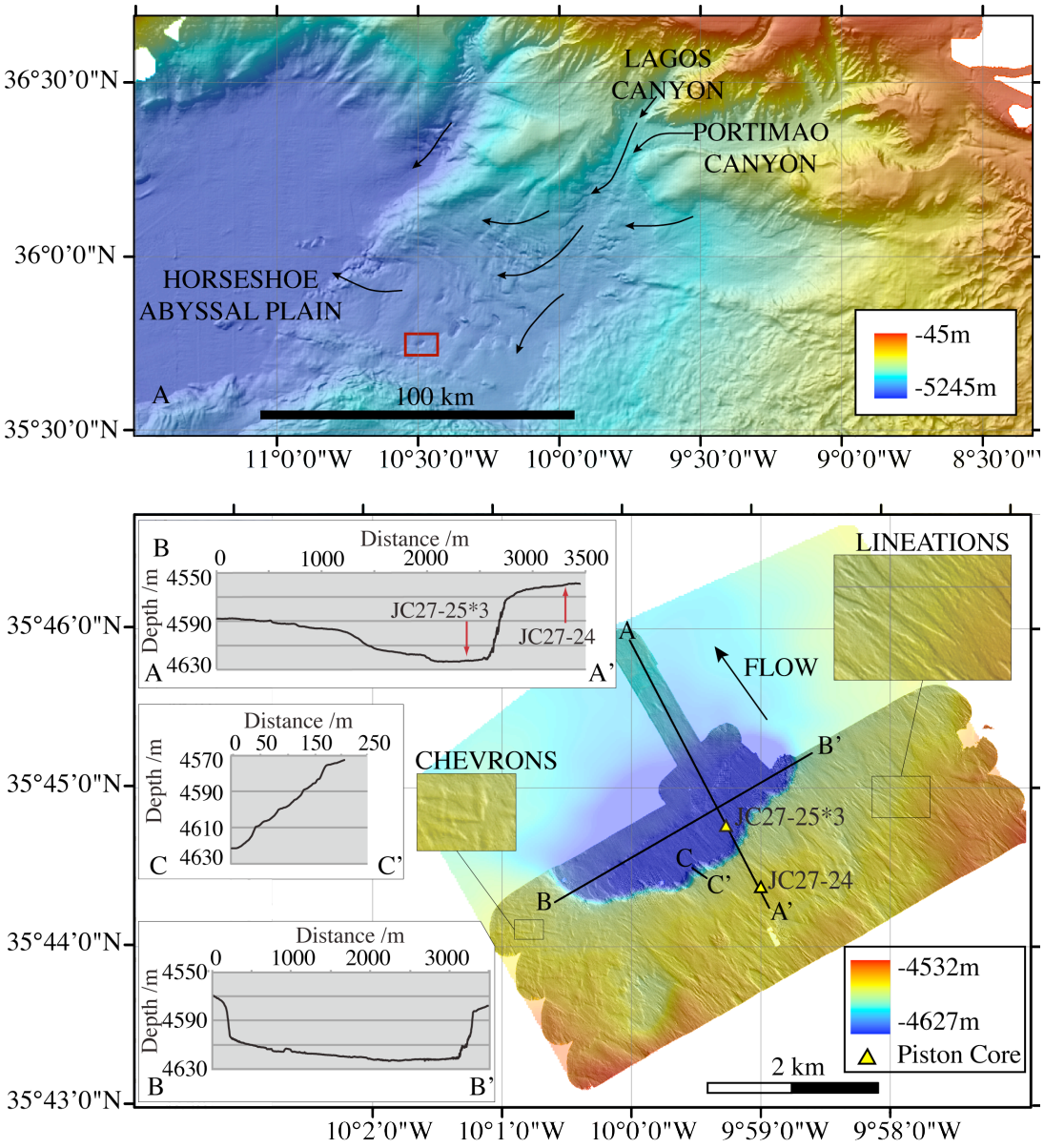

Figure 6.4. Erosional scours in Horseshoe Valley, offshore southwest Portugal. (A) Composite image of SWIM multibeam bathymetry data showing the regional morphology of Horseshoe Valley (Zitellini et al., 2009). Note the large scours in the central valley. Black arrows show interpreted flow pathways. Red box indicates the location of Autosub6000 data. (B) High-resolution Autosub6000 image and cross-sectional profiles across a giant oval-shaped scour in Horseshoe Valley. Additional depth information (pastel colors) is derived from AUV depth profiler data. Inset images show depositional chevrons and erosional lineations adjacent to the scour. Additional depth information (pastel colors) is derived from AUV depth profiler data. Locations of cores shown in Figure 6.5 are indicated.

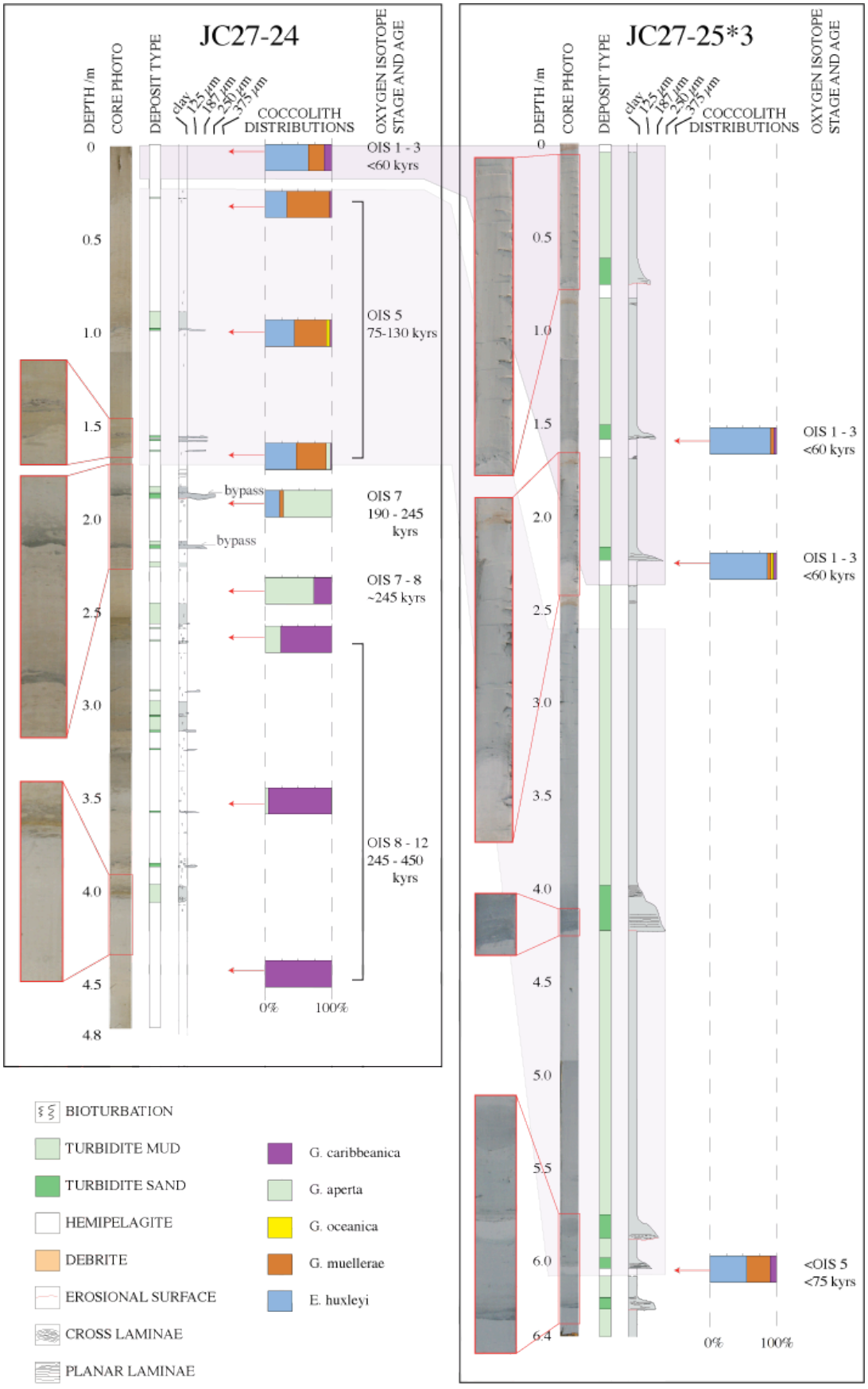
JC27-24
DEPTH /m
CORE PHOTO
DEPOSIT TYPE
clay
125 µm
187 µm
250 µm
375 µm
COCCOLITH DISTRIBUTIONS
OXYGEN ISOTOPE STAGE AND AGE
0
0.5
1.0
1.5
2.0
2.5
3.0
3.5
4.0
4.5
4.8
OIS 1 - 3
<60 kyrs
OIS 5
75-130 kyrs
bypass
bypass
OIS 7
190 - 245
kyrs
OIS 7 - 8
~245 kyrs
OIS 8 - 12
245 - 450
kyrs
0%
100%
JC27-25*3
DEPTH /m
CORE PHOTO
DEPOSIT TYPE
COCCOLITH DISTRIBUTIONS
OXYGEN ISOTOPE STAGE AND AGE
0
0.5
1.0
1.5
2.0
2.5
3.0
3.5
4.0
4.5
5.0
5.5
6.0
6.4
OIS 1 - 3
<60 kyrs
OIS 1 - 3
<60 kyrs
<OIS 5
<75 kyrs
0%
100%
BIOTURBATION
TURBIDITE MUD
TURBIDITE SAND
HEMIPELAGITE
DEBRITE
EROSIONAL SURFACE
CROSS LAMINAE
PLANAR LAMINAE
G. caribbeanica
G. aperta
G. oceanica
G. muellerae
E. huxleyi

Figure 6.5. Core data from Horseshoe Valley scour. For locations see Figure 6.4. Data include core photos, graphic logs and interpretations, and coccolith ratios from hemipelagic sediments that provide dating control (see key for species). OIS = Oxygen Isotope Stage. Core JC27-24 recovered sediments from smooth seafloor upslope of the scour headwall, while core JC27-25*3 was taken from within the scour. Note the thick mud deposits within the scour, compared to the zone of dominant bypass outside the scour.

6.5.3. Setúbal Canyon mouth

Setúbal Canyon is one of the largest canyons crossing the west Iberian margin, extending seawards from the continental shelf near Lisbon to the Tagus Abyssal Plain at 4840 m water depth (Figure 6.1, Figure 6.6a) (Lastras et al., 2009). Erosional features have previously been documented in the lower canyon and canyon mouth, using medium-resolution (30 kHz) sidescan sonar (see inset in Figure 6.6a). New high-resolution images within the canyon mouth reveal irregular crescentic scours that are elongate perpendicular to flow, with 'horns' pointing downstream (Figure 6.6b). These scours are up to 1.0 km in length and width. One large isolated scour reaches a maximum depth of 14 m and has a steep headwall with slope angles up to 30º; it shallows gently downstream over a distance of several hundred meters (profile A-A'; Figure 6.6b,c). Two other scours are partly amalgamated, with headwall slope angles of up to 35º and a maximum depth of 22 m (profiles B-B' and C-C'; Figure 6.6b,c).

Core JC27-39 sampled sediments from within the largest isolated scour (Figure 6.6b and Figure 6.7) and contains 50 cm of hemipelagite underlain by 3.35 m of debrite. The debrite comprises remobilised lower canyon sediments, including 1) thin-bedded turbidites (terrace facies), 2) canyon floor gravels containing lithic clasts up to 7.5 cm in size, and 3) coarse sands with rip-up clasts up to 6.0 cm across. It seems likely that this debrite is the same as that identified by Arzola et al. (2008) that covers much of the lower canyon mouth area. The overlying hemipelagite therefore represents shutdown of the system in the last few thousand years.

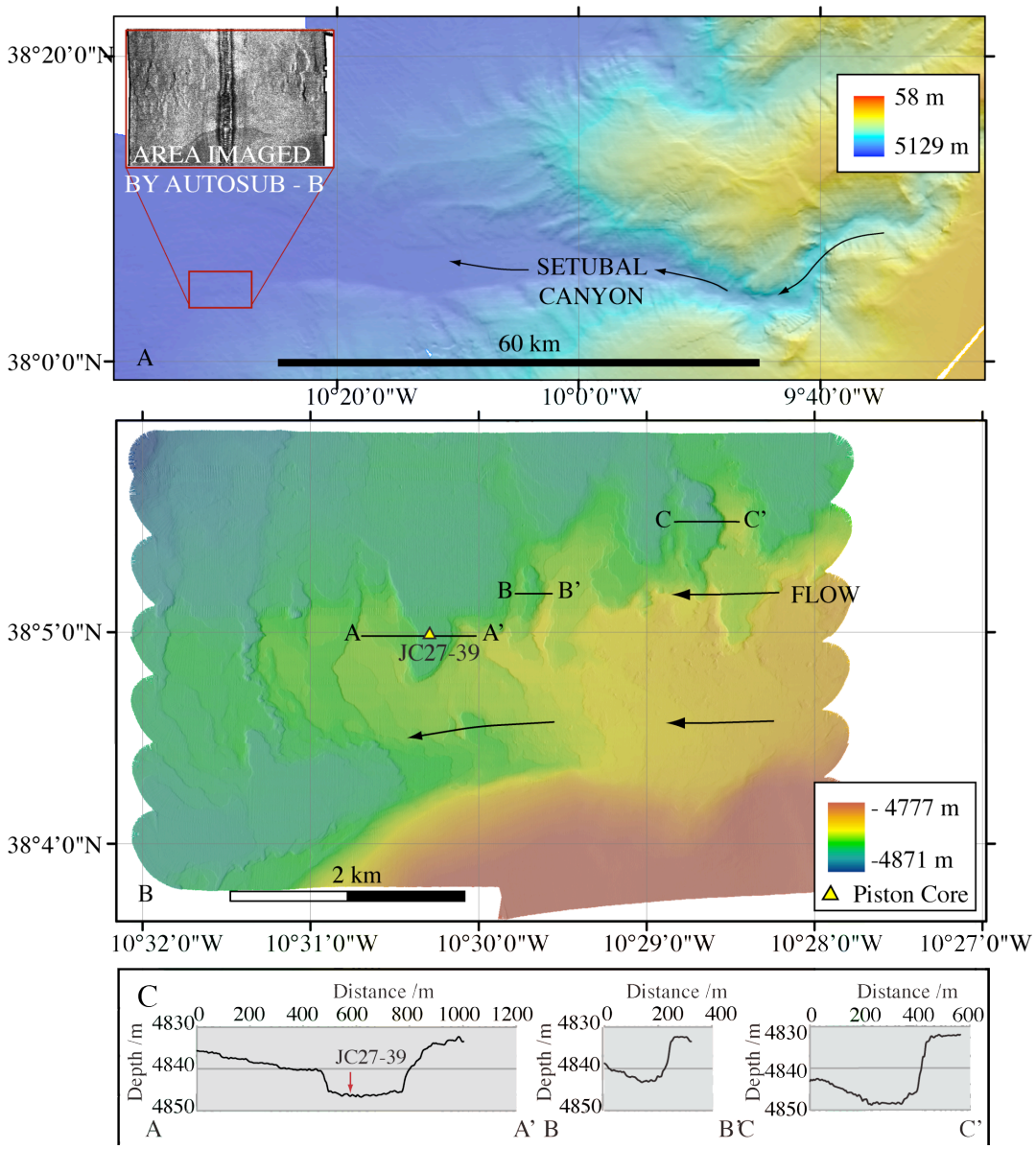

Figure 6.6. Erosional scours in Setúbal Canyon mouth, offshore west Portugal. (A) Regional EM120 multibeam bathymetry showing the morphology of lower Setúbal Canyon. Black arrows show interpreted flow pathways. Inset figure shows TOBI 30 kHz sidescan sonar profile of the scoured region (located by the red rectangle on EM120 data and corresponding to the Autosub6000 image). Light tones are high backscatter. (B) High-resolution Autosub6000 image of crescent-shaped scours. Location of piston core shown in Figure 6.7 is shown. (C) Cross-sectional profiles across a series of crescentic scours. Profile locations shown in (B).

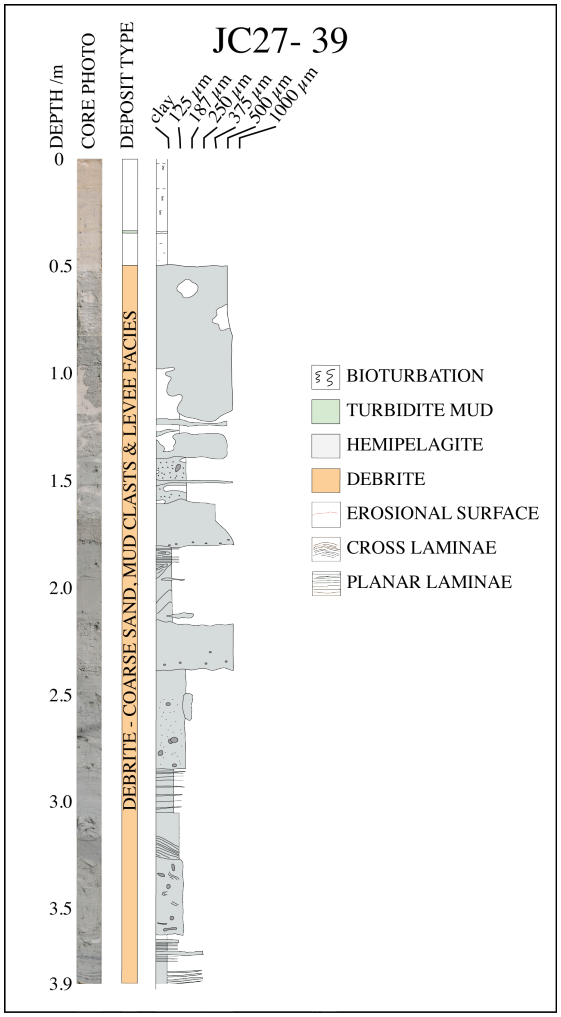

Figure 6.7. Core data from Setúbal Canyon mouth scour. For location see Fig. 6. Data include core photo and graphic log with interpretation. Core contains a thick mass transport deposit overlain by hemipelagic drape.

6.5.4. Whittard Channel margin

The Whittard Canyon and Celtic Fan link the southern Irish Sea and English Channel palaeo-river systems to the deep northwestern Bay of Biscay (Figure 6.1, Figure 6.8a) (Droz et al., 1999; Zaragosi et al., 2000). Hull-mounted multibeam bathymetry data from the fan surface reveal course of the main Whittard Channel, locally flanked by levees draped with fine-grained sediment waves (Figure 6.8a). High-resolution AUV images across the western margin of distal Whittard Channel reveal three distinct morphological features (Figure 6.8b). These include (i) a portion of the active Whittard Channel with a smooth flat thalweg, (ii) a heavily scoured channel margin, and (iii) a pair of large-scale sediment waves in the overbank area of the active channel.

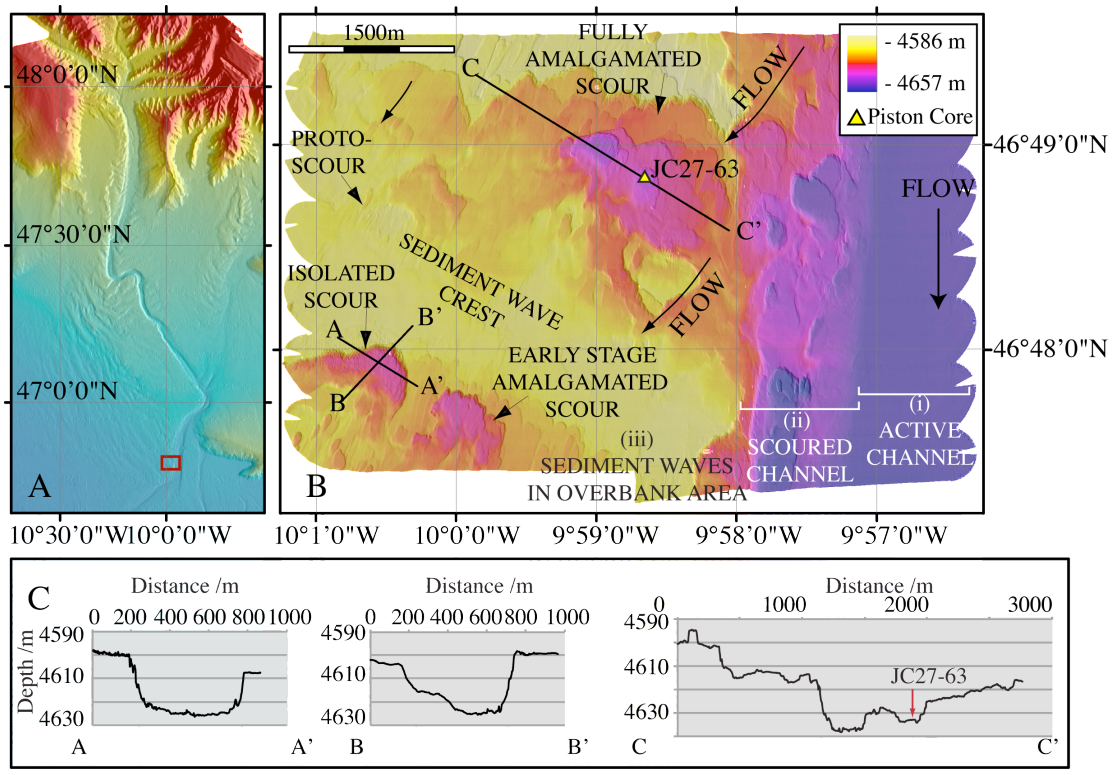

Figure 6.8. Erosional scours on Whittard Channel margin, northern Biscay margin. (A) Regional multibeam bathymetry showing the morphology of Whittard Canyon and Channel. Note the presence of large-scale sediment waves in overbank areas beyond channel bends. Red rectangle shows location of Autosub6000 image. (B) High-resolution Autosub6000 image of scours adjacent to Whittard Channel, in an area of fine-grained sediment waves. Location of piston core shown in Figure 6.9 is shown. Note morphological contrast between smooth channel floor and scoured channel margins and sediment wave troughs. (C) Cross-sectional profiles across isolated and amalgamated scours. Profile locations shown in (B).

Four types of erosional scour can be recognised in the overbank area: protoscour, isolated scour, early-stage amalgamated scour, and fully amalgamated scour. All of the scours have developed on lee slopes or in troughs of sediment waves. Protoscours are zones of shallow erosion that are up to 100 m long and 40 m wide; they are shallow and flat-floored, with internal slope angles <10° and a maximum vertical relief of 8 m. Isolated scours up to 890 m wide, 550 m long and 30 m deep have a uniform 'heel' shape and do not exhibit any signs of coalescing from smaller features; internal slope angles are generally low (<10°), with steeper slopes (22°-50°) confined to the outer limits of the scour (profiles A-A' and B-B', Figure 6.8b,c). One early-stage amalgamated scour has a distinctive scalloped headwall rim and low

relief interior hummocks that are characteristic of scour remnants following amalgamation (profile C-C', Figure 6.8b,c). This scour is up to 18 m deep and is 750 m wide and 480 m long; internal slope angles range from 23°-56°. The largest erosional feature within the imaged area is a late-stage amalgamated scour that extends for >2500 m in the across-slope direction and >1300 m downslope. Of all the scour types documented in this area, this region of amalgamated scour displays both the deepest level of scour and the steepest slopes (50 m and >62°, respectively). The scoured zone has an irregular outer rim and, unlike the other scours, an irregular floor (profile C-C', Figure 6.8b,c).

Two cores were collected across one of the imaged sediment waves. Core JC27-63 sampled 2.3 m of sediment from a broad region of amalgamated scour in a wave trough (Figure 6.8b, Figure 6.9), and is dominated by a single deposit of 1.7 m thickness. This deposit comprises a thin medium-grained basal sand, overlain by a thick ungraded structureless mud. The sand and mud layers are separated by a grain size break (Figure 6.9). Other deposits sampled at the base of the core comprise interbedded organic-rich turbidites with erosive bases and thin mud caps. Core JC27-62 was recovered from a smooth wave crest located 1695 m to the north (just off the area covered by AUV bathymetry; Figure 6.8). This core is dominated by thin-bedded turbidites composed of fine sand bases and thin mud caps; these typical levee-type deposits show an overall upward fining and thinning between 0.9 and 3.7 m (Figure 6.9). The upper 0.9 m of the core comprises several thicker turbidites (up to 7 cm thick), which are overlain by 53 cm of hemipelagite. There is no evidence for the thick mud deposit visible in core JC27-63. Insufficient hemipelagic sediments are present for coccolith dating, but comparison with other cores in the region suggests a Late Glacial turbidite succession overlain by Holocene hemipelagite.

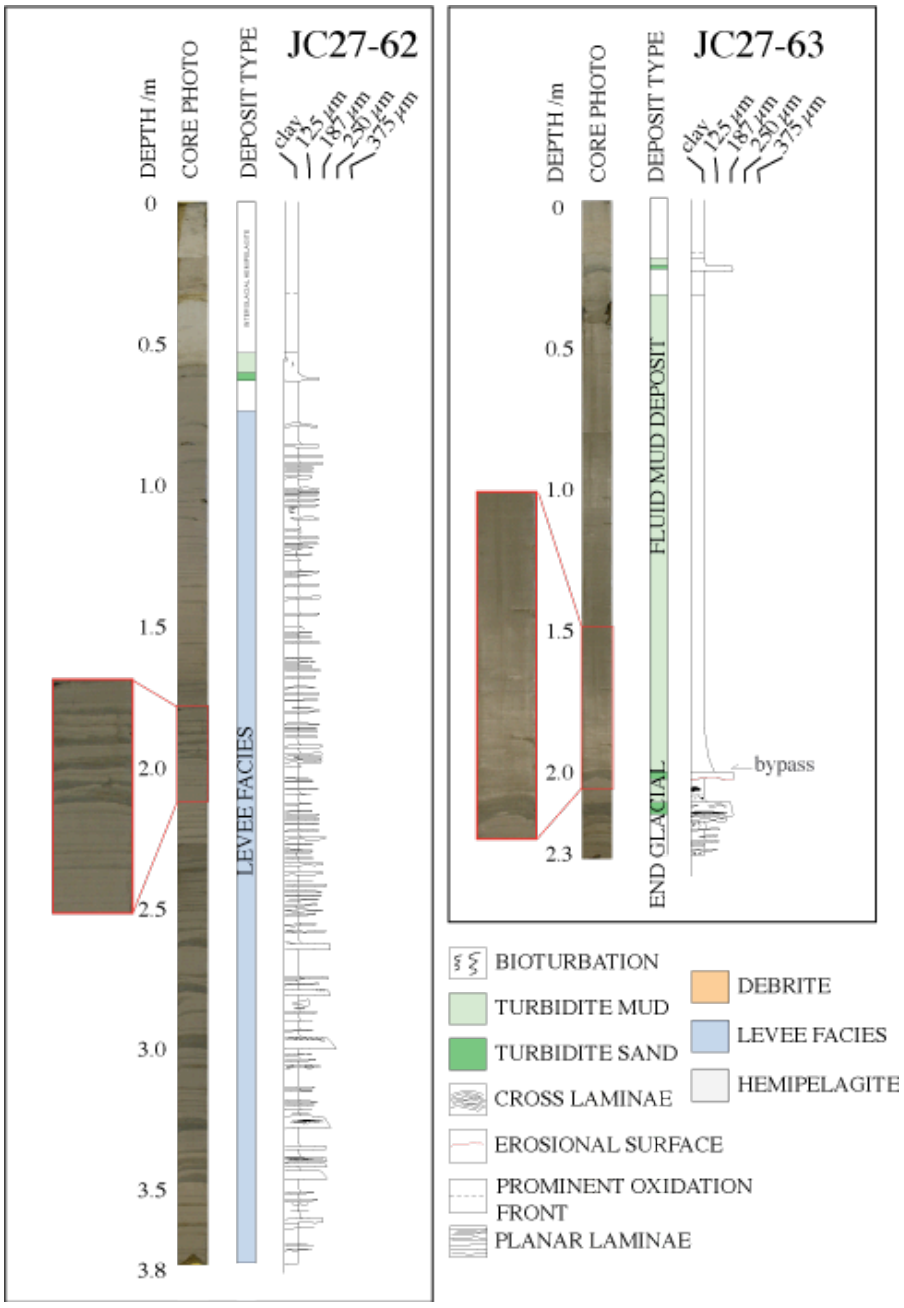

Figure 6.9. Core data from Whittard Channel margin scours. For locations see Figure 6.8. Data include core photos and graphic logs and interpretations. Core JC27-62 recovered sediments from a sediment wave crest just north of the imaged area, while core JC27-63 was taken from within a scour. Note the thick mud deposit within the scour, which is not present in the sequence recovered from outside the scour.

6.6. Interpretation and discussion

Scour morphologies and sizes

The high-resolution images presented here provide detailed insight into the

dimensions, morphology and infill of erosional scours in a variety of deep-water environments. Based upon these morphologic data, four types of isolated erosional scour are identified (6.6.1), as are amalgamated erosional scours (6.6.2). These are then summarised and identified (Figure 6.10):

6.6.1. Isolated erosional scours

Isolated erosional scours have a smooth and continuous outer rim with a regular internal morphology and a broadly symmetrical U-shaped across-slope profile. They are relatively flat-bottomed, with steeper slopes of 20°-50° confined to scour margins. Their downslope profile is asymmetric, with a steep headwall and more gradual downslope opening. The examples of isolated scours presented here reveal four distinctly different types of scour shape and size:

Spoon-shaped scours display a regular elliptical shape in planform, and are elongated in the downslope direction (e.g. scours 1 and 2 in Figure 6.2b). Spoon shaped scours are the only type of scour that narrows and, importantly, closes in the downslope direction. Their elliptical planform produces a low width-to-length ratio of ~0.4. Other examples of spoon-shaped scours include the Cerro Toro Formation of northern Chile (Winn and Dott, 1979; Jobe et al., 2009), Albian Black Flysch of northern Spain (Vicente Bravo and Robles, 1995), Ross Formation of Ireland (Elliott, 2000a,b; Lien et al., 2003), and the modern Valencia Channel mouth in the western Mediterranean Sea (Palanques et al., 1995; Morris et al., 1998).

Heel-shaped scours have outward-flaring limbs that originate at a central, upslope location (Figure 6.8b). The downslope termination of the scour develops via gradual shallowing across the scour width; scour limbs continue to flare out until this termination. Heel-shaped scours are wider than they are long, resulting in width-to-length ratios of up to 1.6. Other published examples of scours exhibiting a heel-shaped morphology occur on the Rhone Neofan off southern France (Kenyon et al., 1995; Torres et al., 1997; Wynn et al., 2002a; Bonnel et al., 2005) and on Redondo Fan offshore California (Normark et al., 2009)

Crescentic scours have a broadly lunate shape with two downslope-pointing limbs (Figure 6.6b). The downslope profile varies across the width of the scour, with more rapid downslope shallowing in the centre of the scour compared to the limbs. Unlike heel-shaped scours, the area between the terminations of the two limbs is positive relief. They are as wide as, or wider than, they are long, with a resultant width-to-length ratio of ~1.3. Crescentic scours have previously been described from the canyon-basin transition zone off west Portugal (Wynn et al., 2002a) and the Valencia Channel mouth (Palanques et al., 1995; Morris et al., 1998).

Oval scours have an elliptical planform that is elongated in the across-slope direction. The large oval scour imaged in this study (Figure 6.4b) displays a more irregular rim than spoon-shaped scours; this may be due to a significantly steeper headwall resulting in small-scale retrogressive mass wasting. Oval scours can be very large; the example documented in the Horseshoe Valley is the widest and deepest isolated scour in the study area. Oval scours have also been from Eel Canyon, offshore California, where they were described as quasi-circular topographic depressions (Lamb et al., 2008).

The original controls on morphology of isolated scours remain poorly understood, especially as some examples show lateral variations in scour morphology within the same system, e.g. Valencia Channel mouth (Palanques et al., 1995; Morris et al., 1998). In addition, as seen in this study, scours in comparable environments can look very different, e.g. Agadir and Setúbal Canyon mouths (Figure 6.2, Figure 6.6). This study speculates that a complex interplay of substrate character (e.g. sand/mud ratio, consolidation rate), seafloor morphology (e.g. slope angle, degree of channelisation), flow character (e.g. volume, velocity, density) and flow frequency are important factors contributing to scour morphology and dimensions.

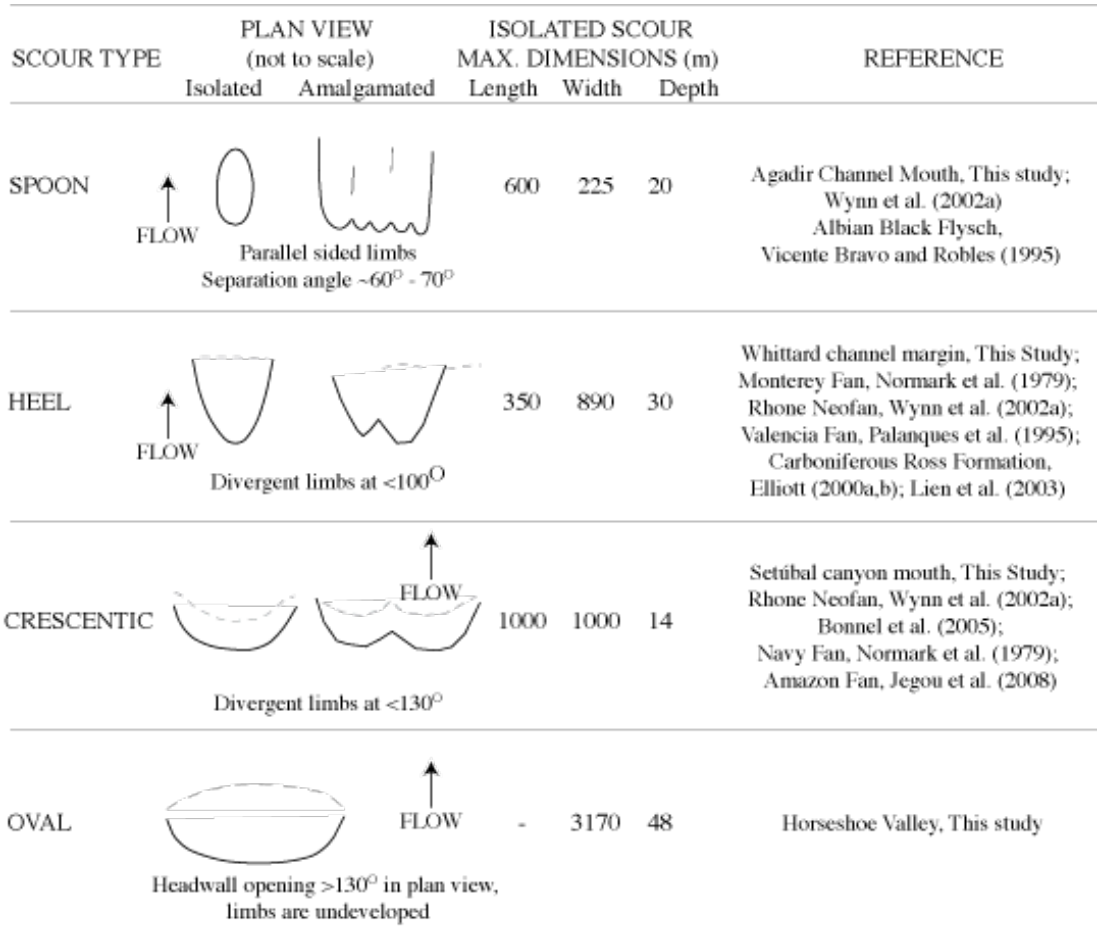

Figure 6.10. Summary figure showing morphology and dimensions of the four isolated and amalgamated scour types documented in this study. Examples of comparable scours from both modern and ancient systems are also listed

6.6.2. Amalgamated erosional scours

Regions of amalgamated scour develop via lateral coalescing of isolated scours, consequently the overall size of amalgamated scours exceeds that of the isolated scours that form them. The morphology of amalgamated scours is defined both by the character and number of isolated scours that have been amalgamated. The upslope portions of amalgamated scour rims are cuspate (Figure 6.2b, Figure 6.8b), where each cusp is a relic of a former isolated feature that has since been incorporated into the amalgamated region. Erosional remnants of former isolated scour margins are commonly preserved on the floor of amalgamated scours, and take the form of irregular topography, hummocks, or elongate ridges of positive relief (Figure 6.2b, Figure 6.8c).

Of the types of isolated scours characterised above, spoon-shaped, heel-shaped and crescentic scours all develop into broad regions of amalgamated scour (Figure 6.2b, Figure 6.6b, Figure 6.8b). In each case, the nature of the amalgamated region becomes highly irregular, although some key characteristics remain that allow the character of former isolated scours to be identified. In the case of spoon-shaped scours, the outer margins and inner remnant topography of the amalgamated region are aligned in the downslope direction, while the irregular upslope rim comprises a number of narrow, steep, and tightly rounded cusps (Figure 6.2b). In comparison, the rims of heel-shaped or crescentic amalgamated scours comprise gently rounded cusps and maintain their widely flaring character (Figure 6.6b, Figure 6.8b). Amalgamated regions that grow via the coalescing of crescentic scours continue to shallow downslope more rapidly towards the centre of the scour than at the margins, therefore retaining the overall crescentic shape.

It is notable that the oval isolated scour in the Horseshoe Valley is about 3 km wide (Figure 6.4b), which is wider than any region of amalgamated scour documented in this study. It is a fully isolated scour, with no evidence for amalgamation and no comparable isolated scours visible on the adjacent seafloor (Figure 6.4b). This has been interpreted to result from structural control (Terrinha et al., 2009; Duarte et al., 2010). However it is also possible that amalgamation is partly controlled by spacing of isolated scours, whereby this example has developed to a scale rarely achieved by isolated examples because it is located many kilometres away from adjacent scours. Overall, it appears that the point at which amalgamation occurs is controlled by the spacing, rate of lateral expansion and longevity of original isolated scours.

6.6.3. Sedimentary deposits within and adjacent to scours

Core data presented here reveal significant variation in the sedimentary fill of scours in different systems, which is a function of differing flow volume, velocity and sediment character. Major changes in sediment character inside and outside of scours within the same system are also documented, as well as temporal changes in sedimentation. For example, in Agadir Canyon mouth the thickest turbidite sands are developed *outside* of the scoured zone, on a gently sloping area of canyon floor that

appears to have been dominantly aggradational in the last 60 kyrs. The presence of sand-to-mud grain-size breaks and thin mud caps indicates bypass of the fine-grained suspended load (Figure 6.2, Figure 6.3). In contrast, the area of amalgamated scour contains a >320 kyr erosional hiatus at 3.4 m overlain by a thickening and fining-upwards sequence of dominantly fine-grained turbidites, suggesting a temporal reduction in flow velocity at this location. The deepest isolated scour displays two significant hiatuses, the youngest of which occurs between OIS 3 and 7 and represents at least 130 kyrs. This hiatus is overlain by a series of thin muddy turbidites indicating dominant bypass of both the sand and mud load (Figure 6.3). Overall, the observed sedimentation pattern suggests that the axis of erosion is shifting northwards across Agadir Canyon mouth, with the deepest isolated scours cutting into the gently sloping northern canyon floor, and the region of amalgamated scour in the canyon axis being progressively infilled during the last 130 kyrs. The whole of the imaged area appears to have been aggradational in the last 60 kyrs, although significant deposit heterogeneity across the imaged area (2 km wide) indicates a complex flow regime that is likely influenced by local seafloor morphology.

The giant oval scour in Horseshoe Valley is filled with a relatively young sequence of thick muddy turbidites, comparable to the amalgamated scour in Agadir Canyon mouth. Individual turbidite muds are up to 1.6 m thick, and appear to be wholly aggradational (Figure 6.5). In contrast, the area immediately upslope of the oval scour is an area of dominant bypass, with poorly developed thin turbidites and a condensed hemipelagic sequence that suggests associated minor erosion and/or bypass. A thick turbidite mud, also approaching 1.6 m thickness, is evident in the floor of an overbank scour adjacent to Whittard Channel (Figure 6.8, Figure 6.9). There is no indication for similar deposits in core outside of the scoured area. Overall, it would appear that broad deep scours are able to effectively trap thick turbidite muds, even though the bulk of the flow is fully bypassing. These muds may be travelling as relatively high concentration fluid mud layers towards the tail of the flow (e.g. McCave and Jones, 1988), possibly generated through post-depositional remobilisation. This interpretation is supported by the uniform, ungraded appearance of mud deposits. Some scours also act as ponds for debris flows, exemplified by the

thick debrite trapped within a scour in Setubal Canyon mouth (Figure 6.6, Figure 6.7).

6.6.4. Insights into scour genesis

As with previous studies (Mutti and Normark, 1987; Normark and Piper, 1991), this study links the development of large isolated and amalgamated scours to areas of significant flow expansion, such as canyon mouths and channel overbanks (Figure 6.2, 6.4, 6.6, 6.8). Underlying structure, such as sediment waves or thrust faults, may also locally influence location of individual scours (e.g. oval scour in Horseshoe Valley; Terrinha et al., 2009; Duarte et al., 2010).

High-resolution multibeam bathymetry data documented here provide additional new insights into scour genesis. A key observation is that isolated scours merge laterally through time into larger areas of amalgamated scour (Figure 6.2, Figure 6.8). The morphology of original isolated scours is often preserved as a series of scour rims on the headwall of the amalgamated scour, and a lateral transition from isolated to amalgamated scour can also be observed in response to lateral migration of the axis of erosion (e.g. Agadir Canyon mouth; Figure 6.2). Synchronous existence of infilling amalgamated scours and actively eroding isolated scours in Agadir Canyon mouth during the Late Quaternary (60-130 kyrs) is of particular interest, as it shows that amalgamated scours can become abandoned while adjacent isolated scours are actively forming. Microfossil-based dating suggests that development of isolated scours, lateral amalgamation, and eventual infilling in this system may take tens to hundreds of thousands of years, probably due to the low event frequency (one major flow every 10 kyrs; Wynn et al., 2002b).

Scour abandonment and infilling may also occur in response to a general system shutdown, e.g. during sea-level highstand, represented by Holocene hemipelagic drape in Setubal Canyon mouth and Whittard Channel scours (Figure 6.7, Figure 6.9). Scours may also be plugged by canyon/channel margin failures, e.g. the debrite fill in Setubal Canyon mouth scour (Figure 6.7). Muddy scour fills may, therefore, be generated by both allocyclic factors, e.g. changing/reducing sediment supply, and autocyclic factors, e.g. canyon thalweg migration or canyon margin failure.

6.6.5. Morphologic features associated with scours

The V-shaped chevrons imaged alongside a giant oval scour in Horseshoe Valley (Figure 6.4b) morphologically resemble erosional chevrons described from the Setubal Canyon mouth, offshore west Iberia (Wynn et al., 2002a). However the limbs of chevrons imaged in Horseshoe Valley are positive relief features, indicating that they are depositional in origin. They are therefore comparable to depositional chevrons, also up to 200 m across, reported from beyond the mouth of Valencia Channel, where they are thought to be composed of coarse sand-sized sediments moving over a muddy substrate (Palanques et al., 1995; Morris et al., 1998).

Erosional lineations were also imaged adjacent to the oval scour in Horseshoe Valley (Figure 6.4b). These features closely resemble longitudinal streaks identified by Wynn et al. (2002a) and Morris et al. (1998) from modern canyon/channel mouth environments. However, those documented here are significantly smaller and more closely spaced. Isolated erosional lineations are up to 80 m long, whereas lineations that exceed 80 m in length are coalesced with adjacent features.

6.7. Conclusions

In this study a series of new high-resolution images of deep-water scours have been combined with sedimentological and chronological data to provide new insights into scour morphology, sedimentology and genesis as follows:

1. Modern deep-water scours may be studied at a level of detail usually unique to outcrop studies, by using (i) AUV-mounted high-resolution multibeam bathymetry, (ii) sedimentological data derived from piston cores placed precisely within imaged areas, and (iii) microfossil-based dating of cored sediments, which provides a chrono-stratigraphic framework for scour genesis.
2. By nesting these AUV-based (outcrop-scale) datasets within lower resolution multibeam bathymetry and deep-towed sidescan sonar data, this study allows precise paleo-environmental interpretations not generally deducible in outcrop-scale studies.
3. Scours documented in high-resolution in this study cover a size range of 40 to 3170 m wide, and 8 to 48 m deep, effectively ‘bridging the gap’ between

outcrop studies and traditional (low-resolution) seafloor data. Deep-water erosional scours are therefore documented to occur along a continuum of sizes, from cm to km scale.

4. Isolated scours documented in this study are associated with canyon/channel termini and margins, and display four different morphologies: spoon-shaped, heel-shaped, crescent-shaped and oval-shaped.
5. Isolated scours may coalesce into broad areas of amalgamated scour; evidence for the presence of isolated scours is commonly preserved within the region of amalgamation as a series of scour rims on the scour headwall, or as remnants on the scour floor.
6. Scour abandonment and infilling events vary between and within systems, and may occur in response to thalweg migration, general system shutdown, changes in flow character, or plugging by mass transport deposits.
7. Scours can accumulate considerable thicknesses of turbidite muds while significant levels of bypass may occur synchronously in the surrounding area. Depositional character of flows can therefore vary dramatically across short distances (tens to hundreds of meters).
8. Other macro-features may be associated with regions of scour in deep-water environments, such as V-shaped chevrons and erosional lineations.

7. Thesis synthesis

7.1. Introduction

The research presented here incorporates a multidisciplinary approach to understand the formation, dynamics and sedimentology of a subset of elliptically shaped scours. Three investigative approaches are utilised and are presented in Chapters 3-6:

(i) experimental simulations of erosional environments

(ii) the analysis of ancient turbidite systems

(iii) the analysis of modern seafloor systems.

This chapter summarises and integrates the findings of the three research approaches, and discusses how the findings may be combined to further our understanding of all erosional bedforms. This synthesis also addresses the objectives outlined in Chapter 1.

7.2. Principal scientific advances

This thesis has fulfilled its principal aims and offers significant scientific advances to the understanding of scours in deep-sea environments. Each of the three investigative approaches outlined above has provided new and unique insights into the dynamics of erosional bedforms. The principal scientific advances are summarised below:

7.2.1. First experimental generation of flutes in open channel flows on initially smooth mud beds

Experimental work presented in Chapter 3 provides, for the first time, experimentally generated flutes formed in open channel flows from an initially smooth bed. The significance of these findings is five fold:

(1) The development of flutes on initially smooth mud beds demonstrates that flutes do not require pre-existing and/or significant defects upon which to nucleate (c.f. Allen, 1971), but rather the erosive flow may create bed defects during the course of the experiment;

(2) Experiments demonstrate that flutes may be generated in open channel flows, whereas previous attempts have failed (e.g. Rucklin, 1938; Dzulynski and Walton, 1963; Allen, 1969) or not been attempted (Allen, 1971);

(3) the experimental flutes developed and expanded as stable bedforms, eroded by sand-laden flows and formed coevally with other erosional features. These bedforms were therefore not transient features (contra Rucklin, 1938; Allen, 1969; 1971), loading structures (contra Dzulynski and Walton, 1963; Dzulynski, 1965; Dzulynski and Simpson, 1966), or tool marks (contra Dzulynski and Simpson, 1966; Dzulynski, 1996);

(4) Electronically obtained morphological bed data collected during each experiment are the first such data for experimental flutes, and provide the first quantification of experimentally generated erosional bedforms. The data provide time-series cross-sectional profiles that allow the precise tracking of bedforms with respect to time;

(5) Other erosional features formed in association with experimental flutes include pock-marks, gullies and potholes; these have not previously been generated during experimental investigations of erosion in mud beds. These new bedforms therefore contribute original data on experimental erosional bedform research, and pave the way for new experimental investigations regarding their formation.

7.2.2. Genetic model of megaflutes in sedimentary systems

Fieldwork that investigated the occurrence and stratigraphic context of megaflutes in the Carboniferous Ross Sandstone Formation (Co. Clare, SW Ireland), culminated in the first model that recognises the abundance of such features and places them in a depositional context that accounts for the panoply of sedimentary and stratigraphic features (Chapter 4). The model is based upon bed-scale data that reveal thickening-upward packages within the outcrops, and further reveal the systematic occurrence of megaflutes within these packages. Results show that the packages are the result of the progradation of lobe-elements, whereby each individual package records a vertical trend from distal- to proximal-deposits, accompanied by an increasing frequency of megaflutes, and ultimately the development of broad erosional surfaces.

A six-stage model for lobe-element evolution is developed that documents successive phases of deposition, sediment bypass, erosion and lobe abandonment. This new model provides a mechanism for lobe-element switching, explains the

development of thickening-upwards successions, and provides an explanation for the occurrence of megaflutes within prograding lobe-elements. Furthermore, the work applies recently established nomenclature and associated processes regarding the building-blocks of lobes (of Deptuck et al., 2008) to the Ross Sandstone outcrops for the first time, and provides a new and up-to-date interpretation for the intensively studied and widely debated outcrops of the Ross Sandstone.

7.2.3. First explanation of how megaflutes form within sand beds

Previous studies of flutes, megaflutes and large-scale scours have shown that they occur in host-beds of highly variable lithology. Thus, flutes occur within host-beds of mud, megaflutes are encountered within host-beds of sandstone and sandstone conglomerates, and large-scale scours on the modern seafloor occur within hemipelagic sediments and turbiditic sands/muds. Key questions have existed regarding the genetic link between these host sediment types and their erosive bedforms, for example how can steep-sided megaflutes form and be preserved in a sand substrate? This thesis provides the first insight into a potential link (Chapter 5). Data presented for the sandstones of the Ross Sandstone Formation form the first analysis of its kind, and reveal the microstructure, diagenesis and quantitative mineralogy of the deposits. The results indicate that the sandstones contained up to 18 – 30 % clay and would therefore have exhibited considerable cohesive strength after deposition. This existence of mud-rich sands in terminal lobe-element positions provides a first clarification to the enigma of how megaflutes and ripples co-exist on sandstone bedding surfaces of the Ross Sandstone. However, it raises new questions regarding the flow processes involved in emplacing and eroding mud-rich sand in deep-sea environments, and the bedforms that would be expected to form.

7.2.4. First definition for megaflutes

Despite featuring widely in published literature of ancient turbidite systems and in some analyses of modern turbidite systems, the term “megaflute” has, until now, escaped a definition. In-depth analyses of the Ross Sandstone megaflutes and comparison with other ancient examples such as the Albian Black Flysch (northern Spain) allow for the first detailed definition (Chapter 5): megaflutes are erosional features that are parabolic in planform with rims that point upstream and flare out downstream, they may be spoon shaped or horseshoe shaped (with a median ridge),

and range from 0.4 - 8 m wide, 0.8 - 25 m long, and occur up to 0.10 - 0.65 m deep. Megaflutes occur almost exclusively within rippled surfaces and exhibit smooth interiors, and may coalesce laterally to produce amalgamated megaflutes. Megaflutes are also in part dependent upon the lithology and thickness of host sediments whereby host-sediments must possess some cohesive properties, and megaflute depth must not exceed host sandstone thickness. The processes of megaflute formation are linked to regions of increased turbulence intensity, such as at channel terminations. Data presented in this thesis demonstrate, in the case of the Ross Formation, that megaflutes form in distal-to-medial lobe-element environments. Further detailed outcrop studies are now required in order to assess whether megaflutes form in a broader range of environments, such as with modern elliptical scours.

7.2.5. First high-resolution imaging of deep-water scours along the northeast Atlantic margin

This thesis presents data from a pioneering investigation of modern seafloor scours along the northeast Atlantic margin (Chapter 6). High-resolution bathymetric images of scours at water depths of between 4200 m and 4850 m were obtained via an AUV that operated at <100 m height above the seafloor. The data have a pixel size of 2 x 2 m, which is an unprecedented level of detail for bathymetry obtained from a true deep-water environment. The investigation represents a significant step-forward in the analysis of modern deep-water environments, and serves to transform the way such environments are investigated. The implications of these data on the sedimentological understanding and dynamics of deep-water scours are numerous:

(1) scours imaged in high-resolution range from 40 – 3170 m wide and 8 – 48 m deep and bridge the gap between outcrop studies and traditional (low resolution) seafloor data;

(2) scours are associated with canyon/channel termini and margins, and may be further influenced by underlying structure, such as sediment waves or faults;

(3) isolated scours exhibit four different morphologies: spoon-shaped, heel-shaped, crescent-shaped and oval-shaped;

(4) isolated scours may coalesce to produce amalgamated scours, however amalgamated scours may become abandoned while isolated scours are actively forming;

(5) the morphology of amalgamated scours are defined by both the number and morphology of the isolated scours that form them;

(6) single turbidity currents events may deposit considerable thicknesses of turbidite muds within scours (i.e. no sand) and substantial turbidite sands outside the region of scour. This suggests that scours are capable of effectively trapping thick turbidite muds even though the bulk of the flow is fully bypassing the scour;

(7) thick turbidite muds may represent relatively high concentration fluid mud layers that are transported towards the tail-end of turbidity currents;

(8) aside from infilling by multiple flow events, scour infilling or abandonment may occur in response to general system shutdown (driven by widely ranging environmental factors) or being plugged by unique density current events;

(9) other features may be associated with regions of scour in deep-water environments, such as V-shaped chevrons and erosional lineations.

7.3. Do flutes, megaflutes and large-scale scours relate to one another in terms of morphology and genesis?

The investigations of flutes, megaflutes and large-scale scours presented in this thesis demonstrate that many morphological similarities exist between the different scales of bedforms. These fall into in three classes:

(i) spoon-shaped flute forms
(ii) horseshoe-shaped flute forms
(iii) gully forms

Despite the dramatically different scales of observation, each class of bedform is recognised in the three environments investigated in this study. Different bedform morphologies identified within the classes are documented in Table 7-1.

	Spoon-shaped flute forms	Horseshoe-shaped flute forms	Gully forms
Laboratory environment (Chapter 3)	Narrow and broad flutes	Broad flutes	Gullies
Ancient turbidite system (Chapters 4 and 5)	Megaflutes	Horseshoe megaflutes	Stepped-scours and flat-bottomed scours
Modern seafloor environment (Chapter 6)	Spoon-, heel- and oval-shaped scours	Crescent-shaped scours	Lineations

Table 7-1. A summary table listing the morphological forms belonging to the three classes of erosional bedforms documented in this thesis.

7.3.1. The morphology of spoon-shaped flute forms

The class of spoon-shaped flute forms comprises concave-up erosional hollows. They typically exhibit bilateral symmetry, with a median plane aligned parallel to flow (Figure 7.1 and 7.2). Their across-flow profile is U-shaped, and their downstream profile displays a steeply inclined lee slope, and a more gently sloping stoss slope. Some occurrences exhibit lateral furrows at their widest points, which creates a mild deviation from the model spoon-shape; such occurrences are cuspate along their U-shaped across-flow profiles (see Figure 7.1). Width to length ratios range from 2:1 to 1:2, and forms may be aligned parallel to- or transverse to flow; the unique character of an exceptionally wide example (width to length ratio of 4:1) is attributed to the influence of underlying structural control (see Chapter 6). This illustrates that the morphology of spoon-shaped flute forms may deviate from typical forms when affected by non flow-related factors. Forms that have coalesced laterally exhibit cuspate rims and may contain remnant erosional features of the former isolated forms.

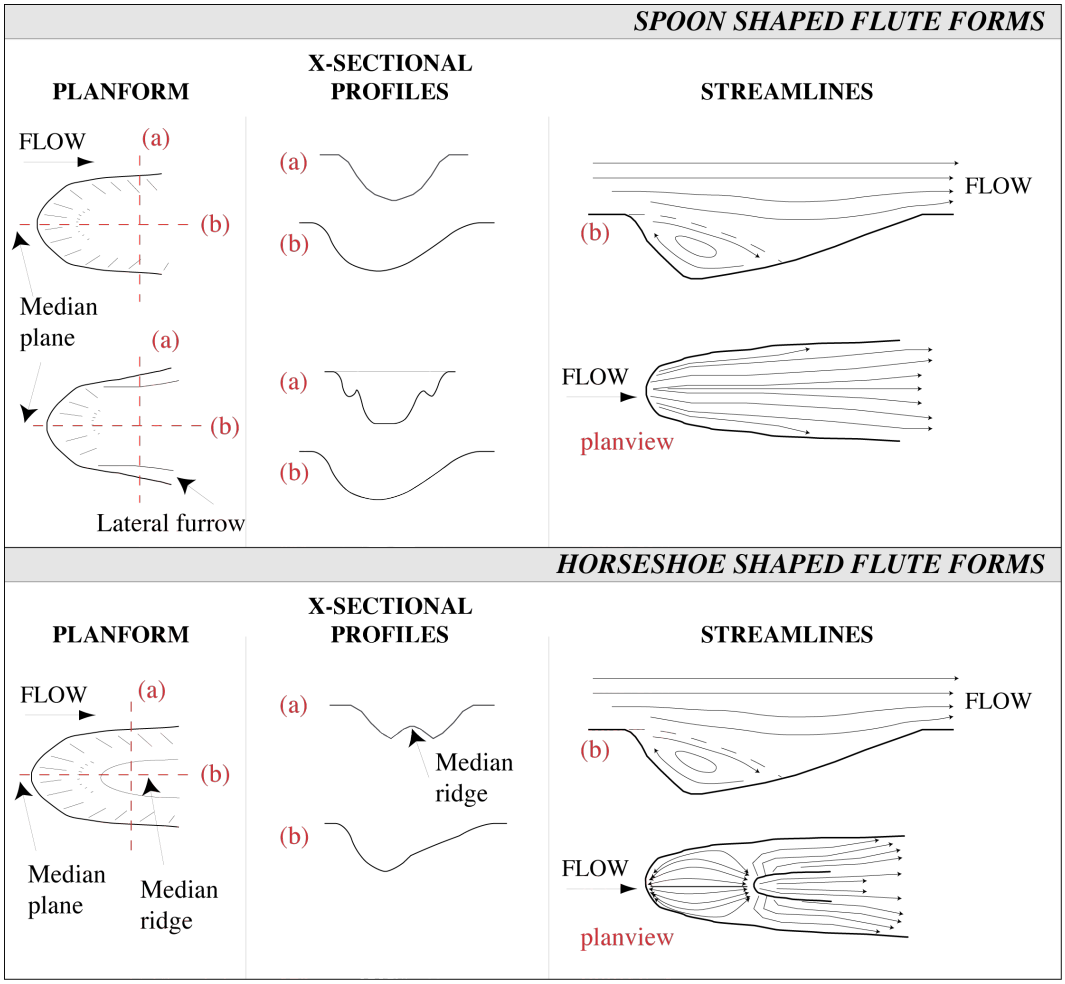

Figure 7.1. Summary figure showing the principal morphological features and streamlines associated with spoon-shaped and horseshoe-shaped flute forms. Position of cross-sectional profiles in planview schematics is shown by red dashed line. Streamline figures modified after Allen (1971, 1984, p. 283).

7.3.1. The morphology of horseshoe-shaped flute forms

The planform morphology of horseshoe-shaped flute forms is similar to that of spoon-shaped flute forms; with upstream pointing parabolic rims, and bilateral symmetry with a median plane aligned parallel to flow (Figure 7.1, Figure 7.3). However, horseshoe-shaped flute forms contain an internal median ridge that provides positive relief within the otherwise hollow feature; this ridge is eroded into the substrate (not a depositional feature) within the flute form. Owing to the presence of the median ridge, the cross-sectional profile is W-shaped across-flow (see Figure 7.1). Observations presented in this thesis suggest that horseshoe-shaped flute forms

are not associated with lateral furrows. Width to length ratios are ~1:1, and always occur between the limits of 2:1 and 1:2. Horseshoe-shaped forms that coalesce laterally retain their horseshoe-shaped morphology and median ridges, and create an amalgamated feature with multiple internal ridges.

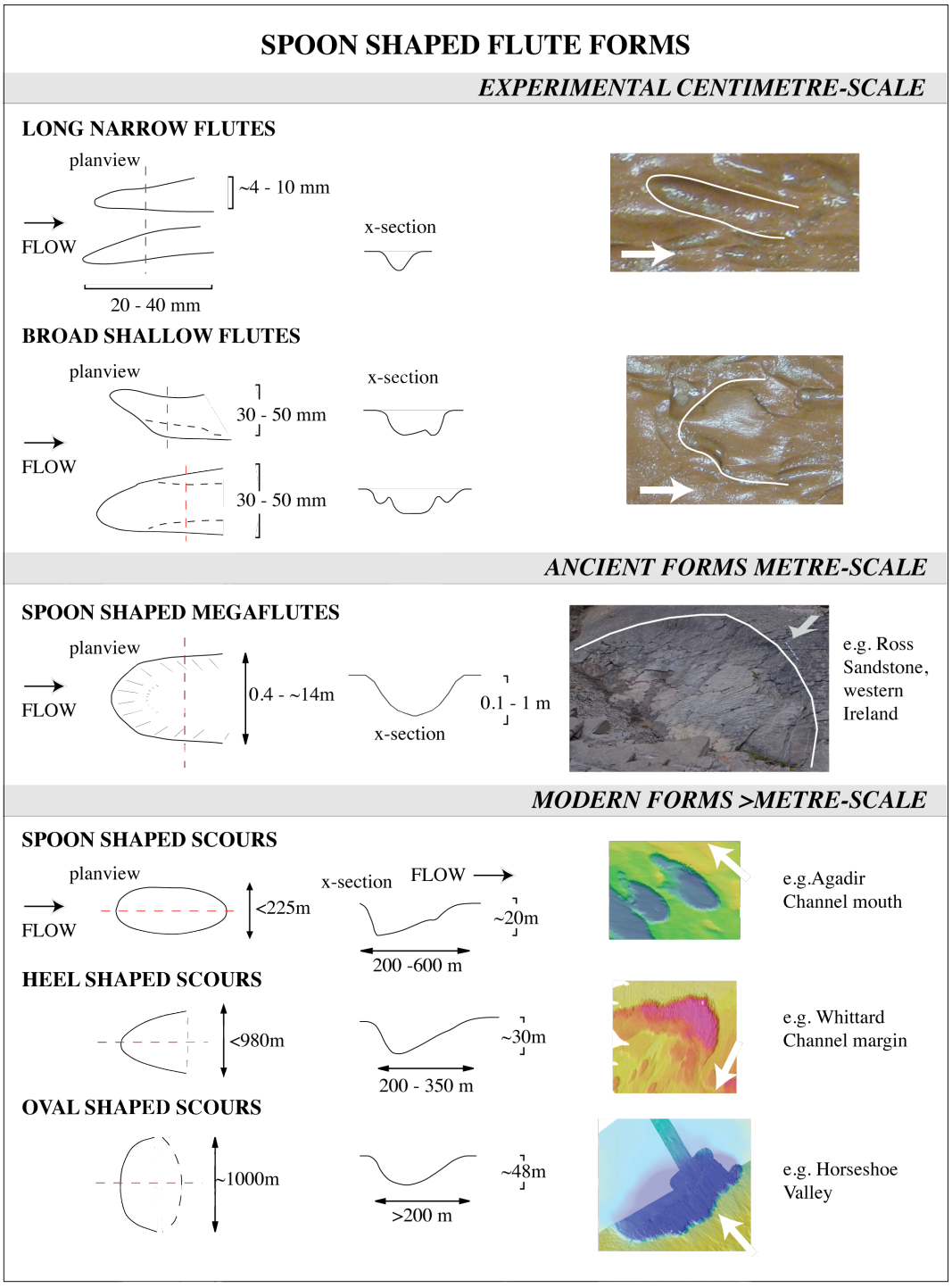

Figure 7.2. A summary figure showing the morphology of bedforms belonging to the class of "spoon-shaped flute forms" observed in laboratory, ancient and modern systems. Position of cross-sectional profiles in planview schematics is shown by red dashed line. Illustrative

photographs (laboratory and ancient system) and bathymetric images (modern system) are presented; solid white lines indicate the location of bedform rims, and flow/palaeoflow directions are indicated by white arrows.

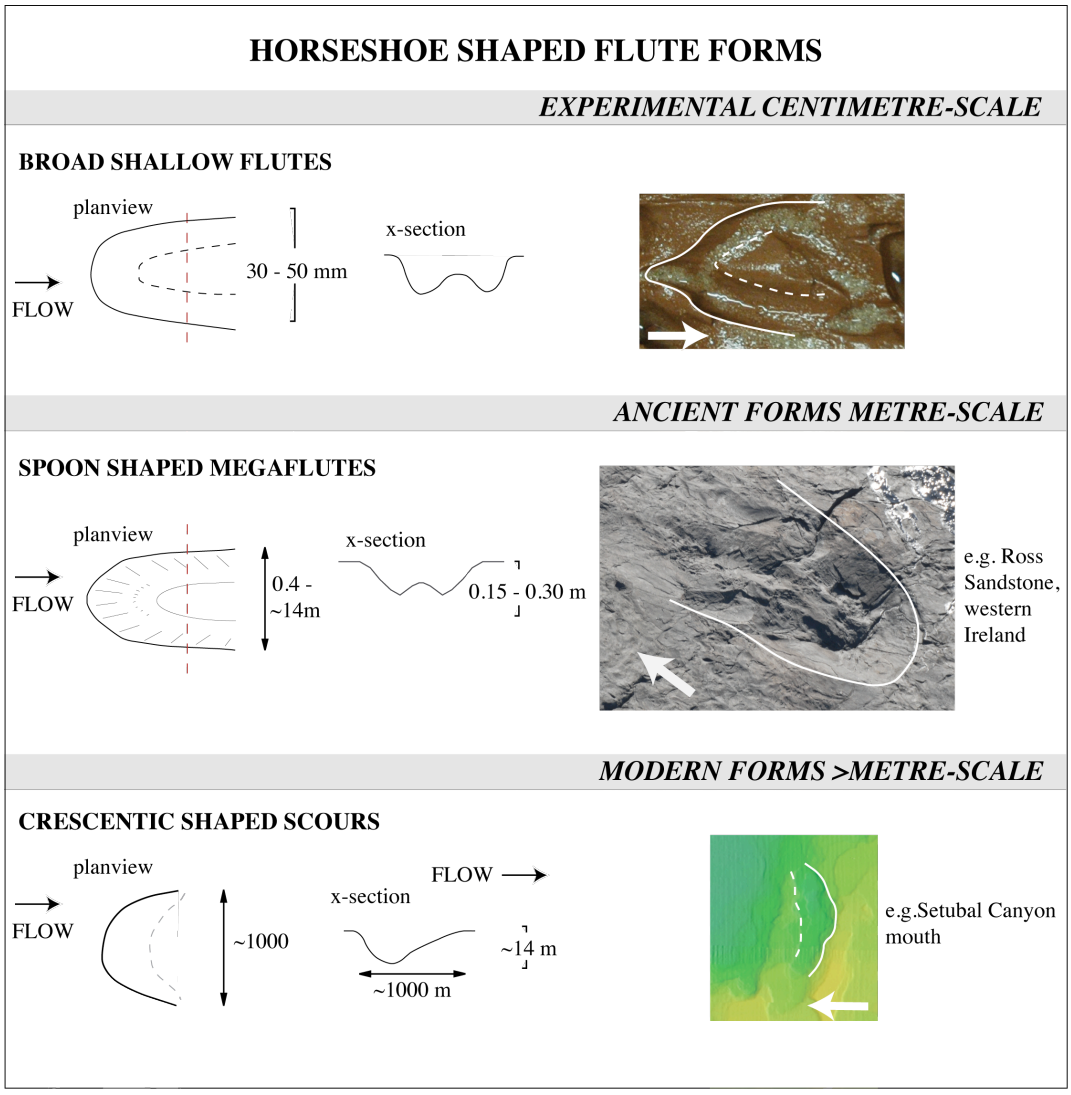

Figure 7.3. A summary figure showing the morphology of bedforms belonging to the class of "horseshoe-shaped flute forms" observed in laboratory, ancient and modern systems. Position of cross-sectional profiles in planview schematics is shown by red dashed line. Illustrative photographs (laboratory and ancient system) and bathymetric images (modern system) are presented; solid white lines indicate the location of bedform rims, and flow/palaeoflow directions are indicated by white arrows.

7.3.2. The genesis of spoon-shaped and horseshoe-shaped flute forms

The morphologies and dimensions of the spoon-shaped and horseshoe-shaped flute forms are very similar; the principal feature that distinguishes the forms is the presence of a central median ridge (Figure 7.1). Both classes are considered to be flute-like in form with similar formational processes; in fact in the Carboniferous Ross Sandstone, spoon-shaped and horseshoe-shaped forms of megaflutes commonly occur within the same thickening-upward packages. Furthermore, fully exposed megaflutes of both form types are of directly comparable widths and depths (Figure 5.10). The stratigraphic occurrence of these forms in the Ross Sandstone indicates that their formation is associated with the termination of prograding lobe-element feeder-channels, and flute forms in modern deep-water environments are also associated with canyon/channel terminations but in much larger distributary and depositional systems. These forms have previously been linked with regions of flow expansion such as at canyon/channel termini or overbank positions, and published examples of scours in modern and ancient seafloor environments are most commonly associated with hydraulic jumps. However, findings presented in this thesis suggest that deep-sea scours are not exclusively formed by hydraulic jumps. Rather, underlying structural controls, or the subtle effects of depositional topography (for example, associated with lobe elements) may influence scour development. Flute forms were certainly generated under experimental conditions without the presence of a hydraulic jump. Furthermore, scours may develop in regions of flow expansion in distal lobe-element positions that are too distal or not sizeable enough to invoke hydraulic jump.

7.3.3. The morphology and genesis of gully forms

Gully forms are linear features that are arranged approximately parallel to flow; they have relatively flat bottoms with steeply inclined edges. In laboratory and modern seafloor environments they are observed in planform, and in outcrop they are observed primarily in cross section (Figure 7.4). However, width to depth ratios between environments are comparable, ranging mostly from 25:1 to 35:1 (infrequent,

particularly low profile outcrop examples have width to depth ratios of 1:5). Gully forms always occur in close proximity to spoon- and horseshoe-shaped flute forms.

Although the origins of gully forms remain enigmatic (see experimental conclusions of Allen, 1984), the data presented here allows comparisons to be made with other erosional bedforms. The close temporal and spatial proximity of gully forms with flute-forms (see Chapter 6; Wynn et al., 2002b) indicate that they form in regions that are associated with turbulent and erosive cells.

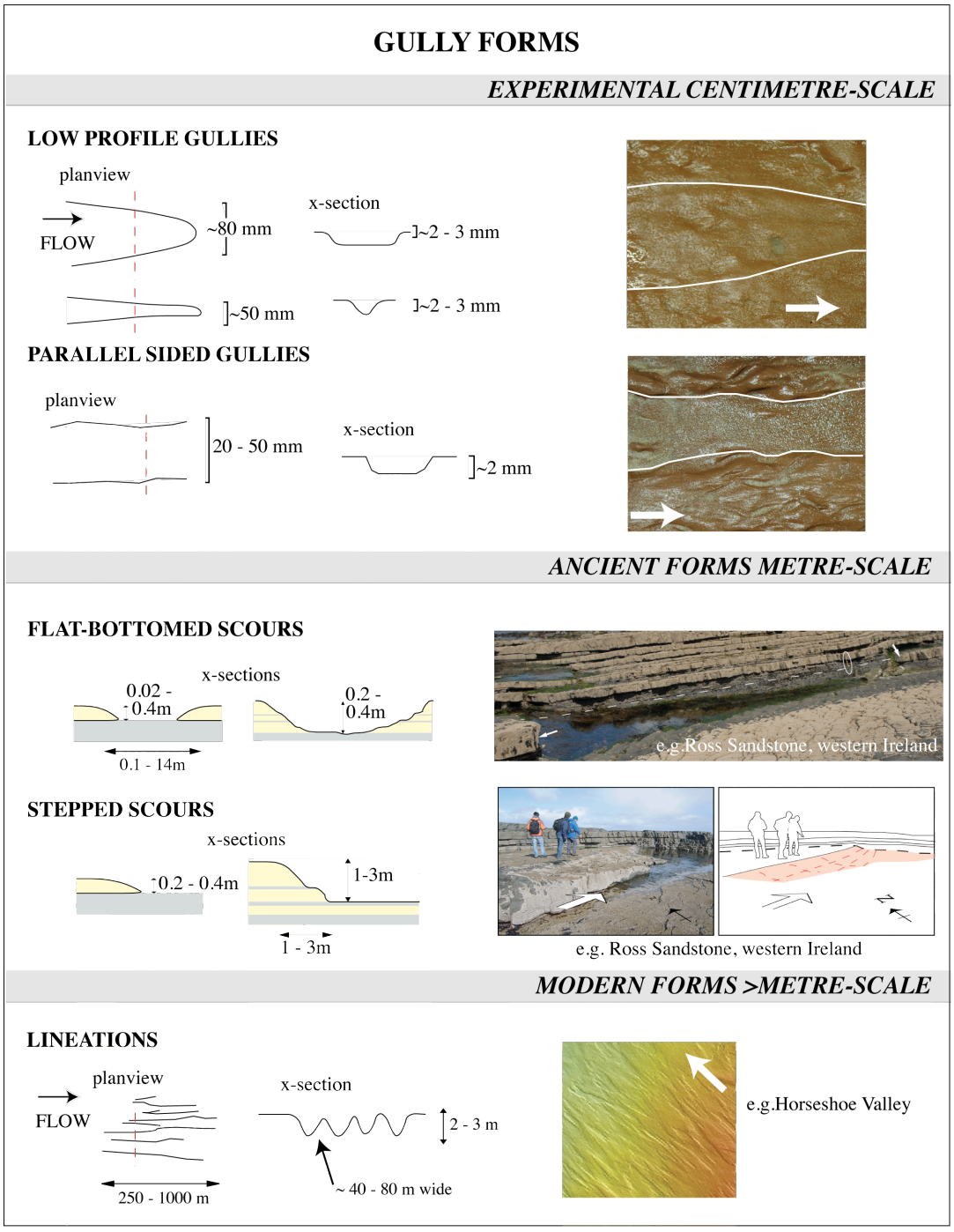

Figure 7.4. A summary figure showing the morphology of bedforms belonging to the class of "gully forms" observed in laboratory, ancient and modern systems. Illustrative photographs (laboratory and ancient system) and bathymetric images (modern system) are presented; solid white lines indicate the location of fully rims, and flow/palaeoflow directions are indicated by white arrows.

7.4. Do erosional bedforms naturally form in three distinct size groups, or is this an artifact of how they are documented?

It is clear that integrating studies of erosional bedforms observed in the laboratory, outcrop, and on the modern seafloor remains a major challenge, largely due to the differing spatio-temporal scales involved (Morris and Normark, 2000). In particular, there is a significant size gap between most erosional forms documented in outcrop (typically several centimetres to a few metres across and less than a metre deep), and the resolution of those imaged on the modern seafloor (10s to 100s of metres across and several metres deep). Over 30 years ago, Normark et al. (1979) documented flute-shaped depressions up to 500 m wide and 15 m deep on Navy Fan, and suggested that "*there is probably a continuity in size between the flute-shaped depressions on Navy Fan and observed flute marks in ancient turbidites*". However, limited detailed data comparing modern and ancient systems has previously made it difficult to verify the suggestion made by Normark et al. (1979). This thesis is the first attempt to quantitatively address the classification of erosional bedforms by scale.

AUV obtained high-resolution images from modern deepwater environments presented in Chapter 6 display outcrop-resolution data of modern seafloor scours. In fact, spoon-shaped and horseshoe-shaped "flute forms" documented in this thesis occur along a continuous range of sizes (Table 7-2), and thus demonstrates that the existing notion that classic-flutes, megaflutes and modern deepwater scours occur in distinct categories is incorrect. Data presented in this thesis provide evidence, for the first time, for the existence of a continuous range in sizes of deepwater scours, from centimetre-scale to kilometre-scale.

	Experimental investigations	Outcrop investigation	Modern seafloor investigation
Width /m	0.004 – 0.050	0.44 – 8.00	40 - 3170
Depth /m	~0.01	0.10 – 0.65	8 – 48
Length /m	~0.05	0.80 - >25.00	350 – 600

Table 7-2. Summary table showing the dimensions of documented examples of the class of "flute forms" presented in this thesis, for the three investigation environments of laboratory (experimental; Chapter 3), outcrop (Ross Sandstone, western Ireland; Chapters 4 and 5) and modern seafloor (Chapter 6).

7.4.1. Future work

This investigation has provided an understanding of the formation, dynamics and classification of elliptically shaped erosional bedforms. However, new questions now remain to be answered:

- This thesis presents the first experimentally produced flute forms in muds within an open channel flow, and generated a variety of other bedforms not previously formed under experimental conditions. Further experimental work across a range of flow conditions (depth, velocity, slope) and substrate types (cohesive strengths) is now needed to further investigate this range of bedforms, and to further define the class of flute-forms.

- It is clear that there is a strong relationship between the development of erosional bedforms and the nature of the substrate sediments. However megaflutes in ancient sediments are preserved predominantly in sands whereas modern seafloor scours occur in muds and sands. Further investigations of the host substrate types in outcrop (both modern and ancient seafloor) are needed to further assess this relationship.

- Despite the considerable advances made in documenting the range of erosional bedform sizes in this thesis, the size range is not yet completely continuous. It is likely that further modern seafloor investigations and continuing advances in AUV technology will continue to document modern

seafloor scours at an increasingly smaller scale. Such results are expected to further confirm the continuous range of deepwater scours.

References

Allen, J. R. L. 1965. Scour marks in snow. *Journal of Sedimentary Petrology*, **35**, 331-338.

Allen, J. R. L. 1968a. On criteria for the continuance of flute marks, and their implications. *Geologie en Mijnbouw,* **47**, 3-16.

Allen, J. R. L. 1968b. Flute marks and flow separation. *Nature*, **219**, 602-604.

Allen, J. R. L. 1969. Erosional current marks of weakly cohesive mud beds. *Journal of Sedimentary Petrology*, **39**, 607-623.

Allen, J. R. L. 1970. *Physical Processes of Sedimentation*. Allen and Unwin, London, p.248.

Allen, J. R. L. 1971. Transverse erosional marks of mud and rock: their physical basis and geological significance. *Sedimentary Geology,* **5**, 167-385.

Allen, J. R. L. 1973. Development of flute-mark assemblages, 1. Evolution of pairs of defects. *Sedimentary Geology,* **10**, 157-177.

Allen, J. R. L. 1975. Development of flute-mark assemblages, 2. Evolution of trios of defects. *Sedimentary Geology,* **13**: 1-26.

Allen, J. R. L., 1984, Sedimentary structures, their character and physical basis. Developments in sedimentology: Amsterdam, Elsevier, v. 1 and 2.

Amos, K.J., Peakall, J., Bradbury, P.W., Roberts, M., Keevil, G. and Gupta, S. 2010. The influence of bend amplitude and planform morphology on flow and sedimentation in submarine channels. *Marine and Petroleum Geology*, **27**, 1431-1447.

Anderton, R., 1995. Sequences, cycles and other nonsense: are submarine fan models any use in reservoir geology. *In:* Hartley, A.J. and Prosser, D.J. (eds), *Characterization of Deep Marine Clastic Systems*. Geological Society Special Publication, **94**, 5-11.

Arzola, R.G., Wynn, R.B., Lastras, G., Masson, D.G., Weaver, P.P.E. 2008. Sedimentary features and processes in the Nazaré and Setúbal submarine canyons, west Iberian margin. Marine Geology, **250**, 64–88.

Baas, J.H., Best, J.L., Peakall, J. and Wang, M. 2009. A phase diagram for turbulent, transitional and laminar clay suspension flows. *Journal of Sedimentary Research*, **79**, 162-183.

Beaubouef, R.T. 2004. Deep-water leveed–channel complexes of the Cerro Toro Formation, Upper Cretaceous, southern Chile. *AAPG Bulletin*, **88**, 1471–1500.

Biscaye, P.E. 1965. Mineralogy and sedimentation of recent deep-sea clay in the Atlantic Ocean and adjacent seas and oceans. *GSA Bulletin*, **76**, 803-832.

Bonnel, C., Dennielou, B., Droz, L., Mulder, T. and Berne, S. 2005. Architecture and depositional pattern of the Rhône Neofan and recent gravity activity in the Gulf of Lions (western Mediterranean). *Marine and Petroleum Geology*, **22**, 827-843.

Bourget, J., Zaragosi, S., Mulder, T., Schneider, J.-L., Garlan, T., Van Toer, A., Mas., V and Ellouz-Zimmermann, N. 2009. Hyperpycnal-fed turbidite lobe architecture and recent sedimentary processes: A case study from the Al Batha turbidite system, Oman margin. *Sedimentary Geology*, in press.

Bouma, A.H., 1962, Sedimentology of some Flysch deposits: A graphic approach to facies interpretation: Amsterdam, Elsevier, 168 p.

Brooks, P.C. 2001. Experimenal study of erosional cyclic steps. M.S. Thesis, University of Minnesota, London.

Carr, M., and Gardner, M.H. 2000. Portrait of a Basin-Floor Fan for Sandy Deep-Water Systems, Permian Brushy Canyon Formation. *In:* Bouma, A.H., Stelting, C.E., and Stone, C.G. (eds), *Fine-Grained Turbidite Systems and Submarine Fans*, AAPG Memoir 72/SEPM Special Publication, **68**, 215-232.

Chapin, M.A., Davies, P., Gibson, J.L. and Pettingill, H.S. 1994. Reservoir architecture of turbidite sheet sandstones in laterally extensive outcrops, Ross Formation, Western Ireland. GCSSEPM Foundation 15th Annual Research Conference, Submarine Fans and Turbidite Systems, 53-68.

Chen, C. and Hiscott, R.N. 1999. Statistical analysis of turbidite cycles in submarine fan successions: tests for short-term persistence. *Journal of Sedimentary Research*, **69**, 486-504.

Chuan, F.A., Bjorlykke, K. and Lowrey, C.J. 2001. Closed-system curial diagenesis in reservoir sandstones: examples from the Garn Formation at Haltenbanken area, offshore mid-Norway. *Journal of Sedimentary Research,* **71**, 15-26.

Clark, J.D. and Pickering, K.T. 1996. Submarine Channels: Process and Architecture. London, Vallis Press, 231.

Collinson, J.D., Martinsen, O., Bakken, B. and Kloster, A. 1991. Early fill of the Western Irish Namurian Basin: a complex relationship between turbidites and deltas. *Basin Research*, **3**, 223-242.

Crane, W.H. and Lowe, D.R. 2008. Architecture and evolution of the Paine channel complex, Cerro Toro Formation (Upper Cretaceous), Silla Syncline, Magallanes Basin, Chile. *Sedimentology*, **55**, 979–1009.

Cutler, K.B., Edwards, R.L., Taylor, F.W., Cheng, H., Adkins, J., Gallup, C.D., Cutler, P.M., Burr, G.S. and Bloom, A.L. 2003. Rapid sea-level fall and deep ocean temperature change since the last interglacial period. *Earth and Planetary Science Letters*, **206**, 253-271.

Dennielou, B., Jouanneau, J.-M., Marsset, T. and Savoye, B., 2003. Vitesses d'accumulation des sédiments, fréquence des dépôts, âge et durée de vie des corps sédimentaires sur l'éventail turbiditique profond du Zaire. 9ème Congrès des Sédimentologues Français, Bordeaux, 162–163.

Deptuck, M.E., Piper, D.W., Savoye, B. and Gervais, A. 2008. Dimensions and architecture of late Pleistocene submarine lobes off the northern margin of East Corsica: *Sedimentology*, **55**, 869-898.

Droz, L., Auffret, G.A., Savoye, B., Bourillet, J.F. 1999. L'e´ventail profond de la marge Celtique: stratigraphie et e´volution se´dimentaire. *Comptes Rendus de l'Académie des Sciences, Paris, Earth and Planetary Scienc*es, **328**, 173–180.

Duarte, J.C., Terrinha, P., Rosas, F.M., Valadares, V., Pinheiro, L.M., Matias, L., Magalh˜aes, V. and Roque, C. 2010. Crescent-shaped morphotectonic features in the Gulf of Cadiz (offshore SW Iberia). *Marine Geology*, **271**, 236-249.

Dutton, S.P., Flanders, W.A. and Barton, M.D. 2003. Reservoir characterization of a Permian deep-water sandstone, East Ford field, Delaware basin, Texas. *AAPG Bulletin*, **87**, 609–627.

Dzulynski, S. and Sanders, J.E. 1962. Current marks on firm mud bottoms. *Transactions of the Conneticut Academy of Arts and Sciences*, **42**; 57-96.

Dzulynski, S. and Simpson, F. 1966. Influence of bottom irregularities on experimental scour markings: Annales De La Société Géologique De Pologne, **36**, 285-294.

Dzulunski, S. and Walton, E. K. 1963. Experimental production of sole markings: Transactions of the Edinburgh Geological Society, **19**, 279-305.

Dzulynski, S. 1965. New data on experimental production of sedimentary structures: Journal of Sedimentary Petrology, **35**, 196-212.

Dzulynski, S. 1996. Erosional and deformational structures in single sedimentary beds: a genetic commentary. *Annales Societatis Geologorum Poloniae*, **66**, 101-189.

Dzulynski, S. 2001. Atlas of sedimentary structures from the Polish Flysch Carpathians. Material for 12th Meeting of the Association of European Geological Societies. *ING UJ*, Krakow. p. 65.

Elliott, T. 2000a. Depositional architecture of a sand-rich, channelised turbidite system: the Upper Carboniferous Ross sandstone formation, Western Ireland. *In:* Weimer, P., Slatt, R.M., Coleman, J., Rosen, N.C., Nelson, H., Bouma, A.H., Styzen, M.J. and Lawrence, D.T. (eds) *Deep-water reservoirs of the World*, GCSSEPM Foundation 20th Annual Research Conference, 342-364.

Elliott, T. 2000b. Megaflute erosion surfaces and the initiation of turbidite channels. *Geology*, **28**, 119-122.

Finnie, I. and Kabil, Y. H. 1965. On the formation of surface ripples during erosion. *Wear*, **8**, 60-69.

Fildani, A. and Normark, W.D. 2004. Late Quaternary evolution of channel and lobe complexes of Monterey Fan. *Marine Geology,* **206**, 199-223.

Fildani, A., Normark, W.R., Kostic, S. and Parker, G. 2006. Channel formation by flow stripping: large-scale scour features along the Monterey East Channel and their relation to sediment waves. *Sedimentology*, **53**, 1265-1287.

Flood, R.D. 1983. Classification of sedimentary furrows and a model for furrow initiation. *Geological Society of America Bulletin*, **94**, 630-639.

Frenz, M., Wynn, R.B., Georgiopoulou, A., Bender, V.B., Hough, G., Masson, D.G., Talling, P.J. and Cronin, B.T. 2009. Provenance and pathways of late Quaternary turbidites in the deep-water Agadir Basin, northwest African margin. *International Journal of Earth Sciences*, **98**; 721-733.

Freudenberg, W. 1933. Die Gurich-Berckhemer'schen Wulste. *Z. Deutsch. Geol. Ges*. 86: 59.

Gervais, A., Savoye, B., Mulder, T., Gonthier, E. 2006. Sandy modern turbidite lobes: a new insight from high resolution seismic data. *Marine and Petroleum Geology*, **23**, 485–502.

Ghibaudo, G. 1980. Deep-sea fan deposits in the Macigno Formation (Middle-Upper Oligocene) of the Gordana Valley, Northern Apennines, Italy. *Journal of Sedimentary Petrology*, **50**, 723-742.

Groenenberg, R.M., Hodgson, D.M., Prélat, A., Luthi, S.M. and Flint, S.S. 2010. Flow-deposit interaction in submarine lobes: insights from outcrop observations and realizations of a process-based numerical model. *Journal of Sedimentary Research*, **80**, 252-267.

Gurich, G. 1933. Schriigschichtungsbogen und zapfenformige FliesswiJlste im "Flagstone'"yon Pretoria und ~ihnliche Vorkommnisse in Quartzit yon Kuibis, S.W.A., dem Schilfsandstein yon Maulbronn u.a. Z. *Deut. Geol. Ges.,* 85: 652--664.

Hampson, G. J., Elliott, T. and S. J. Davies. 1997. The application of sequence stratigraphy to Upper Carboniferous fluvio-deltaic strata of the onshore UK and Ireland: Implications for the southern North Sea. *Journal of the Geological Society, London*, **154**, 719–733.

Hanquiez, V., Mulder, T., Toucanne, S., Lecroart, P., Bonnel, C., Marchès, E. and Gonthier, E. 2009. The sandy channel–lobe depositional systems in the Gulf of Cadiz: Gravity processes forced by contour current processes. *Sedimentary Geology*, in press.

Haq, B.U. and Schutter, S.R. 2008. A chronology of Paleozoic sea-level changes. *Science*, **322**, 64-68.

Hesse, R. and Dalton, E. 1995. Turbidite channel/overbank deposition in a Lower Devonian orogenic shelf basin, Fortin Group of Gaspe/Peninsula, Northern Appalachians, Canada. *Journal of Sedimentary Research,* **B65**, 44–60.

Hilton, V.C. 1995. Sandstone architecture and facies from the *Annot* Basin of the SW Alpine foreland basin, SE France. *In:* Pickering, K.T., Hiscott, R.N., Kenyon, N.H., Ricci Lucchi, F., and Smith, R.D.A. Eds., Atlas of Deep Water Environments: Architectural style in turbidite systems. London, Chapman & Hall, p. 227-235.

Hiscott, R.N. 1980. Depositional framework of sandy mid-fan complexes of Tourelle Formation, Ordovician, Quebec. *AAPG Bulletin*, **64**, 1052-1077.

Hiscott, R.N. 1981. Deep-sea fan deposits in the Macigno Formation (Middle-Upper Oligocene) of the Gordana Valley, Northern Apennines, Italy – Discussion. *Journal of Sedimentary Petrology*, **51**, 1015-1033.

Hiscott, R.N., Hall., F.R. and Pirmez, C. 1997. Turbidity-current overspill from the Amazon channel: texture of the silt/sand load, paleoflow from anisotropy of magnetic susceptibility and implications for flow processes. *In:* Flood, R.D., Piper, D.J.W., Klaus, A., and Peterson, L.C. (eds) *Proceedings of the Ocean Drilling Program, Scientific Results*, **155**, 53–78. Ocean Drilling Program, College Station, TX.

Hodgson, D.M., Flint, S.S., Hodgetts, D., Drinkwater, N.J., Johannessen, E.P. and Luthi, S. 2006. Stratigraphic evolution of fine-grained submarine fan systems, Tanqua depocentre, Karoo Basin, South Africa. *Journal of Sedimentary Research*, **76**, 20–40.

Hodson, F. 1954a. The beds above the Carboniferous Limestone in northwest County Clare, Eire. *Quarterly Journal of the Geological Society, London*, **109**, 259–283.

Hodson, F. 1954b. The Carboniferous rocks of Foynes Island, Co. Limerick. Geological Magazine, **91**, 153–160.

Hodson, F. and Lewarne, G.C. 1961. A mid-Carboniferous Namurian basin in parts of the counties of Limerick and Clare, Ireland. *Quarterly Journal of the Geological Society, London*, **117**, 307–333.

Huvenne, V. A. I., McPhail, S.D., Wynn, R.B., Furlong, M. and Stevenson, P. 2009. Mapping Giant Scours in the Deep Ocean. *EOS (Transactions, American Geophysical Union*, **90**, 274-275.

Imran, J., Parker, G., and Katopodes, N. 1998. A numerical model of channel inception on submarine fans. *Journal of Geophysical Research*, **103**, 1219-1238.

Jegou, I., Savoye, B., Pirmez, C. and Droz, L. 2008. Channel-mouth lobe complex of the recent Amazon Fan: The missing piece. *Marine Geology*, **252**: 62-77.

Jobe, Z.R., Bernhardt, A., Fosdick, J.C. and Lowe, D.R. 2009. Cerro Toro Channel Margins, Sierra del Toro. *In:* Fildani, A., Hubbard, S.M. and Romans, B.W. Eds., Stratigraphic evolution of deep-water architecture: Examples of controls and depositional styles from the Magallanes Basin, southern Chile 2009. SEPM Field Trip Guidebook No. 10, p. 31-33.

Johnson, S.D., Flint, S.S., Hinds, D. and Wickens, H.d.V. 2001. Anatomy of basin floor to slope turbidite systems, Tanqua Karoo, South Africa: sedimentology, sequence stratigraphy and implications for subsurface prediction. *Sedimentology*, **48**, 987–1023.

Jones, L.S. & Schumm, S.A. 1999. Causes of avulsion: an overview. *In:* Smith, N.D. & Rogers, J. (eds) *Fluvial Sedimentology VI*, *IAS Special Publication*, **28**, 171–178.

Kármán, Yh. Von, 1930 Mechanische Ähnlichkeit und Turbulenz. Nachrichten der Akademie der Wissenschaften Göttingen, Math.-Phys. Klasse, 58.

Kane, I.A., Kneller, B.C., Dykstra, M., Kassem, A. and McCaffrey W.D. 2007. Anatomy of a submarine channel-levee: an example from Upper Cretaceous slope sediments, Rosario Formation, Baja California, Mexico. *Marine and Petroleum Geology*, **24**, 540-563.

Kane, I.A., McCaffrey, W.D. and Peakall, J. 2008. Controls on sinuosity evolution within submarine channels. *Geology*, **36**, 287–290.

Kane, I.A., Dykstra, M.L., Kneller, B.C., Tremblay, S. and McCaffrey W.D. 2009a. Architecture of a coarse-grained channel-levee system: the Rosario Formation, Baja California, Mexico. *Sedimentology*, **56**, 2207-2234.

Kane, I.A., McCaffrey, W.D. and Martinsen, O.J. 2009b. Alogenic vs. autogenic controls on megaflute formation. *Journal of Sedimentary Research,* **79**, 643-651.

Kane, I.A. 2010. Development and flow structures of sand injectites: The Hind Sandstone Member injectite complex, Carboniferous, UK. *Marine and Petroleum Geology*, **27**, 1200-1215

Kane, I.A., McCaffrey, W.D. and Peakall, J. 2010. On the origin of paleocurrent complexity within deep marine channel levees. *Journal of Sedimentary Research*, **80**, 54-66.

Karpova, G.V. 1969. Clay mineral post-sedimentary ranks in terrigenous rocks. *Sedimentology,* **13**, 5-20.

Keevil, G.M., McCaffrey, W.D. and Peakall, J. 2008. Flow evolution in submarine channel bends: experimental insights into flow tuning. AAPG Convention, San Antonio, Texas.

Kenyon, N. H. and Millington, J. 1995. Contrasting deep-sea depositional systems in the Bering Sea. *In:* Pickering, K.T., Hiscott, R.N., Kenyon, N.H., Ricci Lucchi, F., and Smith, R.D.A. Eds., Atlas of Deep Water Environments: Architectural style in turbidite systems. London, Chapman & Hall, p. 196–202.

Kenyon, N.H., Millington, J., Droz, L. and Ivanov, M.K. 1995. Scour holes in channel-lobe transition zone on the Rhone Cone, *In:* Pickering, K.T., Hiscott, R.N., Kenyon, N.H., Ricci Lucchi, F., and Smith, R.D.A. Eds., Atlas of Deep Water Environments: Architectural style in turbidite systems. London, Chapman & Hall, p. 212-215.

Kidd, R.B., Lucchi, R.G., Gee, M. and Woodside, J.M., 1998. Sedimentary processes in the Stromboli Canyon and Marsili Basin, SE Tyrrhenian Sea: results from side-scan sonar surveys. *Geo-Marine Letters*, **18**, 146-154.

Klaucke, I., Masson, D.G., Kenyon, N.H. and Gardner, J.V. 2004. Sedimentary processes of the lower Monterey Fan channel and channel-mouth lobe. *Marine Geology*, **206**, 181-198

von Komar, P.D. 1971. Hydraulic jumps in turbidity currents. *Bulletin of the Geological Society of America*, **82**, 1477-1488.

Kostic, S. and Parker, G. 2006. The response of turbidity currents to a canyon-fan transition: internal hydraulic jumps and depositional signatures. *Journal of Hydraulic Research*, **44**, 631–653.

Koyama, T. and Ikeda, H. 1998. Effect of riverbed gradient on bedrock channel configuration: a flume experiment. *Proceedings of the Environmental Research Centre, Tsukuba University, Japan*, ***23***; 25-34.

Kraus, E. 1935. Uber Sandsteinmulste. *Z. Deutsch. Geol. Ges.* 87: 334-360.

Kuijpers, A., Hansen, B., Huhnerbach, V., Larsen, B., Nielsen, T., Werner, F. 2002. Norwegian Sea overflow through the Faeroe-Shetland gateway as documented by bedforms. *Marine Geology,* **188**, 147-164.

Lamb, M.P., Parsons, J.D., Mullenbach, B.L., Finlayson, D.P., Orange, D.L. and Nittrouer, C.A. 2008. Evidence for superelevation, channel incision, and formation of cyclic steps by turbidity currents in Eel Canyon, California. *Geological Society of America Bulletin,* **120**, 463-475.

Larue, D.K. and Hovadik, J. 2006. Connectivity of channelised reservoirs: a modelling approach. *Petroleum Geoscience*, **12**, 291-308.

Lastras, G., Arzola, R.G., Masson, D.G., Wynn, R.B., Huvenne, V.A.I., Huhnerbach, V. and Canals, M. 2009. Geomorphology and sedimentary features in the Central Portuguese submarine canyons, western Iberian margin. *Geomorphology*, **103**; 310-329.

Lee, S.E., Talling, P.G., Ernst, G.G.J. and Hogg, A.J. 2002. Occurrence and origin of submarine plunge pools at the base of the US continental slope. *Marine Geology*, **185**, 363-377.

Leeder, M.R. 1999. Sedimentology and sedimentary basins: from turbulence to tectonics. London, Blackwell Science, p. 199.

Leeder, M.R., Mack, G.H., Peakall, J. and Salyards, S.L. 1996. First quantitative test of alluvial stratigraphic models: Southern Rio Grande rift, New Mexico. *Geology*, **24**, 87–90.

Lien T., Walker, R.G. and Martinsen, O.J. 2003. Turbidites in the Upper Carboniferous Ross Formation, western Ireland: reconstruction of a channel and spillover system. *Sedimentology*, **50**, 113-148.

Mackey, S.D. and Bridge, J.S. 1995. Three-dimensional model of alluvial stratigraphy: theory and application. *Journal of Sedimentary Research*, **B65**, 7–31.

Martinsen, O. J., T. Lien, and R. G. Walker. 2000. Upper Carboniferous deep-water sediments, western Ireland: Analogs for passive-margin turbidite plays. *In:* Weimer, P. Slatt, R.M., Coleman, J., Rosen, N. C., Nelson, H., Bouma, A.H., Styzen, M.J. and Lawrence D.T. (eds) *Deep-water reservoirs of the world*: GCSSEPM Foundation 20th Annual Research Conference, 533–555.

Martinsen, O.J. and Collinson, J.D. 2002. The Western Irish Namurian Basin reassessed – a discussion. *Basin Research*, **14**, 523-542.

Martinsen, O.J., Lien, T., Walker, R.G. and Collinson, J.D. 2003. Facies and sequential organisation of a mudstone-dominated slope and basin floor succession: the Gull Island Formation, Shannon Basin, Western Ireland. *Marine and Petroleum Geology*, **20**, 789-807.

Maslin, M., Knutz, P.C. and Ramsay, T. 2006. Millenial-scale sea-level control on avulsion events on the Amazon Fan. *Quaternary Science Reviews*, **25**, 3338-3345.

Masson, D.G., Kenyon, N.H., Gardner, J.V. and Field, M.E. 1995. Monterey Fan: channel and overbank morphology. *In:* Pickering, K.T., Hiscott, R.N., Kenyon, N.H., Ricci Lucchi, F., and Smith, R.D.A. (eds) *Atlas of Deep Water Environments: Architectural style in turbidite systems*, Chapman & Hall, London, 47-79.

Masson, D.G., Wynn, R.B., Bett, B.J., 2004. Sedimentary environment of the Faeroe-Shetland Channel and Faeroe Bank channels, NE Atlantic, and the use of bedforms as indicators of bottom current velocity in the deep ocean. *Sedimentology*, **51**, 1-35.

Maxson, J. H. & Campbell, I. 1935. Stream fluting and stream erosion. *Journal of Geology*, 43; 729-744.

Maxson, J. H. 1940. Fluting and faceting of rock fragments. *Journal of Geology*, 48; 717-751.

McCave, I.N., Chandler, R.C., Swift, S.A., Tucholke, B.A. 2002. Contourites of the Nova Scotian continental rise and HEBBLE area. *Geological Society of London Memoir,* **22**, 21-38.

Middleton, G.V. 1966a. Experiments of density and turbidity currents. 1: Motion of the head. *Canadian Journal of Earth Sciences*, 3; 523-546.

Middleton, G.V. 1966b. Experiments of density and turbidity currents. 2: Uniform flow of density currents. *Canadian Journal of Earth Sciences*, 3; 627-637.

Middleton, G.V. 1966c. Experiments of density and turbidity currents. 3: Deposition of sediment. *Canadian Journal of Earth Sciences*, 4; 475-505.

Millington, J.J. and Clark, J.D. 1995. The Charo/Arro Canyon-Mouth sheet system,

south-central Pyrenees, Spain: A structurally confined influence zone of sediment dispersal. *Journal of Sedimentary Research,* **65**, 443-454.

Morris, S. A., Kenyon, N.H., Limonov, A.H. and Alexander, J. 1998. Downstream changes of large-scale bedforms in turbidites around the Valencia channel mouth, north-west Mediterranean: implications for palaeoflow reconstruction. *Sedimentology*, **45**, 365–377.

Morris, W.R. and Normark, W.R., 2000, Sedimentologic and geometric criteria for comparing modern and ancient sandy turbidite elements. *In:* Weimer, P., Slatt, R.M., Coleman, J., Rosen, N.C., Nelson, H., Bouma, A.H., Styzen, M.J. and Lawrence, D.T. (Eds), Deep-water reservoirs of the World, GCSSEPM Foundation 20th Annual Research Conference, p. 606-628.

Mutti, E. 1974. Examples of ancient deep-sea fan deposits from circum-Mediterranean geosynclines. SEPM Special Publication, **19**, 92-105.

Mutti, E. 1984. The Hecho Eocene Submarine Fan system, south-central Pyrenees, Spain. *Geo-marine Letters*, **3**, 199-202.

Mutti, E. 1992. Turbidite sandstones. AGIP-Istituto di Geologia, Universita` di Parma; San Donato Milanese, p. 275.

Mutti, E. and Normark, W.R. 1987. Comparing examples of modern and ancient turbidite systems: problems and concepts. *In:* Legget, J.K. and Zuffa, G.G. (eds) *Marine Clastic Sedimentology: Concepts and Case Studies*, Graham and Troutman, London, 1–38.

Mutti, E. and Normark, W.R. 1991. An integrated approach to the study of turbidite systems. *In:* Weimer, P. and Link, M.H (eds) *Seismic Facies and Sedimentary Processes of Submarine Fans and Turbidite Systems*, Springer-Verlag, New York, 75-106.

Mutti, E. and Sonnino, M. 1981. Compensation cycles: a diagnostic feature of turbidite sandstone lobes. IAS 2nd Eur. Meet., Bologna, Italy, 120–123.

Naidu, A.S., Burrell, D.C. and Hood, D.W. 1971. Clay mineral composition and geologic significance of some Beaufort Sea sediments. *Journal of Sedimentary Petrology*, **41**, 691-694.

Nelson, C.H., Twichell, D.C., Schwab, W.C., Lee, H.J., Kenyon, N.H. 1992. Upper Pleistocene turbidite sand beds and chaotic silt beds in the channelized, distal, outer-fan lobes of the Mississippi fan. *Geology,* **20**, 693–696.

Normark, W.R., 1970, Growth patterns of deep-sea fans. PhD Thesis, University of California, San Diego.

Normark, W.R., Piper, D.J.W. and Hess, G.R. 1979. Distributary channels, sand lobes, and mesotopography of Navy submarine fan, California borderland, with applications to ancient submarine fan sediments. *Sedimentology,* **26**, 749-774.

Normark, W.R. and Piper, D.J.W. 1991. Initiation processes and flow evolution of turbidity currents: implications for the depositional record, *in* R. H. Osborne,

ed., From shoreline to abyss: SEPM Special Publication **46**, 207–230.

Normark, W.R., Paull, C.K., Caress, D.W., Ussler, W. and Sliter, R., 2009, Fine-scale relief related to Late Holocene channel shifting within the floor of the upper Redondo Fan, offshore Southern California. *Sedimentology*, **56**, 1690-1740.

Palanques, A., Kenyon, N.H., Alonso, B., and Limonov, A. 1995. Erosional and depositional patterns in the Valencia channel mouth: an example of a modern channel-lobe transition zone. *Marine Geophysical Researches*, **17**, 503–517.

Parker, G. and Izumi, N. 2000. Purely erosional and solitary steps created by flow over a cohesive bed. *Journal of fluid mechanics,* **419**; 302-238.

Parsons, J.D., Schweller, W.J., Stelting, C.W., Southard, J.B., Lyons, W.J. and Grotzinger, J.P., 2002. A preliminary experimental study of turbidite fan deposits. *Journal of Sedimentary Research*, **72**, 619–628.

Peakall, J., McCaffrey, W.D. and Kneller, B.C. 2000a. A process model for the evolution, morphology and architecture of sinuous submarine channels. *Journal of Sedimentary Research,* **70**, 434–448.

Peakall, J., Leeder, M.R., Best, J. and Ashworth, P. 2000b. River response to lateral tilting: a synthesis and some implications for the modelling of alluvial architecture in extensional basins. *Basin Research*, **12**, 413–424.

Pett, J.W. and Walker, R.G. 1971a. Relationship of flute cast morphology to internal sedimentary structures in turbidites. *Journal of Sedimentary Petrology*, **41**, 114-128.

Pett, J.W. and Walker, R.G. 1971b. Relationship of flute cast morphology to internal sedimentary structures in turbidites - Reply. *Journal of Sedimentary Petrology*; 1156-1158.

Pickering, K.T. 1981. Two types of outer fan lobe sequence, from the late Precambrian Kongsfjord Formation Submarine Fan, Finnmark, North Norway. *Journal of Sedimentary Petrology*; **51***,* 1277–1286.

Pickering, K.T., Hiscott, R.N. and Hein, F.J. 1989. Deep Marine Environments: Clastic Sedimentation and Tectonics. Unwin Hyman, London, p. 416.

Pickering, K.T., Hiscott, R.N., Kenyon, N.H., Ricci Lucchi, F., and Smith, R.D.A. (eds) *Atlas of Deep Water Environments: Architectural style in turbidite systems*, Chapman & Hall, London, 47-79.

Piper, D.J.W., Hiscott, R.N. and Normark, W.R. 1999. Outcrop-scale acoustic facies analysis and latest Quaternary development of Hueneme and Dume submarine fans, offshore California. *Sedimentology*, **46**, 47-78.

Piper, D.J.W. and Deptuck, M. 1997, Fine-grained turbidites of the Amazon Fan: facies characterization and interpretation. *In:* Flood, R.D., Piper, D.J.W., Klaus, A., and Peterson, L.C. (eds) *Proceedings of the Ocean Drilling Program, Scientific Results*, **155**, 79–108. Ocean Drilling Program, College Station, TX.

Piper, D.J.W., Shor, A.N., Farre, J.A., O'Connell, S., Jacobi, R., 1985. Sediment slides and turbidity currents on the Laurentian Fan: Sidescan sonar observations near the epicentre of the 1929 Grand Banks earthquake. *Geology,* **13**; 538-541.

Piper, D.J.W. and Normark, W.R. 2001. Sandy fans; from Amazon to Hueneme and beyond. *AAPG Bulletin*, **85**, 1407–1438.

Pirmez, C. and Flood, R.D. 1995. Morphology and structure of Amazon Channel. *In:* Flood, R.D., Piper, D.J.W., Klaus, A. et al. (eds) *Proceedings of the Ocean Drilling Program, Initial Reports*, **155**, 23-45. Ocean Drilling Program, College Station, TX.

Posamentier, H.W. 2003. A linked shelf-edge delta and slope-channel turbidite system: 3D seismic case study from the eastern Gulf of Mexico. *In:* Roberts, H.H., Rosen, N.C., Fillon, R.H. and Anderson, J.B. (eds) *Shelf-margin deltas and linked down slope petroleum systems: global significance and future exploration strategy*: Proceedings, 23rd GCSSEPM Foundation Bob. F. Perkins Research Conference, 115-134.

Potter, D.P. and Shaw, J. 2009. Shaded seafloor relief, Placentia Bay southeast, offshore Newfoundland and Labrador; Geological Survey of Canada, Map 2147A, scale 1:50,000.

Pyles, D.R., 2004. On the stratigraphic evolution of a structurally confined submarine fan, Carboniferous Ross Sandstone, Western Ireland. Unpublished PhD dissertation, University of Colorado at Boulder, 322 pp.

Prélat, A., Hodgson, D.M. and Flint, S.S. 2009. Evolution, architecture and hierarchy of distributary deep-water deposits: a high-resolution outcrop investigation from the Permian Karoo Basin, South Africa. *Sedimentology*, **56**, 2132-2154.

Pyles, D.R., 2004. On the stratigraphic evolution of a structurally confined submarine fan, Carboniferous Ross Sandstone, Western Ireland. Unpublished PhD dissertation, University of Colorado at Boulder, 322 pp.

Pyles, D.R., 2007. Architectural Elements in a Ponded Submarine Fan, Carboniferous Ross Sandstone, Western Ireland. *In:* Nilsen, T.H., Shew, R.D., Steffens, G.S. and Studlick, J.R.J. (eds) *Atlas of deep-water outcrops*. AAPG Studies in Geology, **56**, CD-ROM, p. 19.

Pyles, D.R. 2008. Multiscale stratigraphic analysis of a structurally confined submarine fan: Carboniferous Ross Sandstone, Ireland. *AAPG Bulletin*, **92**, 557-587.

Pyles, D.R. and Jennette, D.C. 2009. Geometry and architectural associations of co-genetic debrite–turbidite beds in basin-margin strata, Carboniferous Ross Sandstone (Ireland): Applications to reservoirs located on the margins of structurally confined submarine fans. *Marine and Petroleum Geology*, **26**, 1974-1996.

Remacha, E, and Fernandez, L.P. 2003. High-resolution correlation patterns in the turbidite systems of the Hecho Group (South-Central Pyrenees, Spain). *Marine and Petroleum Geology*, **20**, 711–726.

Ribeiro Machado, L.C., Kowsmann, R.O., de Almeida, W. Jr, Murakami, C.Y., Schreiner, S., Miller, D.J., Orlando, P. and Piauilino, V. 2004. Geometry of the proximal part of the modern turbidite depositional system of the Carapebus Formation, Campos Basin: a model for reservoir heterogeneities. *Boletim de Geociencias da Petrobras*, **12**, 287–315.

Ricci-Lucchi, F. 1975. Depositional cycles in two turbidite formations of northern Apennines (Italy). *Journal of Sedimentary Petrology*, **45**, 3-43.

Ricci-Lucchi, F. 1984. The deep-sea fan deposits of the Miocene Marnoso-Arenacea Formation, northern Apennines. *Geo-marine Letters*, **3**, 203-210.

Ricci-Lucchi, F. and Valmori, E. 1980. Basin-wide turbidites in a Miocene, oversupplied deep-sea plain: a geometrical analysis. *Sedimentology*, **27**, 241-270.

Rider, M.H. 1974. The Namurian of west County Clare. *Proceedings of the Royal Irish Academy*, **74B**, 125-142.

Roveri, M. 2002. Sediment drifts of the Corsica Channel, northern Tyrrhenian Sea. *Geol. Soc. London. Memoir,* **22**, 191-208.

Rücklin, H., 1938, Strömungsmarken im unteren Muschelkalk des Saarlandes: Senckenbereiana*,* **20**, 94-114.

Stow, D.A.V. and Bowen, A.J. 1980. A physical model for the transport and sorting of fine-grained sediment by turbidity currents. *Sedimentology*, **27**, 31–46.

Stow, D.A.V., Faugeres, J.C., Gonthier, E., Cremer, M., Llave, E., Hernández-Molina, F.J., Luis Somoza, V Díaz-del-Río, 2002a. Faro-Albufeira drift complex, northern Gulf of Cadiz. *Geological Society of London Memoir,* **22**, 137-154.

Stow, D.A.V., Hernandez-Molina, F.J., Llave, E., Sayago-Hil, M., Diaz del Rio, V. and Branson, A. 2009. Bedform-velocity matrix: The estimation of bottom current velocity from bedform observations. *Geology*, **37**, 327-330.

Savoye, B., Babonneau, N., Dennielou, B. and Bez, M. 2009. Geological overview of the Angola-Congo margin, the Congo deep-sea fan and its submarine valleys. *Deep-Sea Research II*, **56**, 2169-2182.

Schulz, M. 2002. On the 1470-year pacing of Dansgaard-Oeschger warm events. *Paleoceanography*, **17**, 1014, doi:10.1029/2000PA000571.

Shor, A.N., Piper, D.J.W., Hughes Clarke, J.E. and Mayer, L.A. 1990. Giant flute-like scour and other erosional features formed by the Grand Banks turbidity current. *Sedimentology*, **37**, 631-645.

Siddall, M., Rohling, E.J., Thompson, W.G. and Waelbroek, C. 2008. Marine isotope stage 3 sea level fluctuations: data synthesis and new outlook. *Reviews of Geophysics*, **46**, RG4003.

Stow, D.A.V. and Bowen, A.J. 1980. A physical model for the transport and sorting of fine-grained sediment by turbidity currents. *Sedimentology*, **27**, 31–46.

Strachan, L.J. 2002. Slump-initiated and controlled syndepositional sandstone remobilization: An example from the Namurian of County Clare, Ireland. *Sedimentology*, **49**, 25–41.

Straub, K.M., Mohrig, D.C., Buttles, J., McElroy, B., and Pirmez, C. 2008. Interactions between turbidity currents and topography in aggrading sinuous submarine channels: A laboratory study. *Geological Society of America Bulletin*, **120**, 368-385.

Sullivan, M., Jensen, G., Goulding, F., Jennette, D., Foreman, L. and Stern, D. 2000. Architectural analysis of deep-water outcrops: implications for exploration and development of the Diana Sub-Basin, western Gulf of Mexico. *In:* Weimer, P., Slatt, R.M., Coleman, J., Rosen, N.C., Nelson, H., Bouma, A.H., Styzen, M.J. and Lawrence, D.T. (eds) *Deep-water reservoirs of the World*, GCSSEPM Foundation 20th Annual Research Conference, 1010-1031.

Sumner, E.J., Talling, P.J. and Amy, L.A. 2009. Deposits of flows transitional between turbidity current and debris flow. *Geology*, **37**, 99-994.

Talling, P. J., Wynn, R. B., Masson, D. G., Frenz, M., Cronin, B.T., Schiebel, R., Akhmetzhanov, A.M., Dallmeier-Tiessen, S., Benetti S., Weaver, P.P.E., Georgiopoulou, A., Zu¨hlsdorff, C. and Amy, L.A., 2007, Onset of submarine debris flow deposition far from original giant landslide. *Nature*, **450**, 541-544.

Terrinha, P., Matias, L., Vicente, J., Duarte, J., Luís, J., Pinheiro, L., Lourenço, N., Diez, S., Rosas, F, Magalhães, V., Valadares, V., Zitellini, N., Mendes Víctor, L. and MATESPRO Team. 2009. Morphotectonics and Strain Partitioning at the Iberia-Africa plate boundary from multibeam and seismic reflection data. *Marine Geology,* **267**, 156-174.

Torres, J., Droz, L., Savoye, B., Terentieva, E., Cochonat, P., Kenyon, N.H. and Canals, M. 1997. Deep-sea avulsion and morphosedimentary evolution of the Rhône Fan Valley and Neofan during the Late Quaternary (north-western Mediterranean Sea). *Sedimentology*, **44**, 457–477.

Toucanne, S., Zaragosi, S., Bourillet, J.F., Naughton, F., Cremer, M., Eynaud, F. and Dennielou, B. 2008. Activity of the turbidite levees of the Celtic-Armorican margin (Bay of Biscay) during the last 30,000 years: Imprints of the last European deglaciation and Heinrich events. *Marine Geology*, **247**, 84-103.

Tucholke, B.E. 1982. Origin of longitudinal triangular ripples on the Nova Scotian continental rise. *Nature,* **296**, 735-737.

Tucholke, B.E., Hollister, C.D., Biscaye, P.E., Gardner, W.D. 1985. Abyssal current character determined from sediment bedforms on the Nova Scotian continental rise. *Marine Geology*, **66**, 43-47.

Twichell, D.C., Schwab, W.C., Nelson, C.H., Kenyon, N.H. and Lee, H.J. 1992. Characteristics of a sandy depositional lobe in the outer Mississippi fan from SeaMARCIA sidescan sonar images. *Geology*, **20**, 689–692.

Vicente Bravo, J. C. and S. Robles. 1995. Large-scale mesotopographic bedforms from the Albion Black Flysch, northern Spain: characterization, setting and comparison with recent Channel-Lobe Transition Zones analogues, *in* K. T. Pickering, R. N. Hiscott, N. H. Kenyon, F. Ricci Lucchi, and R. D. A. Smith, eds., Atlas of deep water environments: architectural style in turbidite systems: London, Chapman and Hall, p. 216–226.

Walderhaug, O. 1996. Kinetic modeling of quartz cementation and porosity loss in deeply buried sandstone reservoirs. *Bulletin of the American Association of Petroleum Geologists,* **80***,* 731-745.

Walker, R.G. and Mutti, E. 1973. Turbidite facies and facies associations. *In:* Middleton, G.V and Bouma A. (eds) *Turbidites and Deep-water Sedimentation*, SEPM Pacific Section Short Course, 119-157.

Weimer, P. 1991. Seismic facies, characteristics and variations in channel evolution, Mississippi Fan (Plio-Pleistocene), Gulf of Mexico. *In:* Weimer, P. and Link, M.H. (eds) *Seismic Facies and Sedimentary Processes of Submarine Fans and Turbidite Systems*. Springer, New York, 323–347.

Weaver, P. P. E. & Kuijpers, A. 1983. Climatic control of turbidite deposition on the Madeira Abyssal Plain. *Nature,* **306**, 360–363.

Weaver, P. P. E. 1994. Determination of turbidity current erosional characteristics from reworked coccolith assemblages, Canary Basin, N. E. Atlantic. *Sedimentology*, **41**, 1025-1038.

Weaver, P.P.E., Wynn, R.B., Kenyon, N.H. and Evans, J. 2000. Continental margin sedimentation, with special reference to the north-east Atlantic margin. *Sedimentology*, **47**, 239-256.

Winn, R.D. and Dott, R.H., 1979, Deep-water fan-channel conglomerates of Late cretaceous age, southern Chile. *Sedimentology*, **26**, 203-228.

Wignall, P.B. and Best, J.L. 2000. The Western Irish Namurian Basin reassessed. *Basin Research*, **12**, 59-78.

Wignall, P.B. and Best, J.L. 2002. Reply to: The Western Irish Namurian Basin reassessed - a discussion by O.J. Martinsen & J.D. Collinson. *Basin Research*, **14**, 531-542

Wynn, R.B., Kenyon, N.H., Masson, D.G, Stow, D.A.V. and Weaver, P.E. 2002a. Characterisation and recognition of deep-water channel-lobe transition-zones. *AAPG Bulletin*, **86**, 1441-1462.

Wynn, R.B., Weaver, P.P.E., Stow, D.A.V., and Masson, D.G. 2002b. Turbidite depositional architecture across three interconnected deep-water basins on the Northwest African margin. *Sedimentology*, **49**, 669-695.

Wynn, R.B., Cronin, B.T. and Peakall, J. 2007. Sinuous deep-water channels: Genesis, geometry and architecture. *Marine and Petroleum Geology*, **24**, 341–387.

Zaragosi, S., Auffret, G.A., Fauge`res, J.-C., Garlan, T., Pujol, C. and Cortijo, E. 2000. Physiography and recent sediment distribution of the Celtic Deep-Sea Fan, Bay of Biscay. *Marine Geology*, **169**, 207-237.

Zitellini, N., Gracia, E., Matias, L., Terrinha, P., Abreu, M.A., DeAlteriis, G., Henriet, J.P., Danobeitia, J.J., Masson, D.G., Mulder, T., Ramella, R., Somoza, L. and Diez, S., 2009, The quest for the Africa-Eurasia plate boundary west of the Strait of Gibraltar. *Earth and Planetary Science Letters*, **280**, 13–50.

Appendix A
List megaflutes and scours in modern and ancient environments

Fan Name/ Reference	Imagery	Water depth (m)	Number of scours	Change in slope gradient (for CLTZ)	Scour Depth (m)	Scour Width (m)	Scour Length (m)	Comments
AGADIR								
Wynn et al., 2002a	-30 kHz deep-towed side scan sonar (TOBI) -7kHz and 3.5kHz profiles -piston cores	4250	Multiple, Many tens	Changes from rom 0.2 – 0.04	np	250 - 500 (isolated) Also amalgamated zone ~1000	500 (isolated)	-30km long erosional zone -Channel-lobe transition zone extends 60km from mouth
This study	-AUV mounted EM2000 multibeam -piston cores -EM120 multibeam -SBP120 and 3.5kHz sub-bottom profilers	4265	Tens, Plus regions of amalgamation	-	8 - 20	50 - 225	150 - 600	- Channel-lobe transition zone setting
ALBIAN BLACK FLYSCH, N. SPAIN								
Vicente Bravo and Robles, 1995	Outcrop work – 3D sketches and photo-montages	n/a	~Not specified, probably several	n/a	1 – 5	5 – 50	Downstream exposures are poor or difficult to discern	-Directly compared to Normark et al. (1979) Navy fan work -Composed of sands and gravels, must have formed under upper flow regimes - Channel-lobe transition zone setting -shows multi-episodic

scour and fill

1

CERRO TORO FM, MAGALLANES BASIN, N CHILE	Imagery	Water depth (m)	No scours	Slope Grad.	Scour Depth (m)	Scour Width (m)	Scour Length (m)	Notes
Wynn and Dott, 1979	*Outcrop work*	n/a	Multiple, tens	n/a	1.5	np	np	
Jobe et al., 2009	Outcrop work	n/a	Multiple, tens	n/a	"Canoe" flutes, no dimensions given, shown in photograph, meters in size			-region forms channel margin deposits of proximal axial channel belt
EEL CANYON	Imagery	Water depth	No scours	Grad	Depth	Width	Length	Notes
Lamb et al., 2008	-15.5kHz Hydrosweep system (echosounder?)	1000 - 1600	~7	n/a		Wavelength of steps = 2000 m Step height ~150 m		Scours generated at cyclic steps by superelevated turbidity currents that escape a 90° bend in the Eel Canyon -Steps occur within larger channel-like feature extending from canyon bend
HUENEME FAN								
Piper et al., 1999	-hi-res boomer system, 540 J fired at 0.75s and a 5 m 10-element hydrophone array ??	~1000	Multiple	Np		-1-2 m deep -50-200m apart		-on scoured-lobe subelement -attributed to the passage of flows with a high proportion of silt but a efficiency in sand, which erode sand as they pass down the fan. The low settling velocity of silt resulted in slow deceleration, permitting extended traction transport and scour. These flow therefore tended to locally bypass, scour and/or deposit only thing/widespread beds on middle fan

LAGOS-PORTIMAO FAIRWAY								
This study	-AUV mounted EM2000 multibeam -piston cores -EM120 multibeam -SBP120 and 3.5kHz sub-bottom profilers	4570	1	-	50	3000	>2000	-Single oval scour in channel mouth region -flanked by depositional chevrons and erosional (?) lineations

2

LAURENTIAN FAN	Imagery	Water depth (m)	No scours	Slope Grad.	Scour Depth (m)	Scour Width (m)	Scour Length (m)	Notes
Shor et al., 1990	- sidescan sonar image -multibeam	2800	1 +other erosional features	0.02° (+ flow expansion due to valley widening)	100 (giant) 10-20 (smaller)	np	1 (giant)	Giant flute is one off – more common smaller depressions occur in linear series -apparently cut by the 1929 Grand Banks turbidity current
LISBON CANYON MOUTH								
Wynn et al., 2002a	-30kHz deep towed side scan sonar (TOBI) -deep towed 7kHz profiles	4800	Tens, plus chevron scours, and an additional zone of waves/scours 70km from channel mouth	np	~4600	3000 (amalgamated) 800 (chevrons) -1500 wide (second zone)	6000 (amalgamated) 1000 (chevrons) -3000 long (second zone)	- Channel-lobe transition zone setting -40km long zone of erosional scours -75km away is additional zone of scours and sediment waves
MONTEREY								

Masson et al., 1995	-30kHz sidescan sonar (TOBI) -7kHz profiler data	Not given	Implies many, tens?	n/a	From tens – ~1000 m in diameter		-scours in overbank area concentrated adjacent to the outside of meander bends, suggesting an origin related to spillover of channellised flows -dominance of erosional features over those of depositional origin -surface represents complex equilibrium between erosion and deposition, rather than dominantly erosional	
Klaucke et al., 2004	-30-32kHz sidescan sonar and 7kHz hi-res sub-bottom profiler (TOBI) -6.5kHz sidescan sonar (GLORIA)	Not given	Implies many, tens?	np	From tens – ~1000 m in diameter			-develop in overbank area of alternating mud and graded silt -develop alongside trains of sediment
Monterey East: Fildani and Normark, 2004	-Deep-tow side looking sonar -3.5kHz reflection profiles -multibeam bathymetry -sed core	3400	4	n/a	Up to 110	2500 - 3500	2000 – 5000	-flow stripping at meander 20-40m deep, 3km wide breach in Shepard Meander levee leads to series of deep scours
Monterey East: Fildani et al., 2006	-3.5kHz seismic reflection profiles -multibeam bathymetry -deep tow sidescan -sediment core samples	3400	4	n/a	80 - 200	3500 - 4500	3000 - 6000	-flow stripping at meander (Above) -cyclic steps created by Froude-supercritical flow over erodible bed, leading to cyclic steps which are either net-erosional (scours) or net-depositional (sed waves)

NAVY								
Normark et al. 1979	-110kHz side scan sonar -4kHz seismic reflection profiles -echo sounder	~1770	30	n/a	20	50 - >500	<400	Located on outer levee slopes, or between and along active channels
Vicente Bravo and Robles, 1995	-Authors used data from Normark et al., 1979 Compared to outcrops in Albian Black Flysch – which are similar in size to smallest resolvable features on Navy Fan							
PLACENTIA BAY								
Potter and Shaw, 2009	-multibeams: Kongsburg-Simrad EM1000, EM1002, EM710, EM3002	~20	Multiple, tens to hundreds	Np	-several meters	<200	>500	-contentious origin, linked to 1929 Grand Banks earthquake, but other causes are "more likely" (none given)
REDONDO FAN								
Normark et al., 2009	AUV mounted 200kHz 1ox1o multibeam sonar, and 2-16kHz sub-bottom profiler (navigation aided by 300kHz Doppler velocity log at depths <130m, and GPS at surface) -ROV vibracores	650 - 700	>10 on two different scales	n/a	30 (Giant-scour) 6 - 20 (small scours)	200 (Giant-scour) 90 – 100 (small scours)	>400 (Giant-scour) 100 - 180 (small scours)	-48 cm mud fill in giant scour -linear sets of depressions (on two scales) formed adjacent to sediment waves -formation is attributed to recurrent cyclic steps due to recurrent overflow events
ROSS SANDSTONE, CO. CLARE, IRELAND	**Imagery**	**Water depth (m)**	**No scours**	**Slope Grad.**	**Scour Depth (m)**	**Scour Width (m)**	**Scour Length (m)**	**Notes**
Chapin et al., 1994	Outcrop work – multiple vertical	n/a	Multiple, tens	n/a	0.3 – 3.5	1.5 – 6	np	Scour types include bedding plane scours,

	logs, analysis of photo-montages					but some are >30 m		megaflutes and stepped-scours and form a continuum of erosive processes -generated by (i) hydraulic jump associated with slope change at CLTZ or overbank or (ii) disturbances from vortices in flow induced by irregular topography
Elliott, 2000a,b	Outcrop work – multiple vertical logs	n/a	Multiple, tens	n/a	0.5 - 3	1 – 45	5 – 25	-linked to widespread surfaces termed megaflute erosion surfaces -MES are indicative of powerful, single, large-volume turbidity currents that were non-depositional and initiated channels
Lien et al., 2003	Outcrop work – multiple vertical logs	n/a	Multiple	n/a	~3	1 - 40	At least 25	-erosion linked to the final stages of spillover at the bends of sinuous channels
Macdonald et al., in prep	Ourcrop work – multiple vertical logs, correlative panels	n/a	Multiple, tens	n/a	<1	3-15+	n/p	- Channel-lobe transition zone setting on lobe-element scale -scouring associated with flow expansion at termination of lobe-element feeder channel
RHONE	**Imagery**	**Water**	**No scours**	**Slope Grad.**	**Scour Depth (m)**	**Scour Width (m)**	**Scour Length (m)**	**Notes**

RHONE	Imagery	Water depth(m)	No scours	Slope Grad.	Scour Depth (m)	Scour Width (m)	Scour Length (m)	Notes
Kenyon et al. 1995	-30kHz sidescan sonar -5kHz profiles	np	Tens	"Changes from 1 in 100 to 1 in 200"	20	1000	np	-CLTZ -flow expansion, hydraulic jump
Wynn et al. 2002a	-30 kHz deep-towed side scan sonar (TOBI) -5 kHz profiles	~2300	Multiple, 10's to 100	Changes from 0.6° to 0.3°	20	np	1000	-CLTZ -Scours seen up to 30 km beyond CLTZ.
SAN LUCAS								
Normark, 1970	-side scan sonar -3.8kHz profiles	~2900	Not specified, figures suggest ~7	np	Not specified, figures suggest ~10	-Not specified, figures suggest dimensions of ~50m x ~200m		-imaged steep-walled depressions and hummocky topography
Normark and Piper, 1991, p. 220	-side scan sonar		8 large Many small	0.028°	50-60	np	500-600	Re-interpretation of Normark (1970), no new data obtained
SETUBAL CANYON MOUTH								
This study	- AUV mounted EM2000 multibeam -piston cores -EM120 multibeam -SBP120 and 3.5kHz sub-bottom profilers	4840	10-20 Also amalgamated scours	-	14 (isolated) 22 (amalgamated)	~2000 (many are 'open')	1000 (isolated)	-CLTZ
VALENCIA CHANNEL MARGIN								
Morris et al., 1998	-30kHz high-res side scan sonar (MAK1)	~2800	Multiple, tens, chevron bedforms, linear bedforms	Flat channel floor has slope of 0.17	~2 (Chevrons)	200 (Chevrons & megaflutes)	70 (Chevrons)	-CLTZ

	-gravity cores		and mega-flutes					
WHITTARD CHANNEL MARGIN								
This study	-AUV mounted EM2000 multibeam -piston cores -EM120 multibeam -SBP120 and 3.5kHz sub-bottom profilers	4600	Tens, plus regions of amalgamation	-	30 (isolated) 18 (amalgamated)	890 (isolated) 750 (amalgamated)	550 (isolated) 480 (amalgamated)	-Scouring in overbank area of channel -four scales of scouring documented: proto-, isolated-, amalgamated-, and fully-amalgamated

Appendix B
List of MATLAB scripts

Convert.m

Script converts ultrasonic probe data matrices into XYZ format

```
[a,a1,a2,a3,a4,a5,a6,a7,a8,a9,a10,a11,a12] = textread('FILENAME.txt','%f %f %f %f %f %f %f %f %f %f %f %f %f %f %f','delimiter',' ')
count=1
all= horzcat(a,a1,a2,a3,a4,a5,a6,a7,a8,a9,a10,a11,a12)
f=length(a)
b1=ones(f,1)
b1=b1+count
b1=b1-1
c1=horzcat(a,b1,a1)
count=count+1
b2=ones(f,1)
b2=b2+count
b2=b2-1
c2=horzcat(a,b2,a2)
count=count+1
b3=ones(f,1)
b3=b3+count
b3=b3-1
c3=horzcat(a,b3,a3)
count=count+1
b4=ones(f,1)
b4=b4+count
b4=b4-1
c4=horzcat(a,b4,a4)
count=count+1
b5=ones(f,1)
b5=b5+count
b5=b5-1
c5=horzcat(a,b5,a5)
count=count+1
b6=ones(f,1)
b6=b6+count
b6=b6-1
c6=horzcat(a,b6,a6)
count=count+1
b7=ones(f,1)
b7=b7+count
b7=b7-1
c7=horzcat(a,b7,a7)
count=count+1
b8=ones(f,1)
b8=b8+count
b8=b8-1
c8=horzcat(a,b8,a8)
count=count+1
b9=ones(f,1)
b9=b9+count
b9=b9-1
c9=horzcat(a,b9,a9)
count=count+1
b10=ones(f,1)
```

```
b10=b10+count
b10=b10-1
c10=horzcat(a,b10,a10)
count=count+1
b11=ones(f,1)
b11=b11+count
b11=b11-1
c11=horzcat(a,b11,a11)
count=count+1
b12=ones(f,1)
b12=b12+count
b12=b12-1
c12=horzcat(a,b12,a12)
combined=vertcat(c1,c2,c3,c4,c5,c6,c7,c8,c9,c10,c11,c12)
dlmwrite('FILENAME.txt',combined,'delimiter',' ','newline', 'pc','precision','%.2f')
```

Plot.m

Script interpolates and plots compiled XYZ files using contour plots. This script was used to plot both field and experimental data.

```
data = importdata('FILENAME.txt','\t');
x_A = data(:,1);
y_A = data(:,2);
z_A = data(:,3);

xres = 500; yres = xres;

xspaceA = linspace(min(x_A),max(x_A),xres);
yspaceA = linspace(min(y_A),max(y_A),yres);

[X_A,Y_A,Z_A] = griddata(x_A,y_A,z_A,xspaceA(:)',yspaceA(:),'linear', {'QJ'});

figure
contourf(X_A,Y_A,(-1*Z_A),100,'linestyle','none'), colorbar('westoutside'), hold on
caxis([-12.6 -10.8])
xlim([2000 2500])

X = X_A;
Y = Y_A;
Z = -1*(Z_A);
```

PlotXsection.m

Script plots a line of cross section between specified points (X_a, Y_a) and (X_b, Y_b), between the y-limits of y_A and y_B, and the x-limits of x_A and x_B. This script was used to plot both field and experimental data.

plotXsection(X,Y,Z, X_a,Y_a,X_bY_b)
ylim([y_A y_B])
xlim([x_A and x_B])

Appendix C

Macdonald, H.A., Peakall, J., Wignall, P. and Best, J. *In prep*. Sedimentation in deep-sea lobe elements: implications for the origin of thickening-upwards sequences.

SEDIMENTATION IN DEEP-SEA LOBE ELEMENTS: IMPLICATIONS FOR THE ORIGIN OF THICKENING-UPWARDS SEQUENCES

Heather A. Macdonald*[1], Jeff Peakall[1], Paul B. Wignall[1] and Jim Best[2]

[1]*Earth Surface Science Institute, School of Earth and Environment, University of Leeds, Leeds, LS2 9JT, UK.*

[2]*Departments of Geology and Geography and Ven Te Chow Hydrosystems Laboratory, University of Illinois, IL 61801, USA.*

**Corresponding author (email: h.macdonald@see.leeds.ac.uk)*

Abstract:

The frequency and origin of upward-thickening packages in the sediments of deep-sea environments has been a topic of much recent debate. Excellent bed-scale exposures in the Carboniferous Ross Formation, western Ireland, allow individual surfaces to be traced laterally and the detailed architecture of whole packages to be evaluated using multiple vertical logs. The deposits comprise architectural elements including bed-sets, lobe-elements and composite lobes, with the lobe-elements being arranged in upward-thickening depositional packages. Results show that these packages are the result of the progradation of each lobe-element, whereby each individual package records a vertical trend from distal- to proximal-deposits accompanied by an increasing frequency of megaflutes and ultimately the development of broad erosional surfaces. We propose a six-stage model for lobe-element evolution that documents successive phases of deposition, sediment bypass, erosion and lobe abandonment. This new model provides a mechanism for lobe-elements switching and explains the development of thickening-upward successions. This allows the re-examination of existing process-models for these sedimentary packages in deep-sea sediments.

Submarine lobes form a key component of submarine fans, and although they have been extensively studied (e.g., Walker and Mutti, 1973; Mutti, 1974; Ricci-Lucchi, 1975; Hiscott, 1980; Mutti and Normark, 1987; Twichell et al., 1992; Nelson et al., 1992; Piper et al., 1999; Piper and Normark, 2001; Ribeiro Machado et al., 2004; Gervais et al., 2006; Deptuck et al., 2008; Bourget et al., 2009; Prélat et al., 2009), their formative processes still remain relatively poorly understood. In particular, key questions remain concerning the relative importance of progradation and aggradation in submarine lobes, and how such processes are manifested and identified in the rock record (Mutti and Sonnino, 1981; Hiscott, 1981; Chen and Hiscott, 1999; Deptuck et al., 2008; Prélat et al., 2009). Recent advances in understanding the sedimentary architecture of submarine fans have been made based upon analysis of large-scale geometries interpreted from seismic, bathymetric or acoustic datasets (e.g., Gervais et al., 2006; Deptuck et al., 2008; Jegou et al., 2008; Bourget et al., 2009), and numerical modelling (Groenenberg et al., 2010). These studies have led to the recognition of hierarchies of internal sedimentary architecture (e.g. Twichell et al., 1992; Piper et al., 1999; Deptuck et al., 2008; Prélat et al., 2009), and culminated in two very similar four-level hierarchies, based on subsurface data (Deptuck et al., 2008) and outcrop data (Prelat et al., 2009). The hierarchy of Deptuck et al. (2008) was based upon small, confined lobes of the Corsican trough, and comprises bed/bed-sets (deposits from a single flow), lobe-elements (stacked beds and bed-sets), composite-lobes (stacked lobe elements) and lobe complexes (stacked composite lobes). However, understanding the detailed process mechanics within and between these individual levels has been limited by the poor resolution of these techniques and the absence of detailed facies and bed-level descriptions.

Outcrop studies often provide bed-level detail, although they typically lack both the scale and three-dimensional control on architecture observed in seismic data and modern studies (but see Prélat et al. (2009) who present a recent notable exception). Early work concentrated on analysis of vertical sequences and placed much emphasis on the presence of asymmetrical sequences, particularly thickening-upwards packages (Walker and Mutti, 1973; Mutti, 1974; Ricci-Lucchi, 1975; Ghibaudo, 1980; Ricci-Lucchi and Valmori, 1980). These sequences were interpreted either as the result of progradation (e.g., Mutti, 1974; Ricci-Lucchi, 1975, 1984) or the subtle lateral shifts that form compensation cycles (Mutti and Sonnino, 1981; Mutti, 1984; Pickering et al., 1989). This body of work was questioned by Hiscott (1981) who argued that the sequences recognised by Ghibaudo (1980) could simply be the result of the chance distribution of beds. Subsequent statistical analysis of a broader range of deep-marine sequences (Chen and Hiscott, 1999) also concluded that in the studied sections the lobe deposits showed no consistent thickness trends. The absence of asymmetric vertical stacking patterns was attributed both to the myriad factors controlling turbidite thickness and distribution, and to the importance of aggradation relative to progradation in turbidite lobes (Hiscott, 1981; Chen and Hiscott, 1999). In the lobes of deep-sea fans, sediment aggradation is not controlled principally by sea-level, as in fluvio-deltaic lobes, and therefore accommodation space is always available and progradation is deemed less important (Hiscott, 1981; Chen and Hiscott, 1999). However, despite these arguments, thickening-upwards packages in lobes have continued to be recognised (e.g., Mutti and Normark, 1991; Mutti, 1992; Anderton, 1995; Carr and Gardner, 2000; Elliott, 2000a,b; Lien et al., 2003; Hodgson et al., 2006; Pyles 2007), but their origin and frequency of occurrence remains enigmatic; we address this enigma herein.

Outcrop studies have examined lobes in two and three-dimensional exposures (e.g., Chapin et al., 1994; Carr and Gardner, 2000; Johnson et al., 2001; Remacha and Fernandez, 2003; Hodgson et al., 2006; Pyles, 2007, 2008; Prélat et al., 2009), and have concentrated principally on the nature, dimensions and hierarchy of the architectural elements, and the overall evolution of these lobe systems. However, these studies have not specifically addressed the detailed process mechanics of small-scale (*c*. several metres) packages, or the origins of cyclicity. The present paper examines lobe-element dynamics, *sensu* Deptuck et al. (2008), and thickening-up sequences, through analysis of outcrops from parts of the Carboniferous Ross Sandstone, Western Ireland, which have been widely recognised as exhibiting thickening-upwards packages (Elliott, 2000a,b; Lien et al., 2003; Pyles 2007). Past research has interpreted these sequences either as deep-sea lobes or as spillover lobes adjacent to channels (Chapin et al., 1994; Sullivan et al., 2000; Lien et al., 2003; Pyles, 2007, 2008), or as channels and channel wings on the basin-floor (Elliott, 2000a,b). These previous studies have dominantly used single vertical sedimentary logs, or larger-scale correlation panels of 'key' identified surfaces. Herein, we utilise a series of detailed bed-by-bed scale correlation panels constructed from multiple closely-spaced logs, in combination with laterally tracing continuous individual surfaces, in order to examine the lateral and vertical variations of all beds within these sections. The presence of an array of different erosional features is used, in combination with the spatial distribution of beds, to re-examine previous palaeoenvironmental interpretations, and propose a new model for the development of thickening-upward lobe-elements within the Ross Sandstone. This model recognizes major phases of sediment deposition, bypass, erosion and lobe abandonment, and is used to discuss the origin of some thickening-up sequences in deep-sea lobes.

Regional Setting

The Carboniferous Shannon Basin

The Shannon Basin is a structurally-confined basin that developed throughout the Carboniferous in response to subsidence over the Iapetus suture (Collinson et al., 1991; Martinsen et al., 2000, 2003; Wignall and Best, 2000, 2002; Martinsen and Collinson, 2002; Pyles, 2007, 2008). The basin-fill comprises an initially deepening, then shallowing-upward succession, punctuated by laterally-continuous condensed sections (previously termed "marine bands") that provide a biostratigraphic framework for the basin (Hodson, 1954a,b; Hodson and Lewarne, 1961; Rider, 1974; Collinson et al., 1991; Hampson et al., 1997; Wignall and Best, 2000, 2002; Martinsen and Collinson, 2002; Pyles, 2008). The basin consists of a Visean limestone overlain by a clastic Namurian (upper Mississippian-lower Pennsylvanian) fill, including deep-water shales (Clare Shale Formation ~ 100% shale), turbiditic sandy submarine-fan deposits (Ross Sandstone Formation ~ 60% sandstone), unstable muddy delta-slope deposits (Gull Island Formation ~ 23% sandstone) and fluvio-deltaic shelf margin deposits (Central Clare Group cyclothems ~ 25% sandstone) (Rider, 1974; Collinson et al., 1991; Wignall and Best, 2000, 2002; Martinsen and Collinson, 2002; Pyles, 2008).

The Ross Sandstone

The submarine fan deposits of the Ross Sandstone have been intensively studied in recent years, in part owing to their excellent and continuous exposure along the coast of County Clare, but also because their sedimentary architecture is analogous to many deep-water petroleum reservoirs in the Gulf of Mexico (e.g. Chapin et al., 1994; Sullivan et al., 2000; Pyles, 2008). The Ross Sandstone has a maximum thickness of 500 m and comprises interbedded sandstones, siltstones and mudstones that have been interpreted as mudstone sheets, turbidites, channels and associated slumps (Rider, 1974; Collinson et al., 1991; Martinsen et al., 2000; Wignall and Best, 2000; Strachan, 2002; Lien et al., 2003; Pyles, 2007, 2008). The Ross Sandstone documents an overall progradational history recorded by the progressive north-eastward expansion of the area of turbidite sandstone deposition (Wignall and Best, 2000). In outcrops in SW County Clare, the progradational trend is shown by the vertical change in the proportions of internal architectural elements, where mudstone sheets dominate the lowermost deposits, the middle Ross Sandstone is dominated by lobes, and both channels and slumps become more common in the upper Ross Sandstone (Strachan 2002; Pyles, 2008). However, the dominant architectural element in the Ross Sandstone is suggested to be lobes (56% average by area; Pyles, 2007).

Much of the Ross Sandstone is characterised by interbedded sandstones and mudstones that are organised into broad thickening-upward packages (Elliott, 2000a,b; Lien et al., 2003; Pyles 2007). Packages are typically 1 - 7 m thick, and where complete can be subdivided into three parts (Fig. 1): i) an initial finely parallel-laminated mudstone unit; ii) a series of interbedded silty mudstone and sandstone deposits, and iii) an overlying structureless amalgamated sandstone unit. The degree of amalgamation within the upper sandstone varies across the beds, allowing some bedding surfaces and intervening mudstone deposits to be preserved. Important features that occur at varying heights through these packages are *megaflutes*, a type of large flute-like erosional bedform that provides evidence for highly localized erosion within an otherwise largely depositional environment. The distribution of megaflutes, together with the depositional environment of these cyclical packages, has been widely debated, with palaeoenvironmental reconstructions ranging from: i) aggrading lobes within a structurally-confined, rapidly subsiding, basin (Pyles, 2007, 2008), where scouring developed in regions of channel-to-lobe transition (Chapin et al., 1994), through ii) scouring on channel flanks via single, catastrophic, channel-initiating flows that subsequently infilled via low-magnitude, high-frequency turbidity currents (Elliott, 2000a,b), to iii) deposition and scouring within spillover lobes at the bends of sinuous submarine channels (Lien et al., 2003). A key aspect of the research presented herein has been to help resolve these conflicting interpretations.

Methodology, dataset and study area

The present-day geomorphology of the study area consists of both cliff exposures and extensive foreshore platforms. The cliffs allow laterally-continuous lobe deposits to be traced across distances of up to 2000 m revealing that average lobe dimensions are 1900 m wide and 2 m thick (Pyles, 2007). In order to evaluate depositional processes, we have focussed upon accessible coastal exposures at Ross Bay, Ross Point and Kilbaha Bay (Fig. 2). The former two locations have not previously been

recorded in bed-set detail, whereas the sections at Kilbaha Bay (Fig. 2c) have been previously studied by Elliott (2000a; his Channel 4). The present dataset comprises 53 sedimentary logs that were used to construct three correlation panels.

Measured sections

The three measured sections detailed herein occur within the middle Ross Sandstone (Kilbaha Bay) and the upper (Ross Bay and Ross Point). The sections comprise cyclical thickening-upwards packages (Fig. 1). The sandstones are fine-grained and commonly structureless (Bouma horizon Ta), although fluted bases, planar lamination (Bouma horizon Tb) and ripple cross-lamination (Bouma horizon Tc) are not uncommon. Occasionally, mud chips are contained within sandstone beds, particularly within thicker (>0.30 m) and/or amalgamated sandstones where clasts are 0.02 – 0.15 m long. Mudstone beds are nearly always planar laminated with some very thin (<1 mm) fine-sand stringers. Within the thickening-upward packages, two scales of erosional surfaces and structures exist: (i) broad scour surfaces with steps that may fully, or almost-fully, cut out thick (>0.50 m) sandstone beds (Fig. 3A,B), and (ii) megaflutes. These latter show a much wider range of styles and sizes than previously recorded (e.g. Chapin et al., 1994; Elliott 2000a,b; Lien et al., 2003), including cross-sectional profiles with a U-shape (Fig. 3A,B), megaflutes with internal hummocks (Fig. 3B) and megaflutes with planform shapes that range from widely-flaring (Fig. 3A) to arcuate (Fig. 3B). These various types of erosive feature are often preserved on the same bedding surface, where the scalloped rims of megaflutes occur along broad erosional surfaces.

Ross Bay (Fig. 3A)

The package documented from Ross Bay (Figs 2 and 3A) is situated 7.2 m above the previously illustrated "classic megaflute" surface of Leeder (1999), Elliott, (2000b) and Lien et al. (2003). It occurs within a succession of >10 thickening-up packages that begin with mudstone intervals that vary considerably in thickness (Figure 4). Contrary to previous reports that considered the packages to exhibit solely a coarsening-up motif (e.g. Elliott, 2000a; Lien et al. 2003; Pyles 2008), the basal strata show a fining-upward trend with thin interbedded ripple sandstone and siltstone passing upwards into dark shales, although the predominant trend is one of coarsening upwards (Fig. 4). This is manifested as a progressive increase in sandstone bed thickness and an associated decline in the thickness of shale/siltstone interbeds. The thickest beds are ~1m thick although this is attributable to amalgamation of 2-3 or more beds (Fig. 4).

The package chosen for detailed study exhibits a sequence of distinct erosional events, with the lowest erosion surface (labelled 'a', Fig. 3A) truncating a thin-sand that is only 0.25 m from the base of the package. Overlying this thin sand is a 0.50 m thick tabular sand that has two megaflutes eroded into its upper surface (labelled 'b', Fig. 3A), each measuring ~3 m wide and possessing ~0.25 m of erosive relief. Despite being immediately adjacent to one another, these megaflutes have different sediment infills, with one being firstly infilled with 0.1 m of sand whilst the other is initially infilled with 0.1 m of mud. Overlying both of these initial infills is a series of interbedded muds and sands that show amalgamation up-section. These muds and sands are themselves partially eroded by a broad scour surface (labelled

'c', Fig. 3A) that extends across the width of the exposure and has a vertical relief of ~1.5 m. This scour surface is the main erosive feature within the package, and hosts at least 3 megaflutes and one stepped-scour (inset figures, Fig. 3A). This major erosional surface is infilled by interbedded sand-rich deposits, some of which display further megaflutes (labelled 'd', Fig. 3A), which are then overlain by amalgamated sandstone beds. This whole thickening-up package is overlain by a significant thickness of mudstone at the base of an overlying thickening-upward package.

Ross Point (Fig. 3B)

The Ross Point section is located in an intertidal position, immediately below the Ross Slump (Figs 2 and 3B). A thickening-upward package lies on a laterally-continuous amalgamated sandstone that has an undulating, erosive upper contact (labelled 'a', Fig. 3B). The earliest interbedded muds and sands of the overlying thickening-upward package have ponded within the erosive topography of this upper surface. The first major erosional surface (1.3 m from the base of package in the northwest; labelled 'b' Figure 3B) is laterally persistent and hosts a stepped scour that nearly removes a 1.1 m thick tabular sand; to the south-east, the erosional surface becomes difficult to discern within an erosive amalgamated sandstone (Fig. 3b). This major erosional surface is progressively infilled by interbedded sands and muds, which are then succeeded by amalgamated sands. Megaflutes occur in these upper sandstones; one fully-exposed example (inset figure, Fig. 3B) measures 3 m wide, 7 m long and 0.55 m in vertical relief, and is initially draped with a mud-chip conglomerate with clasts up to 0.25 m long. These megaflutes are otherwise passively filled with sandstone and thin discontinuous muds (Fig. 3B).

Kilbaha Bay (Fig. 3C)

The Kilbaha Bay section (Figs 2 and 3C) is located at the easternmost headland of the bay approximately 5 m below the top of the exposure. The base of the package is marked by a laterally-continuous mudstone (labelled 'a', Fig. 3C), which is overlain by ~2 m of interbedded sandstones (with some mudstone intervals) that shows progressive amalgamation to the west. Two of the lowermost interbedded sandstones (labelled 'b' and 'c', Fig. 3C) have erosional upper surfaces and are cut-out locally by stepped scours. These surfaces are filled with other thick interbedded sandstones, one of which has a widespread upper erosional surface that hosts megaflutes (>2 m wide; labelled 'd', Fig 3C). Overlying this is a series of interbedded sandstones and mudstones, which culminate in a thick, amalgamated sandstone. This succession is partially eroded by a widespread erosional scour surface, with a vertical relief of up to 2 m, which also hosts megaflutes (3 – 15 m wide) upon the amalgamated sandstone (labelled 'e', Fig. 3C). This broad scour surface is then filled with interbedded sands and mud, and is overlain by a thick mudstone interval that marks the beginning of the next thickening-upward package.

Sedimentary model: erosive bypass within prograding lobe-elements

Based on these detailed sections, we attribute the thickening-up packages observed in the Ross Sandstone to deposition on prograding lobes within a distributary submarine fan. The deposits exhibit the classical features of deep-sea lobes (e.g., Mutti and Normark, 1987): 1) relatively tabular and laterally-extensive beds; 2) distinct packages bounded by parallel surfaces; 3) a dominance of thick sandstone beds alternating with mudstones and thinner-bedded sandstones; 4) amalgamation of sandstone beds; 5) scours and 6) thickening-up packages. By analogy with other studies in turbiditic environments (Twichell et al., 1992; Piper and Normark, 2001; Gervais et al., 2006; Deptuck et al., 2008; Bourget et al., 2009; Hanquiez et al., 2009), and in accord with Pyles and Jennette (2009), we interpret each thickening-up package to represent one lobe-element, which in turn stack to produce composite lobes. The basal mudstone part of the packages mark a period of lobe-element shutdown, recorded by thin, fining-upward successions, and its presence is dependent upon the degree of avulsion (lateral distance and time scale) experienced by a subsequent lobe-element.

Based on these observations, a six-stage model for the development of each lobe-element and its erosive features can be proposed (Fig. 5): (t1) Initially, in a dominantly depositional distal lobe-element setting, interbedded sands and muds accumulate from successive turbidity currents, and the bed shear stresses from these expanding and decelerating flows are insufficient to generate any erosional bedforms. (t2) As the lobe-element progrades and aggrades, increasing erosion is manifested by the generation of megaflutes. Thicker sands are deposited by higher velocity flows that deposit erosively amalgamated beds. (t3) With further progradation and aggradation of the lobe, the frequency of megaflutes becomes greater as the intensity of sediment bypass increases. (t4) The period of maximum bypass represents arrival of the distributary channel at a proximal position within the lobe-element; the erosive surface is here termed a proximal lobe bypass surface. At this stage, megaflutes may develop and join laterally or become incorporated into the margin of the bypass surface. (t5) Bypass intensity decreases as lobe-element abandonment is initiated; deposition rates increase resulting in a net accumulation of sediment and the passive filling of the proximal lobe bypass surface. The remaining erosive features become draped or compensationally-filled by larger flows. (t6) Complete avulsion, perhaps linked to the infill of these first small channels, leads to the prograding lobe-element being abandoned. Sediment accumulation at this locality is initially composed of thin sand/mud interbeds and then solely by mud that marks the beginning of a new thickening-up package, and the generation of a new lobe-element.

The occurrence of megaflutes, distributary channels and proximal lobe bypass surfaces

In this model proposed herein, the location of erosive features within the lobe-element deposits, including megaflutes and broader bypass surfaces, is determined by their proximality within the prograding and aggrading lobe. Furthermore, megaflutes form as a result of the increased flow velocities that may be expected at the channel to lobe-element transition region, and develop in a proximal lobe-element position. Such localities have also been proposed to be zones in which hydraulic jumps may occur that may favour the production of local scour (Normark

et al., 1979; Chapin et al., 1994). Their occurrence within the upper portions of thickening-up packages therefore spans medial- to late-stage proximal deposits (Fig. 3). In the lowermost parts of the packages, the megaflutes likely represent the erosive products of larger flows, and with continued progradation an increasing proportion of the flows generate more megaflutes. At this stage, the largest flows begin to develop broad erosive surfaces on which megaflutes can form, grow and coalesce. With continued progradation, a more proximal setting is reached and the phase of maximum sediment bypass occurs via the arrival of the lobe-element distributary channel, eventually culminating in formation of a proximal lobe bypass surface. This surface erodes through earlier proximal and medial deposits, and precedes the initiation of lobe abandonment. The observed increase in erosional intensity within these thickening-upwards packages points to a gradual and progressive increase in the local velocity of the turbidity currents at any given location.

Support for this model is provided by recent work on subsurface and modern deep-sea environments, which shows repeated erosion and the formation of megaflutes in regions of flow expansion between confined and unconfined flow. Examples include the San Lucas Fan and the Agadir, Lisbon and Setubal Canyons where scours are common in these modern channel-lobe transition zones, and in the Rhône Neofan and Monterey Fan, where flows are beginning to initiate new lobe / overbank deposits (Normark, 1970; Masson et al., 1995; Wynn et al., 2002; Bonnel et al., 2005; Fildani et al., 2006).

Discussion

Comparison with existing models

The model presented here builds on earlier interpretations of lobes for these sequences (Chapin et al., 1994, Pyles, 2007, 2008) but is in contrast to models invoking ‘channels with channel-wings’ (Elliott, 2000a,b), and channel spillover lobes (Lien et al., 2003).

Channels, channel wings and channel initiation

Elliott (2000a,b) suggested that the successions examined here were channels with broader, sheet-like, thickening-upward, and overall coarsening-upward, channel wing deposits. The basal surfaces of the channel wings in Elliott’s model exhibit megaflutes along discrete surfaces and were interpreted as marking periods of widespread erosion and subsequent localised channelization by giant single flows. These discrete surfaces, termed *megaflute erosion surfaces* were envisaged to occur on the upper surface of thick, amalgamated sandstones, and pass laterally into channel axes. Several problems exist with this ‘channel-wing’ model: (1) it fails to record the occurrence of megaflutes both within the amalgamated sandstones and upon interbedded sands lower in the packages (see also Lien et al., 2003), and does not account for the fact that there is therefore a progressive increase in the degree of erosion that occurs within each package; (2) it fails to recognise that once the main megaflute erosion surface is formed, it may continue to be subjected to subsequent *filling- and cutting-* events, i.e. it does not have to form via a single catastrophic

event explicit in the model; (3) the model provides no explanation for the repetition of numerous thin packages, which presumably must arise through frequent channel avulsion in this model. Trunk channels (rather than the distributary channels envisaged here) are typically long-lived conduits with low avulsion rates (e.g., Weimer, 1991; Pirmez and Flood, 1995; Savoye et al., 2009); (4) it implies the proportion of channels-fills in the Ross Sandstone is very high. Indeed, Elliott (2000a) considered such channel fills the dominant element of the mid-and upper parts of the Ross Sandstone, much higher than in any other known example (e.g. Clark and Pickering, 1996; Wynn et al., 2007); (5) it contrasts with previous work on the infill of submarine channels that have typically been shown to be fining-upwards successions, sometimes associated with thinning-upwards packages, but not thickening- and coarsening-upwards sequences (e.g., Chen and Hiscott, 1999); (6) paradoxically, the 'channel-wing' model suggests that the packages predominantly consist of 'laterally extensive sheet-like' deposits (Elliott, 2000a p. 367), and thus presumably must be dominantly unconfined, yet are all considered as channel elements.

The model presented herein addresses all of these points and recognises distributary channels and broad erosion surfaces within dominantly unconfined lobe sequences. Critically, we show that the 'megaflute erosion surfaces' are just one of many erosional surfaces in each thickening-upward package, and that they represent erosion by many of the most erosive flows (see also Pyles and Jennette, 2009). This suggests that channels, at least distributary channels such as these, are formed by multiple events rather than single catastrophic events. It further suggests that the previous consensus on the initiation of trunk channels via numerous erosive events (e.g., Clark and Pickering, 1996; Imran et al., 1998; Posamentier, 2003) remains valid.

Spillover lobes

A contrasting model associates megaflute development with spillover lobes at the bends of sinuous channels (Lien et al., 2003). This 'spillover' model proposes that mudstones at the base of the packages represent deposition furthest from the channel, and that the coarser-grained, thickening-up, sequences represent spillover lobes formed as the channels migrated laterally, with channel avulsion occurring at the top of each thickening-up unit. Overbank flow is assumed to occur only at the outside of channel bends, with homogeneous mudstones occurring immediately adjacent to other parts of the channel representing older overbank deposits or the deposits of distal flows that are overspilling at the outer channel bend (Lien et al., 2003; their figure 23). A number of key difficulties arise with this model: (1) overbank sediment from submarine channels does not comprise solely homogeneous muds in more distal locations, but rather displays thin interlaminated beds, graded beds and base-missing sequences (Stow and Bowen, 1980; Mutti and Normark, 1987; Kane et al., 2007, 2009); (2) there is substantial evidence to suggest that fine-grained overbank flow occurs at all points along a channel, particularly for the largest flows. Therefore, overbank areas immediately adjacent to channels are proximal deposits, not older deposits or the distal deposits of overspill from outer channel bend apices (as implied by figure 23 of Lien et al., 2003) (e.g. Hesse and Dalton, 1995; Peakall et al., 2000a; Kane et al., 2007, 2008, 2010; Crane and Lowe, 2008); (3) the deposits in channel

overbank areas typically fine-upwards (e.g., Hiscott et al., 1997; Piper and Deptuck, 1997; Beaubouef, 2004; Kane et al., 2007) and would also be expected to typically show decreasing erosional features with time as flow confinement increases. In fact, levees typically show only minimal erosional features (e.g., Kane et al. 2007); (4) true levee sequences do not show thickening-upwards cyclicity, but are instead marked by complex patterns with both thinning-up and thickening-upwards packages (e.g., Mutti and Normark, 1987; Kane et al., 2007); (5) similarly repeated thickening-upwards cycles are not observed in other spillover lobes (e.g., Dutton et al., 2003); (6) trunk channels, rather than the distributary channels envisaged herein, are typically long-lived conduits with low avulsion rates (e.g., Weimer, 1991; Pirmez and Flood, 1995; Savoye et al., 2009); (7) given the high proportion of lobes in this environment (56%; Pyles 2007) and high avulsion rates, channels should be more abundant and show higher degrees of inter-connectivity (e.g., Mackey and Bridge, 1995; Leeder et al., 1996; Larue and Hovadik, 2006); (8) The model of Lien et al. (2003) is, in part, predicated on the idea that the thin (~2 m thick) thickening-upwards packages seen in the Ross Sandstone are interpreted as lobe fringe deposits (when compared to typical 3-15 m thickening-upwards lobe deposits; Mutti and Normark, 1987), but this is not commensurate with observations of significant erosion.

Existing lobe models

The present paper shows how erosional features develop on two types of widespread erosional surface and that erosion is distributed in a systematic manner within the stratigraphic architecture of these sediments. The bed-scale analysis used herein reveals the erosive and depositional processes involved in building the fundamental element of the depositional system: the lobe element (Prélat et al., 2009), and is in agreement with the history of depositional lobes outlined by Pyles and Jennette (2009), based in large part on Pyles (2004), with observations from Pyles (2007, 2008) that focuses on much larger, inaccessible, cliff-sections that are laterally-extensive and continuous.

Progradation relative to aggradation in lobes

The relative importance of aggradation versus progradation in deep-sea lobes has been controversial (e.g., Mutti, 1974; Ricci-Lucchi, 1975, 1984; Hiscott, 1981; Chen and Hiscott, 1999). Whilst it is clear that aggradation is a rapid process in deep-sea lobes as accommodation space is always available, there is less clarity on the degree of progradation, if any, that may occur. Progradation was considered to be prevalent in deep-sea lobes from early field studies (e.g., Mutti, 1974; Ricci-Lucchi, 1975, 1984), yet the thickening-up cyclical packages used in support of this argument were challenged (see below), leading to a view that there was only limited progradation in deep-sea lobes (Chen and Hiscott, 1999). In particular, evidence for progradation from outcrop studies, other than from putative asymmetric cyclical packages, is lacking. The integrated model of lobe-element evolution postulated herein addresses this limitation, combining a number of key lines of evidence: i) progressive increases in the periodicity of erosion, ii) the associated increasing magnitude of this erosion over time, iii) increasing flow confinement over time, and iv) clearly-defined,

repetitive, thickening-upwards packages. Such evidence indicates that over time at-a-point flow velocities increased, in part driven by increasing confinement. The proposed model can be explained through purely autocyclic behaviour, where a lobe develops and the distributary channel progressively progrades over the lobe. As the lobe-element aggrades, and the lateral gradients consequently increase, then avulsion becomes progressively more likely (cf. Mackey and Bridge, 1995; Jones and Schumm, 1999; Peakall et al. 2000b; Parsons et al., 2002). Once avulsion takes place, there is a relatively rapid decrease in the energy of flows received at the original location, and a new lobe-element is initiated elsewhere. Repetition of this autocyclical sequence results in repeated thickening-upwards packages.

An alternative explanation is that the cyclical increases in erosion frequency, erosion magnitude, bed thickness and flow confinement are the result of progressive and repeated changes in externally-controlled flow magnitude. In this scenario, lobe progradation is not required, and lobe aggradation could be more dominant; yet, even here, a degree of progradation would be expected given that flow sizes would be increasing. There are, however, two main weaknesses of such an explanation. Firstly, it is unclear what external factor(s) might lead to such repeatable changes in external conditions. The timescales of formation for lobe-elements are very rapid, whilst avulsion frequency of lobe-elements in the Ross Sandstone is unknown, modern systems have avulsion frequencies for lobe-elements of <5 kyr for smaller systems (Deptuck et al., 2008) such as the Ross, and even higher frequencies (0.6-1.5 kyr) in larger systems such as the Amazon and Zaire Fans (Dennielou et al., 2003; Jegou et al., 2008). These rates are orders of magnitude faster than Milankovitch sequences but may scale to the types of millenial-scale fluctuations identified in Pleistocene records such as Isotope Stage 3 (e.g., Cutler et al., 2003; Siddall et al., 2008) and linked to channel avulsion in the Amazon channel (Maslin et al., 2006). It is unknown whether such high frequency fluctuations were present in the Namurian (Haq and Schutter, 2008), but even if these are assumed, then it is questionable whether most millenial fluctuations are sufficiently high-frequency and repeatable, with the possible exception of Dansgaard-Oeschger events (e.g., Schulz, 2002; Siddall et al., 2008). Secondly, recent experimental work has shown that submarine channels act to regulate the size of flows that travel through them (Keevil et al., 2008; Straub et al., 2008; Amos et al., 2010), thus in large part eliminating the influence of any external forcing, even if present. The rationale behind these experiments is relatively simple; consider the case of a larger than average flow in a channel with any significant sinuosity such as those identified in the Ross (e.g., Elliott, 2000a; Sullivan et al., 2000; Lien et al., 2003). As this larger flow approaches the first bend, enhanced overspill occurs due to centrifugal forces; the process is repeated at each subsequent bend until the flow has been regulated to a similar size that is able to traverse the main channel with only limited progressive overbank loss of material.

In summary, the autocyclic model proposed herein honours the field-data and provides a set of coherent process explanations for the formation of these packages. The alternative explanation of repeated and progressive external forcing of flows appears improbable, as it lacks compelling underlying forcing mechanisms. Furthermore, even if such external drivers were present, then autocyclic behaviour operating within the trunk channels would act to reduce the impact of these variations at the point of lobe-element deposition. The underlying processes have

implications for the relative amounts of progradation to aggradation observed; the proposed lobe-element dynamics model, in contrast to the ideas on external forcing, demonstrates an important component of progradation at the lobe-element scale.

A mechanism for thickening-up distributions

The presence and origin of thickening-up sequences in deep-sea lobes has been debated. A number of workers have suggested that thickening-up distributions do not generally occur in lobes and have demonstrated that some early interpretations were incorrect (Hiscott, 1981; Anderton, 1995; Chen and Hiscott, 1999). However, thickening-up packages continue to be recognised within lobe sequences, and have been attributed either to lobe progradation or to subtle lateral migration producing compensation cycles (e.g., Mutti, 1974; Mutti and Sonnino, 1981, Pickering et al., 1989; Lien et al., 2003; Pyles, 2007). Given that progradation in lobes has previously been considered to be limited (Chen and Hiscott, 1999), then the compensation-cycle model has been prevalent, relating sequences to lateral changes (Mutti and Sonnino, 1981; Mutti, 1984; Pickering et al., 1989). Given the widespread application of compensation cycles, it is perhaps instructive to revisit the basis of the compensation cycle model. A progressive shift in a single direction will make for a localised thickening-up sequence (e.g., Hiscott, 1981). However, to examine full compensational cycles, the original block model of Mutti and Sonnino (1981) is used herein (Fig. 6A), and shows that only some areas exhibit thickening-up sequences, whilst others predict thinning-up or more complex sequences. Consequently, a succession consisting only of thickening-up cycles is very unlikely to form from compensation cycles (e.g. Chen and Hiscott, 1999).

The model presented herein provides a mechanism for generating thickening-up sequences at all points laterally across a section (Fig. 6B), with the exception being low-relief distributary channels that would typically show local fining-up, and possibly thinning-up sequences. However, these channels are volumetrically of limited importance. The thickening-up sequences occur as a consequence both of larger flows at-a-point over time, due to progradation and enhanced flow confinement, and critically to consequent increased bed erosion and amalgamation. The presence of erosion is key since it will act to partly offset any natural variability in initial flow volumes, because the thickening-upwards trend is not purely a bed-by-bed variation but instead is largely envisaged to be a function of the extent of progressive bed amalgamation. Importantly, the degree of progradation relative to aggradation that is required to achieve such thickening-up sequences is greatly reduced when the dominant control is not the individual flow size and associated bed thickness, but instead a relatively subtle shift from preservation of mud interbeds to progressive erosion of these mud caps.

Support for such a progradational and aggradational model for submarine lobes is provided by both high-resolution seismic studies of modern lobes, and outcrop examples with excellent three-dimensional control. Some small-scale modern fans have been observed to undergo significant progradation whilst undergoing aggradation (e.g., Gervais et al., 2006; Hanquiez et al., 2009), and bed-correlations in the Permian Karoo Basin demonstrate progradation of submarine lobes in this basin (Hodgson et al., 2006; Prélat et al., 2009). Although aggradation is

dominant in these examples, progradation still occurs, with consequent implications for the preserved sedimentary characteristics as demonstrated in the present model.

The model presented herein thus demonstrates how thickening-up sequences may form in prograding lobes with periodic erosive flows. However, it is not proposed that all lobes will display such trends, as originally postulated by early outcrop studies. Lobes that exhibit more limited erosion are less likely to display thickening-up sequences. Equally, lobes that display more limited progradation and commensurately greater relative aggradation (e.g., Deptuck et al., 2008) and / or lateral migration, will be less likely to exhibit thickening-up packages. The ultimate controls on the degree of progradation, aggradation, and lateral migration remain to be explored.

Conclusions

Repeated thickening-upwards sequences within the Ross Sandstone are shown to exhibit progressive increases in erosional periodicity, bed amalgamation, and scour, culminating in broad erosional surfaces and an abrupt return to mud-deposition. A model of lobe-element dynamics is proposed that integrates these observations. Lobe-element progradation in association with aggradation leads to a progressive increase, at any given point in the system, in the local magnitude of flows, resulting in increased erosion and sediment bypass, and ultimately the development of broad erosive surfaces associated with low-relief distributary channels. Avulsion and lobe-element switching, most likely as a result of increased lateral gradients, subsequently lead to rapid abandonment and a return to background sedimentation.

This model of lobe-dynamics has led to a reassessment of previous environmental interpretations, including spillover lobes, and channels with channel wings. These alternative models are shown to be inconsistent with the outcrop observations. Additionally, implications from the model include the rejection of previous arguments (based on these sections) that submarine channel initiation is the product of giant single flows. Instead the previous consensus on channel initiation via numerous erosive events is reasserted.

The model of lobe-element dynamics outlined herein provides a mechanism for thickening-upwards sequences within lobes. Furthermore, our work suggests that the progressive thickening-upwards pattern occurs through a combination of locally larger flows, and increased bed amalgamation. This produces thickening-upwards sequences at all points, with the exception of volumetrically insignificant low-relief channel infills. In contrast, existing models based on the lateral movement of deposits in compensation cycles result in a variety of vertical sequences and are unlikely to result in cyclical thickening-upwards packages. The present dataset thus demonstrates that progradation can, in certain cases, form thickening-upwards sequences, and furthermore that as a result of bed amalgamation the degree of progradation to aggradation does not have to be high.

Heather Macdonald is funded by a NERC Open CASE Studentship (NER/S/A/2006/14147) at The University of Leeds, tied with The Geology and

Geophysics Group, NERC Strategic Research Division, NOCS. We thank Esther Sumner and Rachael Dale for assistance and discussion in the field, Darren Box for useful discussion on the Ross Sandstone, and David Pyles for providing a useful and constructive review of an earlier version of the manuscript. Authors thank reviewers David J.W. Piper and David M. Hodgson and subject editor for Gary Hampson for valuable comments and suggestions, which greatly improved the manuscript.

References

Amos, K.J., Peakall, J., Bradbury, P.W., Roberts, M., Keevil, G. and Gupta, S. 2010. The influence of bend amplitude and planform morphology on flow and sedimentation in submarine channels. *Marine and Petroleum Geology*, **27**, 1431-1447.

Anderton, R. 1995. Sequences, cycles and other nonsense: are submarine fan models any use in reservoir geology. *In:* Hartley, A.J. and Prosser, D.J. (eds), *Characterization of Deep Marine Clastic Systems*. Geological Society Special Publication, **94**, 5-11.

Beaubouef, R.T. 2004. Deep-water leveed–channel complexes of the Cerro Toro Formation, Upper Cretaceous, southern Chile. *AAPG Bulletin*, **88**, 1471–1500.

Bonnel, C., Dennielou, B., Droz, L., Mulder, T. and Berne, S. 2005. Architecture and depositional pattern of the Rhône Neofan and recent gravity activity in the Gulf of Lions (western Mediterranean). *Marine and Petroleum Geology*, **22**, 827-843.

Bourget, J., Zaragosi, S., Mulder, T., Schneider, J.-L., Garlan, T., Van Toer, A., Mas., V. and Ellouz-Zimmermann, N. 2009. Hyperpycnal-fed turbidite lobe architecture and recent sedimentary processes: A case study from the Al Batha turbidite system, Oman margin. *Sedimentary Geology*, in press.

Carr, M., and Gardner, M.H. 2000. Portrait of a Basin-Floor Fan for Sandy Deep-Water Systems, Permian Brushy Canyon Formation. *In:* Bouma, A.H., Stelting, C.E., and Stone, C.G. (eds), *Fine-Grained Turbidite Systems and Submarine Fans*, AAPG Memoir 72/SEPM Special Publication, **68**, 215-232.

Chapin, M.A., Davies, P., Gibson, J.L. and Pettingill, H.S. 1994. Reservoir architecture of turbidite sheet sandstones in laterally extensive outcrops, Ross Formation, Western Ireland. GCSSEPM Foundation 15th Annual Research Conference, Submarine Fans and Turbidite Systems, 53-68.

Chen, C. and Hiscott, R.N. 1999. Statistical analysis of turbidite cycles in submarine fan successions: tests for short-term persistence. *Journal of Sedimentary Research*, **69**, 486-504.

Clark, J.D. and Pickering, K.T. 1996. Submarine Channels: Process and Architecture. London, Vallis Press, 231.

Collinson, J.D., Martinsen, O., Bakken, B. and Kloster, A. 1991. Early fill of the Western Irish Namurian Basin: a complex relationship between turbidites and deltas. *Basin Research*, **3**, 223-242.

Crane, W.H. and Lowe, D.R. 2008. Architecture and evolution of the Paine channel complex, Cerro Toro Formation (Upper Cretaceous), Silla Syncline, Magallanes Basin, Chile. *Sedimentology*, **55**, 979–1009.

Cutler, K.B., Edwards, R.L., Taylor, F.W., Cheng, H., Adkins, J., Gallup, C.D., Cutler, P.M., Burr, G.S. and Bloom, A.L. 2003. Rapid sea-level fall and deep ocean temperature change since the last interglacial period. *Earth and Planetary Science Letters*, **206**, 253-271.

Dennielou, B., Jouanneau, J.-M., Marsset, T. and Savoye, B., 2003. Vitesses d'accumulation des sédiments, fréquence des dépôts, âge et durée de vie des corps sédimentaires sur l'éventail turbiditique profond du Zaire. 9ème Congrès des Sédimentologues Français, Bordeaux, 162–163.

Deptuck, M.E., Piper, D.J.W., Savoye, B. and Gervais, A. 2008. Dimensions and architecture of late Pleistocene submarine lobes off the northern margin of East Corsica: *Sedimentology*, **55**, 869-898.

Dutton, S.P., Flanders, W.A. and Barton, M.D. 2003. Reservoir characterization of a Permian deep-water sandstone, East Ford field, Delaware basin, Texas. *AAPG Bulletin*, **87**, 609–627.

Elliott, T. 2000a. Depositional architecture of a sand-rich, channelised turbidite system: the Upper Carboniferous Ross sandstone formation, Western Ireland. *In:* Weimer, P., Slatt, R.M., Coleman, J., Rosen, N.C., Nelson, H., Bouma, A.H., Styzen, M.J. and Lawrence, D.T. (eds) *Deep-water reservoirs of the World*, GCSSEPM Foundation 20th Annual Research Conference, 342-364.

Elliott, T. 2000b. Megaflute erosion surfaces and the initiation of turbidite channels. *Geology*, **28**, 119-122.

Fildani, A., Normark, W.R., Kostic, S. and Parker, G. 2006. Channel formation by flow stripping: large-scale scour features along the Monterey East Channel and their relation to sediment waves. *Sedimentology*, **53**, 1265-1287.

Gervais, A., Savoye, B., Mulder, T. and Gonthier, E. 2006. Sandy modern turbidite lobes: a new insight from high resolution seismic data. *Marine and Petroleum Geology*, **23**, 485–502.

Ghibaudo, G. 1980. Deep-sea fan deposits in the Macigno Formation (Middle-Upper Oligocene) of the Gordana Valley, Northern Apennines, Italy. *Journal of Sedimentary Petrology*, **50**, 723-742.

Groenenberg, R.M., Hodgson, D.M., Prélat, A., Luthi, S.M. and Flint, S.S. 2010. Flow-deposit interaction in submarine lobes: insights from outcrop observations and realizations of a process-based numerical model. *Journal of Sedimentary Research*, **80**, 252-267.

Hampson, G. J., Elliott, T. and S. J. Davies. 1997. The application of sequence stratigraphy to Upper Carboniferous fluvio-deltaic strata of the onshore UK and Ireland: Implications for the southern North Sea. *Journal of the Geological Society, London*, **154**, 719–733.

Hanquiez, V., Mulder, T., Toucanne, S., Lecroart, P., Bonnel, C., Marchès, E. and Gonthier, E. 2009. The sandy channel–lobe depositional systems in the Gulf of Cadiz: Gravity processes forced by contour current processes. *Sedimentary Geology*, in press.

Haq, B.U. and Schutter, S.R. 2008. A chronology of Paleozoic sea-level changes. *Science*, **322**, 64-68.

Hesse, R. and Dalton, E. 1995. Turbidite channel/overbank deposition in a Lower Devonian orogenic shelf basin, Fortin Group of Gaspe/Peninsula, Northern Appalachians, Canada. *Journal of Sedimentary Research,* **B65**, 44–60.

Hiscott, R.N. 1980. Depositional framework of sandy mid-fan complexes of Tourelle Formation, Ordovician, Quebec. *AAPG Bulletin*, **64**, 1052-1077.

Hiscott, R.N. 1981. Deep-sea fan deposits in the Macigno Formation (Middle-Upper Oligocene) of the Gordana Valley, Northern Apennines, Italy – Discussion. *Journal of Sedimentary Petrology*, **51**, 1015-1033.

Hiscott, R.N., Hall., F.R. and Pirmez, C. 1997. Turbidity-current overspill from the Amazon channel: texture of the silt/sand load, paleoflow from anisotropy of magnetic susceptibility and implications for flow processes. *In:* Flood, R.D., Piper, D.J.W., Klaus, A., and Peterson, L.C. (eds) *Proceedings of the Ocean Drilling Program, Scientific Results*, **155**, 53–78. Ocean Drilling Program, College Station, TX.

Hodgson, D.M., Flint, S.S., Hodgetts, D., Drinkwater, N.J., Johannessen, E.P. and Luthi, S. 2006. Stratigraphic evolution of fine-grained submarine fan systems, Tanqua depocentre, Karoo Basin, South Africa. *Journal of Sedimentary Research*, **76**, 20–40.

Hodson, F. 1954a. The beds above the Carboniferous Limestone in northwest County Clare, Eire. *Quarterly Journal of the Geological Society, London*, **109**, 259–283.

Hodson, F. 1954b. The Carboniferous rocks of Foynes Island, Co. Limerick. Geological Magazine, **91**, 153–160.

Hodson, F. and Lewarne, G.C. 1961. A mid-Carboniferous Namurian basin in parts of the counties of Limerick and Clare, Ireland. *Quarterly Journal of the Geological Society, London*, **117**, 307–333.

Imran, J., Parker, G., and Katopodes, N. 1998. A numerical model of channel inception on submarine fans. *Journal of Geophysical Research*, **103**, 1219-1238.

Jegou, I., Savoye, B., Pirmez, C. and Droz, L. 2008. Channel-mouth lobe complex of the recent Amazon Fan: The missing piece. *Marine Geology*, **252**: 62-77.

Johnson, S.D., Flint, S.S., Hinds, D. and Wickens, H.d.V. 2001. Anatomy of basin floor to slope turbidite systems, Tanqua Karoo, South Africa: sedimentology, sequence stratigraphy and implications for subsurface prediction. *Sedimentology*, **48**, 987–1023.

Jones, L.S. & Schumm, S.A. 1999. Causes of avulsion: an overview. *In:* Smith, N.D. & Rogers, J. (eds) *Fluvial Sedimentology VI*, *IAS Special Publication*, **28**, 171–178.

Kane, I.A., Kneller, B.C., Dykstra, M., Kassem, A. and McCaffrey W.D. 2007. Anatomy of a submarine channel-levee: an example from Upper Cretaceous slope sediments, Rosario Formation, Baja California, Mexico. *Marine and Petroleum Geology*, **24**, 540-563.

Kane, I.A., McCaffrey, W.D. and Peakall, J. 2008. Controls on sinuosity evolution within submarine channels. *Geology*, **36**, 287–290.

Kane, I.A., Dykstra, M.L., Kneller, B.C., Tremblay, S. and McCaffrey W.D. 2009. Architecture of a coarse-grained channel-levee system: the Rosario Formation, Baja California, Mexico. *Sedimentology*, **56**, 2207-2234.

Kane, I.A., McCaffrey, W.D. and Peakall, J. 2010. On the origin of paleocurrent complexity within deep marine channel levees. *Journal of Sedimentary Research*, **80**, 54-66.

Keevil, G.M., McCaffrey, W.D. and Peakall, J. 2008. Flow evolution in submarine channel bends: experimental insights into flow tuning. AAPG Convention, San Antonio, Texas.

Larue, D.K. and Hovadik, J. 2006. Connectivity of channelised reservoirs: a modelling approach. *Petroleum Geoscience*, **12**, 291-308.

Leeder, M.R. 1999. Sedimentology and sedimentary basins: from turbulence to tectonics. London, Blackwell Science, p. 199.

Leeder, M.R., Mack, G.H., Peakall, J. and Salyards, S.L. 1996. First quantitative test of alluvial stratigraphic models: Southern Rio Grande rift, New Mexico. *Geology*, **24**, 87–90.

Lien T., Walker, R.G. and Martinsen, O.J. 2003. Turbidites in the Upper Carboniferous Ross Formation, western Ireland: reconstruction of a channel and spillover system. *Sedimentology*, **50**, 113-148.

Mackey, S.D. and Bridge, J.S. 1995. Three-dimensional model of alluvial stratigraphy: theory and application. *Journal of Sedimentary Research*, **B65**, 7–31.

Martinsen, O. J., T. Lien, and R. G. Walker. 2000. Upper Carboniferous deep water sediments, western Ireland: Analogs for passive-margin turbidite plays. *In:* Weimer, P. Slatt, R.M., Coleman, J., Rosen, N. C., Nelson, H., Bouma, A.H., Styzen, M.J. and Lawrence D.T. (eds) *Deep-water reservoirs of the world*: GCSSEPM Foundation 20th Annual Research Conference, 533–555.

Martinsen, O.J. and Collinson, J.D. 2002. The Western Irish Namurian Basin reassessed – a discussion. *Basin Research*, **14**, 523-542.

Martinsen, O.J., Lien, T., Walker, R.G. and Collinson, J.D. 2003. Facies and sequential organisation of a mudstone-dominated slope and basin floor succession: the Gull Island Formation, Shannon Basin, Western Ireland. *Marine and Petroleum Geology*, **20**, 789-807.

Maslin, M., Knutz, P.C. and Ramsay, T. 2006. Millenial-scale sea-level control on avulsion events on the Amazon Fan. *Quaternary Science Reviews*, **25**, 3338-3345.

Masson, D.G., Kenyon, N.H., Gardner, J.V. and Field, M.E. 1995. Monterey Fan: channel and overbank morphology. *In:* Pickering, K.T., Hiscott, R.N., Kenyon, N.H., Ricci Lucchi, F., and Smith, R.D.A. (eds) *Atlas of Deep Water Environments: Architectural style in turbidite systems*, Chapman & Hall, London, 47-79.

Mutti, E. 1974. Examples of ancient deep-sea fan deposits from circum-Mediterranean geosynclines. SEPM Special Publication, **19**, 92-105.

Mutti, E. 1984. The Hecho Eocene Submarine Fan system, south-central Pyrenees, Spain. *Geo-marine Letters*, **3**, 199-202.

Mutti, E. 1992. Turbidite sandstones. AGIP-Istituto di Geologia, Universita` di Parma; San Donato Milanese, p. 275.

Mutti, E. and Normark, W.R. 1987. Comparing examples of modern and ancient turbidite systems: problems and concepts. *In:* Legget, J.K. and Zuffa, G.G. (eds) *Marine Clastic Sedimentology: Concepts and Case Studies*, Graham and Troutman, London, 1–38.

Mutti, E. and Normark, W.R. 1991. An integrated approach to the study of turbidite systems. *In:* Weimer, P. and Link, M.H (eds) *Seismic Facies and Sedimentary Processes of Submarine Fans and Turbidite Systems*, Springer-Verlag, New York, 75-106.

Mutti, E. and Sonnino, M. 1981. Compensation cycles: a diagnostic feature of turbidite sandstone lobes. IAS 2nd Eur. Meet., Bologna, Italy, 120–123.

Nelson, C.H., Twichell, D.C., Schwab, W.C., Lee, H.J., Kenyon, N.H. 1992. Upper Pleistocene turbidite sand beds and chaotic silt beds in the channelized, distal, outer-fan lobes of the Mississippi fan. *Geology,* **20**, 693–696.

Normark, W.R. 1970. Growth pattern of deep-sea fans. *AAPG Bulletin*, **54**, 2170-2195.

Normark, W.R., Piper, D.J.W. and Hess, G.R. 1979. Distributary channels, sand lobes, and mesotopography of Navy submarine fan, California borderland, with applications to ancient submarine fan sediments. *Sedimentology,* **26**, 749-774.

Parsons, J.D., Schweller, W.J., Stelting, C.W., Southard, J.B., Lyons, W.J. and Grotzinger, J.P., 2002. A preliminary experimental study of turbidite fan deposits. *Journal of Sedimentary Research*, **72**, 619–628.

Peakall, J., McCaffrey, W.D., Kneller, B.C. 2000a. A process model for the evolution, morphology and architecture of sinuous submarine channels. *Journal of Sedimentary Research,* **70**, 434–448.

Peakall, J., Leeder, M.R., Best, J. and Ashworth, P. 2000b. River response to lateral tilting: a synthesis and some implications for the modelling of alluvial architecture in extensional basins. *Basin Research*, **12**, 413–424.

Pickering, K.T., Hiscott, R.N. and Hein, F.J. 1989. Deep Marine Environments: Clastic Sedimentation and Tectonics. Unwin Hyman, London, p. 416.

Piper, D.J.W. and Deptuck, M. 1997, Fine-grained turbidites of the Amazon Fan: facies characterization and interpretation. *In:* Flood, R.D., Piper, D.J.W., Klaus, A., and Peterson, L.C. (eds) *Proceedings of the Ocean Drilling Program, Scientific Results*, **155**, 79–108. Ocean Drilling Program, College Station, TX.

Piper, D.J.W. and Normark, W.R. 2001. Sandy fans; from Amazon to Hueneme and beyond. *AAPG Bulletin*, **85**, 1407–1438.

Piper, D.J.W., Hiscott, R.N. and Normark, W.R. 1999. Outcrop-scale acoustic facies analysis and latest quaternary development of Hueneme and Dume submarine fans, offshore California. *Sedimentology,* **46**, 47–78.

Pirmez, C. and Flood, R.D. 1995. Morphology and structure of Amazon Channel. *In:* Flood, R.D., Piper, D.J.W., Klaus, A. et al. (eds) *Proceedings of the Ocean Drilling Program, Initial Reports*, **155**, 23-45. Ocean Drilling Program, College Station, TX.

Posamentier, H.W. 2003. A linked shelf-edge delta and slope-channel turbidite system: 3D seismic case study from the eastern Gulf of Mexico. *In:* Roberts, H.H., Rosen, N.C., Fillon, R.H. and Anderson, J.B. (eds) *Shelf-margin deltas and linked down slope petroleum systems: global significance and future exploration strategy*: Proceedings, 23rd GCSSEPM Foundation Bob. F. Perkins Research Conference, 115-134.

Prélat, A., Hodgson, D.M. and Flint, S.S. 2009. Evolution, architecture and hierarchy of distributary deep-water deposits: a high-resolution outcrop investigation from the Permian Karoo Basin, South Africa. *Sedimentology*, **56**, 2132-2154.

Pyles, D.R., 2004. On the stratigraphic evolution of a structurally confined submarine fan, Carboniferous Ross Sandstone, Western Ireland. Unpublished PhD dissertation, University of Colorado at Boulder, 322 pp.

Pyles, D.R., 2007. Architectural Elements in a Ponded Submarine Fan, Carboniferous Ross Sandstone, Western Ireland. *In:* Nilsen, T.H., Shew, R.D., Steffens, G.S. and Studlick, J.R.J. (eds) *Atlas of deep-water outcrops*. AAPG Studies in Geology, **56**, CD-ROM, p. 19.

Pyles, D.R. 2008. Multiscale stratigraphic analysis of a structurally confined submarine fan: Carboniferous Ross Sandstone, Ireland. *AAPG Bulletin*, **92**, 557-587.

Pyles, D.R. and Jennette, D.C. 2009. Geometry and architectural associations of co-genetic debrite–turbidite beds in basin-margin strata, Carboniferous Ross Sandstone (Ireland): Applications to reservoirs located on the margins of structurally confined submarine fans. *Marine and Petroleum Geology*, **26**, 1974-1996.

Remacha, E, and Fernandez, L.P. 2003. High-resolution correlation patterns in the turbidite systems of the Hecho Group (South-Central Pyrenees, Spain). *Marine and Petroleum Geology*, **20**, 711–726.

Ribeiro Machado, L.C., Kowsmann, R.O., de Almeida, W. Jr, Murakami, C.Y., Schreiner, S., Miller, D.J., Orlando, P. and Piauilino, V. 2004. Geometry of the proximal part of the modern turbidite depositional system of the Carapebus Formation, Campos Basin: a model for reservoir heterogeneities. *Boletim de Geociencias da Petrobras*, **12**, 287–315.

Ricci-Lucchi, F. 1975. Depositional cycles in two turbidite formations of northern Apennines (Italy). *Journal of Sedimentary Petrology*, **45**, 3-43.

Ricci-Lucchi, F. 1984. The deep-sea fan deposits of the Miocene Marnoso-Arenacea Formation, northern Apennines. *Geo-marine Letters*, **3**, 203-210.

Ricci-Lucchi, F. and Valmori, E. 1980. Basin-wide turbidites in a Miocene, oversupplied deep-sea plain: a geometrical analysis. *Sedimentology*, **27**, 241-270.

Rider, M.H. 1974. The Namurian of west County Clare. *Proceedings of the Royal Irish Academy*, **74B**, 125-142.

Savoye, B., Babonneau, N., Dennielou, B. and Bez, M. 2009. Geological overview of the Angola-Congo margin, the Congo deep-sea fan and its submarine valleys. *Deep-Sea Research II*, **56**, 2169-2182.

Schulz, M. 2002. On the 1470-year pacing of Dansgaard-Oeschger warm events. *Paleoceanography*, **17**, 1014, doi:10.1029/2000PA000571.

Siddall, M., Rohling, E.J., Thompson, W.G. and Waelbroek, C. 2008. Marine isotope stage 3 sea level fluctuations: data synthesis and new outlook. *Reviews of Geophysics*, **46**, RG4003.

Stow, D.A.V. and Bowen, A.J. 1980. A physical model for the transport and sorting of fine-grained sediment by turbidity currents. *Sedimentology*, **27**, 31–46.

Strachan, L.J. 2002. Slump-initiated and controlled syndepositional sandstone remobilization: an example from the Namurian of County Clare, Ireland. *Sedimentology*, **49**, 25–41.

Straub, K.M., Mohrig, D.C., Buttles, J., McElroy, B., and Pirmez, C. 2008. Interactions between turbidity currents and topography in aggrading sinuous

submarine channels: A laboratory study. *Geological Society of America Bulletin*, **120**, 368-385.

Sullivan, M., Jensen, G., Goulding, F., Jennette, D., Foreman, L. and Stern, D. 2000. Architectural analysis of deep-water outcrops: implications for exploration and development of the Diana Sub-Basin, western Gulf of Mexico. *In:* Weimer, P., Slatt, R.M., Coleman, J., Rosen, N.C., Nelson, H., Bouma, A.H., Styzen, M.J. and Lawrence, D.T. (eds) *Deep-water reservoirs of the World*, GCSSEPM Foundation 20th Annual Research Conference, 1010-1031.

Twichell, D.C., Schwab, W.C., Nelson, C.H., Kenyon, N.H. and Lee, H.J. 1992. Characteristics of a sandy depositional lobe in the outer Mississippi fan from SeaMARCIA sidescan sonar images. *Geology*, **20**, 689–692.

Walker, R.G. and Mutti, E. 1973. Turbidite facies and facies associations. *In:* Middleton, G.V and Bouma A. (eds) *Turbidites and Deep-water Sedimentation*, SEPM Pacific Section Short Course, 119-157.

Weimer, P. 1991. Seismic facies, characteristics and variations in channel evolution, Mississippi Fan (Plio-Pleistocene), Gulf of Mexico. *In:* Weimer, P. and Link, M.H. (eds) *Seismic Facies and Sedimentary Processes of Submarine Fans and Turbidite Systems*. Springer, New York, 323–347.

Wignall, P.B. and Best, J.L. 2000. The Western Irish Namurian Basin reassessed. *Basin Research*, **12**, 59-78.

Wignall, P.B. and Best, J.L. 2002. Reply to: The Western Irish Namurian Basin reassessed - a discussion by O.J. Martinsen & J.D. Collinson. *Basin Research*, **14**, 531-542

Wynn, R.B., Kenyon, N.H., Masson, D.G, Stow, D.A.V. and Weaver, P.E. 2002. Characterisation and recognition of deep-water channel-lobe transition-zones. *AAPG Bulletin*, **86**, 1441-1462.

Wynn, R.B., Cronin, B.T. and Peakall, J. 2007. Sinuous deep-water channels: Genesis, geometry and architecture. *Marine and Petroleum Geology*, **24**, 341–387.

Figure captions

Figure 1. A typical, complete thickening-upward package of the Ross Sandstone at Ross Bay, recording an upward trend of (i) thick mudstone interval, (ii) interbedded sand and mud deposits, (iii) thick, amalgamated sandstone.

Figure 2. Location map showing the study area and overall location of the Carboniferous Shannon Basin, western Ireland (after Pyles, 2007). Inset maps show the location of studied areas, A. Ross Bay, B. Ross Point, and C. Kilbaha Bay. Low water mean (L.W.M.) and high water mean (H.W.M) are marked respectively.

Figure 3. Cross profiles of measured sections from three studied locations. Profiles show sandstone and mudstone deposits, major erosional surfaces, stepped scours and megaflutes. A. Ross Bay (52°35'3.12"N, 9°52'36.52"W);

sedimentary log in south-westernmost part of outcrop is also shown in Figure 4, B. Ross Point (52°35'24.75"N 9°52'42.67"W), C. Kilbaha Bay (approx. 52°34'17.46"N 9°50'50.10"W). Time periods (t1-t6) are marked on the left hand side of each figure and link to the periods identified in Figure 5.

Figure 4. Sedimentary log showing the sedimentology of three thickening-upward packages from the upper Ross Sandstone, Ross Bay. Palaeocurrents measured from ripples show a consistent NE flow direction. Where the palaeocurrent is the average of multiple readings the total number of readings is provided in brackets. Lateral variation within the central coarsening-up packages is depicted in Figure 3A.

Figure 5 A six-stage sedimentary model for erosive bypass within prograding terminal lobe-elements in the Ross Sandstone. The schematic lobe-elements are prograding relative to the fixed-position red dashed line. Cross-sections depict interbedded sandstone (yellow) and mudstone (grey), and illustrate the deposits associated with each stage at the fixed-position red line.

Figure 6 Diagram showing vertical changes in sedimentation of sand (white) and mud (black), whereby packages are defined by lobe-element (LE) surfaces. A. Diagram showing the origin of compensation cycles (CC), and how thickness trends vary across the width of the cycles; upper part after Mutti and Sonnino (1981). Lobe-elements bases are shown schematically as flat based as with the original Mutti and Sonnino (1981) figure, however, the underlying surface will show subtle topographic relief that likely controls the position of the next lobe-element. Under this concept of compensation cycles, each cycle is capped by horizontal muds that accumulate during periods of shutdown. Note that across the diagram, thinning- and thickening-upward trends are observed together with regions of no thickness change. Only (iv) shows exclusively thickening-upward trends. B. Diagram showing the thickening-upward (TU) trends generated by prograding lobe-elements, as presented here. Thickening-upward trends are observed across the lobe-element, and are only interrupted by localised erosion generated by lobe-element bypass surfaces, as in (iii). Average total lobe with is ~1900 m (Pyles, 2007).

Figure 1

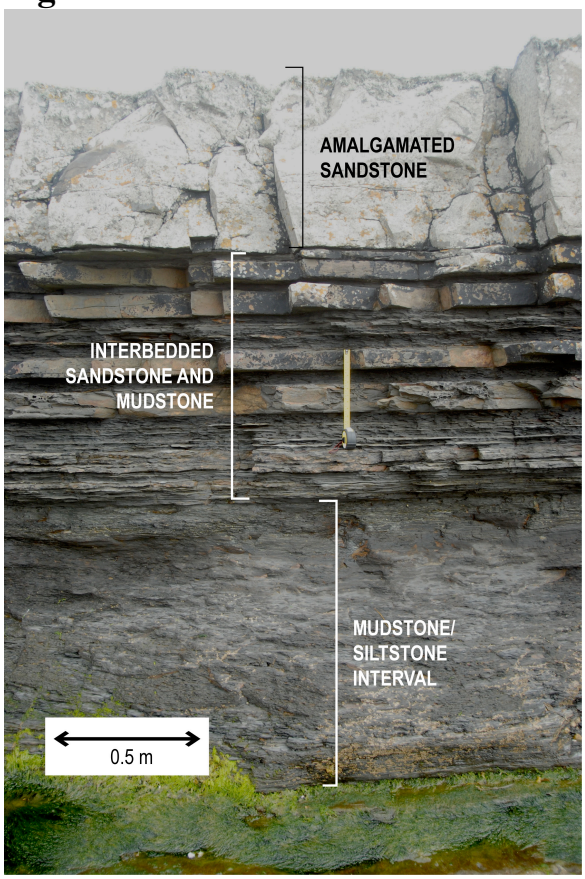

Figure 2

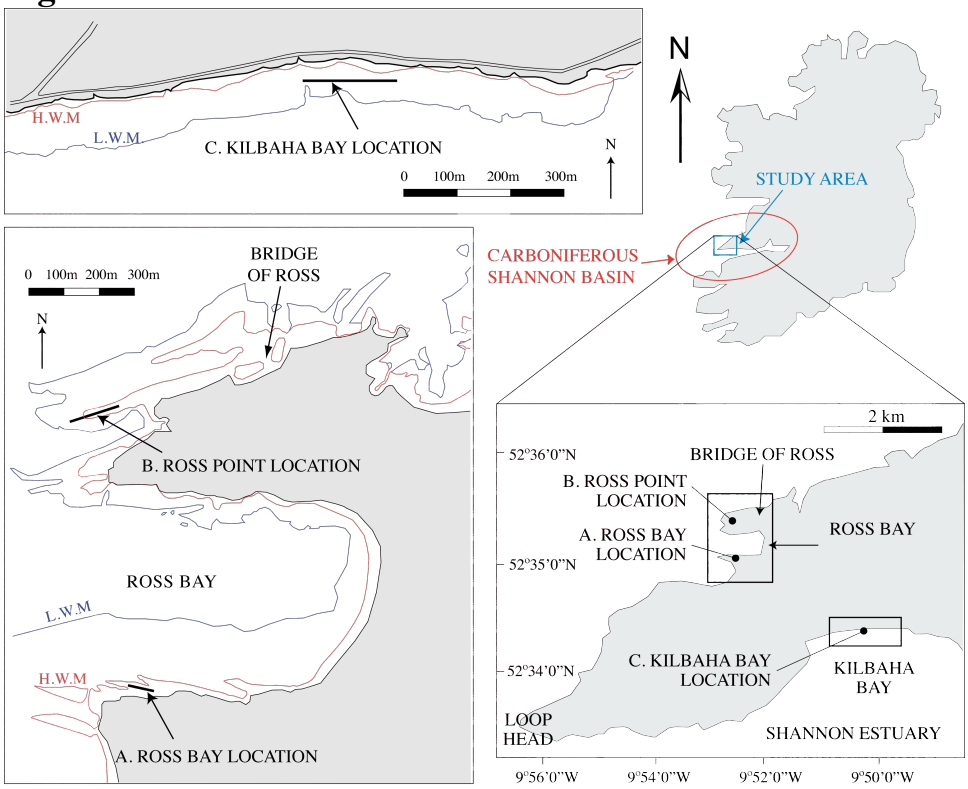

Figure 3

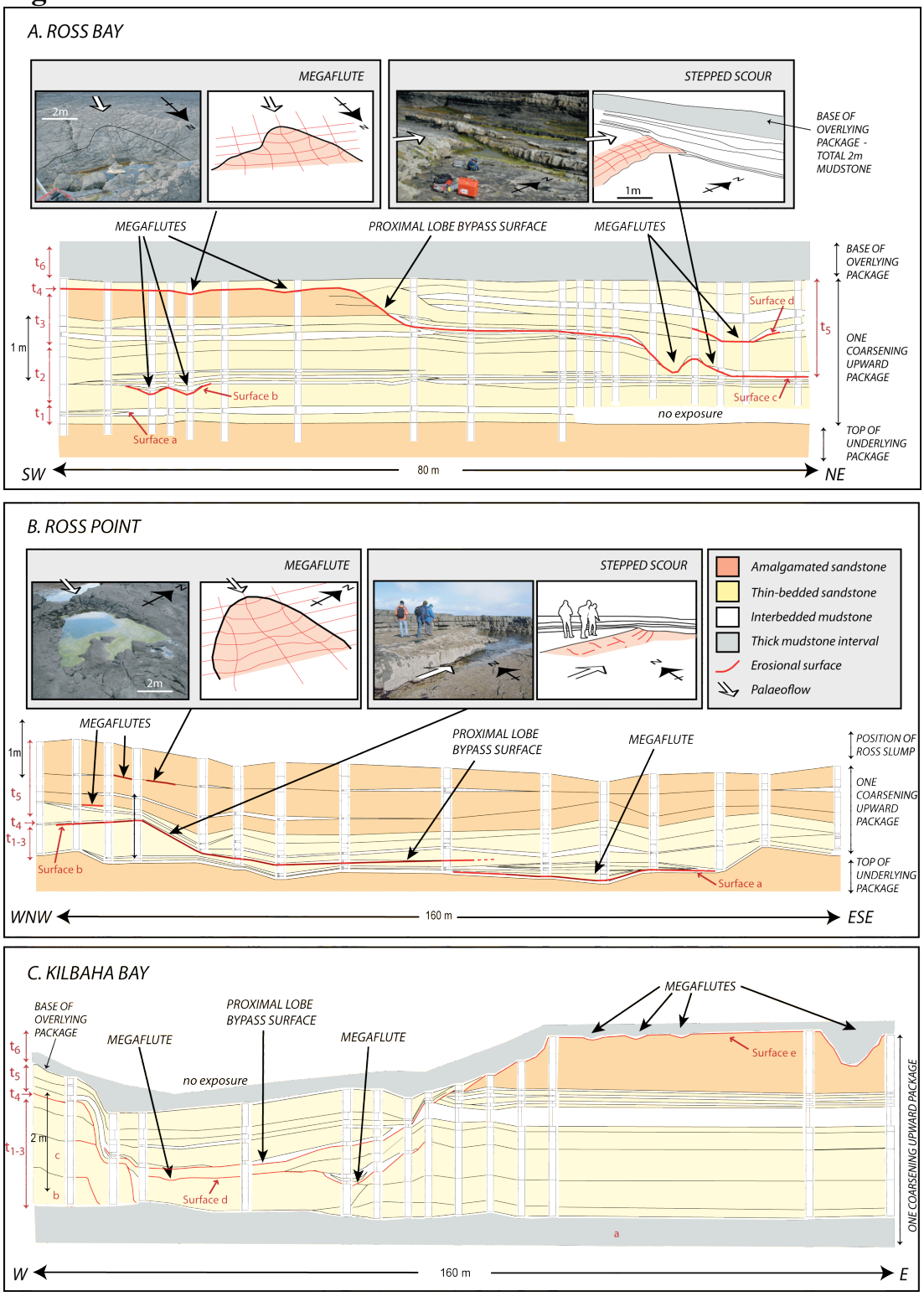
A. ROSS BAY
MEGAFLUTE
STEPPED SCOUR
2m
1m
BASE OF OVERLYING PACKAGE - TOTAL 2m MUDSTONE
MEGAFLUTES
PROXIMAL LOBE BYPASS SURFACE
MEGAFLUTES
t6
t4
t3
t2
t1
1 m
t5
Surface a
Surface b
Surface c
Surface d
no exposure
BASE OF OVERLYING PACKAGE
ONE COARSENING UPWARD PACKAGE
TOP OF UNDERLYING PACKAGE
SW
80 m
NE
B. ROSS POINT
MEGAFLUTE
STEPPED SCOUR
2m
Amalgamated sandstone
Thin-bedded sandstone
Interbedded mudstone
Thick mudstone interval
Erosional surface
Palaeoflow
MEGAFLUTES
PROXIMAL LOBE BYPASS SURFACE
MEGAFLUTE
1m
t5
t4
t1-3
Surface b
Surface a
POSITION OF ROSS SLUMP
ONE COARSENING UPWARD PACKAGE
TOP OF UNDERLYING PACKAGE
WNW
160 m
ESE
C. KILBAHA BAY
BASE OF OVERLYING PACKAGE
MEGAFLUTE
PROXIMAL LOBE BYPASS SURFACE
MEGAFLUTE
MEGAFLUTES
t6
t5
t4
t1-3
2 m
c
b
a
no exposure
Surface d
Surface e
ONE COARSENING UPWARD PACKAGE
W
160 m
E

Figure 4

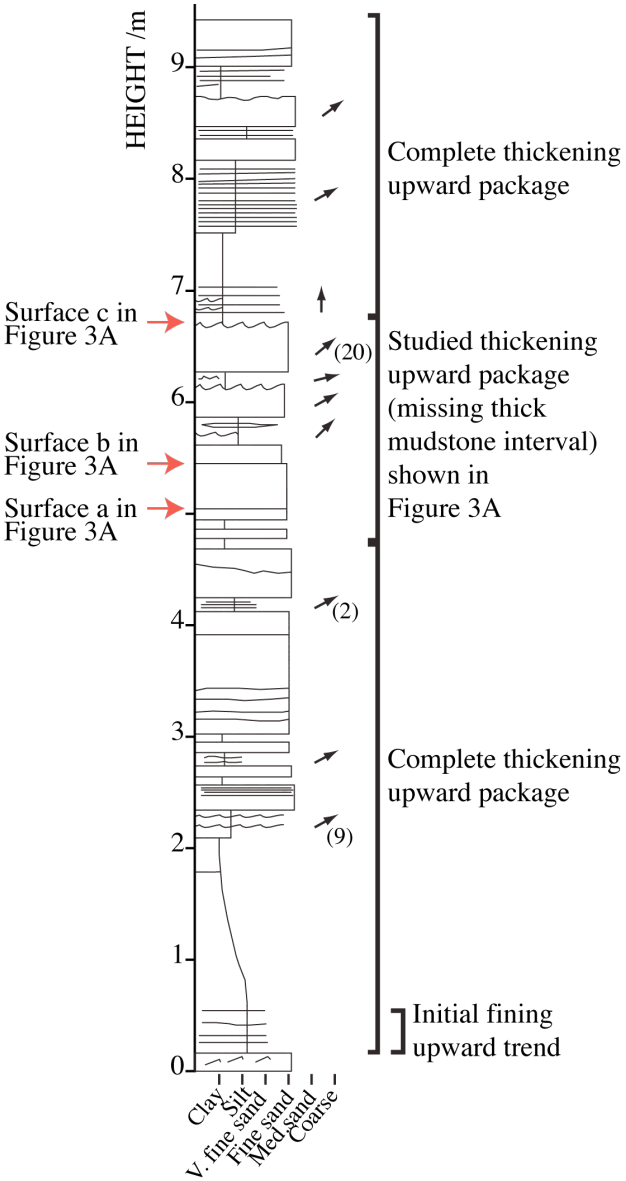
HEIGHT /m
9
8
7
6
4
3
2
1
0
Surface c in Figure 3A
Surface b in Figure 3A
Surface a in Figure 3A
(20)
(2)
(9)
Complete thickening upward package
Studied thickening upward package (missing thick mudstone interval) shown in Figure 3A
Complete thickening upward package
Initial fining upward trend
Clay
Silt
V. fine sand
Fine sand
Med sand
Coarse

Figure 5

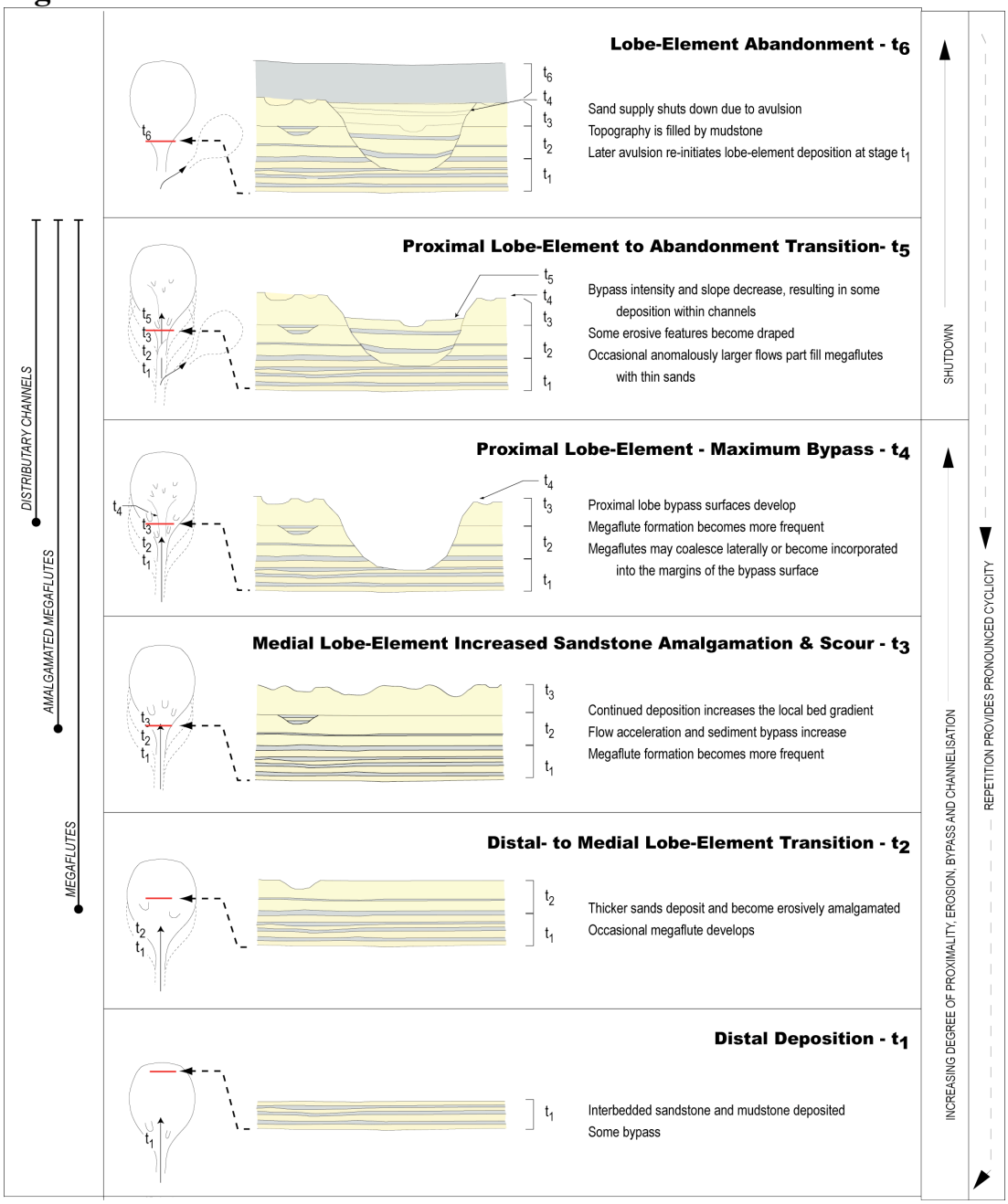
Lobe-Element Abandonment - t6
Sand supply shuts down due to avulsion
Topography is filled by mudstone
Later avulsion re-initiates lobe-element deposition at stage t1
Proximal Lobe-Element to Abandonment Transition- t5
Bypass intensity and slope decrease, resulting in some deposition within channels
Some erosive features become draped
Occasional anomalously larger flows part fill megaflutes with thin sands
Proximal Lobe-Element - Maximum Bypass - t4
Proximal lobe bypass surfaces develop
Megaflute formation becomes more frequent
Megaflutes may coalesce laterally or become incorporated into the margins of the bypass surface
Medial Lobe-Element Increased Sandstone Amalgamation & Scour - t3
Continued deposition increases the local bed gradient
Flow acceleration and sediment bypass increase
Megaflute formation becomes more frequent
Distal- to Medial Lobe-Element Transition - t2
Thicker sands deposit and become erosively amalgamated
Occasional megaflute develops
Distal Deposition - t1
Interbedded sandstone and mudstone deposited
Some bypass
DISTRIBUTARY CHANNELS
AMALGAMATED MEGAFLUTES
MEGAFLUTES
SHUTDOWN
INCREASING DEGREE OF PROXIMALITY, EROSION, BYPASS AND CHANNELISATION
REPETITION PROVIDES PRONOUNCED CYCLICITY

Figure 6

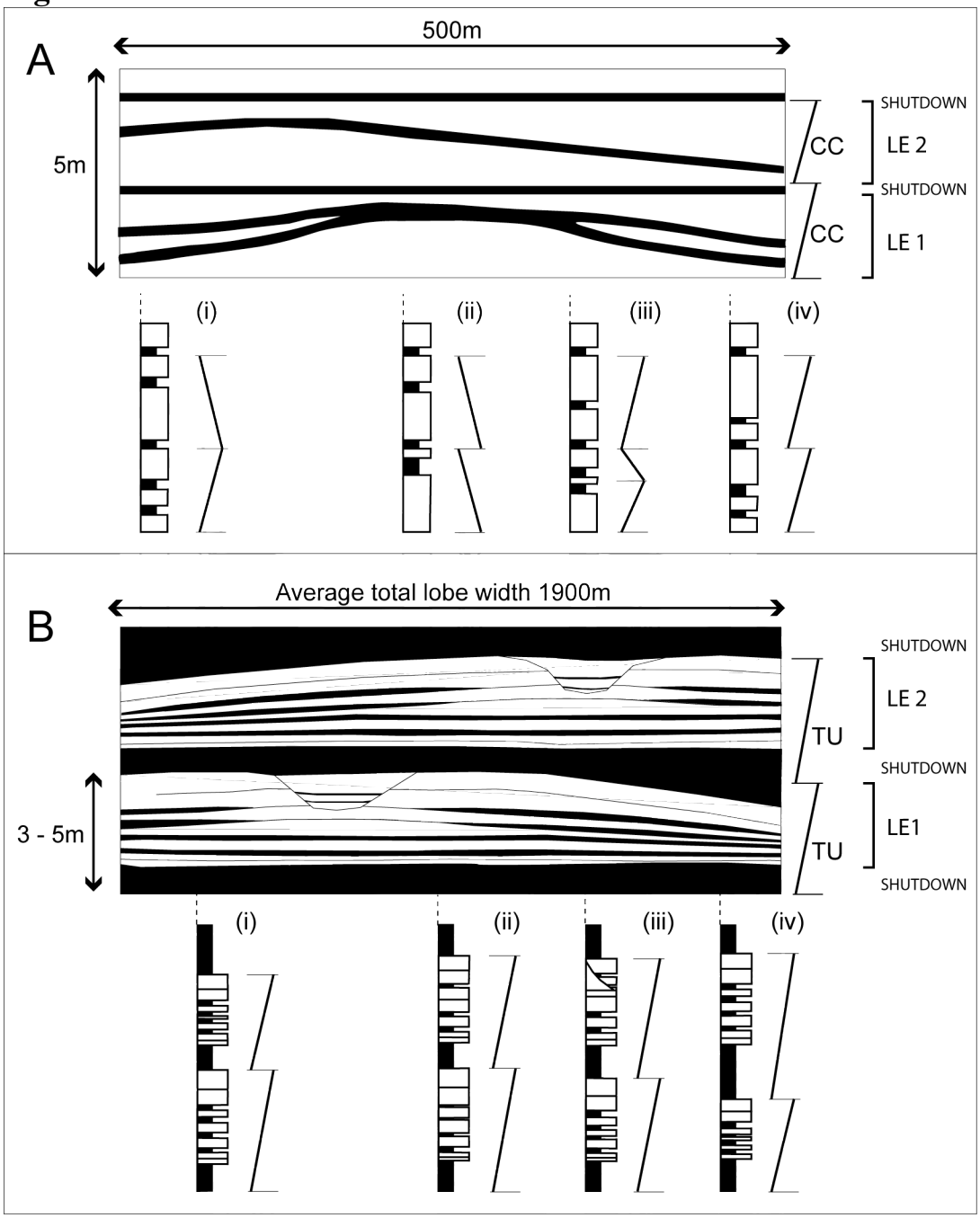
A
500m
5m
CC
CC
SHUTDOWN
LE 2
SHUTDOWN
LE 1
(i)
(ii)
(iii)
(iv)
B
Average total lobe width 1900m
3 - 5m
TU
TU
SHUTDOWN
LE 2
SHUTDOWN
LE1
SHUTDOWN
(i)
(ii)
(iii)
(iv)

Appendix D

Macdonald, H.A. Wynn, R.B., Huvenne, V.A.I., Weaver, P.P.E., McPhail, S.D., Masson, D.G. and Peakall, J. *In review*. High-resolution imaging of deep-water erosional scours along the northeast Atlantic margin: Bridging the gap between modern and ancient turbidite systems.

High-resolution imaging of deep-water erosional scours along the northeast Atlantic margin: Bridging the gap between modern and ancient turbidite systems

Heather A. Macdonald[1*], Russell B. Wynn[2], Veerle A.I. Huvenne[2], Philip P.E. Weaver[2], Stephen D. McPhail[2], Douglas G. Masson[2] and Jeff Peakall[1]

[1]School of Earth and Environment, Leeds University, Leeds, LS2 9JT, UK
[2]National Oceanography Centre, Southampton, European Way, Southampton, SO14 3ZH, UK

Corresponding author email: h.macdonald@see.leeds.ac.uk

ABSTRACT

A series of large-scale erosional scours are described from four modern deep-water canyon/channel systems along the northeast Atlantic continental margin. Regional-scale geophysical data indicate that most scours occur in zones of rapid flow expansion, e.g. channel mouths or overbank areas. High-resolution images of the scours cover ~25 km^2 at 2x2 m pixel size, and were obtained using Autosub6000, an Autonomous Underwater Vehicle equipped with an EM2000 multibeam bathymetry system. Ground-truthing of scour fills and inter-scour areas was achieved using accurately located piston cores that targeted specific sites within imaged areas, while microfossil-based dating provides temporal constraints on scour genesis. Imaged scours range from 40-3170 m wide and 8-48 m deep, effectively 'bridging the gap' between traditional scales of analysis of outcrop and modern systems. These results confirm that deep-water scours can range in size from centimeter- to kilometer-scale. Four distinct morphologies of isolated scour are identified: spoon-shaped, heel-shaped, crescent-shaped and oval-shaped. Isolated scours are shown to coalesce laterally into broad regions of amalgamated scour that may be several kilometers across. Depositional V-shaped chevrons and erosional lineations are imaged in some inter-scour areas. Core data reveal that scour erosion, abandonment and infilling vary temporally and spatially both within and between systems, and occur in response to allocyclic (e.g. changing sediment supply) and autocyclic controls (e.g. canyon thlaweg migration or channel margin failure). Erosional hiatuses within scour fills may represent hundreds of thousands of years of time, and yet leave little visible record. Local scour morphology may generate significant lateral heterogeneity in sediment deposition, even during periods of non-erosion. Scours can also effectively trap thick fluid mud and debris flow deposits that leave little or no record on adjacent seafloor; they may therefore preserve information on local flow events during relatively quiescent periods, e.g. sea-level highstands.

INTRODUCTION TO DEEP-WATER EROSIONAL SCOURS

Large-scale erosional scours are indicative of the passage of highly erosive turbidity currents that are often voluminous and fully bypassing. They are a key component of many deep-water channels and fans, and have been intensively studied in both modern (e.g. Normark, 1970; Normark et al., 1979; Shor et al., 1990; Kenyon et al., 1995; Wynn et al., 2002a; Fildani et al., 2006, Normark et al., 2009) and ancient submarine environments (e.g. Vicente Bravo and Robles, 1995; Elliott, 2000a,b; Lien et al., 2003).

Research on deep-water erosional scours began in the 1970's, pioneered by Bill Normark and colleagues during their studies of Navy Fan offshore California (e.g. Normark et al., 1979). These studies recognised giant flute-shaped depressions over 500 m wide and 15 m deep on the modern seafloor. Around this time, much smaller examples, up to 1.5 m deep, were documented in Upper Cretaceous submarine fan deposits of the Cerro Toro Formation (Magallanes Basin), southern Chile (Winn and Dott, 1979). Even at this embryonic stage of scour research, it was clear that there were major differences in the scale of feature that could be recognized in modern and ancient settings.

Subsequent to these early findings, increasingly detailed deep-towed sidescan sonar and multibeam bathymetry images of the modern seafloor revealed that large-scale erosional scours are in fact a common feature of many deep-water turbidite systems (for a comprehensive listing of examples, see Table 1). These studies have shown that large-scale scours are broadly restricted to margins or termini of submarine canyons and channels. Examples of scours imaged on channel levee backslopes, or between/along active channels, include Navy Fan (Normark et al., 1979), Laurentian Fan (Shor et al., 1990), Stromboli Canyon (Kidd et al., 1998), Monterey Fan (Masson et al., 1995; Klaucke et al., 2004) and Redondo Fan (Normark et al., 2009). Scours in these examples are up to 20 m deep and 400 m long. In some areas, stepped scours adjacent to channel bends are arranged in linear trains that extend for several kilometers, e.g. Monterey Canyon (Fildani and Normark, 2004; Fildani et al., 2006) and Eel Canyon (Lamb et al., 2008). Scours have also been encountered at the transition zone between canyons or channels and depositional fans and basins. Examples include Valencia Channel mouth (Palanques et al., 1995; Morris et al., 1998), Rhône Neofan (Kenyon et al., 1995; Torres et al., 1997; Wynn et al., 2002a; Bonnel et al., 2005), Umnak Channel mouth (Kenyon and Millington, 1995) and Setubal and Agadir Canyon mouths (Wynn et al., 2002a). These occur either as fields of isolated scours (250-1000 m wide, 500-1000 m long and 14-20 m deep) or as broad zones of amalgamated scour up to 3 km wide. In areas where slope canyons encounter a marked slope break at the base-of-slope, submarine plunge pools up to 1.1 km wide and 75m deep can occur, as along the US continental slope (e.g. Lee et al., 2002). Overall, most large-scale scours are indicative of regions of flow expansion (Mutti and Normark, 1987; Normark and Piper, 1991) induced by a lack of confinement or a change in slope. At these locations, turbidity currents may undergo a hydraulic jump, leading to locally increased turbulence and scouring of underlying sediments (Komar, 1971; Normark et al., 1979; Mutti and Normark, 1987; Lee et al., 2002).

Erosional scours documented in outcrop commonly have meter-scale geometries, such as in the Carboniferous Ross Sandstone of western Ireland (Chapin et al., 1994; Elliott 2000a,b; Lien et al., 2003), the Albian Black Flysch of northern Spain (Vicente Bravo and Robles, 1995), the Lower Eocene Charo Canyon mouth of the Spanish Pyrenees (Millington and Clark, 1995) and the Eocene-Oligocene Annot Sandstone in the French Alps (Hilton, 1995; Morris and Normark, 2000). These outcrop-based studies have helped document the nature of scoured substrates and infilling sediments, e.g. the multi-episodic scour-and-fill geometries visible in sandstones of the Albian Black Flysch (Vicente Bravo and Robles, 1995). However, precise paleo-environmental interpretation of scours in outcrop can be challenging,

as exemplified by observations of the well-studied Carboniferous Ross Sandstone. In this system, scours have been interpreted as occurring in a channel-lobe transition zone (Chapin et al., 1994) on channel flanks via single high-magnitude channel-initiating flows (Elliott, 2000a,b), and in spillover lobes at the bends of sinuous channels (Lien et al., 2003).

Some small-scale erosional features, such as flutes and other sole marks, have been recreated under laboratory conditions (Rücklin, 1938; Dzulynski and Walton, 1963; Dzulynski, 1965; Dzulynski and Simpson, 1966; Allen, 1969; 1971; 1984). However, these are typically several orders of magnitude smaller than documented examples on the modern seafloor. Allen (1971) links the generation of small-scale erosional bedforms (i.e. flutes) to the presence of irregularities on the eroded bed, and Allen's (1971) *defect theory* theoretically relates the size, shape and structure of erosional bedforms (i.e. flutes) to the number and character of these irregularities, and the nature of the erosive flow. To test whether Allen's (1971) defect theory can be up-scaled to large-scale modern scours, Shor et al. (1990) applied it to generation of a giant flute-shaped scour on Laurentian Fan (100 m deep and 1000 m long), which is believed to have been generated by the 1929 Grand Banks turbidity current. Shor et al. (1990) performed calculations using both empirical parameters (from Allen, 1971) and measurements taken from the giant scour. However, both calculations produced durations of scour generation that were considered too small to realistically generate the observed scour; it was therefore assumed that the scour became unusually deep because erosion of seafloor surrounding the scour was hindered by a conglomerate veneer. It therefore remains unclear whether flow processes operating on both small- and large-scale scours are comparable, and whether experimental studies of erosion can be up-scaled to natural examples on the modern seafloor.

HIGH-RESOLUTION AUV IMAGING OF DEEP-WATER SCOURS

It is clear that integrating studies of erosional scours in the laboratory, at outcrop, and on the modern seafloor remains a major challenge, largely due to the differing spatio-temporal scales involved (Morris and Normark, 2000). In particular, there is a significant size gap between most erosional scours documented in outcrop (typically several centimeters to a few meters across and less than a meter deep), and those imaged on the modern seafloor (10's to 100's of meters across and several meters deep). However, recent technological advances in deep-water research may see this gap beginning to close. For example, Normark et al. (2009) utilised an Autonomous Underwater Vehicle (AUV) to obtain unprecedented images of deep-water scours on Redondo Fan, offshore California. They obtained high-resolution multibeam bathymetry and sub-bottom profiles at water depths up to 700 m, by flying the AUV at a height of ~70 m above seafloor. Their multibeam bathymetry data have 1.5 m lateral resolution and 0.3 m vertical accuracy, which is approaching outcrop-scale resolution (Normark et al., 2009). This pioneering study was a first step towards addressing the traditional mismatch in scale, but further high-resolution data are now required to assess how scour dimensions and morphology in different deep-water systems are influenced by local factors, e.g. structural controls, substrate type, flow conditions/frequency, and nature and volume of infilling sediments.

Here, we present four examples of large-scale, deep-water scours associated with canyon and channel systems along the northeast Atlantic continental margin. We have attempted to further address the mismatch in data resolution mentioned above by utilising Autosub6000, which is a newly developed AUV capable of operating close to the seafloor at water depths of up to 6000 m (Huvenne et al., 2009). The AUV was instrumented with a high-resolution multibeam bathymetry system, in order to map the planform morphology of deep-water scours in unprecedented detail. These high-resolution images are combined with accurately targeted piston cores, in order to provide information on erosion history and scour fill. The results provide new insights into scour genesis (particularly large-scale amalgamated scours) and highlight the variability in scour morphology and fill in different turbidite systems along a single stretch of continental margin.

STUDY AREA

This study investigates erosional scours in four deep-water canyon/channel systems along the northeast Atlantic continental margin (Figure). These are: 1) Agadir Canyon mouth, 2) Horseshoe Valley, 3) Setúbal Canyon mouth, and 4) Whittard Channel margin. These locations cover several tectono-climatic settings with a variety of shallow- to deep-water sediment transport regimes (Weaver et al., 2000). For example, Agadir Canyon is dominated by infrequent (1 every ~10,000 yrs), large-volume flows (>10 km^3 of sediment), sourced from the Morocco Shelf (Wynn et al., 2002b), whereas Whittard Channel is dominated by frequent (up to 130 per 1000 yrs) smaller flows, mostly during glacial lowstands when fluvio-glacial outwash supplied sediments directly to the head of Whittard Canyon (Toucanne et al., 2008).

METHODS AND DATA

Geophysical data

The majority of geophysical data presented here were collected during a research expedition on RRS *James Cook* in August 2008 (JC27). Data collected using hull-mounted multibeam bathymetry (EM120) and sub-bottom profilers (SBP120 and 3.5kHz) provide information on the overall planform and cross-sectional geometry of the seafloor. However, the main dataset presented here is high-resolution AUV multibeam bathymetry, collected using an EM2000 system housed within the Autosub6000 AUV. Autosub6000 was able to cover an area of ~25 km^2 within a 24-hour mission, and the EM2000 system was able to image seafloor features with a pixel size of 2x2 m. Data were subsequently processed using the IFREMER software suite 'Caraibes'.

Sedimentological data

A series of shallow piston cores were collected from each of the four work areas, with a maximum penetration of 6.5 m. Core sites were chosen once high-resolution multibeam bathymetry images were downloaded and visualised, and were selected to hit targets >50 m across. RRS *James Cook* is equipped with a Dynamic Positioning (DP) system, while any potential offset created by drift of the corer was monitored using an Ultra Short Base Line (USBL) acoustic positioning system located on the

coring wire at depths of up to 2.5 km. Visual core logging included sediment facies, colour and grain size. All logged deposits were ultimately identified as turbidite, debrite or hemipelagite.

Dating control

Microfossil-based dating of hemipelagic sediments in the studied cores was used to identify erosional hiatuses. Ratios of different coccolith species were identified and a combination of first and last appearance and overall abundance of dominant species then used to develop a chrono-stratigraphy that is tied into the oxygen isotope stratigraphy at specific oxygen isotope stages (OIS) (Weaver and Kuijpers, 1983; Weaver, 1994; Wynn et al., 2002b). Bioturbation of hemipelagic sediments and other potential errors mean that ages are accurate to within ~10%.

RESULTS

Agadir Canyon mouth

Agadir Canyon extends northwestwards over 450 km from the Morocco Shelf (100-200 m water depth) to the eastern Agadir Basin (~4500 m water depth) (Figures 1 and 2a). The canyon is up to 30 km wide and acts as a conduit for large-volume siliciclastic flows (Wynn et al., 2002b; Frenz et al., 2009). Previous studies, utilising medium-resolution (30kHz) sidescan sonar, mapped a major zone of erosion in the canyon mouth area, with km-scale scours focused immediately downstream of an intra-canyon slope break (slope change of 0.2° to 0.04°; Wynn et al., 2002a). Both isolated and amalgamated scours were imaged in the erosion zone (see inset in Figure 2a), but the relationship between the two end members was not clearly resolvable on existing data.

Our new high-resolution imagery (Figure 2b) confirms the presence of both isolated and amalgamated scours, covering an area of ~15 km^2 in the canyon mouth. The deepest erosion is focused within isolated scours along the northern margin of the broad, flat canyon axis; these scours cut into the gently sloping margin of the canyon floor. Isolated scours are spoon-shaped and elongated downslope, with U-shaped cross-sectional profiles that shallow and taper downstream. Maximum scour depths and sidewall slope angles are consistently within the upstream 60% of the scours; the steepest slope angles (20°-50°) are largely confined to scour headwalls and sidewalls (see profiles A-A' and B-B', Figure 2b). Scour dimensions vary between 150-600 m long, 40-225 m wide and 8-20 m deep. Scours 1 and 2 (Figure 2b) are the largest identified isolated scours. Scour 2 exhibits a rim opening and low sidewall slopes (0.5°-6.5°) along its southwest margin, where it borders a region of amalgamated scour. This amalgamated scour displays a broadly flat-bottomed morphology, but includes several erosional remnants within the scour floor and in cuspate rims at scour margins (see cross section C-C', Figure 2b). The imaged area of amalgamated scour extends across >4 km^2 and can be subdivided into smaller zones of amalgamation that are bound by high-standing topography. The headwall of the amalgamated scour comprises a series of cuspate scars, similar in apparent dimensions and morphology to the headwalls of adjacent isolated scours.

Three piston cores were obtained from within the imaged region along a SSW-NNE transect: JC27-09, JC27-12 and JC27-11 (Figures 2b and 3). Core JC27-09 targeted

the floor of the amalgamated scour, and recovered ~4.0 m of sediment including a total of 13 turbidites. The youngest turbidites comprise thin (<5 cm), normally graded, very fine-grained and well-sorted basal sands, with thin planar and cross-laminations (*Tc* and *Td*; Bouma, 1962). Overlying mud caps are up to 65 cm thick, and intervening hemipelagites are present between each turbidite (dated at OIS 1-3; <60 ka). In contrast, older deposits (below 1.8 m core depth and dated at OIS 4-5; 60-130 ka) display 5-10 cm thick, normally graded, medium-grained, planar and cross-laminated basal sands (*Tc* and *Td*), with erosive bases and rip-up clasts; these sands are overlain by comparable thicknesses of turbidite mud. A thin clast-rich muddy debrite overlies an apparent erosional hiatus at 3.4 m that likely occurred around the OIS 5/6 boundary at ~130 ka (Figure 3). Immediately beneath this hiatus are the oldest hemipelagic sediments sampled in the core, which contain *P. lacunosa* and are therefore older than OIS 13 or ~450 ka (Weaver and Kuijpers, 1983; Weaver, 1994). The hiatus therefore corresponds to at least 320 kyrs of erosion and probably represents several meters of missing sediment.

Core JC27-12 targeted the floor of the deepest isolated scour, and recovered 1.0 m of sediment including five turbidites (Figure 3). These turbidites typically display thin (<5 cm), fine- to medium-grained, planar- and cross-laminated basal sands (*Tb* and *Tc*), with 5-15 cm thick overlying mud-caps. Coccolith dating of intervening hemipelagites reveals that the upper three turbidites were deposited during OIS 1-3 (<60 ka). These turbidites are immediately underlain by a hemipelagite dated at OIS 7 (190-245 ka), indicating an erosional hiatus of ~130 kyrs (Figure 3). A further hiatus of >200 kyrs occurs above the lowermost turbidite in the core, as hemipelagite overlying this deposit contains *P.lacunosa* and is therefore older than OIS 13 (>450 ka).

Core JC27-11 sampled ~3.0 m of sediment from an area of relatively smooth seafloor immediately northeast of the scoured area, and contains six texturally immature, sand-rich, poorly-sorted turbidites up to 50 cm thick (Figure 3). The thicker turbidite deposits exhibit erosive bases and contain wavy-, planar- and ripple-cross laminations that are occasionally disturbed by convolute bedding. Coccolith dating reveals an absence of significant hiatuses in JC27-11 (Figure 3), instead showing a relatively young and continuous sequence of sand-rich turbidites (all OIS 1-3; <60 ka).

Visual analysis of the three cores provides compelling evidence for a correlative relationship between the upper three turbidites, based upon turbidite mud colour, relative stratigraphic position, and thickness and colour of intervening hemipelagic intervals. Coccolith dating supports these correlations and indicates that the upper three turbidites were deposited in the last 60 ka (Figure 3). However, the turbidite deposits show remarkable variation between cores, in terms of bed thickness, grain size and sedimentary structures (Figure 3). Cores JC27-09 and JC27-12 also show evidence for significant hiatuses beneath these turbidites, indicating phases of active erosion prior to 60 ka and removal of several meters of sediment.

Horseshoe Valley

The Horseshoe Valley is located offshore southwest Iberia, and is a broad conduit for sediments transported southwestwards from the Lagos and Portimao Canyons to the

Horseshoe Abyssal Plain (Figure 4a) (Terrinha et al., 2009). Hull-mounted multibeam bathymetry data reveal a series of giant scours on the floor of the central fairway, on an overall slope of ~0.5º (Terrinha et al., 2009; Duarte et al., 2010; Figure 4a). The largest scours are up to 5 km wide and 120 m deep, with long axes aligned parallel to slope. Seismic profiles indicate that scour locations are controlled by the underlying thrust fault morphology (Duarte et al., 2010).

Our new high-resolution AUV data focus on a single large-scale, erosional scour that is U-shaped in cross-section and measures ~3 km wide and 50 m deep (Crescentic Depression 1 of Duarte et al., 2010). The scour is oval in planform and, unlike the Agadir Canyon scours, is elongate along slope (i.e. perpendicular to downslope flow). The scour is at ~4600 m water depth and displays average headwall slope angles of 30º, with maximum angles locally reaching 56º (Figure 4b). Profiles of the headwall slope vary across the scour, ranging from smooth and constant to stepwise with distinctive terraced morphology (Profiles A-A' and C-C'; Figure 4b). Two areas of morphologically distinct bedforms flank the scour: V-shaped chevrons to the west and lineations to the southeast and east (see inset figures in Figure 4b). The chevrons are V-shaped positive relief features that are up to 200 m across. Chevron limbs bound a hollow and flat-bottomed central region, and open out in a downstream direction. The lineations are negative relief features that may be fully isolated or amalgamated with other surrounding lineations; they are 40-80 m wide, 250-460 m long and up to 3 m deep. All lineations >80 m in length appear to be amalgamated.

Two piston cores were recovered from the area imaged by high-resolution data (Figures 4b and 5). Core JC27-24, recovered from outside the scour ~700 m upslope of the scour headwall, contains 4.7 m of dominantly hemipelagic sediments interbedded with about 20 thin turbidites. Turbidite deposits are 0.2-12 cm thick, and comprise thinly laminated fine sand bases overlain by structureless muds. In some cases the basal sand is absent. Coccolith ratios reveal that these deposits range in age from OIS 1-3 (<60 ka) to OIS 8-12 (450 ka), and do not appear to be separated by significant hiatuses (Figure 5). In contrast, core JC27-25*3, recovered from the scour floor, is dominated by seven thick turbidites with very different character to those seen outside the scour. The turbidites display texturally mature, normally graded, fine- to medium-grained sand bases that are erosive, up to 25 cm thick and laminated or cross-laminated (*Tb* and *Tc*). Sand bases are overlain by up to 1.5 m of structureless ungraded turbidite mud, and bounding hemipelagites are thin or absent (Figure 5). Coccolith dating shows that the turbidite sequence cored inside the scour is relatively young, with ages restricted to OIS 1-5 (<75 ka). Net accumulation rates during the last 75 kyrs are therefore over three times higher inside the scour compared to the adjacent seafloor.

Setúbal Canyon mouth

Setúbal Canyon is one of the largest canyons crossing the west Iberian margin, extending seawards from the continental shelf near Lisbon to the Tagus Abyssal Plain at 4840 m water depth (Figure 6a) (Lastras et al., 2009). Erosional features have previously been documented in the lower canyon and canyon mouth, using medium-resolution (30 kHz) sidescan sonar (see inset in Figure 6a). New high-resolution images within the canyon mouth reveal irregular crescentic scours that are elongate perpendicular to flow, with 'horns' pointing downstream (Figure 6b). These

scours are up to 1.0 km in length and width. One large isolated scour reaches a maximum depth of 14 m and has a steep headwall with slope angles up to 30º; it shallows gently downstream over a distance of several hundred meters (profile A-A'; Figure 6b,c). Two other scours are partly amalgamated, with headwall slope angles of up to 35º and a maximum depth of 22 m (profiles B-B' and C-C'; Figure 6b,c).

Core JC27-39 sampled sediments from within the largest isolated scour (Figure 6b and 7) and contains 50 cm of hemipelagite underlain by 3.35 m of debrite. The debrite comprises remobilised lower canyon sediments, including 1) thin-bedded turbidites (terrace facies), 2) canyon floor gravels containing lithic clasts up to 7.5 cm in size, and 3) coarse sands with rip-up clasts up to 6.0 cm across. It seems likely that this debrite is the same as that identified by Arzola et al. (2008) that covers much of the lower canyon mouth area. The overlying hemipelagite therefore represents shutdown of the system in the last few thousand years.

Whittard Channel margin

The Whittard Canyon and Celtic Fan link the southern Irish Sea and English Channel palaeo-river systems to the deep northwestern Bay of Biscay (Figures 1 and 8a) (Droz et al., 1999; Zaragosi et al., 2000). Hull-mounted multibeam bathymetry data from the fan surface reveal course of the main Whittard Channel, locally flanked by levees draped with fine-grained sediment waves (Figure 8a). High-resolution AUV images across the western margin of distal Whittard Channel reveal three distinct morphological features (Figure 8b). These include (i) a portion of the active Whittard Channel with a smooth flat thalweg, (ii) a heavily scoured channel margin, and (iii) a pair of large-scale sediment waves in the overbank area of the active channel.

Four types of erosional scour can be recognised in the overbank area: protoscour, isolated scour, early-stage amalgamated scour, and fully amalgamated scour. All of the scours have developed on lee slopes or in troughs of sediment waves. Protoscours are zones of shallow erosion that are up to 100 m long and 40 m wide; they are shallow and flat-floored, with internal slope angles <10º and a maximum vertical relief of 8 m. Isolated scours up to 890 m wide, 550 m long and 30 m deep have a uniform 'heel' shape and do not exhibit any signs of coalescing from smaller features; internal slope angles are generally low (<10º), with steeper slopes (22º-50º) confined to the outer limits of the scour (profiles A-A' and B-B', Figure 8b,c). One early-stage amalgamated scour has a distinctive scalloped headwall rim and low relief interior hummocks that are characteristic of scour remnants following amalgamation (profile C-C', Figure 8b,c). This scour is up to 18 m deep and is 750 m wide and 480 m long; internal slope angles range from 23º-56º. The largest erosional feature within the imaged area is a late-stage amalgamated scour that extends for >2500 m in the across-slope direction and >1300 m downslope. Of all the scour types documented in this area, this region of amalgamated scour displays both the deepest level of scour and the steepest slopes (50 m and >62º, respectively). The scoured zone has an irregular outer rim and, unlike the other scours, an irregular floor (profile C-C', Figure 8b,c).

Two cores were collected across one of the imaged sediment waves. Core JC27-63 sampled 2.3 m of sediment from a broad region of amalgamated scour in a wave trough (Figure 8b and 9), and is dominated by a single deposit of 1.7 m thickness.

This deposit comprises a thin medium-grained basal sand, overlain by a thick ungraded structureless mud. The sand and mud layers are separated by a grain size break (Figure 9). Other deposits sampled at the base of the core comprise interbedded organic-rich turbidites with erosive bases and thin mud caps. Core JC27-62 was recovered from a smooth wave crest located 1695 m to the north (just off the area covered by AUV bathymetry; Figure 8). This core is dominated by thin-bedded turbidites composed of fine sand bases and thin mud caps; these typical levee-type deposits show an overall upward fining and thinning between 0.9 and 3.7 m (Figure 9). The upper 0.9 m of the core comprises several thicker turbidites (up to 7 cm thick), which are overlain by 53 cm of hemipelagite. There is no evidence for the thick mud deposit visible in core JC27-63. Insufficient hemipelagic sediments are present for coccolith dating, but comparison with other cores in the region suggests a Late Glacial turbidite succession overlain by Holocene hemipelagite.

INTERPRETATION AND DISCUSSION

Scour morphologies and sizes

The high-resolution images presented here provide detailed insight into the dimensions, morphology and infill of erosional scours in a variety of deep-water environments. Based upon these morphologic data, we are able to identify the following categories of scour (Figure 10):

Isolated erosional scours

Isolated erosional scours have a smooth and continuous outer rim with a regular internal morphology and a broadly symmetrical U-shaped across-slope profile. They are relatively flat-bottomed, with steeper slopes of 20º-50º confined to scour margins. Their downslope profile is asymmetric, with a steep headwall and more gradual downslope opening. The examples of isolated scours presented here reveal four distinctly different types of scour shape and size:

Spoon-shaped scours display a regular elliptical shape in planform, and are elongated in the downslope direction (e.g. scours 1 and 2 in Figure 2b). Spoon shaped scours are the only type of scour that narrows and, importantly, closes in the downslope direction. Their elliptical planform produces a low width-to-length ratio of ~0.4. Other examples of spoon-shaped scours include the Cerro Toro Formation of northern Chile (Winn and Dott, 1979; Jobe et al., 2009), Albian Black Flysch of northern Spain (Vicente Bravo and Robles, 1995), Ross Formation of Ireland (Elliott, 2000a,b; Lien et al., 2003), and the modern Valencia Channel mouth in the western Mediterranean Sea (Palanques et al., 1995; Morris et al., 1998).

Heel-shaped scours have outward-flaring limbs that originate at a central, upslope location (Figure 8b). The downslope termination of the scour develops via gradual shallowing across the scour width; scour limbs continue to flare out until this termination. Heel-shaped scours are wider than they are long, resulting in width-to-length ratios of up to 1.6. Other published examples of scours exhibiting a heel-shaped morphology occur on the Rhone Neofan off southern France (Kenyon et al., 1995; Torres et al., 1997; Wynn et al., 2002a; Bonnel et al., 2005) and on Redondo Fan offshore California (Normark et al., 2009)

Crescentic scours have a broadly lunate shape with two downslope-pointing limbs (Figure 6b). The downslope profile varies across the width of the scour, with more rapid downslope shallowing in the centre of the scour compared to the limbs. Unlike heel-shaped scours, the area between the terminations of the two limbs is positive relief. They are as wide as, or wider than, they are long, with a resultant width-to-length ratio of ~1.3. Crescentic scours have previously been described from the canyon-basin transition zone off west Portugal (Wynn et al., 2002a) and the Valencia Channel mouth (Palanques et al., 1995; Morris et al., 1998).

Oval scours have an elliptical planform that is elongated in the across-slope direction. The large oval scour imaged in this study (Figure 4b) displays a more irregular rim than spoon-shaped scours; this may be due to a significantly steeper headwall resulting in small-scale retrogressive mass wasting. Oval scours can be very large; the example documented in the Horseshoe Valley is the widest and deepest isolated scour in the study area. Oval scours have also been from Eel Canyon, offshore California, where they were described as quasi-circular topographic depressions (Lamb et al., 2008).

The original controls on morphology of isolated scours remain poorly understood, especially as some examples show lateral variations in scour morphology within the same system, e.g. Valencia Channel mouth (Palanques et al., 1995; Morris et al., 1998). In addition, as seen in this study, scours in comparable environments can look very different, e.g. Agadir and Setúbal Canyon mouths (Figures 2b and 6b). We speculate that a complex interplay of substrate character (e.g. sand/mud ratio, consolidation rate), seafloor morphology (e.g. slope angle, degree of channelisation), flow character (e.g. volume, velocity, density) and flow frequency are important factors contributing to scour morphology and dimensions.

Amalgamated erosional scours

Regions of amalgamated scour develop via lateral coalescing of isolated scours, consequently the overall size of amalgamated scours exceeds that of the isolated scours that form them. The morphology of amalgamated scours is defined both by the character and number of isolated scours that have been amalgamated. The upslope portions of amalgamated scour rims are cuspate (Figures 2b and 8b), where each cusp is a relic of a former isolated feature that has since been incorporated into the amalgamated region. Erosional remnants of former isolated scour margins are commonly preserved on the floor of amalgamated scours, and take the form of irregular topography, hummocks, or elongate ridges of positive relief (Figure 2b and 8c).

Of the types of isolated scours characterised above, spoon-shaped, heel-shaped and crescentic scours all develop into broad regions of amalgamated scour (Figures 2b, 6b and 8b). In each case, the nature of the amalgamated region becomes highly irregular, although some key characteristics remain that allow the character of former isolated scours to be identified. In the case of spoon-shaped scours, the outer margins and inner remnant topography of the amalgamated region are aligned in the downslope direction, while the irregular upslope rim comprises a number of narrow, steep, and tightly rounded cusps (Figure 2b). In comparison, the rims of heel-shaped or crescentic amalgamated scours comprise gently rounded cusps and maintain their

widely flaring character (Figures 6b and 8b). Amalgamated regions that grow via the coalescing of crescentic scours continue to shallow downslope more rapidly towards the centre of the scour than at the margins, therefore retaining the overall crescentic shape.

It is notable that the oval isolated scour in the Horseshoe Valley is about 3 km wide (Figure 4b), which is wider than any region of amalgamated scour documented in this study. It is a fully isolated scour, with no evidence for amalgamation and no comparable isolated scours visible on the adjacent seafloor (Figure 4b). This has been interpreted to result from structural control (Terrinha et al., 2009; Duarte et al., 2010). However it is also possible that amalgamation is partly controlled by spacing of isolated scours, whereby this example has developed to a scale rarely achieved by isolated examples because it is located many kilometers away from adjacent scours. Overall, it appears that the point at which amalgamation occurs is controlled by the spacing, rate of lateral expansion and longevity of original isolated scours.

Sedimentary deposits within and adjacent to scours

Core data presented here reveal significant variation in the sedimentary fill of scours in different systems, which is a function of differing flow volume, velocity and sediment character. Major changes in sediment character inside and outside of scours within the same system are also documented, as well as temporal changes in sedimentation. For example, in Agadir Canyon mouth the thickest turbidite sands are developed *outside* of the scoured zone, on a gently sloping area of canyon floor that appears to have been dominantly aggradational in the last 60 kyrs. The presence of sand-to-mud grain-size breaks and thin mud caps indicates bypass of the fine-grained suspended load (Figures 2 and 3). In contrast, the area of amalgamated scour contains a >320 kyr erosional hiatus at 3.4 m overlain by a thickening and fining-upwards sequence of dominantly fine-grained turbidites, suggesting a temporal reduction in flow velocity at this location. The deepest isolated scour displays two significant hiatuses, the youngest of which occurs between OIS 3 and 7 and represents at least 130 kyrs. This hiatus is overlain by a series of thin muddy turbidites indicating dominant bypass of both the sand and mud load (Figure 3). Overall, the observed sedimentation pattern suggests that the axis of erosion is shifting northwards across Agadir Canyon mouth, with the deepest isolated scours cutting into the gently sloping northern canyon floor, and the region of amalgamated scour in the canyon axis being progressively infilled during the last 130 kyrs. The whole of the imaged area appears to have been aggradational in the last 60 kyrs, although significant deposit heterogeneity across the imaged area (2 km wide) indicates a complex flow regime that is likely influenced by local seafloor morphology.

The giant oval scour in Horseshoe Valley is filled with a relatively young sequence of thick muddy turbidites, comparable to the amalgamated scour in Agadir Canyon mouth. Individual turbidite muds are up to 1.6 m thick, and appear to be wholly aggradational (Figure 5). In contrast, the area immediately upslope of the oval scour is an area of dominant bypass, with poorly developed thin turbidites and a condensed hemipelagic sequence that suggests associated minor erosion and/or bypass. A thick turbidite mud, also approaching 1.6 m thickness, is evident in the floor of an overbank scour adjacent to Whittard Channel (Figures 8 and 9). There is no

indication for similar deposits in core outside of the scoured area. Overall, it would appear that broad deep scours are able to effectively trap thick turbidite muds, even though the bulk of the flow is fully bypassing. These muds may be travelling as relatively high concentration fluid mud layers towards the tail of the flow (e.g. McCave and Jones, 1988), possibly generated through post-depositional remobilisation. This interpretation is supported by the uniform, ungraded appearance of mud deposits. Some scours also act as ponds for debris flows, exemplified by the thick debrite trapped within a scour in Setubal Canyon mouth (Figures 6 and 7).

Insights into scour genesis

As with previous studies (Mutti and Normark, 1987; Normark and Piper, 1991), we link the development of large isolated and amalgamated scours to areas of significant flow expansion, such as canyon mouths and channel overbanks (Figures 2, 4, 6 and 8). Underlying structure, such as sediment waves or thrust faults, may also locally influence location of individual scours (e.g. oval scour in Horseshoe Valley; Terrinha et al., 2009; Duarte et al., 2010).

High-resolution multibeam bathymetry data shown here provide additional new insights into scour genesis. A key observation is that isolated scours merge laterally through time into larger areas of amalgamated scour (Figures 2 and 8). The morphology of original isolated scours is often preserved as a series of scour rims on the headwall of the amalgamated scour, and a lateral transition from isolated to amalgamated scour can also be observed in response to lateral migration of the axis of erosion (e.g. Agadir Canyon mouth; Figure 2). Synchronous existence of infilling amalgamated scours and actively eroding isolated scours in Agadir Canyon mouth during the Late Quaternary (60-130 kyrs) is of particular interest, as it shows that amalgamated scours can become abandoned while adjacent isolated scours are actively forming. Microfossil-based dating suggests that development of isolated scours, lateral amalgamation, and eventual infilling in this system may take tens to hundreds of thousands of years, probably due to the low event frequency (one major flow every 10 kyrs; Wynn et al., 2002b).

Scour abandonment and infilling may also occur in response to a general system shutdown, e.g. during sea-level highstand, represented by Holocene hemipelagic drape in Setubal Canyon mouth and Whittard Channel scours (Figures 7 and 9). Scours may also be plugged by canyon/channel margin failures, e.g. the debrite fill in Setubal Canyon mouth scour (Figure 7). Muddy scour fills may therefore be generated by both allocyclic factors, e.g. changing/reducing sediment supply, and autocyclic factors, e.g. canyon thalweg migration or canyon margin failure.

Morphologic features associated with scours

The V-shaped chevrons imaged alongside a giant oval scour in Horseshoe Valley (Figure 4b) morphologically resemble erosional chevrons described from the Setubal Canyon mouth, offshore west Iberia (Wynn et al., 2002a). However the limbs of chevrons imaged in Horseshoe Valley are positive relief features, indicating that they are depositional in origin. They are therefore comparable to depositional chevrons, also up to 200 m across, reported from beyond the mouth of Valencia Channel,

where they are thought to be composed of coarse sand-sized sediments moving over a muddy substrate (Palanques et al., 1995; Morris et al., 1998).

Erosional lineations were also imaged adjacent to the oval scour in Horseshoe Valley (Figure 4b). These features closely resemble longitudinal streaks identified by Wynn et al. (2002a) and Morris et al. (1998) from modern canyon/channel mouth environments. However, those documented here are significantly smaller and more closely spaced. Isolated erosional lineations are up to 80 m long, while lineations that exceed 80 m in length are coalesced with adjacent features.

CONCLUSIONS

In this study a series of new high-resolution images of deep-water scours have been combined with sedimentological and chronological data to provide new insights into scour morphology, sedimentology and genesis as follows:

1. Modern deep-water scours may be studied at a level of detail usually unique to outcrop studies, by using (i) AUV-mounted high-resolution multibeam bathymetry, (ii) sedimentological data derived from piston cores placed precisely within imaged areas, and (iii) microfossil-based dating of cored sediments, which provides a chrono-stratigraphic framework for scour genesis.
2. By nesting these AUV-based (outcrop-scale) datasets within lower resolution multibeam bathymetry and deep-towed sidescan sonar data, we are able to apply precise paleo-environmental interpretations not generally deducible in outcrop-scale studies.
3. Scours documented in high-resolution in this study cover a size range of 40 to 3170 m wide, and 8 to 48 m deep, effectively 'bridging the gap' between outcrop studies and traditional (low-resolution) seafloor data. Deep-water erosional scours therefore occur along a continuum of sizes, from cm to km scale.
4. Isolated scours documented in this study are associated with canyon/channel termini and margins, and display four different morphologies: spoon-shaped, heel-shaped, crescent-shaped and oval-shaped.
5. Isolated scours may coalesce into broad areas of amalgamated scour; evidence for the presence of isolated scours is often preserved within the region of amalgamation as a series of scour rims on the scour headwall, or as remnants on the scour floor.
6. Scour abandonment and infilling events vary between and within systems, and may occur in response to thalweg migration, general system shutdown, changes in flow character, or plugging by mass transport deposits.
7. Scours can accumulate considerable thicknesses of turbidite muds while significant levels of bypass may occur synchronously in the surrounding area. Depositional character of flows can therefore vary dramatically across short distances (tens to hundreds of meters).
8. Other macro-features may be associated with regions of scour in deep-water environments, such as V-shaped chevrons and erosional lineations.

ACKNOWLEDGEMENTS

We would like to thank the Captain, Officers and crew of *RRS James Cook* for their assistance during data collection on JC027. We would particularly like to thank Pete

Stevenson and Maaten Furlong for their assistance with AUV mapping. Esther Sumner is gratefully acknowledged for providing graphic logs of JC027 cores. This project was funded as part of the NERC Oceans 2025 programme. Heather Macdonald is funded by a NERC CASE Studentship (NER/S/A/2006/14147) at University of Leeds. The CASE sponsor is the NSRD Geology and Geophysics group at NOCS.

REFERENCES CITED

Allen, J. R, L., 1969, Erosional current marks of weakly cohesive mud beds: Journal of Sedimentary Petrology, v. 39, p. 607-623.

Allen, J. R. L., 1971, Transverse erosional marks of mud and rock: their physical basis and geological significance: Sedimentary Geology, v. 5, p. 167-385.

Allen, J. R. L., 1984, Sedimentary structures, their character and physical basis. Developments in sedimentology: Amsterdam, Elsevier, v. 1 and 2.

Arzola, R.G., Wynn, R.B., Lastras, G., Masson, D.G., Weaver, P.P.E., 2008, Sedimentary features and processes in the Nazaré and Setúbal submarine canyons, west Iberian margin: Marine Geology, v. 250, p. 64–88.

Bonnel, C., Dennielou, B., Droz, L., Mulder, T. and Berne, S., 2005, Architecture and depositional pattern of the Rhone Neofan and recent gravity activity in the Gulf of Lions (western Mediterranean): Marine and Petroleum Geology, v. 22, p. 827-843.

Bouma, A.H., 1962, Sedimentology of some Flysch deposits: A graphic approach to facies interpretation: Amsterdam, Elsevier, 168 p.

Chapin, M.A., Davies, P., Gibson, J.L. and Pettingill, H.S., 1994, Reservoir architecture of turbidite sheet sandstones in laterally extensive outcrops, Ross Formation, Western Ireland: GCSSEPM Foundation 15th Annual Research Conference, Submarine Fans and Turbidite Systems, p. 53-68.

Droz, L., Auffret, G.A., Savoye, B., Bourillet, J.F., 1999, L'e´ventail profond de la marge Celtique: stratigraphie et e´volution se´dimentaire: Comptes Rendus de l'Académie des Sciences, Paris, Earth and Planetary Sciences, v. 328, p. 173–180.

Duarte, J.C., Terrinha, P., Rosas, F.M., Valadares, V., Pinheiro, L.M., Matias, L., Magalh˜aes, V., Roque, C., 2010, Crescent-shaped morphotectonic features in the Gulf of Cadiz (offshore SW Iberia): Marine Geology, v. 271, p. 236-249.

Dzulynski, S. and Simpson, F., 1966, Influence of bottom irregularities on experimental scour markings: Annales De La Société Géologique De Pologne, v. 36, p. 285-294.

Dzulunski, S. and Walton, E. K., 1963, Experimental production of sole markings: Transactions of the Edinburgh Geological Society, v. 19, p. 279-305.

Dzulynski, S., 1965, New data on experimental production of sedimentary structures: Journal of Sedimentary Petrology, v. 35, p. 196-212.

Elliott, T., 2000a, Megaflute erosion surfaces and the initiation of turbidite channels: Geology, v. 28; p. 119-122.

Elliott, T., 2000b, Depositional architecture of a sand-rich, channelised turbidite system: the Upper Carboniferous Ross sandstone formation, Western Ireland. *In:* Weimer, P., Slatt, R.M., Coleman, J., Rosen, N.C., Nelson, H., Bouma, A.H., Styzen, M.J. and Lawrence, D.T. (Eds), Deep-water reservoirs of the World, GCSSEPM Foundation 20th Annual Research Conference, p. 342-364.

Fildani, A. and Normark, W.D., 2004, Late Quaternary evolution of channel and lobe complexes of Monterey Fan: Marine Geology, v. 206, p. 199-223.

Fildani, A., Normark, W.D., Kostic, S. and Parker, G., 2006, Channel formation by flow stripping: large-scale scour features along the Monterey East Channel and their relation to sediment waves: Sedimentology, v. 53, p. 1265-1287.

Frenz, M., Wynn, R.B., Georgiopoulou, A., Bender, V.B., Hough, G., Masson, D.G., Talling, P.J. and Cronin, B.T., 2009, Provenance and pathways of late Quaternary turbidites in the deep-water Agadir Basin, northwest African margin: International Journal of Earth Sciences, v. 98, p. 721-733.

Hilton, V.C., 1995, Sandstone architecture and facies from the *Annot* Basin of the SW Alpine foreland basin, SE France. *In:* Pickering, K.T., Hiscott, R.N., Kenyon, N.H., Ricci Lucchi, F., and Smith, R.D.A. Eds., Atlas of Deep Water Environments: Architectural style in turbidite systems. London, Chapman & Hall, p. 227-235.

Huvenne, V. A. I., McPhail, S.D., Wynn, R.B., Furlong, M. and Stevenson, P., 2009, Mapping Giant Scours in the Deep Ocean: EOS (Transactions, American Geophysical Union, v. 90, p. 274-275.

Jobe, Z.R., Bernhardt, A., Fosdick, J.C. and Lowe, D.R., 2009, Cerro Toro Channel Margins, Sierra del Toro. *In:* Fildani, A., Hubbard, S.M. and Romans, B.W. Eds., Stratigraphic evolution of deep-water architecture: Examples of controls and depositional styles from the Magallanes Basin, southern Chile 2009. SEPM Field Trip Guidebook No. 10, p. 31-33.

Kenyon, N. H. and Millington, J., 1995, Contrasting deep-sea depositional systems in the Bering Sea. *In:* Pickering, K.T., Hiscott, R.N., Kenyon, N.H., Ricci Lucchi, F., and Smith, R.D.A. Eds., Atlas of Deep Water Environments: Architectural style in turbidite systems. London, Chapman & Hall, p. 196–202.

Kenyon, N.H., Millington, J., Droz, L. and Ivanov, M.K., 1995, Scour holes in channel-lobe transition zone on the Rhone Cone, *In:* Pickering, K.T., Hiscott, R.N., Kenyon, N.H., Ricci Lucchi, F., and Smith, R.D.A. Eds., Atlas of Deep Water Environments: Architectural style in turbidite systems. London, Chapman & Hall, p. 212-215.

Kidd, R.B., Lucchi, R.G., Gee, M. and Woodside, J.M., 1998, Sedimentary processes in the Stromboli Canyon and Marsili Basin, SE Tyrrhenian Sea: results from side-scan sonar surveys: Geo-Marine Letters, v. 18, p. 146-154.

Klaucke, I., Masson, D.G., Kenyon, N.H. and Gardner, J.V., 2004, Sedimentary processes of the lower Monterey Fan channel and channel-mouth lobe: Marine Geology, v. 206, p. 181-198

Komar, P.D., 1971, Hydraulic jumps in turbidity currents: Bulletin of the Geological Society of America, v. 45, p. 747-749.

Lamb, M.P., Parsons, J.D., Mullenbach, B.L., Finlayson, D.P., Orange, D.L. and Nittrouer, C.A., 2008, Evidence for superelevation, channel incision, and formation of cyclic steps by turbidity currents in Eel Canyon, California: Geological Society of America Bulletin, v. 120, p. 463-475.

Lastras, G., Arzola, R.G., Masson, D.G., Wynn, R.B., Huvenne, V.A.I., Huhnerbach, V. and Canals, M., 2009, Geomorphology and sedimentary features in the Central Portuguese submarine canyons, western Iberian margin: Geomorphology, v.103, p. 310-329.

Lee, S.E., Talling, P.G., Ernst, G.G.J. and Hogg, A.J., 2002, Occurrence and origin of submarine plunge pools at the base of the US continental slope: Marine Geology, v. 185, p. 363-377.

Lien T., Walker, R.G. and Martinsen, O.J., 2003, Turbidites in the Upper Carboniferous Ross Formation, western Ireland: reconstruction of a channel and spillover system: Sedimentology, v. 50, p. 113-148.

Masson, D.G., Kenyon, N.H., Gardner, J.V. and Field, M.E., 1995, Monterey Fan: channel and overbank morphology. *In:* Pickering, K.T., Hiscott, R.N., Kenyon, N.H., Ricci Lucchi, F., and Smith, R.D.A. Eds., Atlas of Deep Water Environments: Architectural style in turbidite systems. London, Chapman & Hall, p. 47 - 79.

Millington, J.J. and Clark, J.D., 1995, The Charo/Arro Canyon-Mouth sheet system, south-central Pyrenees, Spain: A structurally confined influence zone of sediment dispersal: Journal of Sedimentary Research, v. 65, p. 443-454.

Morris, S. A., Kenyon, N.H., Limonov, A.H. and Alexander, J., 1998, Downstream changes of large-scale bedforms in turbidites around the Valencia channel mouth, north-west Mediterranean: implications for palaeoflow reconstruction: Sedimentology, v. 45, p. 365–377.

Morris, W.R. and Normark, W.R., 2000, Sedimentologic and geometric criteria for comparing modern and ancient sandy turbidite elements. *In:* Weimer, P., Slatt, R.M., Coleman, J., Rosen, N.C., Nelson, H., Bouma, A.H., Styzen, M.J. and Lawrence, D.T. (Eds), Deep-water reservoirs of the World, GCSSEPM Foundation 20th Annual Research Conference, p. 606-628.

Mutti, E. and Normark, W.R., 1987, Comparing examples of modern and ancient turbidite systems: problems and concepts. *In*: J. K. Leggett and G. G. Zuffa, eds., Marine Clastic Sedimentology: concepts and case studies: London, Graham and Trotman, p. 1–38.

Normark, W.R., 1970, Growth patterns of deep-sea fans. PhD Thesis, University of California, San Diego.

Normark, W.R., Piper, D.J.W and Hess, G.R., 1979, Distributary channels, sand lobes, and mesotopography of Navy Fan, California Borderland, with applications to ancient fant sediments: Sedimentology, v. 26, p. 749–774.

Normark, W.R. and Piper, D.J.W., 1991, Initiation processes and flow evolution of turbidity currents: implications for the depositional record, *in* R. H. Osborne, ed., From shoreline to abyss: SEPM Special Publication 46, p. 207–230.

Normark, W.R., Paull, C.K., Caress, D.W., Ussler, W. and Sliter, R., 2009, Fine-scale relief related to Late Holocene channel shifting within the floor of the upper Redondo Fan, offshore Southern California: Sedimentology, v. 56, p. 1690-1740.

Palanques, A., Kenyon, N.H., Alonso, B., and Limonov, A., 1995, Erosional and depositional patterns in the Valencia channel mouth: an example of a modern channel-lobe transition zone: Marine Geophysical Researches, v. 17, p. 503–517.

Piper, D.J.W., Hiscott, R.N. and Normark, W.R., 1999, Outcrop-scale acoustic facies analysis and latest Quaternary development of Hueneme and Dume submarine fans, offshore California: Sedimentology, v. 46, p. 47-78.

Potter, D.P. and Shaw, J., 2009, Shaded seafloor relief, Placentia Bay southeast, offshore Newfoundland and Labrador; Geological Survey of Canada, Map 2147A, scale 1:50,000.

Rücklin, H., 1938, Strömungsmarken im unteren Muschelkalk des Saarlandes: Senckenbereiana, v. 20, p. 94-114.

Shor, A.N., Piper, D.J.W., Hughes Clarke, J.E. and Mayer, L.A., 1990, Giant flute-like scour and other erosional features formed by the Grand Banks turbidity current: Sedimentology, v. 37, p. 631-645.

Talling, P. J., Wynn, R. B., Masson, D. G., Frenz, M., Cronin, B.T., Schiebel, R., Akhmetzhanov, A.M., Dallmeier-Tiessen, S., Benetti S., Weaver, P.P.E., Georgiopoulou, A., Zu¨hlsdorff, C. and Amy, L.A., 2007, Onset of submarine debris flow deposition far from original giant landslide: Nature, v. 450, p. 541-544.

Torres, J., Droz, L., Savoye, B., Terentieva, E., Cochonat, P., Kenyon, N.H. and Canals, M., 1997, Deep-sea avulsion and morphosedimentary evolution of the Rhône Fan Valley and Neofan during the Late Quaternary (north-western Mediterranean Sea): Sedimentology, v. 44, p. 457–477.

Terrinha, P., Matias, L., Vicente, J., Duarte, J., Luís, J., Pinheiro, L., Lourenço, N., Diez, S., Rosas, F, Magalhães, V., Valadares, V., Zitellini, N., Mendes Víctor, L. and MATESPRO Team., 2009, Morphotectonics and Strain Partitioning at the Iberia-Africa plate boundary from multibeam and seismic reflection data: Marine Geology, v. 267, p. 156-174.

Toucanne, S., Zaragosi, S., Bourillet, J.F., Naughton, F., Cremer, M., Eynaud, F., and Dennielou, B., 2008, Activity of the turbidite levees of the Celtic-Armorican margin (Bay of Biscay) during the last 30,000 years: Imprints of the

last European deglaciation and Heinrich events: Marine Geology, v. 247, p. 84-103.

Vicente Bravo, J. C. and S. Robles., 1995, Large-scale mesotopographic bedforms from the Albion Black Flysch, northern Spain: characterization, setting and comparison with recent Channel-Lobe Transition Zones analogues, *in* K. T. Pickering, R. N. Hiscott, N. H. Kenyon, F. Ricci Lucchi, and R. D. A. Smith, eds., Atlas of deep water environments: architectural style in turbidite systems: London, Chapman and Hall, p. 216–226.

Weaver, P. P. E. & Kuijpers, A., 1983, Climatic control of turbidite deposition on the Madeira Abyssal Plain: Nature, v. 306, p. 360–363.

Weaver, P. P. E., 1994, Determination of turbidity current erosional characteristics from reworked coccolith assemblages, Canary Basin, N. E. Atlantic: Sedimentology, v. 41, p. 1025-1038.

Weaver, P.P.E., Wynn, R.B., Kenyon, N.H. and Evans, J., 2000, Continental margin sedimentation, with special reference to the north-east Atlantic margin: Sedimentology, v. 47, p. 239-256.

Winn, R.D. and Dott, R.H., 1979, Deep-water fan-channel conglomerates of Late cretaceous age, southern Chile: Sedimentology, v. 26, p. 203-228.

Wynn, R.B., Kenyon, N.H., Masson, D.G, Stow, D.A.V. and Weaver, P.E., 2002a, Characterization and recognition of deep-water channel-lobe transition-zones: AAPG Bulletin, v. 86, p. 1441-1462.

Wynn, R.B., Weaver, P.P.E., Stow, D.A.V., and Masson, D.G., 2002b, Turbidite depositional architecture across three interconnected deep-water basins on the Northwest African margin: Sedimentology, v. 49, p. 669-695.

Zaragosi, S., Auffret, G.A., Fauge`res, J.-C., Garlan, T., Pujol, C. and Cortijo, E., 2000, Physiography and recent sediment distribution of the Celtic Deep-Sea Fan, Bay of Biscay: Marine Geology, v. 169, p. 207-237.

Zitellini, N., Gracia, E., Matias, L., Terrinha, P., Abreu, M.A., DeAlteriis, G., Henriet, J.P., Danobeitia, J.J., Masson, D.G., Mulder, T., Ramella, R., Somoza, L. and Diez, S., 2009, The quest for the Africa-Eurasia plate boundary west of the Strait of Gibraltar: Earth and Planetary Science Letters, v. 280, p. 13–50.

Figure Captions

Figure 1. Location map of the four study areas along the northeast Atlantic continental margin. White rectangles show areas covered by Figs 2a, 4a, 6a and 8a. Inset figure shows the Autosub6000 vehicle during deployment.

Figure 2. Erosional scours in Agadir Canyon mouth, offshore northwest Morocco. (A) Regional EM12 multibeam bathymetry showing the morphology of lower Agadir Canyon.

Black arrows show interpreted flow pathways. Inset figure shows TOBI 30 kHz sidescan sonar profile of the scoured region (located by the red rectangle on EM12 data). Light tones are high backscatter. White rectangle shows location of Autosub6000 imagery. (B) High-resolution Autosub6000 image and cross sectional profiles of isolated and amalgamated spoon-shaped scours. Locations of piston cores shown in Fig. 3 are provided.

Figure 3. Core data from Agadir Canyon mouth scours. For locations see Fig. 2. Data include core photos, graphic logs and interpretations, and coccolith ratios from hemipelagic sediments that provide dating control (see key for species). OIS = Oxygen Isotope Stage. Core JC27-09 recovered sediments from within a large amalgamated scour, JC27-12 was taken from within an isolated scour, and JC27-11 sampled sediments adjacent to the scoured zone. Note the marked variability in abundance, thickness and grain size of turbidite deposits, across an area of just over 2 km.

Figure 4. Erosional scours in Horseshoe Valley, offshore southwest Portugal. (A) Composite image of SWIM multibeam bathymetry data showing the regional morphology of Horseshoe Valley (Zitellini et al., 2009). Note the large scours in the central valley. Black arrows show interpreted flow pathways. Red box indicates the location of Autosub6000 data. (B) High-resolution Autosub6000 image and cross-sectional profiles across a giant oval-shaped scour in Horseshoe Valley. Additional depth information (pastel colors) is derived from AUV depth profiler data. Inset images show depositional chevrons and erosional lineations adjacent to the scour. Additional depth information (pastel colors) is derived from AUV depth profiler data. Locations of cores shown in Fig. 5 are indicated.

Figure 5. Core data from Horseshoe Valley scour. For locations see Fig. 4. Data include core photos, graphic logs and interpretations, and coccolith ratios from hemipelagic sediments that provide dating control (see key for species). OIS = Oxygen Isotope Stage. Core JC27-24 recovered sediments from smooth seafloor upslope of the scour headwall, while core JC27-25*3 was taken from within the scour. Note the thick mud deposits within the scour, compared to the zone of dominant bypass outside the scour.

Figure 6. Erosional scours in Setúbal Canyon mouth, offshore west Portugal. (A) Regional EM120 multibeam bathymetry showing the morphology of lower Setúbal Canyon. Black arrows show interpreted flow pathways. Inset figure shows TOBI 30 kHz sidescan sonar

profile of the scoured region (located by the red rectangle on EM120 data and corresponding to the Autosub6000 image). Light tones are high backscatter. (B) High-resolution Autosub6000 image of crescent-shaped scours. Location of piston core shown in Fig. 7 is shown. (C) Cross-sectional profiles across a series of crescentic scours. Profile locations shown in (B).

Figure 7. Core data from Setúbal Canyon mouth scour. For location see Fig. 6. Data include core photo and graphic log with interpretation. Core contains a thick mass transport deposit overlain by hemipelagic drape.

Figure 8. Erosional scours on Whittard Channel margin, northern Biscay margin. (A) Regional multibeam bathymetry showing the morphology of Whittard Canyon and Channel. Note the presence of large-scale sediment waves in overbank areas beyond channel bends. Red rectangle shows location of Autosub6000 image. (B) High-resolution Autosub6000 image of scours adjacent to Whittard Channel, in an area of fine-grained sediment waves. Location of piston core shown in Fig. 9 is shown. Note morphological contrast between smooth channel floor and scoured channel margins and sediment wave troughs. (C) Cross-sectional profiles across isolated and amalgamated scours. Profile locations shown in (B).

Figure 9. Core data from Whittard Channel margin scours. For locations see Fig. 8. Data include core photos and graphic logs and interpretations. Core JC27-62 recovered sediments from a sediment wave crest just north of the imaged area, while core JC27-63 was taken from within a scour. Note the thick mud deposit within the scour, which is not present in the sequence recovered from outside the scour.

Figure 10. Summary figure showing morphology and dimensions of the four isolated and amalgamated scour types documented in this study. Examples of comparable scours from both modern and ancient systems are also listed.

Figure 1

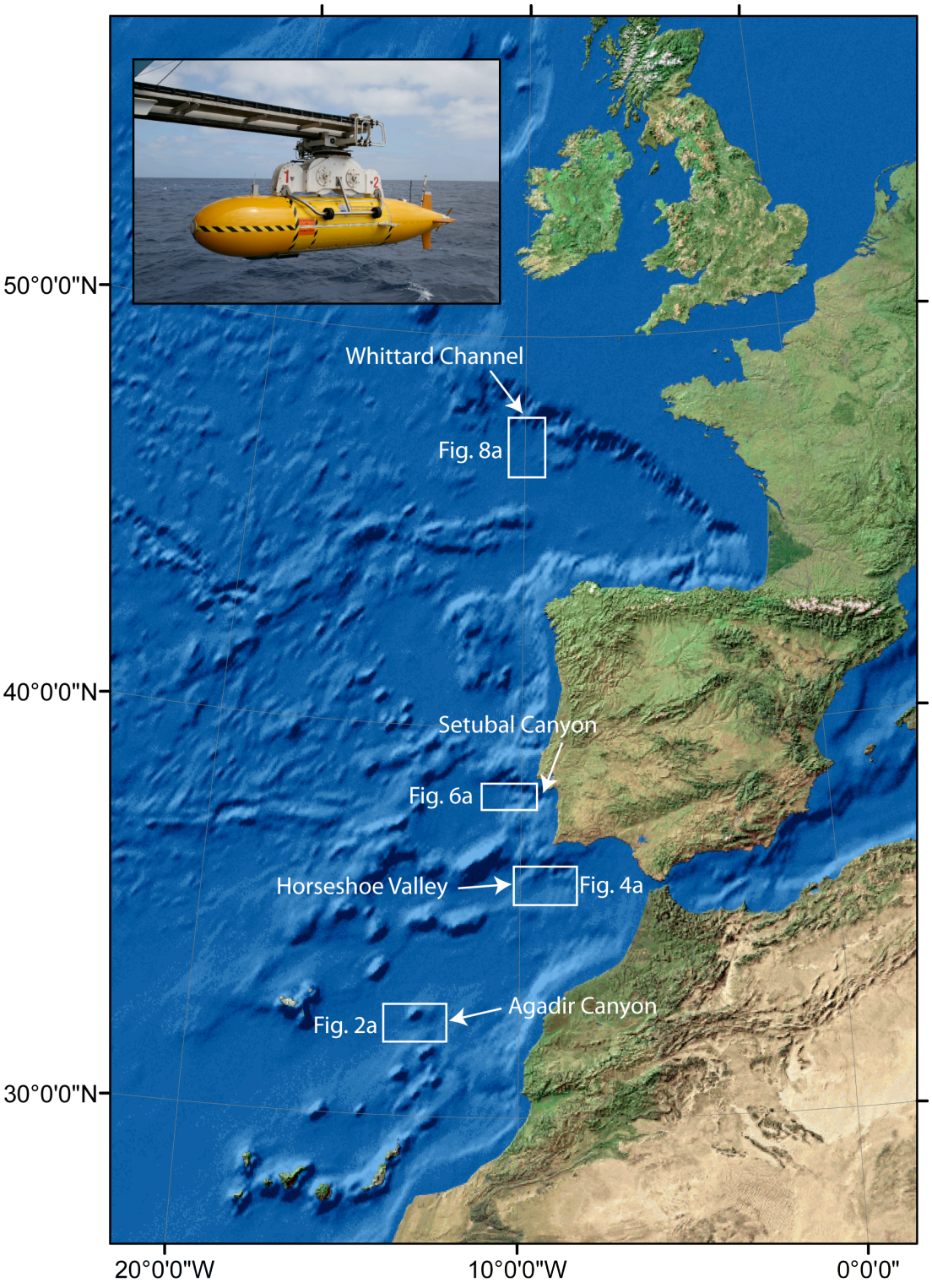

Macdonald et al. Figure 1. .jpg

Figure 2

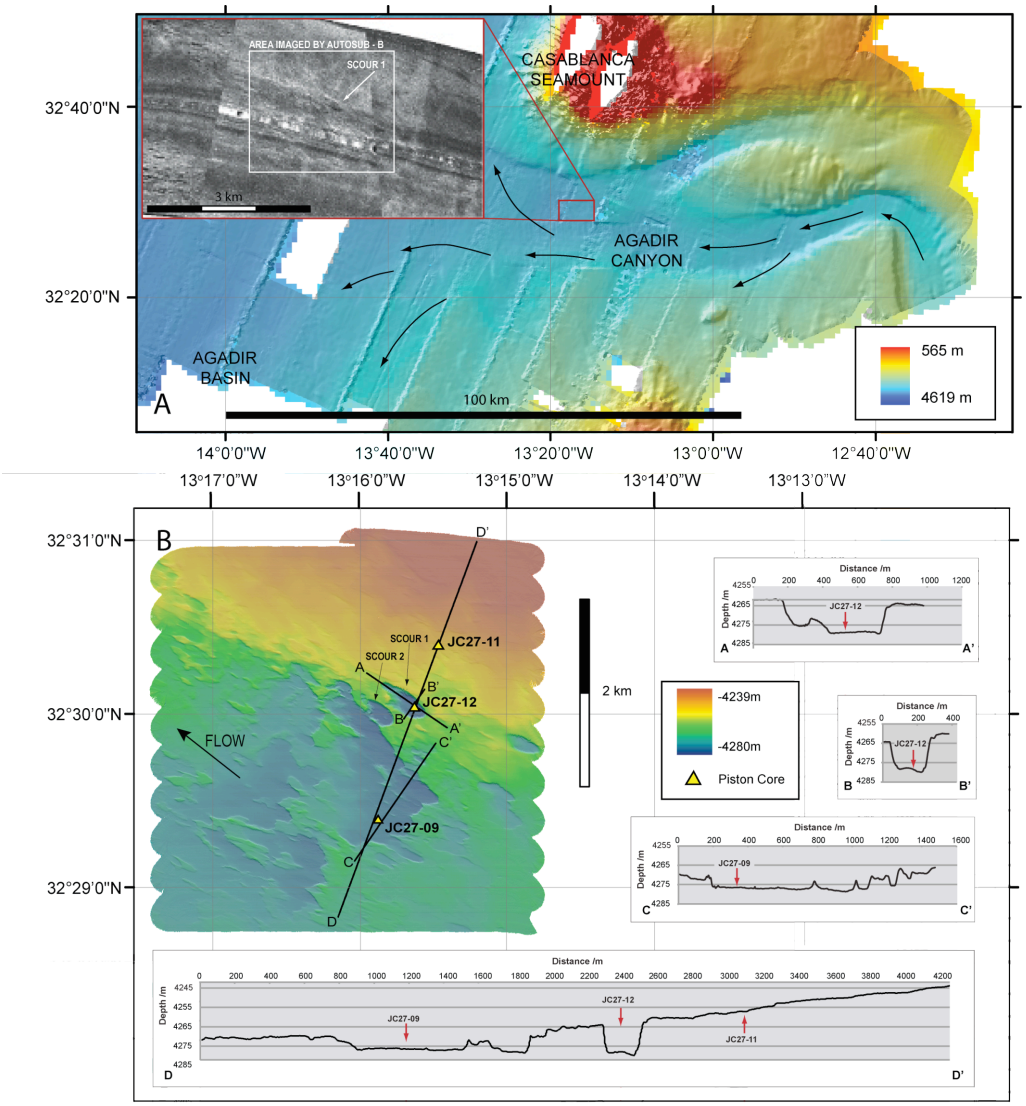

Macdonald et al. Figure 2. .jpg

Figure 3

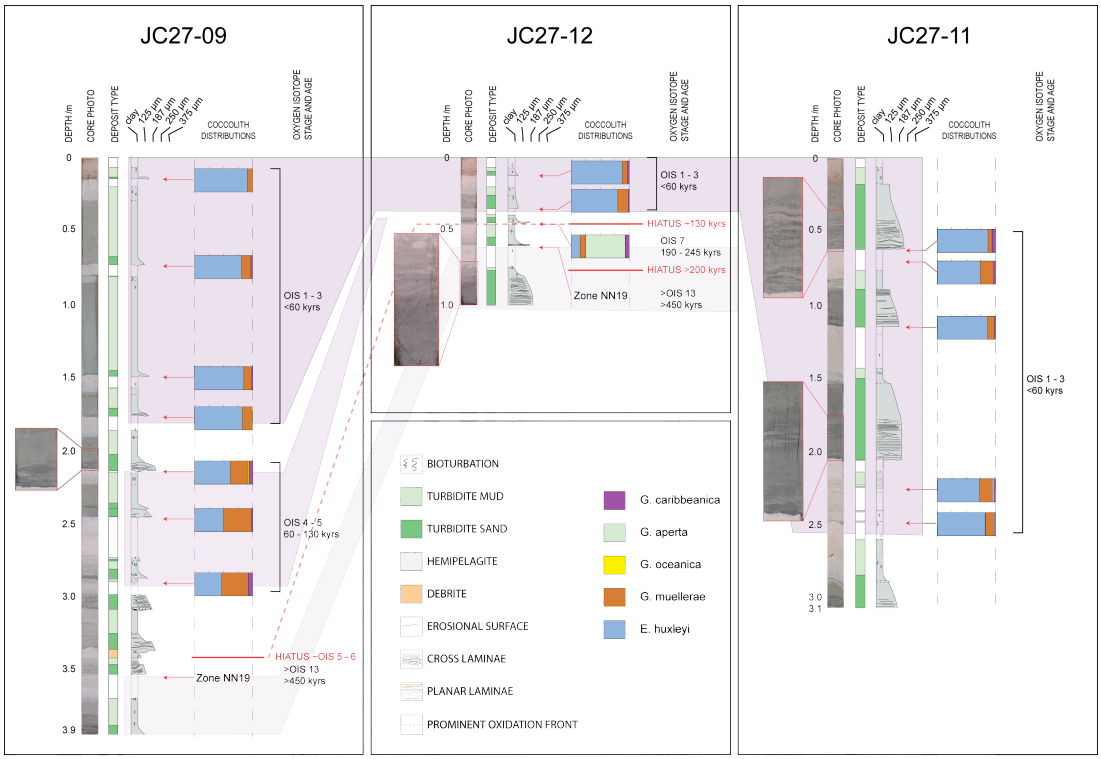

Macdonald et al. Figure 3. .jpg

Figure 4

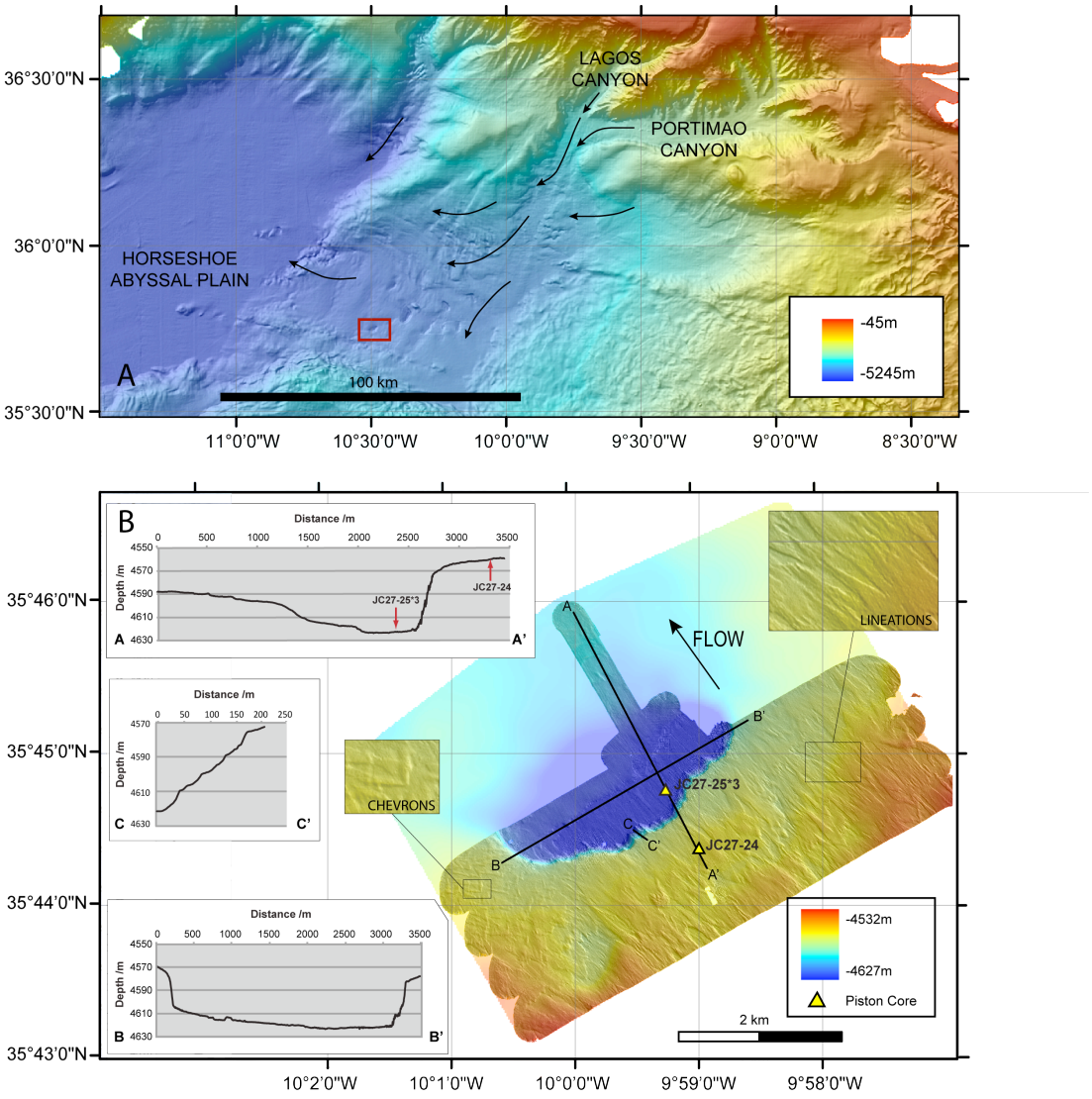

Macdonald et al. Figure 4. .jpg

Figure 5

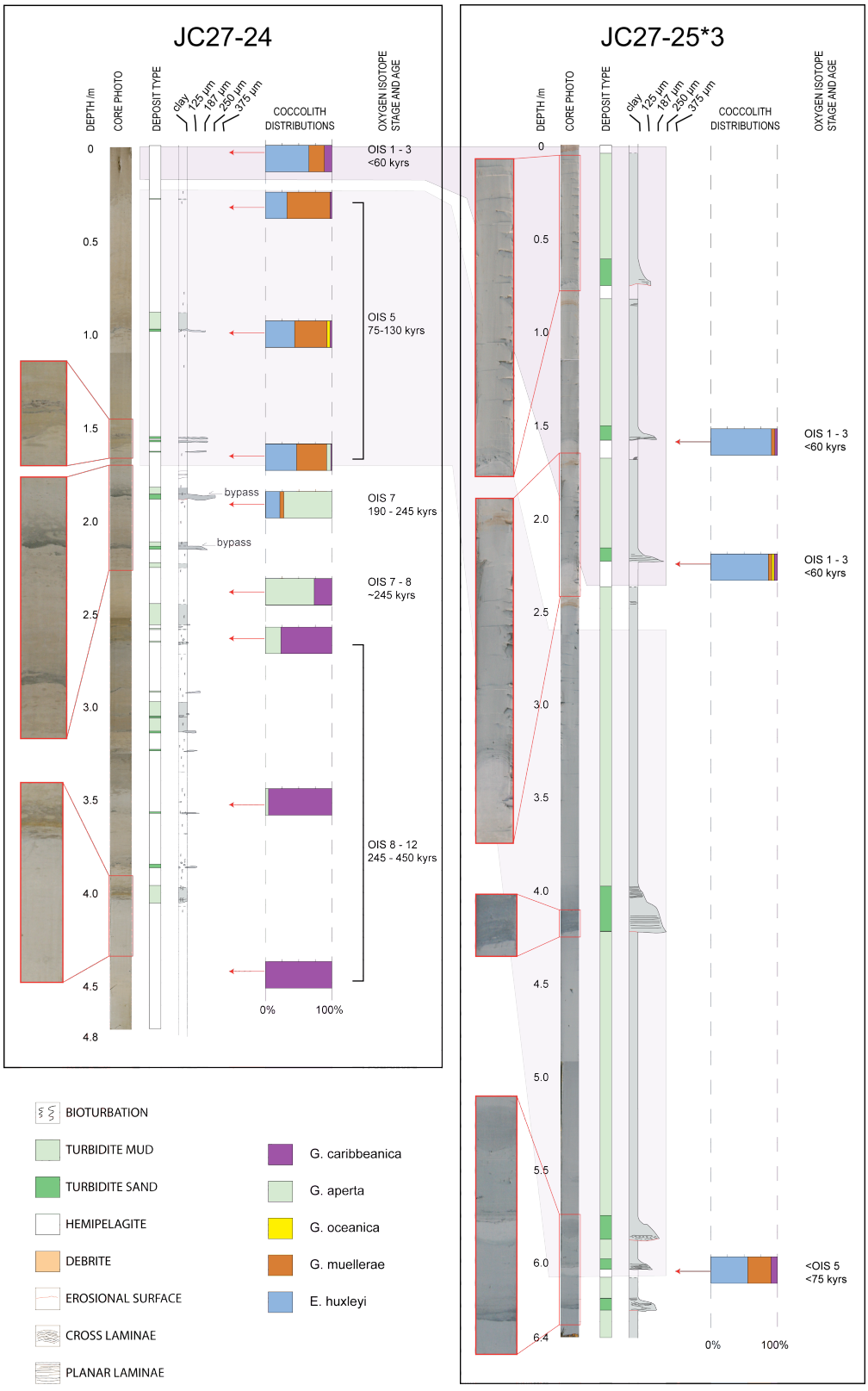

Macdonald et al. Figure 5. .jpg

Figure 6

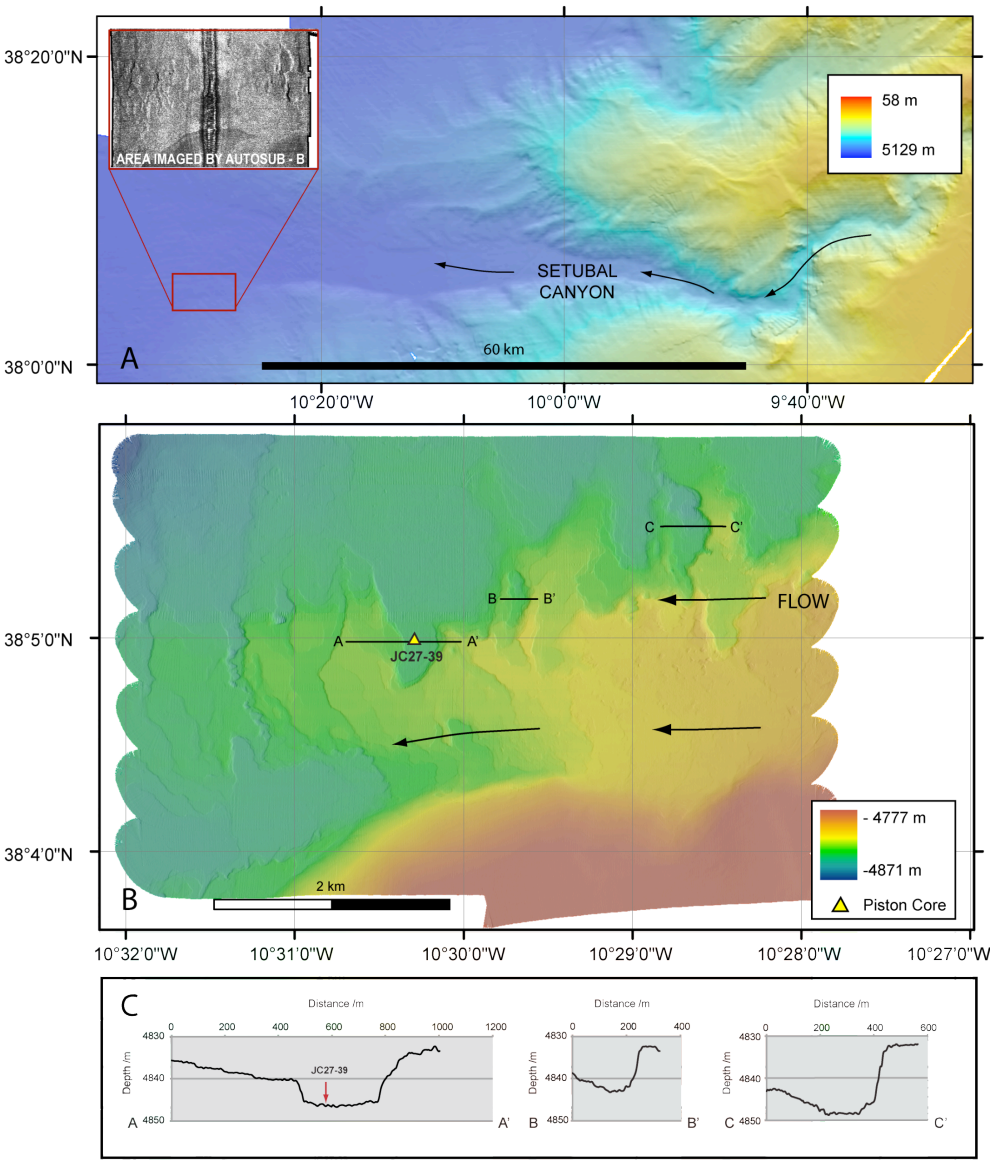

Macdonald et al. Figure 6. .jpg

Figure 7

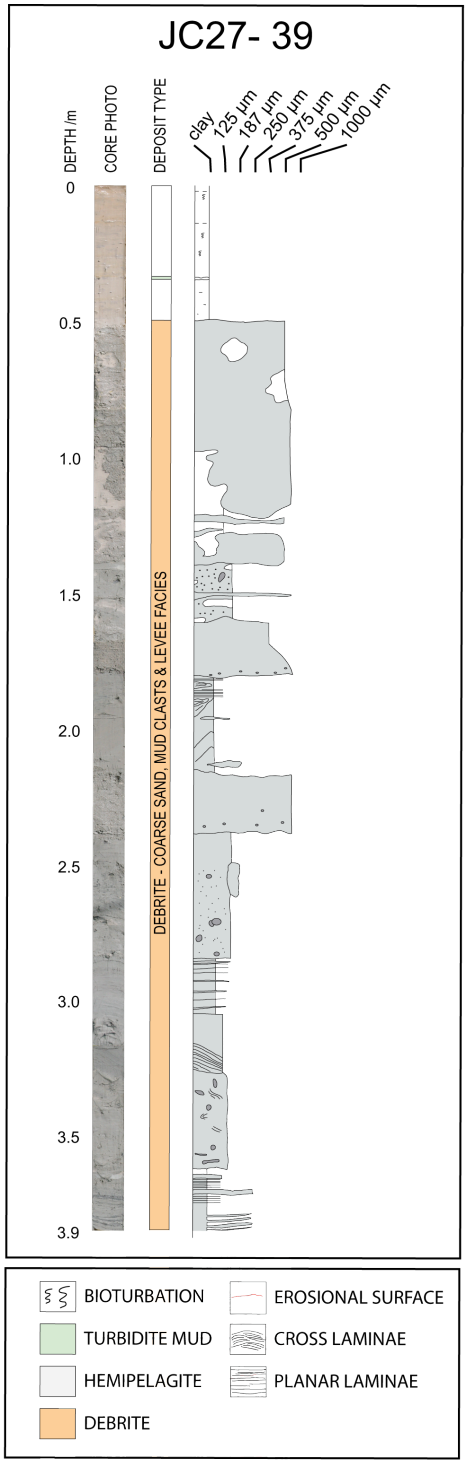

Macdonald et al. Figure 7. .jpg

Figure 8

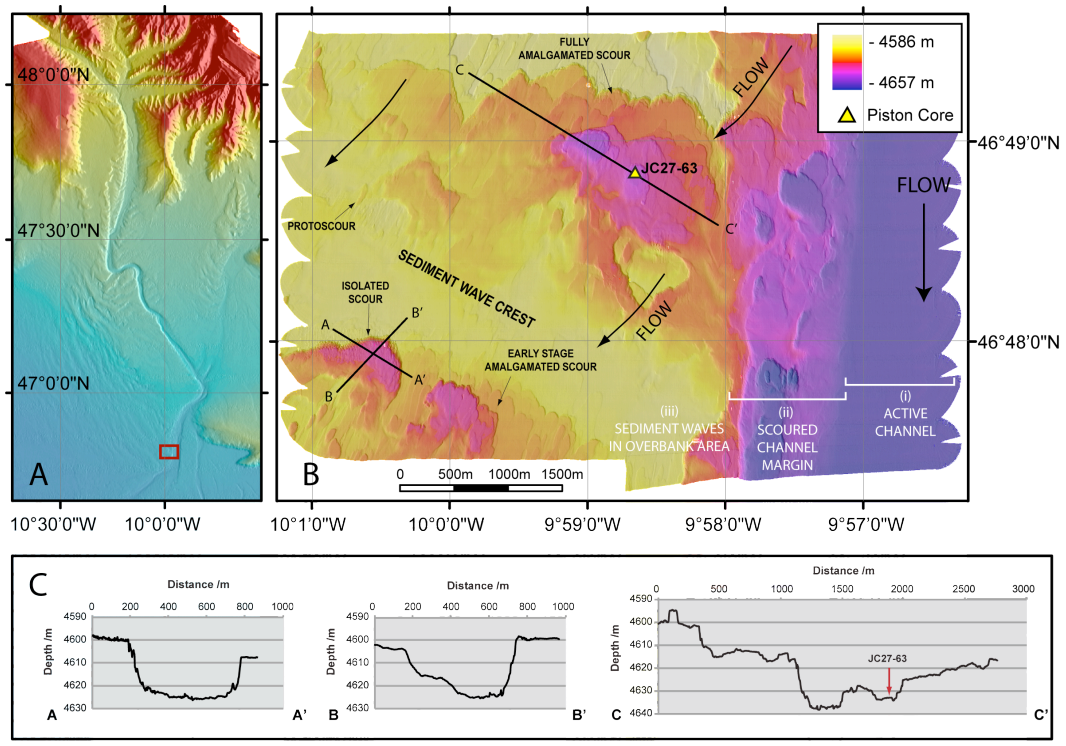

Macdonald et al. Figure 8. .jpg

Figure 9

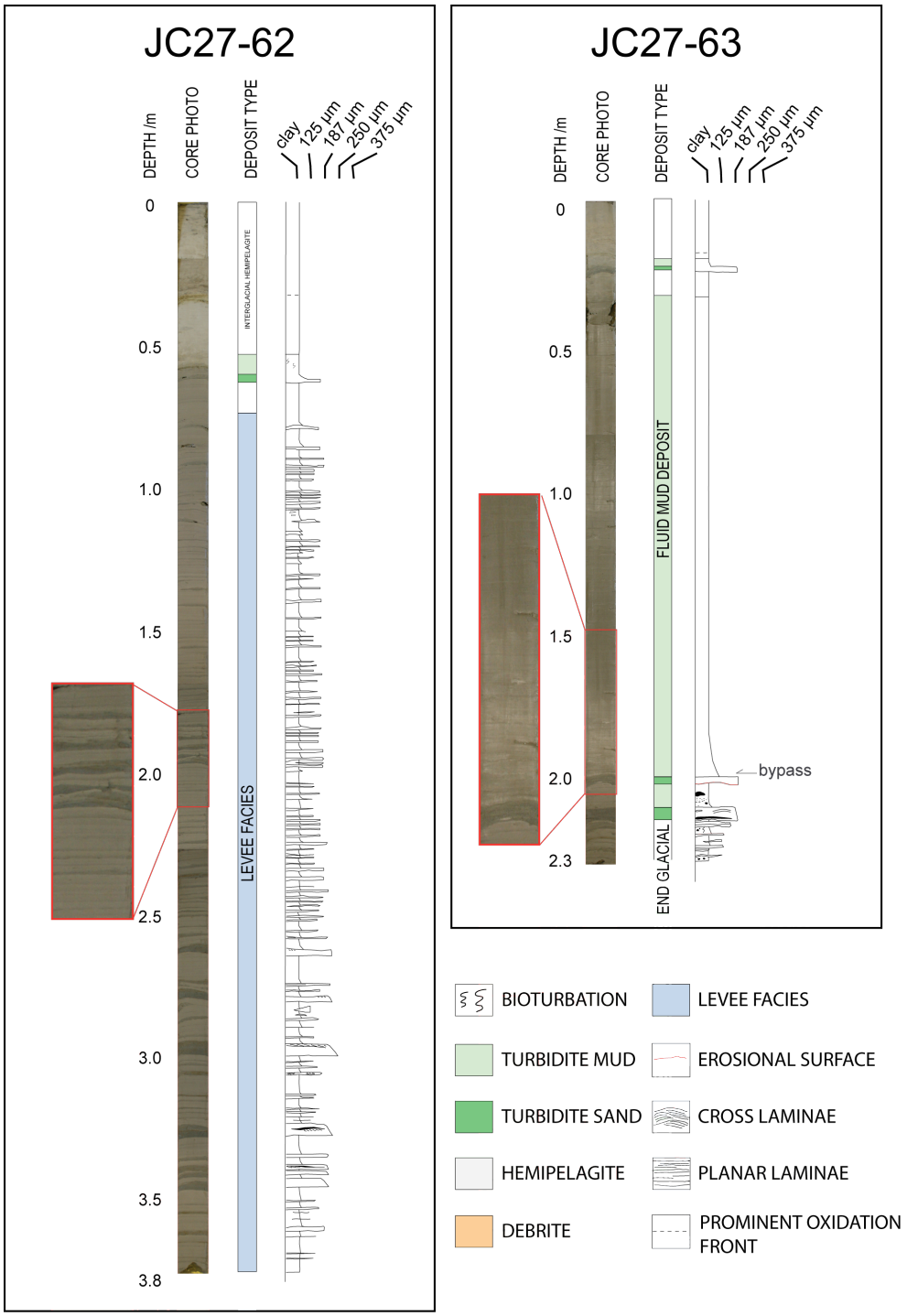

Macdonald et al. Figure 9. .jpg

Figure 10

SCOUR TYPE	PLAN VIEW (not to scale) Isolated Amalgamated	ISOLATED SCOUR MAX. DIMENSIONS (m) Length	Width	Depth	REFERENCE
SPOON	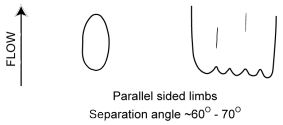 Parallel sided limbs Separation angle ~60° - 70°	600	225	20	Agadir Channel Mouth, This study; Wynn et al. (2002a) Albian Black Flysch, Vicente Bravo and Robles (1995)
HEEL	Divergent limbs at <100°	350	890	30	Whittard channel margin, This Study; Monterey Fan, Normark et al. (1979); Rhone Neofan, Wynn et al. (2002a); Valencia Fan, Palanques et al. (1995); Carboniferous Ross Formation, Elliott (2000a,b); Lien et al. (2003)
CRESCENTIC	Divergent limbs at <130°	1000	1000	14	Setúbal canyon mouth, This Study; Rhone Neofan, Wynn et al. (2002a); Bonnel et al. (2005); Navy Fan, Normark et al. (1979); Amazon Fan, Jegou et al. (2008)
OVAL	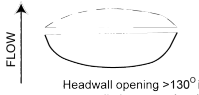 Headwall opening >130° in plan view, limbs are undeveloped	-	3170	48	Horseshoe Valley, This study

Macdonald et al. Figure 10. .jpg